SURFACE PATTERNED NANO- AND MICROARRAYS USING PARYLENE FOR BIOLOGICAL APPLICATIONS

A Dissertation

Presented to the Faculty of the Graduate School

of Cornell University

In Partial Fulfillment of the Requirements for the Degree of

Doctor of Philosophy

by

Christine Pek Boey Tan

January 2011

SURFACE PATTERNED NANO- AND MICROARRAYS USING PARYLENE FOR BIOLOGICAL APPLICATIONS

Christine Pek Boey Tan, Ph. D.

Cornell University 2011

Spatial patterning of biomolecules on a surface with nano- and micrometer precision is important in engineering biological microenvironments. Nano- and micropatterned biological arrays are useful for chemical functionalization of miniaturized biosensors, tissue engineering, high throughput drug screening, and fundamental biophysical and molecular biology studies. Despite the growing demands and applications, current surface patterning techniques are still lacking. Parylene (or poly[p-xylylene]) is a unique family of chemically vapor deposited polymer that is biocompatible, exhibits little to no swelling in aqueous solutions and is amenable to photolithography processing. These characteristics of parylene are attractive for its use as a "peel-able", high fidelity stencil for the surface patterning of biomolecular arrays. Different types of parylene coatings containing substituted functional groups have been developed for biochemical surface modification on virtually any surface.

The two themes that emerge from this work are: i) the use of parylene films with nano/microfabricated openings as a stencil tool for surface patterning (Chapters 2 – 4), and ii) the application of parylene coatings to directly pattern surfaces (Chapters 5 and 6). Chapter 2 describes a new nanofabrication process to create parylene stencils with sub-100nm openings. These stencils can then be combined with inkjet printing to rapidly generate multi-component biomolecular nanoarrays on a single surface. The work in Chapter 3 elucidates the role of cell-cell interactions in tumor angiogenesis through the use of patterned tumor cell arrays. In Chapter 4, a hybrid substrate,

consisting of a hydrophobic parylene stencil with hydrophilic silanized openings, is utilized to control spot drying morphology and improve microarray reproducibility. Parylene-based paper microfluidic devices and their enhanced capabilities are presented in Chapter 5. The work in Chapter 6 involves proteins covalently immobilized onto an array of reactive (aminated) parylene strips. These strips subsequently incorporated with microfluidics for the affinity-based screening and subsequent recovery of aptamers. Chapter 7 is a summary containing unpublished observations of parylene that may serve as a useful starting point for future researchers. These cumulative studies demonstrate that parylene-based surface patterning techniques are versatile for creating nano- and microarrays towards many biological applications.

BIOGRAPHICAL SKETCH

Christine Pek Boey Tan (陈弼梅) was born in the sunny island country of Singapore in 1983. Her remarkable mother, June Tong, single-handedly brought up Christine and her brother, Samuel Tan, with the help of her grandmother, aunts and uncles. By the age of 4, Christine had read the entire World Book encyclopedia that her mother gave to her as a birthday present. As a result of this voracious reading, Christine created minor troubles in primary school by volunteering esoteric answers like "krypton, yttrium and palladium" to her science teacher's simple request to name a chemical element; presumably an early sign for her scientific career.

From 1995–1999, Christine studied at Raffles Girls' Secondary School, where she learned to aspire, strive and dare to be an active creator of a better age for all. Christine attended Hwa Chong Junior College from 2000–2001 and was elected by the students to the 27th Students' Council. Her campaigning motto, "I may not be your best, but my determination will definitely beat the rest", still guides her to this day.

In 2002, Christine was blessed to be one of the five recipients out of the top high school students, to receive the Singapore Technologies International Scholarship for a full overseas tertiary education. She went overseas to study at Imperial College London, graduated with a Bachelor of Engineering (First Class Honors) in Biomedical Engineering, and became the first college graduate in her family. While at Imperial College, Christine was first introduced to scientific research by working in the laboratory of Dr. Danny O'Hare. Her undergraduate research was focused on the electrochemical studies of oxygen evolution during the electrolysis of water on metal surfaces. Christine also helped in Dr. Alexandra Lindsey's dissertation work to develop the micro-optical ring electrode for electrochemical detection of cyanide.

In 2005, Christine joined the research laboratory of Professor Harold Craighead – a dream come true – and pursued her Ph. D. in Biomedical Engineering at

Cornell University. In 2010, she was honored to receive the Graduate Student Excellence in Mentoring Award from the Cornell's Diversity Programs Office, the Nellie Yeh-Poh Lin Whetten Memorial Award from the Cornell Nanoscale Facility, and the Russell and Sigurd Varian Award from the American Vacuum Society. One of the most momentous events in Christine's life occurred in June 2010, when she married Benjamin Cipriany, her trusted colleague whom she met while in the Craighead group, who is now her most endearing life-long friend.

To my Lord Jesus Christ,

my utmost for His highest.

Whatever is foreseen in joy

Must be lived out from day to day.

Vision held open in the dark

By our ten thousand days of work.

Harvest will fill the barn; for that

The hand must ache, the face must sweat.

And yet no leaf or grain is filled

By work of ours; the field is tilled

And left to grace. That we may reap,

Great work is done while we're asleep.

When we work well, a Sabbath mood

Rests on our day, and finds it good.

- X, Sabbaths, Wendell Berry.

ACKNOWLEDGMENTS

There are countless reasons for me to thank God. First, I am grateful for my loving mother, June Tong, who is always encouraging me to reach heavenward and giving me the wings to fly, even though it must surely be difficult for her that I am so far away. I would like to thank my dear brother, Samuel Tan, for being a pillar of strength and comfort for my mother and me during this challenging time. My wonderful husband and colleague, Benjamin Cipriany, has been a patient listening ear and a godly companion to grow alongside. His love for and knowledge of optics and lasers never fail to amaze me. I owe everything to my godfather David So, for enabling me to work on my PhD without distractions or worry about my family back in Singapore. I am grateful to my parents-in-law, Darrell and Suzanne Cipriany for their understanding and support of our busy graduate lives.

I am thankful to Professor Harold Craighead for giving me the freedom to grow and develop as a scientist, and for supporting my inter-collaborative research efforts. Harold embodies visionary foresight, the ability to ask the right questions, and interdisciplinary knowledge, all in one tall package. I feel really privileged to have been trained under the auspices of a scientific giant like him. Professor David Lin deserves to be credited for teaching me all about microarrays, neuronal dissection and culture, and nucleic acids manipulation. Despite his busy schedule, it is admirable how he always makes time to guide his students and even perform hands-on experiments at the laboratory bench with them. I am grateful to Professor Brian Kirby for mentoring me on the importance of setting personal goals and keeping track of my own professional progress. To his credit, I have used some of his personal evaluation forms and skills worksheet in guiding my own undergraduate students. In Fall 2006, I had the pleasure of being a Teaching Assistant for Professor David Putnam's course on drug delivery. I owe him thanks for helping me find my love for teaching and my

students. Professor Claudia Fischbach has been a great role model for me. She is a brilliant woman scientist who is successful in both her professional career and family life. I am also grateful to Claudia for providing a visionary role in experimental design, useful critique when I was writing my first paper, and for teaching me all about angiogenesis and tumor microenvironments. I would like to thank Professor Moonsoo Jin for being a great instructor on the protein engineering and site-directed mutagenesis course, which is my favorite course at Cornell.

I wish to acknowledge the friendship and technical support of the past and present members of the Craighead group, especially Jose Moran-Mirabal, Philip Waggoner, Madhukar Varshney, Keith Aubin, and Leon Bellan. I am indebted to Jose for being one of the best mentors one could ever find, and for imparting the secret arts of parylene to me. I would like to thank Phil and his family (Amanda, Jack and Claire) for their warm friendship. It has been enjoyable working with Phil, especially on the serendipitous discovery of high-Q resonators in air. Not only has Madhukar been helpful in teaching me about protein surface chemistry, he and Shailey have been wonderful friends. I am grateful to Keith for initiating me into the "wonderful playground" of the Cornell cleanroom, and Leon for introducing me to ferrofluids, electrospinning, interesting uses of cotton candy, and how to make the Slow-tator (slow sample rotator). I was also fortunate to work with Kylan Szeto and Aline Cerf – not only are they creative scientists, they have many hidden talents such as microwave marshmallow-fighting and gourmet cooking skills. I am grateful for the friendship and many interesting discussions with Rob Barton.

It has been most rewarding to work with many talented collaborators, many of whom are also great friends. The micropatterned tumor cells array project was featured on the cover of Integrative Biology, thanks to Bo Ri Seo and Daniel Brooks's persistent hard work. Emily Brooks, who is one of my best friends and my matron-of-

honor, has been a great scientist to brainstorm ideas with and to seek biology help. I am grateful to Eric Williams and Steve Rodriguez, for preparing labeled nucleic acids and running microarray experiments. Dr. Huixian Liu (Weill Medical College) taught me cell culture, RT-PCR and ELISA. Kristin Ceniccola was the first undergraduate student I mentored. She ran many time-consuming experiments in pioneering the patterned hydrogels and parylene peel-strips projects – her enthusiasm is amazing! I would like to thank Sun-min Kim who worked with Jose and me, for performing the multilayer parylene patterning experiments. Catherine Pilarz ran preliminary fluorescent immunostaining experiments for the parylene peel-strips project, and helped jump-start the parylene-based paper microfluidics project. I am grateful to my undergraduates for teaching me how to be a better mentor.

I wish to acknowledge the friendship and technical help on parylene from James Brundage from Uniglobe Kisco. Jim and his colleague Bruce Holt also provided the aminated parylene samples. I would also like to thank Dr. Fred Hyde (Epicentre Technologies), Dr. James Catalfamo (Diagnostics Lab, Cornell), and Professor Xia Chu (Hunan University), for technical advice on the parylene peel-strips project.

The staff members of the Cornell Nanoscale Facility (cleanroom) deserve my gratitude for being always ready to help: Rob Ilic, Melanie Claire, Garry Bordonaro, Vince Genova, Meredith Metzler, Dan Woodie and Mike Skvarla. I would like to thank all my friends at Clark Hall; their sunny presence have livened up the gloomy Clark basement: Nathan Ellis (counselor in residence), Rosemary French, Renee King, Lisa Ciaschi, Bonni Jo Davis, Bobby Kenyon, Rodney Bowman, Dave Bowman, Mick Thomas, Linda Hatch, Lenny Freelove, Sned (and his whiskey sour), Ken and Lenny.

I can still remember the day when Belinda Floyd (administrative assistant in the Biomedical Engineering department [BME]) called me in England to tell me that I have been accepted to Cornell. This is the extent of her dedication to her work.

Belinda has been the “wheels” behind our department, ensuring that everything runs smoothly – she is super! My wonderful BME friends: Tunde Babalola, Clarissa Lui, Abhishek Ramkumar, Jun Wu, Evan Spiegel, Alex Daley, Janet Shen, and Gilda Shayan. Flor Cianchetti is one of my best friends and deserves special mention for being here for me during my most difficult times in graduate school.

To my scientific family at Imperial College: Dr. Danny O’Hare and his research group, especially Dr. Alexandra Lindsay, thank you for teaching me the secret arts of electrochemistry, and for sparking my interest in science! I am grateful to the late Professor John Lever for being an exemplary teacher and believing in me. Professor Kim Parker is a fine example of a scientist who is not just a specialist in one narrow field, but also a true scientific scholar in many interdisciplinary areas, and I aspire to be like him. Drs. Mauricio Barahona and Sophia Yaliraki deserve double credit – first, for encouraging me to come to the United States and work with Harold; second, for indirectly bringing me and Ben together.

I am indebted to the Executive Board of Singapore Technologies Pte. Ltd., especially Mrs. Kuan Kwee Jee and Ms. Irene Ang, for awarding me the scholarship to attend college – the stepping-stone to all these adventures! I would like to thank my mentor at Chartered Semiconductor, Dr. Lap Chan, for suggesting that I pursue a Ph.D., and for his continued encouragement all these years.

The Protestant Cooperative Ministry at Cornell has been a wellspring of spiritual refreshing. I am thankful to our minister, Reverend Taryn Mattice, and my brothers and sisters – Luwam Dirar, Eric Howd, Rob Bruce, Andy Poshadel, Eric Monkman, Katie White, Nate and Johanna Goodell, Ben Wang and Melissa Moser.

By the grace of God, I will always remember my time at Cornell fondly, because of these special people who have been here for me.

TABLE OF CONTENTS

LIST OF FIGURES

LIST OF TABLES

LIST OF ABBREVIATIONS

2D	Two-dimensional
3D	Three-dimensional
λExo	Lambda exonuclease
μCP	Micro-contact printing
AFM	Atomic force microscopy
Al	Aluminum
APTES	3-aminopropyltriethoxysilane
APTMS	3-aminopropyltrimethoxysilane
A.U.	Arbitrary unit
bFGF	Basic fibroblast growth factor
BFPRck	Biotinylated phenylalanine-proline-arginine-chloromethylketone
BSA	Bovine serum albumin
CTB	Cholera toxin subunit B
CVD	Chemical vapor deposition
DAPI	4’,6-diamidino-2-phenylindole
$DiIC_{12}$	1,1'-didodecyl-3,3,3',3'-tetramethylindocarbocyanine perchlorate
DMEM	Dulbecco’s modified Eagle’s minimum essential medium
DNA	Deoxyribonucleic acid
DNP	Dinitrophenol
DPN	Dip pen nanolithography
DPPC	1,2-dipalmitoyl-sn-glycero-3-phosphocholine
DNP-cap-DPPE	1,2-dipalmitoyl-sn-glycero-3-phosphoethanolamine-N-[6-[(2,4-dinitrophenyl)amino]hexanoyl]
dsDNA	Double-stranded DNA
DU145	Human prostate carcinoma cell line

EBL	Electron-beam lithography
ECM	Extracellular matrix
EDTA	Ethylenediaminetetraacetic acid
ELISA	Enzyme-linked immunosorbent assay
EMEM	Eagle's minimum essential medium
EMT	Epithelial-mesenchymal transition
ExoI	Exonuclease I
ExoIII	Exonuclease III
FACS	Fluorescence activated cell sorting
FBS	Fetal bovine serum
FWHM	Full-width-at-half-maximum
HDT	Hexadecanethiol
HEPES	4-(2-hydroxyethyl)-1-piperazineethanesulfonic acid
HTB-4	Urinary bladder transitional cell carcinoma cell line
IgE	Immunoglobulin E
IgG	Immunoglobulin G
IL-8	Interleukin-8
MHA	16-mercaptohexadecanoic acid
MIF300	Photoresist developer
MVD	Molecular Vapor Deposition tool from Applied Microstructures
MW	Molecular weight
NIL	Nanoimprint lithography
PBS	Phosphate buffered saline
PCR	Polymerase chain reaction
PE	Phycoerythrin fluorescent dye
PEG	Polyethylene glycol

PEO	Polyethylene oxide
PDGF	Platelet-derived growth factor
PDMS	Polydimethylsiloxane
PI3K	Phosphatidylinositol 3-kinase
PMMA	Polymethylmethacrylate
PNP	Print-and-Peel
PPV	Poly(p-phenylene vinylene)
PSA	Prostate specific antigen
PSD	Percentage standard deviation
OSCC3	Human oral squamous cell carcinoma-3 cell line
RBL	Rat basophil leukemia cell line
R.F.U.	Relative fluorescence unit
RNA	Ribonucleic acid
SELEX	Systematic evolution of ligands by exponential enrichment
SEM	Scanning electron microscopy
SN-59	6-amino-1-napthalenesulfonamide fluorogenic substrate for thrombin
ssDNA	Single-stranded DNA
TAE	Tris Acetate EDTA buffer
TBE	Tris Borate EDTA buffer
TBPB	Tetrabromophenol blue
TGF-α	Transforming growth factor alpha
TNF-α	Tumor necrosis factor alpha
UV	Ultraviolet light
VEGF	Vascular endothelial growth factor
WCA	Water contact angle
ZEP-520	Electron-beam lithography positive-tone resist

LIST OF SYMBOLS

^{o}C	Degrees celsius
^{o}	Degrees (angle)
γ	Surface tension
η	Viscosity
θ	Apparent contact angle
ϕ29	phi29 polymerase
cc	Cubit centimeter
cm	Centimeter
cm^3	Cubit centimeter
D	Average pore diameter of a porous medium
d_1	Length
d_2	Length
Da	Dalton
g	Gram
h	Hour
Hz	Hertz
kDa	Kilo-Dalton
kPa	Kilo-Pascal
ℓ	Distance or length traveled
μg	Microgram
μL	Microliter
μm	Micrometer
M	Molar
m	Meter
m^3	Cubit meter

min	Minute
mg	Milligram
mL	Milliliter
mm	Millimeter
mN	Milli Newtons
nm	Nanometer
s	Second
t	Time
v/v	Volume in volume dilution
w/v	Weight in volume dilution
w	Width

CHAPTER 1

INTRODUCTION[1]

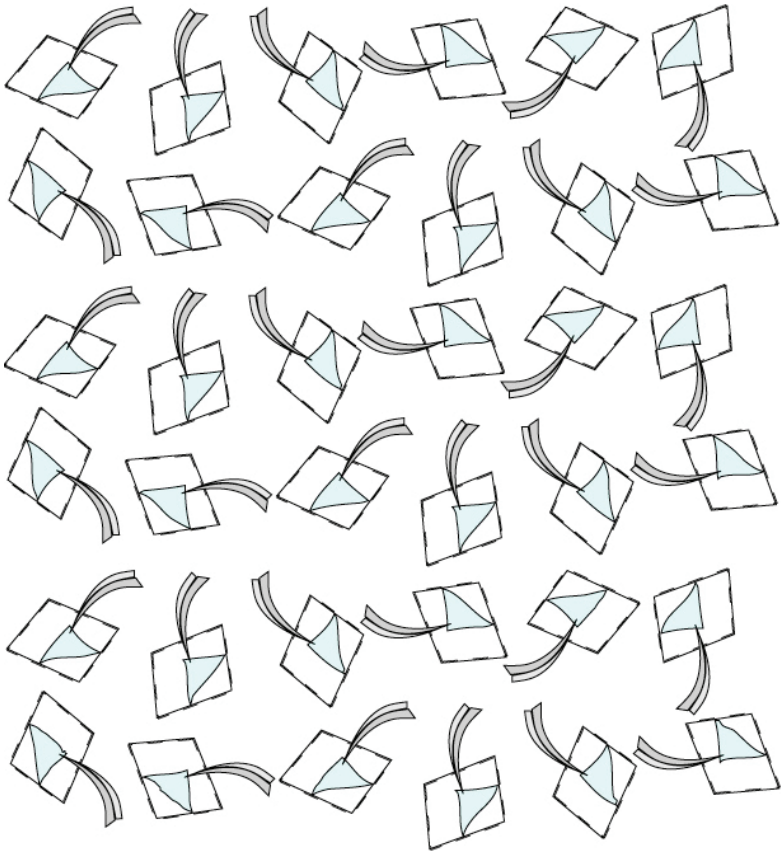

Parylene Peel-Off Pseudo-Tessellation © 2011 Christine Tan.

[1] This chapter is a modified form of the publication: Tan, C.P., Craighead H.G., Surface Engineering and Patterning Using Parylene for Biological Applications, *Materials* 2010, 3, 1803-1832.

1.1 MOTIVATION FOR SURFACE PATTERNING

Surface patterning is the controlled localization and deposition of biochemical molecules on a surface. For several decades now fundamental surface chemistries, such as thiol self-assembly on gold and silanization on glass, have been broadly used to engineer surfaces that allow for covalent linkage of proteins or to resist protein adsorption. In the biomedical community, surface coatings have also been directly applied to create biocompatible or biologically active surfaces for drug delivery systems, biomedical implants and prostheses [1-3]. In particular, these coatings modify the original surface to contain new chemical functionalities suitable for immobilizing proteins, drugs or anti-coagulant agents.

Micropatterning is a toolbox for surface patterning that involves the spatial manipulation and deposition of biomolecules with micro- and nanometer length-scale precision. To create artificial tissues or to even begin unraveling the mysteries of molecular cell biology, the ability to position biomolecules with micro- and nanometer precision is especially important for mimicking biologically relevant environments. For instance in human tissues, the signaling between biomolecular ligands and receptors occur on nanoscale dimensions, while cell-cell interactions and tissue architecture are controlled at the microscale level. Indeed, recent advances in micropatterning [4-10] have enabled a plethora of biological applications ranging from micro total analysis systems (biosensors, microfluidics and microarrays), tissue engineering, and fundamental biophysical studies [11-15]. For example, surfaces of miniaturized biosensors such as nanowires [16], nanoelectromechanical devices [17], and diffraction gratings [18], can be selectively functionalized to carry various biochemical molecules (*e.g.* antibodies, nucleic acids) that would act as biological recognition elements. DNA microarrays are surfaces patterned with arrays of 100-1000s of different nucleic acids to enable large-scale screening of multiple genes at

once [19, 20]. Microarrays have since been extended to cell arrays and protein arrays [21, 22]. Microfluidic channels can be patterned with different biomolecules for portable multiplexed assays [9, 23, 24].

With the advent of micropatterning, there is a desire to pattern biomolecules with increasingly smaller nanoscale resolution, which may perhaps one day reach the dimension of a single biomolecule. This is particularly attractive for enabling research on subcellular structures such as molecular motors and receptor-ligand interactions [8, 25, 26]. Furthermore, this ultra-miniaturization can lead to an increased packing density of a patterned array to include more potential candidates for screening, or faster response time of biosensors [27, 28].

Despite these growing demands and many biological applications, the current surface patterning technologies are imperfect. One crucial question is: how to pattern arrays of different biomolecules on a surface without compromising their biological function? Not only would the ideal surface patterning technique allow for the rapid generation of uniform biomolecular arrays across a range of length scales, it has to be more importantly, biocompatible. There is thus a continual challenge to develop new surface patterning methods and to discover new materials towards this purpose.

1.1.1 Survey of Current Surface Patterning Techniques

Fundamental surface chemistries confer the modified surfaces with desired functional groups (*e.g.* amine, carboxyl, azide, hydroxyl *etc.*) and physico-chemical properties (*e.g.* hydrophobicity, hydrophilicity, resistance to protein adsorption *etc.*). These chemistries include thiol self-assembly on gold, silanization on hydroxyl-rich surfaces like glass, phosphonic acid coordination with multivalent metals *etc*. While some of these chemistries are relatively straightforward and reproducible, they all require their own specific substrate surface to work. Furthermore, it may be difficult to

control the thickness of silane layers [29]. Thus CVD polymeric surface coatings *independent* of the surface material have become popular for direct surface modification [30, 31].

Popularly known micropatterning techniques include dip-pen nanolithography (DPN) [6], microcontact printing (μCP) [7], and inkjet printing [32]. The most accessible method is μCP, which involves the use of elastomeric PDMS stamps to imprint the biomolecules onto a surface. However, the stamp inked with biomolecules can swell in aqueous solutions compromising the pattern fidelity, and the stamp has to be dried that could affect the bioactivity of the molecules. Additionally, it can be difficult to print many different types of biomolecules on a surface due to issues in aligning the PDMS stamps [33]. Inkjet printing is a straightforward patterning technique with high speed and the ability to print multiple types of biomolecules, however its resolution is ~10s μm at best. While dip-pen nanolithography has the best nanopatterning resolution of ~10s of nm, it is a relatively slow technique for patterning microscale features over a large surface area and involves user knowledge of a complex system since it utilizes an atomic force microscopy (AFM) based system. Furthermore, the diversity of different materials DPN can normally print is much smaller compared to inkjet printing. Some improvements have been made to the DPN system, such as using inkjet printing onto the silicon dip pen tips to increase the number of different components printable [34], and an elastomeric polydimethylsiloxane (PDMS) tip that increases the radius of curvature when force is applied to facilitate patterning larger features [35].

Other methods of micropatterning include electron beam lithography to define regions define regions of crosslinked polymer to promote covalent linkage of proteins [4], using streams of flows inside microfluidic channels to pattern stripes of biomolecules and their combinations [9, 23], and using photoresist to pattern areas of

proteins [36]. Again, these methods are limited in terms of how many different types of biomolecules can be patterned on a surface, or require as many different reservoirs and fluidic channels as the number of different biomolecules patterned, or may utilize harsh conditions to remove the patterning resist that can degrade the biomolecules.

Despite many advances being made in the surface patterning technologies and the patterning resolution continually being challenged, the fundamental needs of surface patterning have only been partially met. An ideal surface patterning technique would be: i) biocompatible with the biomolecules that are patterned, retain high pattern uniformity and reproducibility, ii) able to create large surface area arrays of biomolecules rapidly and with high throughput, iii) pattern array features across both micro- and nanometer length scales, iv) able to pattern multi-component species of biomolecules on a single surface, and v) additionally be able to add functional reactive groups independently of the surface material if necessary. Clearly these lofty goals are not easily achieved by a single surface patterning method. The body of work in this dissertation will attempt to address these challenges by developing new capabilities, applications, and methods for surface patterning based on a polymer – parylene.

1.1.2 Motivation for Parylene-Based, Surface Patterned Nano- and Microarrays

Parylene is a family of CVD coated polymers with unique properties such as biocompatibility, pinhole-free conformal coating, low cytotoxicity, and resistance to swelling in aqueous environments. Furthermore, parylene can be chemically inert or chemically reactive depending on the substituted side groups. Traditionally used in semiconductor industries as dielectric layers, parylene is amenable to photolithography micromachining and thus nano- and microscale features can be created in a parylene film. These characteristics of parylene make it amenable and attractive for use in surface patterning. For instance, *chemically inert* parylene-C films

can be utilized as patterning "peel-off" stencils with high patterning fidelity, while *chemically reactive* parylene-A films can be coated onto nearly any surface to directly confer new functional group for covalent linkage of biomolecules and drugs.

Parylene-C "peel-off" stencils have been created and utilized in the first part of this dissertation as a surface patterning method to ameliorate some of these problems associated with current patterning techniques. The first part of this dissertation work relates to parylene "peel-off" stencils and show that they offer many advantages, such as the ability to pattern in a hydrated environment to preserve the bioactivity of the molecules, a patterning resolution of sub-100nm comparable to DPN and μCP, and the rapid generation of uniform nanoarrays containing multi-component proteins. Parylene peel-off is compatible with many existing technologies, such as cell culture methods and traditional microarray processing techniques. Chapters 3 and 4 demonstrate the utility of parylene peel-off in two new applications, specifically to spatiotemporally control the level of cell-cell interaction in tumor cells for angiogenic studies, and to clean up printed spots and reduce the coffee-ring effect (an artifact of drying spots) so as to increase microarray reproducibility.

The physico-mechanical properties of parylene such as hydrophobicity and conformality of the CVD film, as well as the chemical functionalities of parylene conferred by the substituted side groups, allow for a range of new microstructures to be created for several biological microfluidic applications. Moving away from using parylene as a stencil, the second part of this dissertation work is devoted to the use of parylene films for direct surface biochemical modification. In Chapter 5, parylene-C was conformally coated on paper to create a new parylene-paper composite with the porosity of paper and the physico-chemical properties of parylene. Parylene-coated paper is waterproof (hydrophobic) and mechanically flexible. Using adhesive tape and oxygen plasma treatment, channels were patterned on the parylene-paper composites

to transport fluids. These parylene-based paper microfluidic devices were shown to have enhanced capabilities such as combinatorial mixing, concentration gradient generation and protein detection. Another advantage is the ability to tune the lateral flow speeds in different regions of a single device, thereby opening up new assay opportunities for paper-based assays that require sequential delivery of liquid reagents.

Silanization and gold-thiol self-assembled monolayers have been popularly utilized for direct surface modification. However these methods require specific surfaces to work (*e.g.* glass surfaces for silanization and gold surfaces for thiol self-assembly), and the reactions can be difficult to control (*e.g.* silane layers). Chemically reactive parylene can be CVD coated onto nearly any substrate surface to produce uniform films with functional groups. In Chapter 6, proteins are directly covalently coupled onto strips of the chemically reactive aminated form of parylene (parylene-A). These parylene strips are then incorporated into a microfluidic format to first screen for aptamers that bind to these proteins. Each parylene strip can then serve as a tool for individually recovering the sample (aptamer) that binds to the specific protein. This new approach – microfluidic multiplexed sample screening and recovery – can be a powerful tool for high throughput analysis of biomolecules for drug discovery.

The versatility of parylene makes it a useful material for surface patterning, controlling the biochemistry and topography of devices for increasing numbers of biological applications. This introduction will address the role of parylene in surface biochemical modification in several parts. First, the history of parylene, its deposition process and material properties will be introduced. Second, the utility of parylene as a micropatterning stencil template will be discussed. This is followed by a review of the applications of parylene reactive coatings for surface modification. Thereafter, the direct coating of parylene to form microstructures such as membranes and tubes will be discussed.

1.2 BACKGROUND ON THE MATERIAL PARYLENE

1.2.1 History and Chemical Vapor Deposition of Parylene

Parylene was initially observed as the product of vacuum thermal decomposition (pyrolysis) of the common solvent, para-xylene [37]. Despite the relatively high temperatures 700 – 900°C, the yield of parylene film was low. Today, parylene can be deposited more efficiently and easily via a CVD process developed by Gorham [38]. In this CVD process, the dimer precursor [2.2]paracyclophane (or di-para-xylylene) is first vaporized and then undergoes vacuum pyrolysis at temperatures above 550 °C to yield the reactive monomer. The monomer adsorbs to the substrate surface and spontaneously polymerizes at room temperature to form linear, high molecular weight parylene films. Figure 1.1 is the typical CVD process for depositing parylene-C using commercial systems.

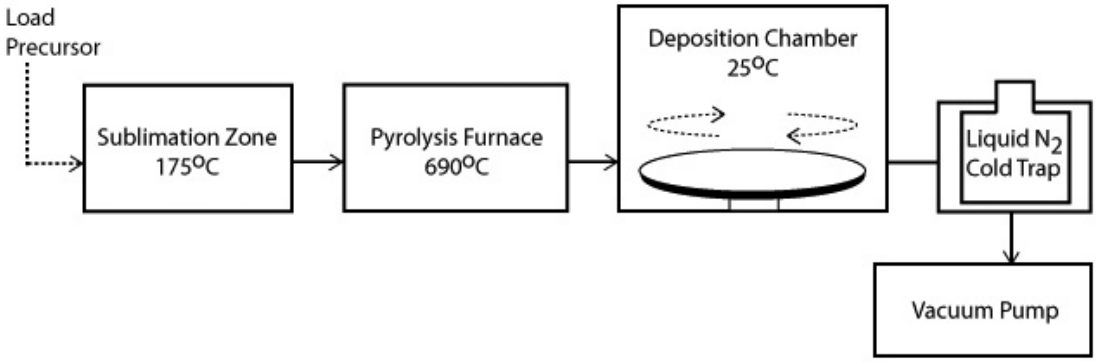

Figure 1.1 CVD polymerization of parylene-C. The precursor is loaded into the sublimation zone (175°C). The sublimed form of the precursor is transported into the furnace (690°C) for pyrolysis into the reactive monomer, which finally polymerizes into parylene spontaneously upon cooling in the deposition chamber (25°C). The substrate stage is usually rotated for increasing the uniformity of deposition.

Figure 1.2(a) shows the chemical reactions underlying the CVD process and the chemical structures of [2.2]para-cyclophane and parylene. The Gorham process enables control of the deposition parameters and full conversion of the precursor into parylene. It is appealing that the substrates are kept at room temperature during deposition, enabling parylene to be coated onto a variety of heat-sensitive substrates without thermal damage. The kinetics of the parylene CVD process have been elegantly reviewed by Fortin and Lu [39]. A key feature is that parylene deposition is under kinetic control. The rate-limiting steps of kinetically controlled CVD are: (1) the adsorption of the monomer onto the substrate, (2) surface migration and possibly bulk diffusion of the monomer, and (3) the chemical reaction (initiation or propagation) at the surface.

Selective deposition of parylene onto localized regions of the substrate can be realized by intervening in any of these rate-limiting steps. For example, several research groups have exploited this to form patterned films of parylene by using either transition metals or their salts to deactivate the monomer reaching the substrate surface [40-42], or localized heating to vary deposition rates at the surface [43-46]. These methods are alternatives to lithography for patterning parylene films. Due to the low sticking coefficient at room temperature [39], parylene is known for its excellent conformal coating of the substrate, even trenches, which is highly attractive for coating biomedical stents. However by suitably engineering the aspect ratios of the trenches and controlling parylene thickness, the otherwise conformal parylene film can be pinched off to form microfluidic tubes [47, 48].

1.2.2 Types of Parylene

The general chemical structure of [2.2]para-cyclophane is shown in Figure 1.2(a). A variety of substituted [2.2]para-cyclophanes exist, whereby functional groups

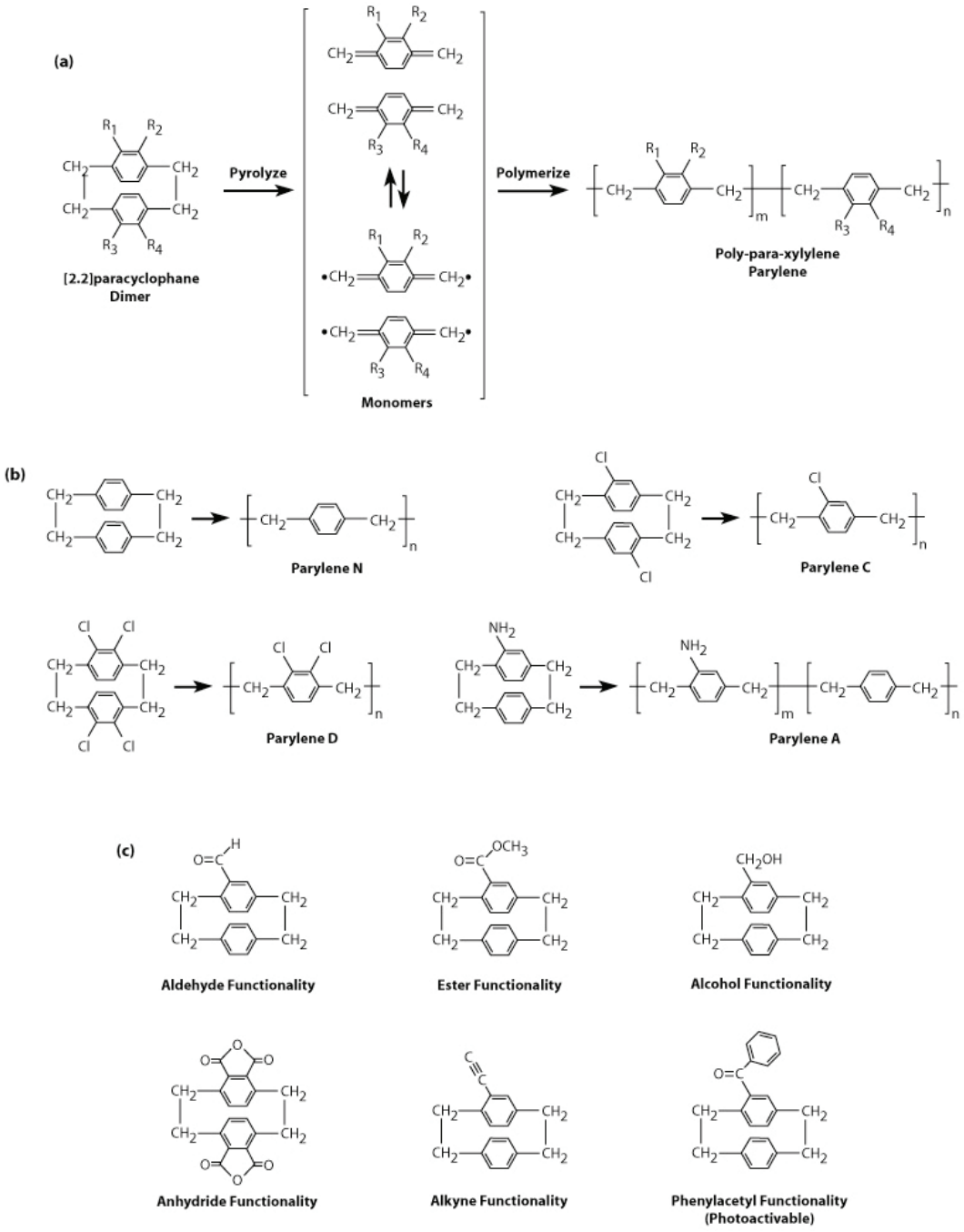

Figure 1.2 (a) Precursor [2.2]paracyclophane and its polymerization into parylene. (b) Types of commercially available precursors and their parylenes. (c) Substituted forms precursors (dimers) of parylene synthesized by research laboratories.

are not modified during the CVD process and allow for the deposition of functionalized parylene films with tailored chemical, mechanical, electrical and optical properties. Functionalized parylene coating is a versatile and simple method to introduce chemical functionalities to a surface, for example a biomedical implant, without the use of external organic solvents and catalysts, thereby reducing contamination and improving biocompatibility. Various [2.2]para-cyclophanes that are commercially available and their parylenes are shown in Figure 1.2(b), and substituted [2.2]para-cyclophanes that have been synthesized by research laboratories [3, 49] are shown in Figure 1.2(c).

Improvements in the chemical synthesis of the substituted precursor have led to parylene films with active functional groups such as carbonyl [50], amine [51], aldehyde [52], ester [53], anhydride [53], alkyne [54], alcohol [55], and photoactivable phenylacetyl [56, 57]. These active groups can further undergo chemical reaction to allow covalent immobilization of drugs [58], disaccharides [52], proteins [59] and polyethylene oxide [57] onto the parylene coated surfaces; these specific applications will be discussed later in the section on reactive parylene coatings. For example, alkynes are of great interest for chemical coupling with azides via "click" chemistry, which has been used in drug discovery, nanobiotechnology and surface chemistry [60]. Furthermore by mixing the ratios of two different types of substituted precursor, a "multipotent" film of parylene containing two different functional groups may also be deposited [61].

1.2.3 Material Properties and Applications of Parylene

Some material properties of commercial parylene are highlighted in Table 1.1. Parylene coatings have been used to protect electronic printed circuit boards, because parylene possesses low permeability to water and gases and forms highly conformal

Table 1.1 Some material properties of commercial available parylenes, data collected from reference [67], data specification sheets from Specialty Coating Systems and Uniglobe Kisco.

	Parylene-N	**Parylene-C**	**Parylene-D**
Density (g/cm^3)	1.11	1.289	1.418
Refractive Index	1.661	1.639	1.669
Melting Point (°C)	420	290	380
Dielectric Constant (60Hz)	2.65	3.15	2.84
Tensile Modulus (GPa)	2.4	3.2	2.84
Elongation to Break (%)	30	200	10
Static Coefficient of Friction	0.25	0.29	0.35
Dynamic Coefficient of Friction	0.25	0.29	0.31
Water Absorption (% in 24h)	<0.1	<0.1	<0.1
Oxygen Gas Permeability $(cc.mm)/(m^2.day)$	15.4	2.8	12.6
Water Vapor Transmission Rate $(g.mm)/(m^2.day)$	0.59	0.08	0.09
Water Contact Angle	79°	87°	97°

pinhole-free coatings. Parylene is amenable to micromachining by photolithography processes, and has been used as dielectric layers in semiconductor industries, as well as anti-stiction coatings for microelectromechanical systems due to its low coefficient of friction [62]. Unique properties such as biocompatibility, the pin-hole free and highly conformal nature of the parylene films, and low water absorption (swelling), have led to their recent adoption for biomedical applications, such as stents, neural electrodes, cardiac pacemakers, intra-oral magnets [63], and high-fidelity micropatterning of biomolecules [64].

1.2.4 Post-Coating Surface Modification of Parylene

The surface free energy of untreated parylene-C films is ~20 mN/m [65], corresponding to a hydrophobic surface with a high static water contact angle (WCA). Different parylenes have different surface properties (hydrophobicity or hydrophilicity), as seen by the different WCA in Table 1.1. This opens up opportunities for controlling and tailoring surface hydrophilicity through the use of parylene coatings. Parylene-C films exposed to oxygen plasma can become permanently hydrophilic due to the destruction of chemical bonds at the parylene surface, and the surface free energy can increase to more than 60 mN/m (WCA decrease to lower than 45°) after just 20s of oxygen plasma [65]. This method of modifying the hydrophilicity of parylene has been exploited for improving cell adhesion to parylene-C surfaces [66]. Untreated parylene films are observed to be resistant to silanization, while oxygen plasma treated parylene surfaces can be silanized using via vapor deposition of aminopropyltrimethoxysilane, as shown by the WCAs in Figure 1.3 [68]. A similar mechanism has been used to functionalize aminodextran and folic acid onto surface acoustic wave devices coated with parylene-C for biosensing [69].

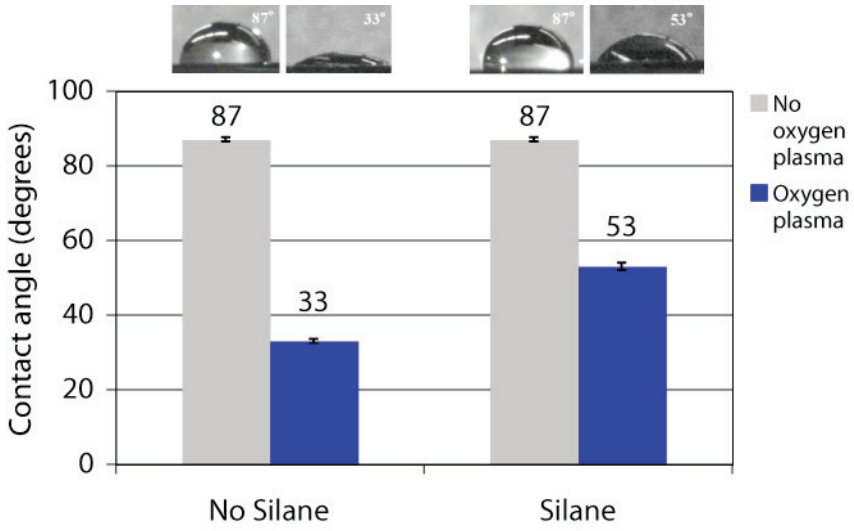

Figure 1.3 WCAs of parylene following different treatments: with 60s oxygen plasma etch and/or silanization with a hydrophilic aminopropyltrimethoxysilane.

1.3 NANO- AND MICROPATTERNING USING PARYLENE PEEL-OFF STENCILS

Surface micropatterning using parylene-C "peel-off" stencils was first pioneered by Ilic and Craighead [64] for patterning proteins and cells on a surface. These stencils were microfabricated using standard photolithography processes illustrated in Figure 1.4(a) (steps 1–4). Briefly, parylene was first coated onto a silicon wafer and a photoresist layer was spun on top of the parylene. Next, the photoresist was exposed by ultraviolet (UV) light and developed, creating features (openings) in the photoresist. The photoresist layer then served as an etch mask during oxygen plasma etching of the underlying parylene layer in the openings. Because photoresist etches at a similar rate as parylene, the photoresist layer has to be thicker than the parylene layer. Finally, the excess photoresist was removed by acetone and isopropanol to leave the parylene stencil on top of the wafer. Steps 5–6 of Figure

1.4(a) outline the procedure for micropatterning. The biomolecule of interest (in this case protein) was incubated onto the parylene stencil coated wafer surface. Thereafter, the parylene stencil can be mechanically "peeled off", as shown in Figure 1.4(b), to spatially pattern proteins in the localized regions defined by the openings. Thus, the parylene stencil also served as a protective coating for excluding the regions outside the openings. In this initial demonstration, arrays of poly-L-lysine, antibodies, mammalian mast cells and bacterial *E.coli* cells were micropatterned. The parylene peel-off approach can be employed in different configurations for micropatterning. For example, parylene peel-off can also be used for patterning cell co-cultures by sequentially patterning the first cell type, then peeling off the parylene and incubating with a second cell type [70]. Multilayer parylene stencils [71, 72] and ultra-thick re-usable parylene stencils [73] have also been developed.

There are two major advantages of parylene stencils. First, parylene is pinhole-free, chemically inert and resists swelling in aqueous solutions. These characteristics allow for biomolecules to be patterned with high fidelity and uniformity using the stencil. mCP is a popular micropatterning technique utilizing elastomeric PDMS stamps that can deform unevenly under pressure, shrink during curing, or swell in solutions. Parylene peel-off alleviates the problems associated with mCP, and increases the uniformity of micropatterning. Second, the parylene peel-off micropatterning approach does not require harsh chemicals and can be performed completely in aqueous environments, which preserves the conformation and activity of sensitive biological species. Other advantages of using parylene stencils for micropatterning include the ability to pattern on a variety of substrate surfaces with large areas rapidly. Figure 1.4(b) shows the parylene peel-off method used in micropatterning 4-inches diameter silicon wafer and 22 mm × 22 mm glass coverslips.

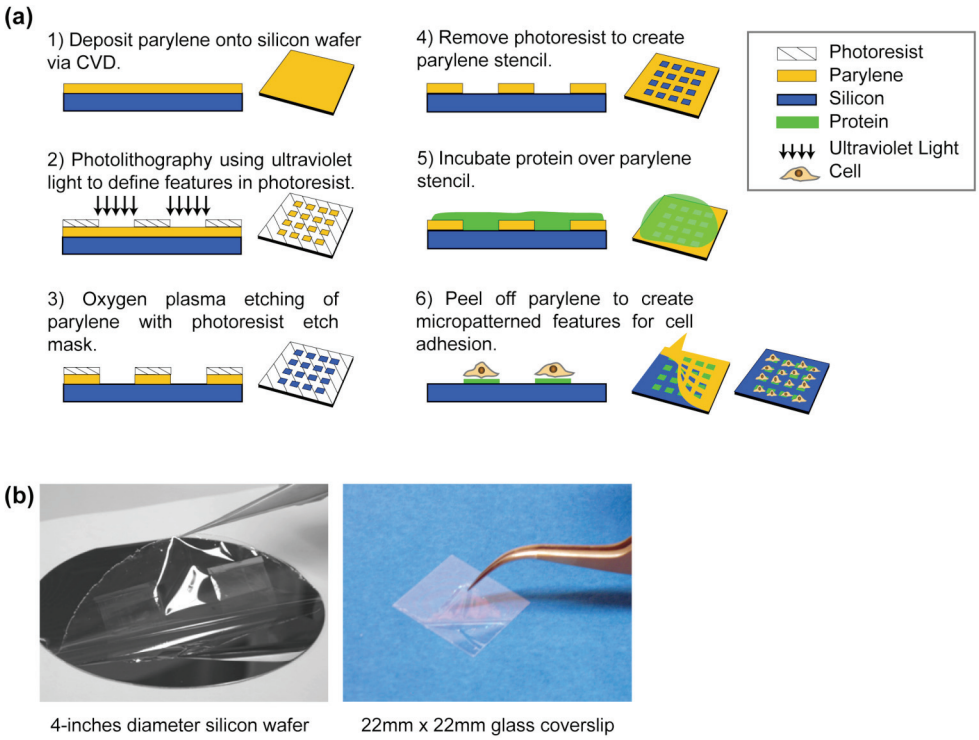

Figure 1.4 (a) Fabrication process of parylene-C stencils and the parylene peel-off micropatterning process. (b) Parylene peel-off has been used to micropattern large areas such as 4-inches diameter silicon wafer and 22mm x 22mm glass coverslips.

1.3.1 Patterned Hydrated Lipid Bilayers

A key advantage of parylene peel-off is the ability to pattern biomolecules in hydrated environments. This is critical for maintaining the bioactivity of proteins and especially the bilayer structure of lipids. As the most stringent test of hydrated patterning, lipid bilayers have been successfully micropatterned using the parylene peel-off approach [74]. Complex arrays of lipid bilayers patterns with different feature shapes and subcellular dimensions containing the antigen dinitrophenol (DNP) have been patterned [75]. Immune cells (rat basophil leukemia [RBL]) were activated by these antigen presenting lipids and extended lamellipodia in the direction along the

lines and square patterns of lipids, shown in Figure 1.5(a)-(c). Furthermore, the RBL cells displayed different morphologies when stimulated with lipids patterns of different shapes and sizes in Figure 1.5(d)-(e). Lipid bilayers of heterogeneous compositions with different functionalities (e.g. presenting antigens, incorporating fluorescent dyes) could be patterned, as shown by the schematic in Figure 1.5(f). The simplicity and adaptability of parylene peel-off for patterning lipids offer a convenient alternative to more complicated lipid patterning approaches such as photopolymerization and electric field-induced reorganization *etc.* [76, 77], and could play a future role in lipidomics.

1.3.2 Patterned Biomolecules Inside Microfluidic Channels

Microfluidic systems hold promise for portable bioassays and interrogation of biomolecules with minimal reagent and sample volume consumption [11-13]. The ability to pattern biomolecules inside the microfluidic channels allows for specific recognition of biological analytes. Patterning inside fluidic channels has been demonstrated by several groups utilizing laminar flows or crossed flows to create combinations of biomolecules [9, 23]. Parylene peel-off stencils can be addressed using fluidic channels for patterning multiple types of biomolecules inside microfluidics [78, 79]. For example, gangliosides embedded in lipid bilayers have been patterned inside microfluidic channels in Figure 1.6(a). In Figure 1.6(b)-(d), this biosensor device was used to detect cholera and tetanus toxin subunits, by measuring the signal from the fluorescently-labeled toxins that bound to the their natural target (gangliosides). Individual channel flows have been used to address openings in parylene stencil, so as the achieve selective spatial patterning of multiple biomolecules on a surface [79]. In the future, parylene could be combined with inkjet printing for multiplexing of biomolecular patterning inside microfluidic channels.

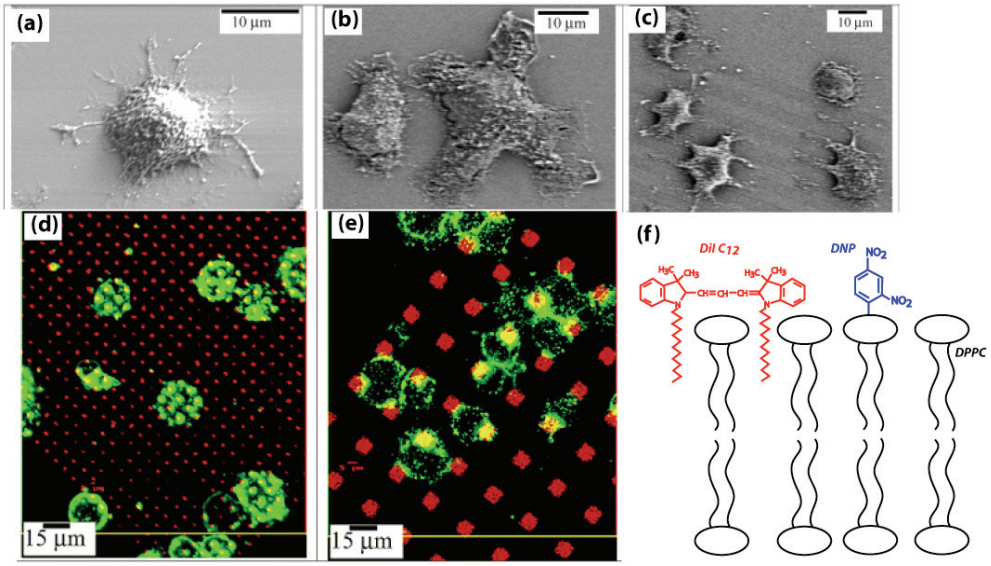

Figure 1.5 Scanning electron micrograph (SEM) images of RBL cells: (a) Resting RBL on a plain silicon surface with lamellipodia randomly spreading on the oxidized silicon substrate; (b) Stimulated RBL at the corner of four patterned squares of lipids; (c) Stimulated RBL over patterned lines of lipids. Gray lines indicate where the antigenic lipids were patterned. Interaction between RBL cells and the patterned lipid bilayer with (d) 1.5 µm pattern, 5 µm period, and (e) 6 µm pattern, 16 µm period. Confocal images of RBL cells sensitized with Alexa 488 anti-DNP IgE (green) on a 1,1'-didodecyl-3,3,3',3'-tetramethylindocarbocyanine perchlorate ($DiIC_{12}$) fluorescently labeled lipid bilayer (red). (f) Schematic showing composition of lipid bilayer patterned in (d): 1,2-dipalmitoyl-sn-glycero-3-phosphocholine (DPPC), 1,2-dipalmitoyl-sn-glycero-3-phosphoethanolamine-N-[6-[(2,4-dinitrophenyl)amino]hexanoyl] (DNP-cap-DPPE) and $DiIC_{12}$ with molar ratio 94.5:5:0.5. DNP (blue) is the antigen for stimulating the mast cells, while $DiIC_{12}$ (red) fluorescently labels the lipid bilayer. Adapted with permission from reference [75]. Copyright 2003 American Chemical Society.

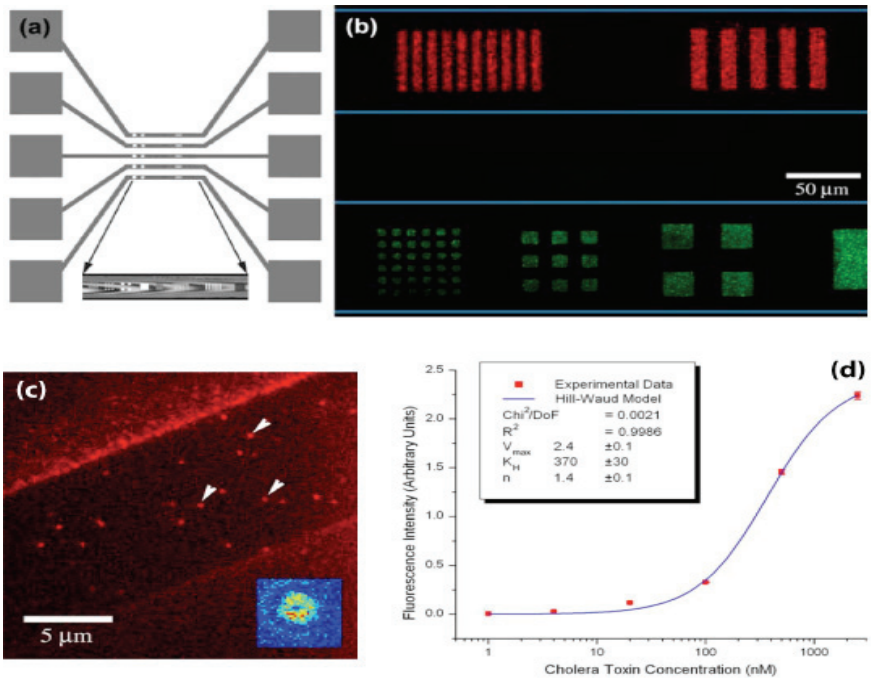

Figure 1.6 Supported lipid bilayer arrays within microfluidic channels. (a) Top view scheme of designed microfluidic trenches and reservoirs and patterned features at the bottom of these trenches (colored marks in central portion). (Inset) Bright field image of top view of patterned trench. (b) Alexa 594-cholera toxin subunit B (CTB) and Alexa 488-tetanus toxin fragment C conjugated toxin fragments segregated from a binary mixture and bound to the lipid bilayer arrays in the microfluidic channels (the channel boundary is represented by the thin horizontal lines). (c) Isolated binding events for cholera toxin observed via total internal reflection fluorescence microscopy. Binding events (arrows) observed in patterned lipid bilayer (strip in center, 10 µm wide) without removal of parylene coating (brighter flanking regions). (Inset) False color intensity plot of a single bound event. (d) Binding assays for CTB. Fluorescence intensity versus concentration plot for successive dilutions images of CTB incubated with patterned lipid bilayer containing gangliosides. (Inset) Hill-Waud model fit parameters. Reprinted from reference [78]. Copyright 2005, with permission from Cell Press, Elsevier.

1.3.3 Co-Culture Cell Arrays

Micropatterning is an attractive method to spatially control the cellular microenvironment and guide cell behavior, which is useful for tissue engineering and cell studies. The biocompatibility of parylene supports cell growth and cultures. The parylene peel-off approach has been demonstrated for directing neuronal cell growth [80] and co-cultures of different cell types [70]. Co-cultures of two or more cell types have been achieved with parylene stencils [70] as outlined in Figure 1.7. In the static mode, the first cell type is seeded onto the openings of the parylene stencil and afterwards the stencil is peeled off and the second cell type seeded onto the surrounding regions. In the dynamic mode, the parylene stencil is coated with collagen after the first cell seeding, and the second cell type is seeded onto the parylene stencil. Afterwards, the stencil can be peeled off to reveal the underlying region for seeding the third cell type. Cell co-cultures can be used for mimicking the cellular microenvironment (*e.g.* liver) for drug testing, and culturing cells that respond to physical or chemical cues from its neighboring cells.

1.3.4 Multi-Layer Parylene Stencils

Surfactants (*e.g.* Tween-20) and protein (bovine serum albumin [BSA]) solutions can be applied as an intermediate separating layer to enable the creation of multilayer parylene films stack. Multilayer parylene stencils have extended the utility of the parylene peel-off micropatterning approach. For example, the total number of different cell types that could be sequentially patterned as co-cultures was increased from three to five using a three-layers parylene stencils compared to just a single layer stencil [72].

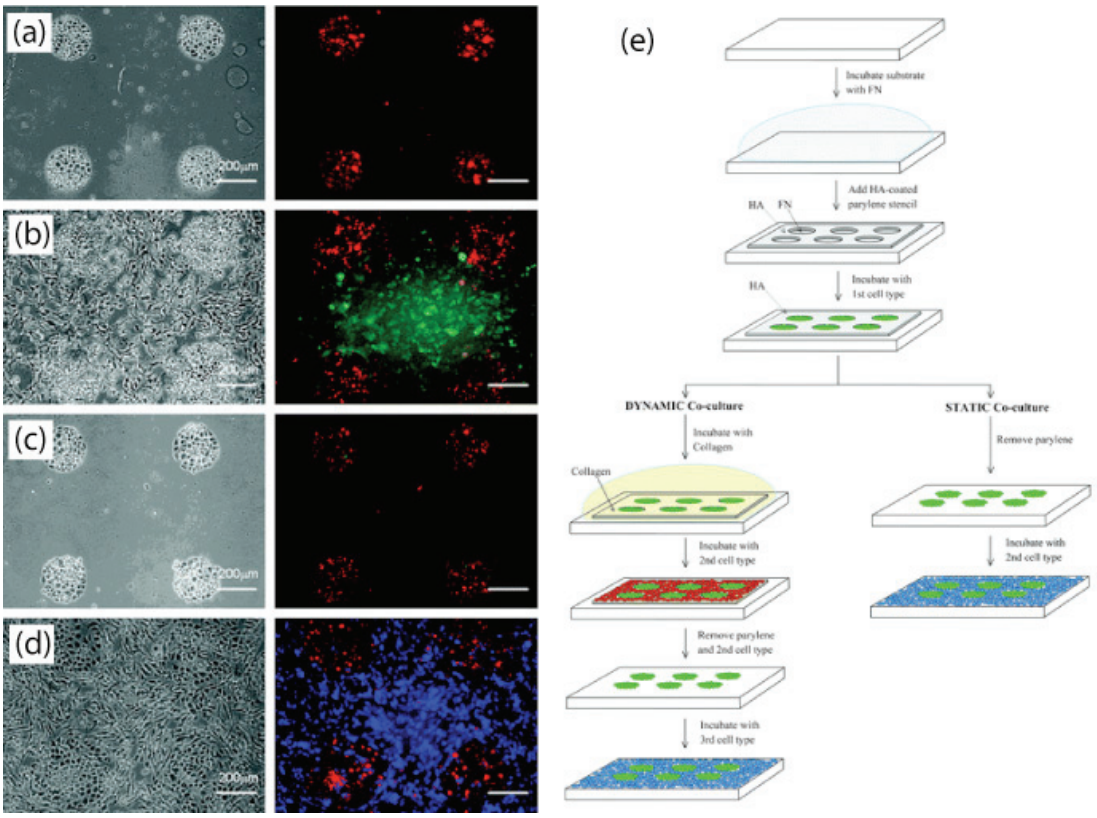

Figure 1.7. Light micrograph (left) and the corresponding fluorescent (right) images of the steps in the formation of dynamic co-cultures using parylene stencils. (a) A hyaluronic acid coated parylene stencil was reversibly sealed on fibronectin treated PDMS and seeded with mouse embryonic stem cells. (b) The patterned co-cultures of mouse embryonic stem cells and hepatocytes. (c) To generate dynamic co-cultures, the stencil was gently peeled away, leaving the embryonic stem cells. (d) After depositing a layer of fibronectin, a third cell type was seeded on the exposed surface. (e) Schematic diagram of the process used to generate static and dynamic co-cultures. Reproduced and adapted from reference [70] by permission of The Royal Society of Chemistry.

The schematic in Figure 1.8 illustrates the patterning of two different biomolecules within close proximity of each other using a two-layers parylene stencil [71]. This can be an alternative patterning approach to laminar flow patterning using microfluidics for patterning two streams of biomolecules separated by subcellular distances [9]. The ability to position two different species with sub-micrometer interval could increase the packing density of biomolecules on microarrays, and improve throughput for screening more candidates per unit area. Furthermore, this work by Kuribayashi also creatively patterned a parylene sheet with the BSA using a top layer of parylene stencil. The stencil was peeled off and the bottom parylene sheet could be rolled up to form a microtube with patterned BSA on its surface.

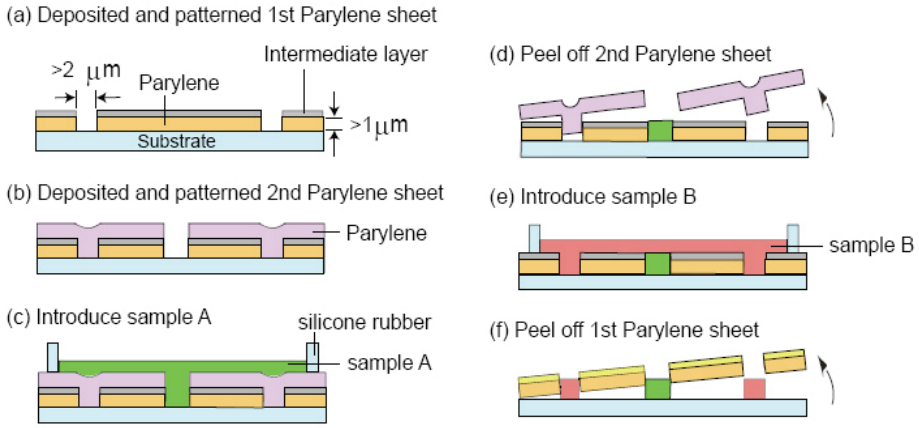

Figure 1.8 Process flow showing the selective patterning of two types of biomolecular samples using sequential multilayer parylene lift-off steps. Reprinted with permission from reference [71]. Copyright (2007) IEEE.

1.3.5 High-Resolution Optical Imaging and Biophysical Studies

Parylene peel-off micropatterning can be a versatile tool for immobilizing biomolecules with subcellular or sub-micrometer feature sizes onto surfaces for high resolution imaging in biophysical studies. Localized micropatterned features can spatially target or activate subcellular receptor-ligand interactions. When combined with high-resolution fluorescence microscopy techniques, biomolecules can be manipulated with nanoscale precision using these patterned surfaces, potentially elucidating the inner workings of cells and shedding new light on biophysical processes. The binding and activity of cellulases have been quantified by fluorescence microscopy of Alexa Fluor 647 labeled cellulases moving along Alexa Fluor 488 labeled cellulose fibrils [81]. These fibrils were immobilized onto glass coverslips using parylene peel-off stencils. Likewise, microtubules have also been patterned onto surfaces for biophysical studies involving the translocation of kinesin along these tubules [82]. Through the use of parylene peel-off micropatterned DNP-lipid arrays, it was discovered that focal adhesion proteins connect the IgE receptors on the surface of immune cells to the cytoskeleton [83]. The spatially defined clustering of receptor-ligands corresponding to the periodicity of the pre-defined micropatterns can provide a convenient and quantitative evaluation of local signaling pathways.

1.4 REACTIVE PARYLENE COATING FOR DIRECT SURFACE MODIFICATION

1.4.1 Functionalized Surface and Microfluidic Channels

Functionalized parylenes with substituted side-groups have been deposited onto surfaces to confer active chemical functionalities. An application of such reactive parylene coatings is for patterning proteins and mammalian cells onto surfaces independent of the substrate material [53], so long as the material can be coated with

parylene. Integrin proteins and cells have been patterned on surfaces coated with functionalized parylene films containing either active ester groups or anhydride groups, as shown in Figure 1.9. Aminated-biotin was microcontact printed using PDMS stamps onto the parylene surface and allowed to react with the ester or anhydride groups. Afterwards, streptavidin-biotin conjugation chemistries were employed to immobilize integrins and cells onto the biotin micropatterns on parylene. Similar strategies for micropatterning surfaces coated with parylene containing reactive functional groups such as alkynes were also reported [54].

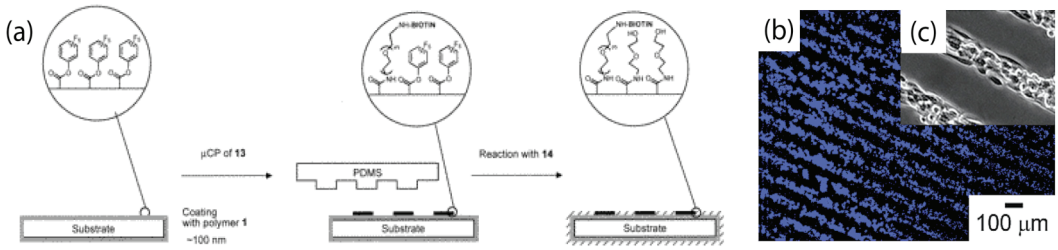

Figure 1.9 (a) Representation of the process that was used for mCP of the amino-functionalized biotin ligand 13 ((+)-biotinyl-3,6,9-trioxaundecanediamine) onto reactive parylene coatings with active ester group. A PDMS stamp, manufactured as a replica from a silicon master, was used for printing ligand 13 onto polymer 1 (parylene coating containing reactive ester group). The remaining surface area was then passivated by reaction with compound 14 (2-(aminoethoxy)ethanol). (b) Fluorescence micrograph of bovine aortic endothelial cells seeded for 24 h on a gold substrate (cell nuclei were stained with bis-benzimide). (c) Enlargement of optical micrograph of the cells seeded for 24 h on a gold substrate. In all cases, the substrate was previously coated with polymer 1 and patterned with ligand 13 to control self-assembly of anti-integrin antibody. The width of each individual line is 50 μm. Adapted with permission from reference [53]. Copyright 2002 American Chemical Society.

Reactive parylene coatings are also convenient for direct surface modification of biomedical implants. R-hirudin, a protein with anticoagulant properties have been covalently linked onto parylene coated surfaces of metallic implants, thereby increasing implant hemocompatibility [51, 58]. Polymeric surfaces such as poly(vinylidenefluoride) can be coated with parylene with amine functional groups to covalently link fibronectin to the surface for improving osteoblast cells adhesion [84]. These studies indicate that reactive parylene coatings are versatile biomaterials for tailoring and engineering surface properties of biomedical implants.

Phenylacetyl groups on parylene coatings can be photoactivated via UV light. Polyethylene oxide (PEO) molecules in close proximity to the surface can then be crosslinked via C-H addition reaction to form PEO hydrogels [56]. These PEO polymerized regions resist protein adsorption. Three-dimensional (3D) micropatterning of BSA and fibrinogen was achieved inside parylene-coated channels independent of topography [57], as shown in Figure 1.10. Parylene films with amine groups have been used to functionalize the internal surface of microfluidics with CD31 antibodies for cell capture and sorting [85]. The CD31 antibodies interact with the antigens expressed on human umbilical-vein endothelial cells and decrease the cells' mobility. This cell sorter device was shown to successfully separate fractions of endothelial from leukocytes that did not express the CD31 antigen, by exploiting differences in cell mobility inside the channels. Microfluidic devices capturing bovine aortic endothelial cells have also been demonstrated using anti-integrin antibodies functionalized inside the microfluidic channel via parylene reactive coatings [59].

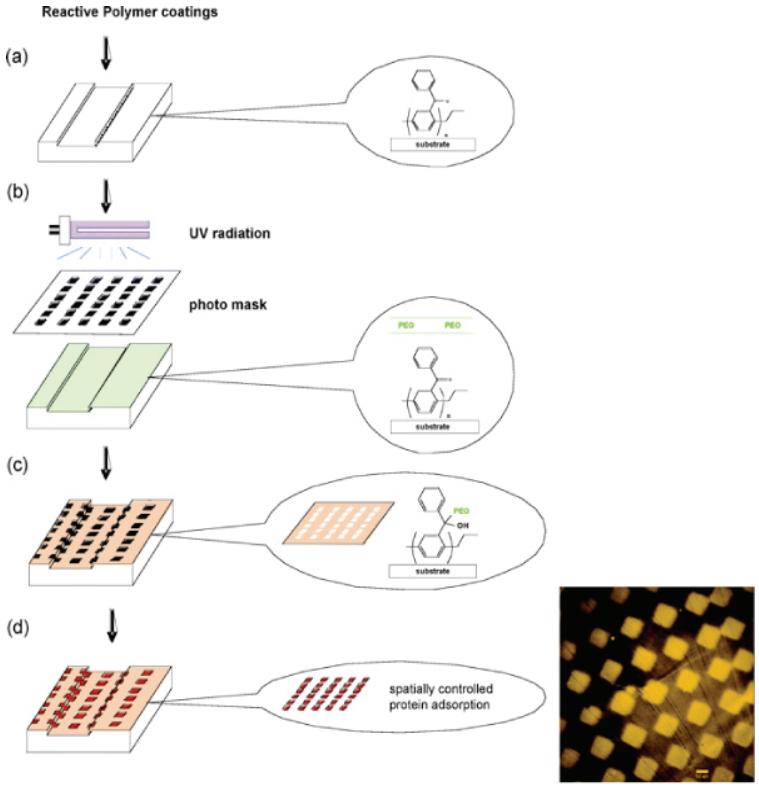

Figure 1.10 Spatially controlled protein adsorption via photopatterning of reactive coatings deposited within microchannels. (a) Reactive coatings are deposited via CVD polymerization. (b) Photopatterning is conducted using a photomask. (c) After rinsing, PEO is selectively immobilized to areas that were exposed to UV radiation (areas surrounding squares). (d) The entire surface is incubated with protein solutions, but proteins preferentially adsorb to non-modified areas. Inset: Surfaces with square patterns of BSA adsorbed onto CVD/PEO-modified silicon substrate. Adapted with permission from reference [57]. Copyright 2005 American Chemical Society.

1.4.2 Vapor-Assisted Microstructures Using Replicas and Templates

By exploiting the conformal nature of parylene coatings, pre-defined channels and microgeometries in materials such as PDMS, have been used as replica and mask templates to assist the vapor deposition of parylene [86, 87].

Figure 1.11(a) is a schematic illustrating the vapor-assisted deposition of parylene by using confined geometries in PDMS. Figure 1.11(b) shows the various microfluidic geometries and channel widths that can be created. The fluorescence indicates successful functionalization of biotin and streptavidin on the internal fluidic surfaces.

Openings with feature sizes as small as 25μm wide separated by a 25μm pitch have been patterned in parylene films using a replica [86]. X-ray photoelectron spectroscopy (XPS) confirmed the presence of parylene in the centre of the microstructure, indicating the monomer vapor was able to reach deep within the replica structure during the CVD process [86].

These methods are simple and adaptable, solventless and lithography-free alternatives towards topologically and chemically designable microstructures from parylene. The advantage is that microfluidics fabricated this way can contain reactive functional groups inside the channels, which are suitable for surface modification with biomolecules later.

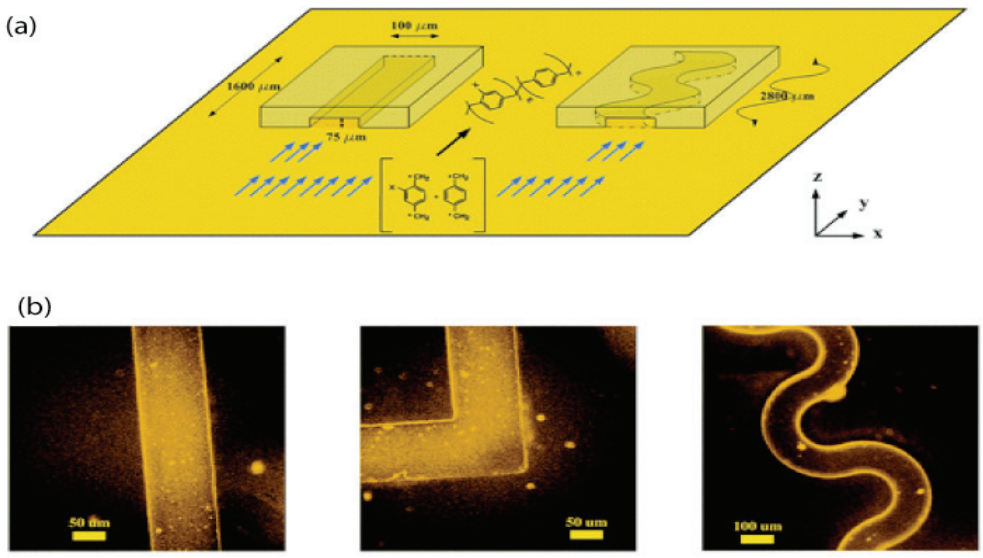

Figure 1.11 (a) CVD polymerization within confined geometries of straight and meandering channels. (b) Fluorescence micrographs of sealed devices coated with parylene containing functional ketone groups, after immobilization of hydrazide−biotin and self-assembly of fluorescent tetramethyl rhodamine isothiocyanate-conjugated streptavidin. Examples are shown in different channel geometries of 75 μm depth and 100 μm width. Adapted with permission from reference [87]. Copyright 2006 American Chemical Society.

1.5 PARYLENE MICROSTRUCTURES

1.5.1 Substrate-Selective Vapor Deposition

Substrate-selective deposition of parylene can be exploited for creating patterned parylene films without the use of lithography. Transition metals, such as iron, and their salts have been reported to inhibit parylene deposition by binding and deactivating the reactive monomer during CVD [41, 88]. As shown in Figure 1.12, gold and silver surfaces that inhibit parylene deposition were microcontact printed with thiols to activate the surfaces for parylene deposition [40]. However, this surface activation can be reversed be passivating the surface with a layer of iron salts, thereby inhibiting parylene deposition again [40]. A systematic study of metals revealed interesting observations that certain metals such as titanium, copper, and nickel can selectively inhibit deposition some types of functionalized parylenes [88]. These studies could have future implications on surface modification and deposition of parylene onto metallic biomedical implants and prostheses.

1.5.2 Parylene Tubes and Microfluidics

Self-sealing parylene tubes can be created by depositing parylene onto high aspect ratio trenches that are etched into a silicon wafer [47, 48]. At a critical thickness of parylene, the top of the trench pinches off to form a sealed parylene tube in Figure 1.13(a). Centimeter-long tubes with inner cross-sectional widths of 400nm to 20μm have been created by this process, and tubes can be peeled off the silicon wafer shown in Figure 1.13(b). The ends of the tubes can be connected to reservoirs using photocurable adhesive as seen in Figure 1.13(c) to create microfluidic channel. In Figure 1.13(d), fluorescent rhodamine B dye was electrokinetically driven through the parylene tube channels without leakage by applying a voltage across the reservoirs. In addition to the obvious applications for microfluidics and biosensors, the

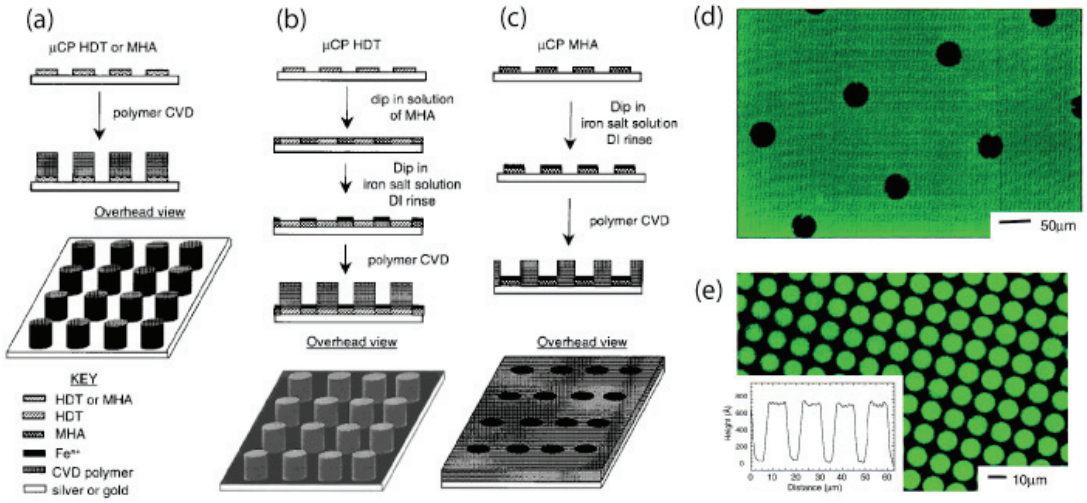

Figure 1.12 Use of mCP to control the growth of CVD parylenes and poly(p-phenylene vinylene) (PPV, a type of parylene) through (a) activation of the surface to polymer growth by mCP of hexadecanethiol (HDT) or 16-mercaptohexadecanoic acid (MHA), (b) deactivation of the printed regions of the surface to polymer growth by mCP of MHA followed by exposure to an iron salt solution and rinse step, and (c) deactivation of the unprinted regions of the surface to polymer growth by mCP HDT on the surface, depositing MHA on the unprinted regions, and exposing the entire surface to a solution of iron salt, followed by a rinse step. Photoluminescence from selectively grown CVD PPV films generated by combining mCP alkanethiols and a growth-inhibiting iron salt: (d) holes in the PPV film (35 μm in diameter) fabricated as shown in (b), using MHA in the printing step and iron(III) chloride as the growth-inhibiting salt; (e) an array of CVD PPV dots (12.5 μm in diameter separated by 2.5 μm) fabricated as shown in (c), using HDT in the printing step, MHA in the unprinted regions, and iron(II) sulfate as the growth-inhibiting salt. Adapted with permission from reference [40]. Copyright 2000 American Chemical Society.

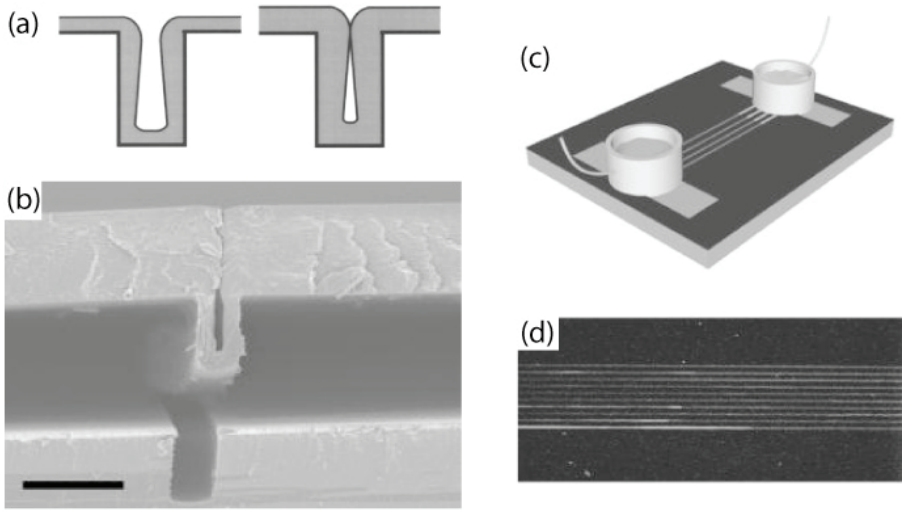

Figure 1.13 (a) Nonconformal step coverage of the high aspect ratio deep trench caused by lack of surface adatom migration. (b) Cross-sectional SEM of a partially delaminated fluidic channel from a high aspect ratio silicon template. Scale bar: 5μm (c) Schematic of the electrokinetic transport of rhodamine B. (d) Fluorescent micrograph of rhodamine B flow near the outlet of a channel. Reprinted with permission from reference [47]. Copyright [2002], American Institute of Physics.

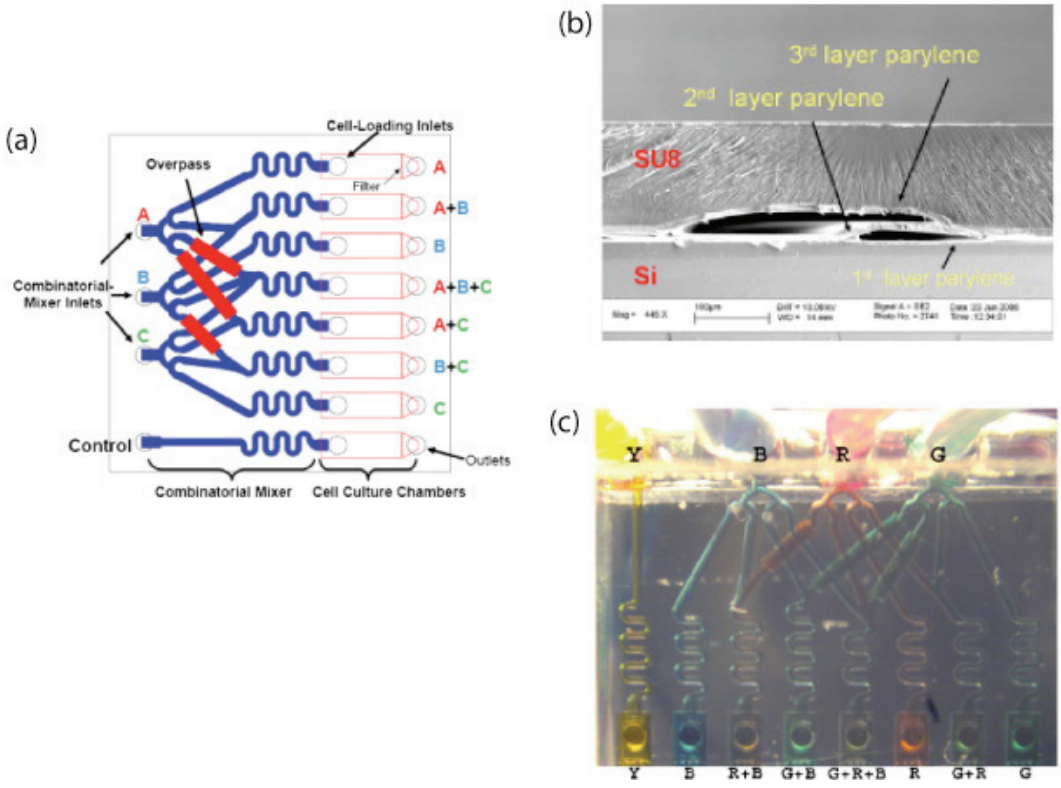

Figure 1.14 (a) Layout of the device design showing the components of the chip. The combinatorial mixer takes in three-input streams and delivers the seven different combinations into the cell culture-chambers. There are several microfluidic "overpass" structures that allow one microchannel to cross over other microchannels. One control channel that receives unmixed input stream is included. Cells can be grown inside the culture-chambers. The chip has a dimension of 1 cm × 1 cm. (b) SEM image of the cross-section of the microfluidic overpass. The overpass has two-level microfluidic channels and such structures will allow two fluidic streams to be separated spatially at the overpass. (c) Combinatorial mixer operated at 0.1μL/min flow rate. As flow rate goes down, molecules have more time to diffuse across the channel for better mixing. Reprinted from reference [89]. Copyright (2008), with permission from Elsevier.

biocompatibility and range of length-scale dimensions of these tubes suggests possible uses for biomedical implantable fluidic networks and artificial blood vessels.

Complicated architectures of 3D parylene microfluidic channels have been realized by monolithic fabrication with a photoresist sacrificial layer. Such devices, shown in Figure 1.14, are used for combinatorial mixing of flows and cell culture [89]. Parylene microfluidic channels have also been micromachined into neural probes with electrodes for recording neural signals and injecting chemicals [90].

1.5.3 Micromachined Structures and Membranes

Neurocages have also been micromachined entirely out of parylene for supporting neuronal cultures and integrating the neurons with electrodes for electrical stimulation and recording action potentials [91-93], show in Figure 1.15. The large central chimney region would isolate the neuronal body (soma), while permitting fine axonal extensions out of the tunnels to form networks with neighboring neurons in Figure 1.15(a). Arrays of neurocages interfaced with electrodes have been utilized for mapping functional neural networks in Figure 1.15(b).

Lipid bilayers can be formed across apertures (~40μm) in microfabricated parylene membranes [94, 95]. These parylene membranes are incorporated between two polymethylmethacrylate (PMMA) plates to form recording wells as shown in Figure 1.16(a)-(c). The lipid bilayers in the recording wells serve as biomimetic cell membranes whereby channel proteins such as α-hemolysin and gramicidin, can be inserted into the bilayer. Ion exchange through the channel proteins can measured as currents, demonstrated by the result in Figure 1.16(d). These biomimetic membranes can be used for investigating ligand and voltage gated ion channels and testing their responses to drugs.

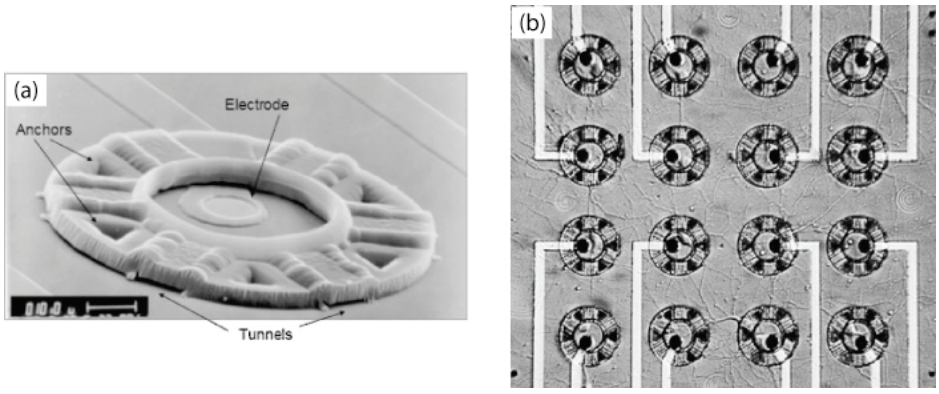

Figure 1.15 (a) SEM of the final neurocage design. The major parts of the neurocage are labeled. A neuron is placed in the central chimney region, near the electrode. Axons and dendrites are free to grow though the tunnels to synapse with other neurons. The cage is made out of 4 µm thick parylene, a biocompatible polymer. Low-stress silicon nitride insulates the gold electrode and leads. Scale bar: 10 µm. (b) 10 days old neuronal culture on chip. Neuron bodies (soma) are trapped in cages, with fine axonal processes outgrowth through the tunnels forming a rich network with surrounding neurons. Reprinted from reference [91]. Copyright (2008), with permission from Elsevier.

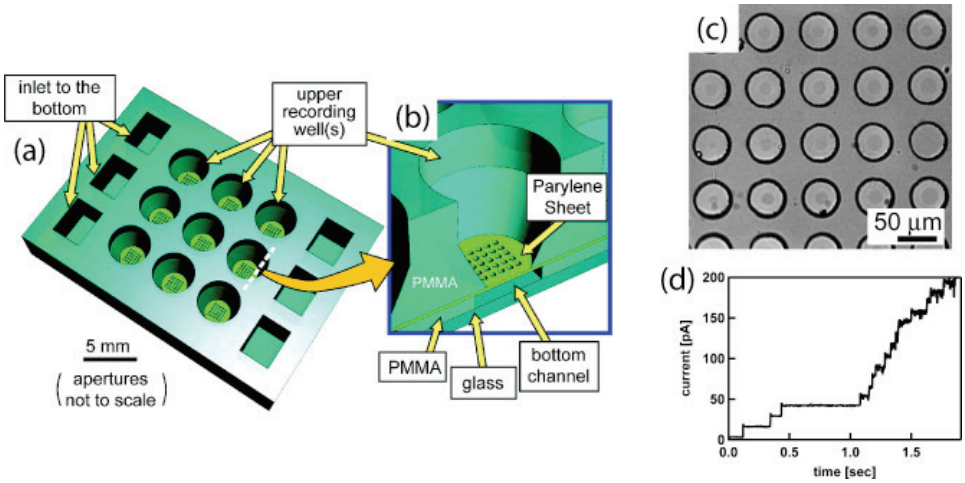

Figure 1.16 Schematic of the lipid bilayer array chip. Adapted with permission from reference [94]. Copyright 2008 American Chemical Society.

REFERENCES

1. Langer, R.; Tirrell, D. A., Designing materials for biology and medicine. *Nature* 2004, 428, 487-492.
2. Mitragotri, S.; Lahann, J., Physical approaches to biomaterial design. *Nature Materials* 2009, 8, 15-23.
3. Nandivada, H.; Chen, H.-Y.; Elkasabi, Y.; Lahann, J., Reactive polymer coatings for biological applications. In *Polymers for biomedical applications*, American Chemical Society: Washington, DC, 2008; pp 283-298.
4. Christman, K. L.; Schopf, E.; Broyer, R. M.; Li, R. C.; Chen, Y.; Maynard, H. D., Positioning multiple proteins at the nanoscale with electron beam cross-linked functional polymers. *Journal of the American Chemical Society* 2009, 131, 521-527.
5. Coyer, S. R.; Garcia, A. J.; Delamarche, E., Facile preparation of complex protein architectures with sub-100-nm resolution on surfaces. *Angewandte Chemie International Edition* 2007, 46, 6837-6840.
6. Lee, K. B.; Park, S. J.; Mirkin, C. A.; Smith, J. C.; Mrksich, M., Protein nanoarrays generated by dip-pen nanolithography. *Science* 2002, 295, 1702-1705.
7. Chen, C. S.; Mrksich, M.; Huang, S.; Whitesides, G. M.; Ingber, D. E., Geometric control of cell life and death. *Science* 1997, 276, 1425-1428.
8. Arnold, M.; Cavalcanti-Adam, E. A.; Glass, R.; Blummel, J.; Eck, W.; Kantlehner, M.; Kessler, H.; Spatz, J. P., Activation of integrin function by nanopatterned adhesive interfaces. *Chemphyschem* 2004, 5, 383-388.
9. Takayama, S.; Ostuni, E.; LeDuc, P.; Naruse, K.; Ingber, D. E.; Whitesides, G. M., Laminar flows - subcellular positioning of small molecules. *Nature* 2001, 411, 1016-1016.

10. Tan, C. P.; Cipriany, B. R.; Lin, D. M.; Craighead, H. G., Nanoscale resolution, multicomponent biomolecular arrays generated by aligned printing with parylene peel-off. *Nano Letters* 2010, 10, 719-725.
11. Whitesides, G. M., The origins and the future of microfluidics. *Nature* 2006, 442, 368-373.
12. Craighead, H., Future lab-on-a-chip technologies for interrogating individual molecules. *Nature* 2006, 442, 387-393.
13. Yager, P.; Edwards, T.; Fu, E.; Helton, K.; Nelson, K.; Tam, M. R.; Weigl, B. H., Microfluidic diagnostic technologies for global public health. *Nature* 2006, 442, 412-418.
14. Khademhosseini, A., *Micro and nanoengineering of the cell microenvironment*. Artech House: Boston, MA, 2008.
15. Khademhosseini, A.; Langer, R.; Borenstein, J.; Vacanti, J. P., Microscale technologies for tissue engineering and biology. *Proceedings of the National Academy of Sciences of the United States of America* 2006, 103, 2480-2487.
16. Zheng, G. F.; Patolsky, F.; Cui, Y.; Wang, W. U.; Lieber, C. M., Multiplexed electrical detection of cancer markers with nanowire sensor arrays. *Nature Biotechnology* 2005, 23, 1294-1301.
17. Waggoner, P. S.; Craighead, H. G., Micro- and nanomechanical sensors for environmental, chemical, and biological detection. *Lab on a Chip* 2007, 7, 1238-1255.
18. St John, P. M.; Davis, R.; Cady, N.; Czajka, J.; Batt, C. A.; Craighead, H. G., Diffraction-based cell detection using a microcontact printed antibody grating. *Analytical Chemistry* 1998, 70, 1108-1111.
19. Lashkari, D. A.; DeRisi, J. L.; McCusker, J. H.; Namath, A. F.; Gentile, C.; Hwang, S. Y.; Brown, P. O.; Davis, R. W., Yeast microarrays for genome wide

parallel genetic and gene expression analysis. *Proceedings of the National Academy of Sciences of the United States of America* 1997, 94, 13057-13062.

20. Schena, M.; Shalon, D.; Davis, R. W.; Brown, P. O., Quantitative monitoring of gene-expression patterns with a complementary-DNA microarray. *Science* 1995, 270, 467-470.
21. MacBeath, G.; Schreiber, S. L., Printing proteins as microarrays for high-throughput function determination. *Science* 2000, 289, 1760-1763.
22. Ziauddin, J.; Sabatini, D. M., Microarrays of cells expressing defined cdnas. *Nature* 2001, 411, 107-110.
23. Dusseiller, M. R.; Niederberger, B.; Stadler, B.; Falconnet, D.; Textor, M.; Voros, J., A novel crossed microfluidic device for the precise positioning of proteins and vesicles. *Lab on a Chip* 2005, 5, 1387-1392.
24. Fan, R.; Vermesh, O.; Srivastava, A.; Yen, B. K. H.; Qin, L. D.; Ahmad, H.; Kwong, G. A.; Liu, C. C.; Gould, J.; Hood, L.; Heath, J. R., Integrated barcode chips for rapid, multiplexed analysis of proteins in microliter quantities of blood. *Nature Biotechnology* 2008, 26, 1373-1378.
25. Huang, B.; Jones, S. A.; Brandenburg, B.; Zhuang, X. W., Whole-cell 3d storm reveals interactions between cellular structures with nanometer-scale resolution. *Nature Methods* 2008, 5, 1047-1052.
26. Jaehrling, S.; Thelen, K.; Wolfram, T.; Pollerberg, G. E., Nanopatterns biofunctionalized with cell adhesion molecule dm-grasp offered as cell substrate: Spacing determines attachment and differentiation of neurons. *Nano Letters* 2009.
27. Dandy, D. S.; Wu, P.; Grainger, D. W., Array feature size influences nucleic acid surface capture in DNA microarrays. *Proceedings of the National Academy of Sciences of the United States of America* 2007, 104, 8223-8228.

28. Squires, T. M.; Messinger, R. J.; Manalis, S. R., Making it stick: Convection, reaction and diffusion in surface-based biosensors. *Nature Biotechnology* 2008, 26, 417-426.

29. Howarter, J. A.; Youngblood, J. P., Optimization of silica silanization by 3-aminopropyltriethoxysilane. *Langmuir* 2006, 22, 11142-11147.

30. Lahann, J., Vapor-based polymer coatings for potential biomedical applications. *Polymer International* 2006, 55, 1361-1370.

31. Lahann, J., Reactive polymer coatings for biomimetic surface engineering. *Chemical Engineering Communications* 2006, 193, 1457-1468.

32. Roth, E. A.; Xu, T.; Das, M.; Gregory, C.; Hickman, J. J.; Boland, T., Inkjet printing for high-throughput cell patterning. *Biomaterials* 2004, 25, 3707-3715.

33. Tien, J.; Nelson, C. M.; Chen, C. S., Fabrication of aligned microstructures with a single elastomeric stamp. *Proceedings of the National Academy of Sciences of the United States of America* 2002, 99, 1758-1762.

34. Wang, Y. H.; Giam, L. R.; Park, M.; Lenhert, S.; Fuchs, H.; Mirkin, C. A., A self-correcting inking strategy for cantilever arrays addressed by an inkjet printer and used for dip-pen nanolithography. *Small* 2008, 4, 1666-1670.

35. Huo, F. W.; Zheng, Z. J.; Zheng, G. F.; Giam, L. R.; Zhang, H.; Mirkin, C. A., Polymer pen lithography. *Science* 2008, 321, 1658-1660.

36. Doh, J.; Irvine, D. J., Photogenerated polyelectrolyte bilayers from an aqueous-processible photoresist for multicomponent protein patterning. *Journal of the American Chemical Society* 2004, 126, 9170-9171.

37. Szwarc, M., New monomers of the quinoid type and their polymers. *Journal of Polymer Science* 1951, 6, 319-329.

38. Gorham, W. F., A new general synthetic method for preparation of linear poly-p-xylylenes. *Journal of Polymer Science Part A: Polymer Chemistry* 1966, 4, 3027-3039.

39. Fortin, J. B.; Lu, T. M., Deposition kinetics for polymerization via the gorham route. In *Chemical vapor deposition polymerization - the growth and properties of parylene thin films*, Kluwer Academic Publishers: Norwell, MA, 2004; pp 41-55.

40. Vaeth, K. M.; Jackman, R. J.; Black, A. J.; Whitesides, G. M.; Jensen, K. F., Use of microcontact printing for generating selectively grown films of poly(p-phenylene vinylene) and parylenes prepared by chemical vapor deposition. *Langmuir* 2000, 16, 8495-8500.

41. Vaeth, K. M.; Jensen, K. F., Transition metals for selective chemical vapor deposition of parylene-based polymers. *Chemistry of Materials* 2000, 12, 1305-1313.

42. Vaeth, K. M.; Jensen, K. F., Selective growth of poly(p-phenylene vinylene) prepared bg chemical vapor deposition. *Advanced Materials* 1999, 11, 814-820.

43. Xu, Y.; Tai, Y. C. *Selective deposition of parylene c for underwater shear-stress sensors*, In Proceedings of TRANSDUCERS 2003, The 12th International Conference on Solid-State Sensors, Actuators and Microsystems, 8-12 June, 2003; pp 1307-1310.

44. Charlson, E. M.; Charlson, E. J.; Sabeti, R., Temperature selective deposition of parylene-c. *Ieee Transactions on Biomedical Engineering* 1992, 39, 202-206.

45. Gazicki, M.; Surendran, G.; James, W.; Yasuda, H., Polymerization of para-xylylene derivatives (parylene polymerization) .3. Heat-effects during

deposition of parylene-n at different temperatures. *Journal of Polymer Science Part A: Polymer Chemistry* 1986, 24, 215-240.

46. Gazicki, M.; Surendran, G.; James, W.; Yasuda, H., Polymerization of para-xylylene derivatives (parylene polymerization) .2. Heat-effects during deposition of parylene-c at different temperatures. *Journal of Polymer Science Part A: Polymer Chemistry* 1985, 23, 2255-2277.

47. Ilic, B.; Czaplewski, D.; Zalalutdinov, M.; Schmidt, B.; Craighead, H. G., Fabrication of flexible polymer tubes for micro and nanofluidic applications. *Journal of Vacuum Science and Technology B* 2002, 20, 2459-2465.

48. Chen, P. J.; Shih, C. Y.; Tai, Y. C., Design, fabrication and characterization of monolithic embedded parylene microchannels in silicon substrate. *Lab on a Chip* 2006, 6, 803-810.

49. Lahann, J.; Langer, R., Novel poly(p-xylylenes): Thin films with tailored chemical and optical properties. *Macromolecules* 2002, 35, 4380-4386.

50. Wahjudi, P. N.; Oh, J. H.; Salman, S. O.; Seabold, J. A.; Rodger, D. C.; Tai, Y. C.; Thompson, M. E., Improvement of metal and tissue adhesion on surface-modified parylene c. *Journal of Biomedical Materials Research: Part A* 2009, 89A, 206-214.

51. Lahann, J.; Hocker, H.; Langer, R., Synthesis of amino[2.2]paracyclophanes - beneficial monomers for bioactive coating of medical implant materials. *Angewandte Chemie International Edition* 2001, 40, 726-728.

52. Nandivada, H.; Chen, H. Y.; Lahann, J., Vapor-based synthesis of poly [(4-formyl-p-xylylene)-co-(p-xylylene)] and its use for biomimetic surface modifications. *Macromolecular Rapid Communications* 2005, 26, 1794-1799.

53. Lahann, J.; Balcells, M.; Rodon, T.; Lee, J.; Choi, I. S.; Jensen, K. F.; Langer, R., Reactive polymer coatings: A platform for patterning proteins and

mammalian cells onto a broad range of materials. *Langmuir* 2002, 18, 3632-3638.

54. Nandivada, H.; Chen, H. Y.; Bondarenko, L.; Lahann, J., Reactive polymer coatings that "Click". *Angewandte Chemie International Edition* 2006, 45, 3360-3363.

55. Lahann, J.; Langer, R., Surface-initiated ring-opening polymerization of epsilon-caprolactone from a patterned poly(hydroxymethyl-p-xylylene). *Macromolecular Rapid Communications* 2001, 22, 968-971.

56. Suh, K. Y.; Langer, R.; Lahann, J., A novel photodefinable reactive polymer coating and its use for microfabrication of hydrogel elements. *Advanced Materials* 2004, 16, 1401-1405.

57. Chen, H. Y.; Lahann, J., Fabrication of discontinuous surface patterns within microfluidic channels using photodefinable vapor-based polymer coatings. *Analytical Chemistry* 2005, 77, 6909-6914.

58. Lahann, J.; Klee, D.; Pluester, W.; Hoecker, H., Bioactive immobilization of r-hirudin on cvd-coated metallic implant devices. *Biomaterials* 2001, 22, 817-826.

59. Lahann, J.; Balcells, M.; Lu, H.; Rodon, T.; Jensen, K. F.; Langer, R., Reactive polymer coatings: A first step toward surface engineering of microfluidic devices. *Analytical Chemistry* 2003, 75, 2117-2122.

60. Moses, J. E.; Moorhouse, A. D., The growing applications of click chemistry. *Chemical Society Reviews* 2007, 36, 1249-1262.

61. Elkasabi, Y.; Chen, H. Y.; Lahann, J., Multipotent polymer coatings based on chemical vapor deposition copolymerization. *Advanced Materials* 2006, 18, 1521-1526.

62. Fortin, J. B.; Lu, T. M., Introduction: Types of parylene and its applications. In *Chemical vapor deposition polymerization - the growth and properties of parylene thin films*, Kluwer Academic Publishers: Norwell, MA, 2004; p 7.

63. Fortin, J. B.; Lu, T. M., In *Chemical vapor deposition polymerization - the growth and properties of parylene thin films*, Kluwer Academic Publishers: Norwell, MA, 2004; p 62.

64. Ilic, B.; Craighead, H. G., Topographical patterning of chemically sensitive biological materials using a polymer-based dry lift off. *Biomedical Microdevices* 2000, 2, 317-322.

65. Hwang, K. S.; Park, J. H.; Lee, J. H.; Yoon, D. S.; Kim, T. S.; Han, I.; Noh, J. H., Effect of atmospheric-plasma treatments for enhancing adhesion of au on parylene-c-coated protein chips. *Journal of the Korean Chemical Society* 2004, 44, 1168-1172.

66. Chang, T. Y.; Yadav, V. G.; De Leo, S.; Mohedas, A.; Rajalingam, B.; Chen, C. L.; Selvarasah, S.; Dokmeci, M. R.; Khademhosseini, A., Cell and protein compatibility of parylene-c surfaces. *Langmuir* 2007, 23, 11718-11725.

67. Fortin, J. B.; Lu, T. M., Film properties. In *Chemical vapor deposition polymerization - the growth and properties of parylene thin films*, Kluwer Academic Publishers: Norwell, MA, 2004; p 58.

68. Tan, C. P.; Moran-Mirabal, J. M.; Brooks, D. J.; Ilic, B. R.; Fischbach, C.; Craighead, H. G. *Surface modification and patterning of biomolecules and cells using a polymer lift-off template*, In Proceedings of MicroTAS 2008, The Twelfth International Conference on Miniaturized Systems for Chemistry and Life Sciences, San Diego, CA, United States, 12-16 Oct, 2008; pp 1552-1554.

69. Lange, K.; Grimm, S.; Rapp, M., Chemical modification of parylene c coatings for saw biosensors. *Sensors and Actuators A: Physical* 2007, 125, 441-446.

70. Wright, D.; Rajalingam, B.; Selvarasah, S.; Dokmeci, M. R.; Khademhosseini, A., Generation of static and dynamic patterned co-cultures using microfabricated parylene-c stencils. *Lab on a Chip* 2007, 7, 1272-1279.

71. Kuribayashi, K.; Hiratsuka, Y.; Yamamura, T.; Takeuchi, S. *Sequential parylene lift-off process for selective patterning of biological materials*, In Proceedings of IEEE MEMS 2007, The 20th International Conference on Micro Electro Mechanical Systems, Kobe, Japan, 21-25 Jan, 2007; pp 501-504.

72. Jinno, S.; Moeller, H. C.; Chen, C. L.; Rajalingam, B.; Chung, B. G.; Dokmeci, M. R.; Khademhosseini, A., Microfabricated multilayer parylene-c stencils for the generation of patterned dynamic co-cultures. *Journal of Biomedical Materials Research: Part A* 2008, 86A, 278-288.

73. Wright, D.; Rajalingam, B.; Karp, J. M.; Selvarasah, S.; Ling, Y. B.; Yeh, J.; Langer, R.; Dokmeci, M. R.; Khademhosseini, A., Reusable, reversibly sealable parylene membranes for cell and protein patterning. *Journal of Biomedical Materials Research: Part A* 2008, 85A, 530-538.

74. Orth, R. N.; Kameoka, J.; Zipfel, W. R.; Ilic, B.; Webb, W. W.; Clark, T. G.; Craighead, H. G., Creating biological membranes on the micron scale: Forming patterned lipid bilayers using a polymer lift-off technique. *Biophysical Journal* 2003, 85, 3066-3073.

75. Orth, R. N.; Wu, M.; Holowka, D. A.; Craighead, H. G.; Baird, B. A., Mast cell activation on patterned lipid bilayers of subcellular dimensions. *Langmuir* 2003, 19, 1599-1605.

76. Morigaki, K.; Baumgart, T.; Jonas, U.; Offenhausser, A.; Knoll, W., Photopolymerization of diacetylene lipid bilayers and its application to the construction of micropatterned biomimetic membranes. *Langmuir* 2002, 18, 4082-4089.

77. Groves, J. T.; Boxer, S. G., Micropattern formation in supported lipid membranes. *Accounts of Chemical Research* 2002, 35, 149-157.

78. Moran-Mirabal, J. M.; Edel, J. B.; Meyer, G. D.; Throckmorton, D.; Singh, A. K.; Craighead, H. G., Micrometer-sized supported lipid bilayer arrays for bacterial toxin binding studies through total internal reflection fluorescence microscopy. *Biophysical Journal* 2005, 89, 296-305.

79. Atsuta, K.; Suzuki, H.; Takeuchi, S., A parylene lift-off process with microfluidic channels for selective protein patterning. *Journal of Micromechanics and Microengineering* 2007, 17, 496-500.

80. Delivopoulos, E.; Murray, A. F.; MacLeod, N. K.; Curtis, J. C., Guided growth of neurons and glia using microfabricated patterns of parylene-c on a sio2 background. *Biomaterials* 2009, 30, 2048-2058.

81. Moran-Mirabal, J. M.; Santhanam, N.; Corgie, S. C.; Craighead, H. G.; Walker, L. P., Immobilization of cellulose fibrils on solid substrates for cellulase-binding studies through quantitative fluorescence microscopy. *Biotechnology and Bioengineering* 2008, 101, 1129-1141.

82. Yoshida, Y.; Yokokawa, R.; Suzuki, H.; Atsuta, K.; Fujita, H.; Takeuchi, S., Biomolecular linear motors confined to move upon micro-patterns on glass. *Journal of Micromechanics and Microengineering* 2006, 16, 1550-1554.

83. Torres, A. J.; Vasudevan, L.; Holowka, D.; Baird, B. A., Focal adhesion proteins connect ige receptors to the cytoskeleton as revealed by micropatterned ligand arrays. *Proceedings of the National Academy of Sciences of the United States of America* 2008, 105, 17238-17244.

84. Klee, D.; Ademovic, Z.; Bosserhoff, A.; Hoecker, H.; Maziolis, G.; Erli, H. J., Surface modification of poly(vinylidenefluoride) to improve the osteoblast adhesion. *Biomaterials* 2003, 24, 3663-3670.

85. Miwa, J.; Suzuki, Y.; Kasagi, N., Adhesion-based cell sorter with antibody-coated amino-functionalized-parylene surface. *Journal of Microelectromechanical Systems* 2008, 17, 611-622.

86. Chen, H. Y.; Lahann, J., Vapor-assisted micropatterning in replica structures: A solventless approach towards topologically and chemically designable surfaces. *Advanced Materials* 2007, 19, 3801-3808.

87. Chen, H. Y.; Elkasabi, Y.; Lahann, J., Surface modification of confined microgeometries via vapor-deposited polymer coatings. *Journal of the American Chemical Society* 2006, 128, 374-380.

88. Chen, H. Y.; Lai, J. H.; Jiang, X. W.; Lahann, J., Substrate-selective chemical vapor deposition of reactive polymer coatings. *Advanced Materials* 2008, 20, 3474-3480.

89. Liu, M. C.; Ho, D.; Tai, Y. C., Monolithic fabrication of three-dimensional microfluidic networks for constructing cell culture array with an integrated combinatorial mixer. *Sensors and Actuators B: Chemical* 2008, 129, 826-833.

90. Takeuchi, S.; Ziegler, D.; Yoshida, Y.; Mabuchi, K.; Suzuki, T., Parylene flexible neural probes integrated with microfluidic channels. *Lab on a Chip* 2005, 5, 519-523.

91. Erickson, J.; Tooker, A.; Tai, Y. C.; Pine, J., Caged neuron mea: A system for long-term investigation of cultured neural network connectivity. *Journal of Neuroscience Methods* 2008, 175, 1-16.

92. Meng, E.; Tai, Y. C.; Erickson, J.; Pine, J. *Parylene technology for mechanically robust neurocages*, In Proceedings of MicroTAS 2003, The Seventh International Conference on Micro Total Analysis Systems, Squaw Valley, CA, United States, 5-9 Oct, 2003; pp 1109-1112.

93. Tooker, A.; Meng, E.; Erickson, J.; Tai, Y. C.; Pine, J., Biocompatible parylene neurocages. *IEEE Engineering in Medicine and Biology Magazine* 2005, 24, 30-33.

94. Le Pioufle, B.; Suzuki, H.; Tabata, K. V.; Noji, H.; Takeuchi, S., Lipid bilayer microarray for parallel recording of transmembrane ion currents. *Analytical Chemistry* 2008, 80, 328-332.

95. Suzuki, H.; Le Pioufle, B.; Takeuchi, S., Ninety-six-well planar lipid bilayer chip for ion channel recording fabricated by hybrid stereolithography. *Biomedical Microdevices* 2009, 11, 17-22.

CHAPTER 2

NANOSCALE RESOLUTION, MULTI-COMPONENT BIOMOLECULAR ARRAYS GENERATED BY ALIGNED PRINTING WITH PARYLENE PEEL-OFF[2]

2.1 INTRODUCTION

Patterned biomolecular arrays with nanoscale features are useful for applications such as tissue engineering, cell cultures, and studying subcellular receptor-ligand interactions and intracellular processes [1-6]. For example, cell behavior such as differentiation, adhesion and proliferation, can be regulated by patterned arrays of extracellular matrix (ECM) proteins with different feature shapes, sizes and spacing [7, 8]. Reducing the feature size of patterned ECM proteins to sub-100nm dimensions can help to elucidate the role of ECM proteins in forming focal adhesions with single-molecule resolution [9]. Furthermore, there is a growing interest to integrate biological and chemical functionalities with miniaturized sensor devices whereby accurate spatial positioning and alignment are crucial, such as nanowire sensors, chemical field-effect transistors, nanoelectromechanical sensors, and diffraction based antibody gratings [10-13]. The diversity of protein molecules and their combinations present in nature requires the highly multiplexed capability of arrays to study the plethora of possible antagonistic and synergistic interactions between receptors and ligands [14, 15]. Hence, it is typical for 10s-1,000s features of different biomaterials and their replicates to be patterned on a large area array and afterwards, allow for cells to interact with the patterned surface [15-19].

---

[2] This chapter is a modified and revised form of the publication: Tan, C.P., Cipriany, B.R., Lin, D.M., Craighead, H.G., Nanoscale Resolution, Multi-component Biomolecular Arrays Generated by Aligned Printing with Parylene Peel-Off, *Nano Letters* 2010, 10, 719-725.

Recent advances in printing and lithography have enabled the generation of patterned arrays with the smallest feature resolution down to 10s of nm. Some common array patterning techniques include AFM based methods such as DPN and its variants [3, 20-22], μCP [23, 24], and inkjet printing [25]. An ideal method for generating biomolecular nanoarrays should have these desired characteristics: i) the ability to offer nanoscale patterning resolution down to 10s of nm, ii) can be easily scalable to enable printing of 100-1,000s of potential ligands, antibodies, or other biomaterials, iii) the ability to print replicates nanoarrays with high-throughput, iv) can print large area nanoarrays, and v) the uniform patterning of the nanoscale features. However, the existing techniques suffer from various limitations that fall short of these ideals.

While DPN is able to achieve nanoscale resolution down to 10s of nm for protein patterning [3, 26], difficulties exist for massive parallel multiplexing because: i) inking the dip-pens using direct inkwells that would occupy $0.5m^2$ for 55,000 pens [27], and ii) the fragility and opacity of silicon-based pen tips make it difficult to align to inkwells [28]. An alternative strategy for multiplexed inking of dip-pens involves using inkjet printing to deliver inks to cantilevers spaced 90μm apart, before using the pens for patterning biological arrays; however mechanical hysteresis in the registration of the inkjet printer with the pens necessitates surface chemical treatments of the pens for correction [29]. Polymer pen lithography utilizing polymeric pen tips have been utilized to alleviate the problems associated with DPN, enabling patterning of features across several length scales covering a $1cm^2$ area in 40 mins [20], and multiplexed protein nanopatterning using inkjet printing delivery of inks [28].

Although many replicate arrays can be rapidly generated by μCP, the patterned array feature sizes are limited and affected by the elastomeric polymer stamps that can deform with pressure, swell and shrink during stamp curing and inking [23, 27].

Additionally, it is challenging to perform alignment of elastomeric stamps to allow for patterning more than three different bio-components on the same array [24].

Finally, inkjet printing is easily scaleable to printing 1,000s of different components, and can rapidly generate replicate arrays with high throughput. However, the inkjet resolution is typically just 50–100μm, depending on the printing buffer composition, substrate hydrophilicity, and environmental humidity.

A key feature of any printing method to generate biomolecular arrays is the use of materials compatible with biological function. Parylene-C is a biocompatible polymer that has been widely used as a stencil for patterning biomolecular arrays with features more than 1μm, creating large area arrays of single-cells, proteins, nucleic acids, lipid bilayers, and cell co-cultures [30-36]. The parylene stencils are pinhole-free, chemically inert and do not swell in aqueous solutions, making them ideal for patterning large area, uniform arrays of biomolecules with superior pattern fidelity. Moreover it is possible to pattern biomolecular arrays using parylene in both dry and hydrated environments, the latter being important for preserving the conformation and functionality of the biomolecules.

In this study, parylene stencils with openings down to sub-100nm feature sizes were nanofabricated and these stencils were utilized to pattern protein features with high pattern fidelity. The Print-and-Peel (PNP) approach is a straightforward nanopatterning approach that combines the high-throughput and scalability of inkjet printing with the simple and uniform patterning capability of parylene peel-off. Using this PNP approach, multi-component nanoarrays of antibodies could be rapidly generated, thereby addressing the limitations of existing patterning methods. This was achieved through the consistent alignment of the inkjet printing on the fabricated parylene stencil, such that each printed spot optimally covered a set of nanoscale openings in the parylene. After inkjet printing the proteins, the parylene was easily

peeled off to leave uniformly patterned arrays of nanoscale protein features, as shown in Figure 2.1. An important extension of this aligned printing process is the ability to overlay spots with different biomolecular compositions onto one another to generate combinatorial nanoarrays of increasing complexity.

2.2 EXPERIMENTAL METHODS

2.2.1 Nanofabrication Process

The fabrication process of the parylene stencil is outlined in Figure 2.1(a). A thin layer of parylene-C from Uniglobe Kisco was chemically vapor coated onto a 4" oxidized silicon wafer (Specialty Coating Systems). Virtually any substrate that is vacuum compatible can be used, such as microscope slides, coverslips *etc.* Thereafter, an aluminum (Al) 15nm thin film was thermally evaporated on top of the parylene. Zeon ZEP-520 resist spun to a 100nm thickness on top of the Al, was baked at 90^{o}C, and exposed by electron beam lithography (EBL) using the JEOL JBX-9300FS. The resist was then developed in n-amyl acetate for 45 seconds and rinsed for 30 seconds in methyl isobutyl ketone and 2-isopropanol. The patterns in the resist were transferred into the Al film using reactive ion etching with $Cl_2/BCl_3/CF_4$ chemistry in a PlasmaTherm 740 etcher. Finally, the nanoscale openings were transferred into the parylene using the patterned Al film as a hard etch mask and oxygen plasma reactive ion etching with the Oxford PlasmaLab 80+ etcher. The Al film was dissolved in MIF300 developer, leaving the parylene stencil on the wafer.

2.2.2 Atomic force microscopy

Tapping mode AFM using a Digital Instruments 3100 system was used to characterize the nanoscale openings fabricated in the parylene stencil, and the nanoscale protein features. The surfaces were probed with a silicon TESP tip at scan

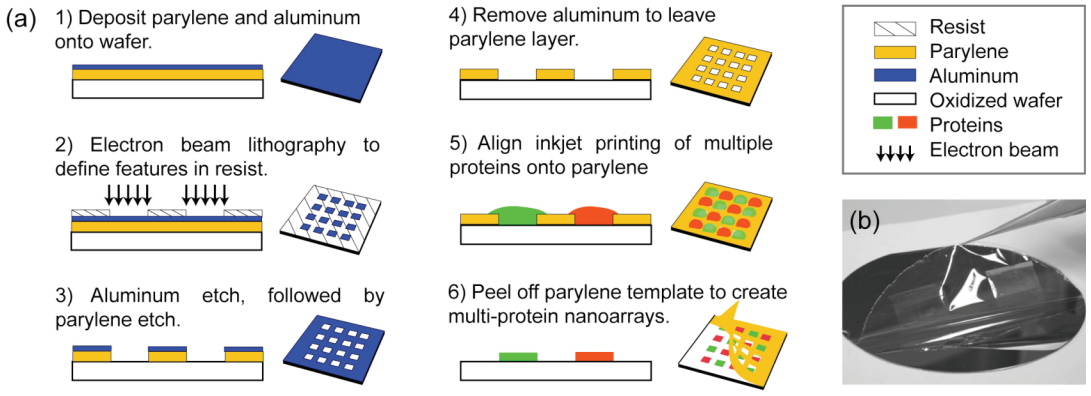

Figure 2.1 (a) Fabrication process of the parylene stencil and the PNP process to generate the protein nanoarrays. Schematic diagrams are not drawn to scale. (b) Mechanically peeling off the parylene stencil from a 4" wafer substrate. For the ease of illustration, the parylene peeling is shown in dry conditions, but the protein nanopatterning and parylene peeling were performed in aqueous environments that did not require drying.

speeds of 0.5–2Hz. The AFM images were post-analyzed using the WSxM v3.0 freeware from Nanotec Electronica. The full-width-at-half-maximum (FWHM) of the cross-sectional profile of a feature was reported as its width to minimize the effect of tip convolution.

2.2.3 Aligned Inkjet Printing Onto Parylene Peel-Off Stencils

Alignment marks – microscale crosses with line widths of 20μm and lengths of 100μm created in the parylene stencil – were used to help locate the positions of the nanoscale openings in the parylene using a high magnification microscope camera. Visual alignment accuracies down to 20μm can be achieved, although this can be easily improved by using a camera with higher magnification. The coordinates of the nanoscale features were calculated and used to program the Marathon Inkjet Microarrayer from Arrayjet for aligned printing of the antibodies spots onto sets of parylene openings. While an inkjet printer was used in this study, the PNP technique would also work for other printing technologies, such as quill-pin spotting and contact printing. Various antibodies tagged with different fluorophores – Alexa Fluor 488 goat anti-rabbit IgG, Alexa Fluor 555 goat anti-rabbit IgG, and Alexa Fluor 647 goat anti-mouse IgG – were diluted in 1:100 v/v in 50% glycerol printing buffer. Each diluted antibody was loaded into a well in a 384-wells microplate and then printed with alignment using the inkjet arrayer. For simplifying the fluorescence colors, only three different fluorescent antibodies were used in this experiment, however 1,000s of different species can be loaded into several microplates and routinely printed as indicated in the inkjet printer specifications provided by the manufacturer. Each printed spot of antibody covers a set of nanoscale openings in the parylene stencil. The parylene stencil was then mechanically peeled away to uniformly pattern multi-component antibodies arrays with different nanoscale feature shapes and sizes. Three

pre-assembled filter cubes from Chroma and Omega Optical were used to collect the fluorescence images, with each cube designed to image one specific fluorophore. The images collected from the three fluorescence channels were overlaid using ImageJ (National Institutes of Health). The final merged image was pseudo-colored – Alexa Fluor 488 (green), Alexa Fluor 555 (blue), and Alexa Fluor 647 (red) – to illustrate the different antibodies patterned.

To achieve combinatorial printing, the printing of a second set of spots was immediately superimposed on top of the first set, to create arrays with different combinations of antibodies per feature. The fluorescence images of the inkjet printed spots corresponding to the three fluorophores were collected and merged to yield a pseudo-color image using ImageJ.

2.2.4 Covalent Immobilization of Small Proteins

Following oxygen plasma etching of the parylene stencils, the oxidized silicon surfaces inside the stencil openings were functionalized with 10% v/v 3-aminopropyltriethoxysilane (APTES) in anhydrous toluene for 1 h, followed by rinsing in toluene, methanol, and water for 15 min. The chips were then treated with 2.5% glutaraldehyde, a homobifunctional linker that would covalently cross-link amine groups on the silane and protein. Small proteins, namely recombinant human interleukin-8 (IL-8, 8kDa, R&D sytems) and tissue growth factor alpha (TGF-α, 5.5kDa, Abcam) were inkjet printed onto the parylene chips at 1μM ceoncentration and incubated for 1 h before rinsing off.

2.2.5 Fibronectin Nanopatterning and Fluorescent Immunostaining

Human fibronectin from Sigma-Aldrich was dissolved in deionized water and diluted in phosphate buffered saline (PBS) to 10 μg/mL. The diluted fibronectin was

manually spotted onto the parylene stencil, incubated for 2 h, and rinsed with water to remove excess unbound fibronectin. The parylene was peeled off with tweezers under water to define an array of nanoscale fibronectin features. The array was kept in hydrated conditions throughout the patterning to preserve the 3D conformation and functionality of the protein. After parylene peel-off, rabbit anti-fibronectin antibody from Sigma-Aldrich and Alexa Fluor 488 conjugated goat anti-rabbit secondary antibody from Invitrogen were used to immunostain the fibronectin features following the manufacturers' protocols and also described elsewhere [30].

Fluorescent immunostaining of the covalently immobilized small proteins was performed using goat anti-IL-8 antibody (R&D systems), mouse anti-TGF-α antibody (Abcam), and secondary Alexa Fluor 488-conjugated donkey anti-goat antibody and Alexa Fluor 647-conjugated donkey anti-mouse antibody.

2.3 RESULTS AND DISCUSSIONS

2.3.1 Nanofabrication Process

Nanoscale openings were created in the parylene stencil, down to sub-100nm feature size, using the above nanofabrication approach. This is the first demonstration of fabricating parylene stencils with such fine resolution, which represents a novel lithographic process in several aspects. Firstly, the smallest opening size that could be fabricated in parylene was limited by the parylene thickness and the accessibility of the oxygen plasma into the openings during etching. The ability to create nanoscale features in parylene is not obvious since previous work using parylene peel-off for biological patterning typically utilized parylene with thicknesses ~1μm or more [30, 31, 33-36], which would inhibit the creation of sub-100nm openings in the parylene stencil. To effectively etch through nanoscale openings in the parylene, it was observed that the aspect ratio (depth:width) of the openings should ideally not exceed

4:1 for plasma accessibility. Moreover, ultra-thin parylene coatings with thickness less than 200nm have been reported to display porous behavior that was tuned to control drug elution [37]. There is a benefit to having the parylene be as thin as possible for the lithographic purpose of creating the smallest features, but at the same time the parylene must be thick enough to achieve its aim as a pin-hole free patterning stencil. Parylene with a thickness of 400nm in this work, which we found to be non-porous and yet thin enough for lithographic processing.

Furthermore, the use of the 15nm Al etch mask was different from previous work involving parylene peel-off whereby photoresist was used as the etch mask [30-34]. Al was an ideal etch mask because it forms a stable oxide layer in the presence of oxygen and maintains etch anisotropy, which prevents lateral widening of the features during pattern transfer into parylene. This lateral widening can be insignificant during the fabrication of micrometer-sized openings in parylene with a photoresist etch mask, but inhibits the accurate reproduction of critical feature dimensions when creating nanometer-sized openings. The ultra-thin Al layer was important for reducing the Al etch time for pattern transfer, thus minimizing lateral widening during Al etch. However, the oxide layer prevented Al from being etched efficiently by the chlorine etch chemistry during the pattern transfer from the ZEP-520 resist layer into the Al film. A breakthrough step at a high power of 450V was essential to remove this oxide layer before the Al film could be completely etched through. This breakthrough step in turn removed the ZEP-520 resist at a faster rate. Thus, the limit of the smallest feature size could be fabricate in the parylene stencil was a function of the etch selectivity, anisotropy, and aspect ratio of the etching steps in the nanofabrication.

The lithography used for fabricating the parylene stencils is not limited to EBL, and could include other high-resolution lithography such as nanoimprint lithography (NIL) [38]. NIL can potentially achieve lithographic resolution similar to

EBL, but could have the added advantage of patterning the same area with high throughput. The use of NIL as an alternative lithographic method to imprint into the resist for the nanofabrication of the parylene stencils is currently being explored.

2.3.2 Characterization of Parylene Peel-Off Stencils and Fibronectin Nanoarrays

In Figure 2.2, the AFM images of arrays of 90nm spots and 180nm lines showed that nanoscale openings of different shapes and sizes could be created in the parylene stencil, due to the new fabrication process utilizing EBL and the Al hard etch mask. Furthermore, the parylene layer was observed to be non-porous, indicating that the 400nm parylene thickness was appropriate for an effective patterning stencil.

Next, these nanofabricated parylene stencils were used to pattern nanoarrays of proteins with high fidelity. Fibronectin, a model protein component of the ECM, was chosen for nanopatterning since it is involved in many biological processes controlling cell fate and behavior [7, 8, 15, 30].

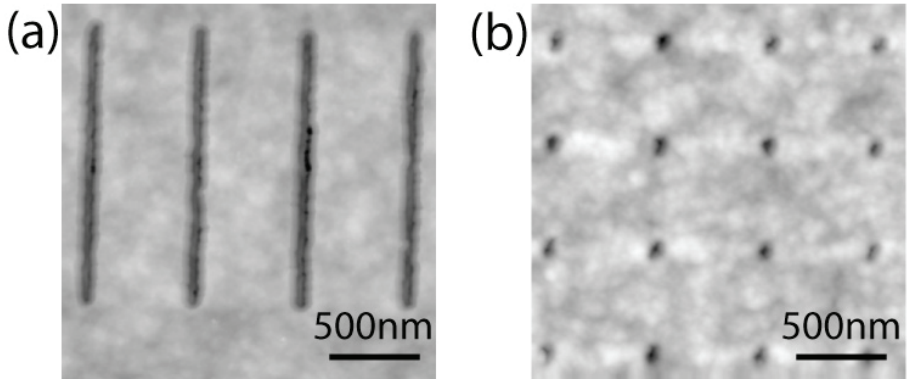

Figure 2.2 AFM images showing arrays of nanoscale openings nanofabricated in the parylene templates – (a) 180nm lines and (b) 90nm spots. The parylene template is pinhole-free at 400nm thickness.

The AFM images taken of the fibronectin arrays in Figure 2.3 showed high fidelity patterns lines with 180 $\pm$ 13 nm widths and spots with 90 $\pm$ 18 nm diameters. A control experiment was also performed, whereby buffer alone was incubated onto the parylene stencil. The control AFM images showed a smooth surface within the openings (data not shown), indicating that arrays of fibronectin were indeed patterned in Figure 2.3. Due to the chemical inertness of parylene and its resistance to swelling in hydrated environments, the fibronectin features were replicated with high fidelity and nanoscale resolution. The cross-sectional height profile of the fibronectin features revealed a relatively uniform height distribution of 4–5nm, comparable to another prior study [39]. It is postulated that the apparent heterogeneity within each 90nm spot was due to fibronectin aggregates being adsorbed, since fibronectin has been reported to adopt a compact globular structure under low ionic strength [39]. It is anticipated that in the future, reducing the feature size of patterned ECM proteins to nanoscale dimensions may help improve the resolution of studies in cell polarity and focal adhesion formation [9, 40].

Fluorescent immunostaining was performed to further confirm the presence of the patterned fibronectin features. Figure 2.4(a) shows a differential contrast microscopy image of the original parylene stencil with both microscopic and nanoscale openings. The micrometer-sized number and line were used to help locate the 180nm nanoscale lines demarcated by the arrows. Fluorescent features were observed in Figure 2.4(b), indicating that we had successfully patterned fibronectin with high fidelity and also preserved the functionality of the protein. The 90nm spot openings and fluorescent features could not be visualized by optical microscopy because the feature size was drastically smaller than the diffraction limit. It was however possible to see the dim fluorescence of the 180nm lines demarcated by the arrows in Figure 2.4(b).

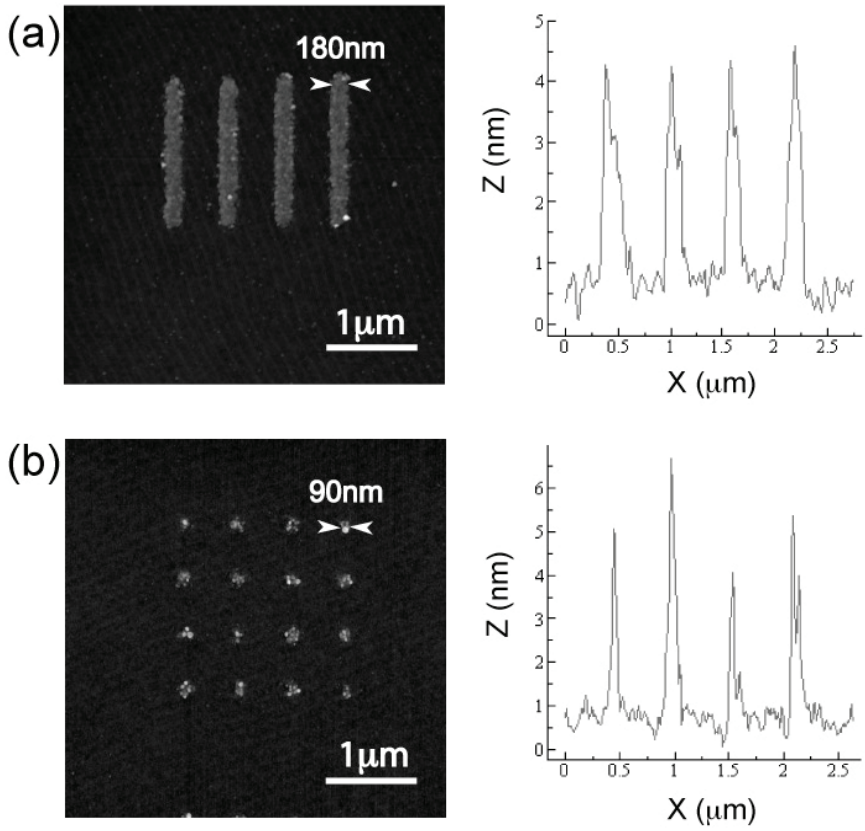

Figure 2.3 AFM images and the cross-sectional profiles of patterned fibronectin nanoarrays – (a) 180nm lines and (b) 90nm spots. The fibronectin patterns were replicated with high fidelity from the parylene templates. The cross-sectional profiles were taken from a span across four array features on each image, and the FWHM of each peak was measured as the feature width. The heights of the patterned fibronectin features were relatively uniform at 4–5nm.

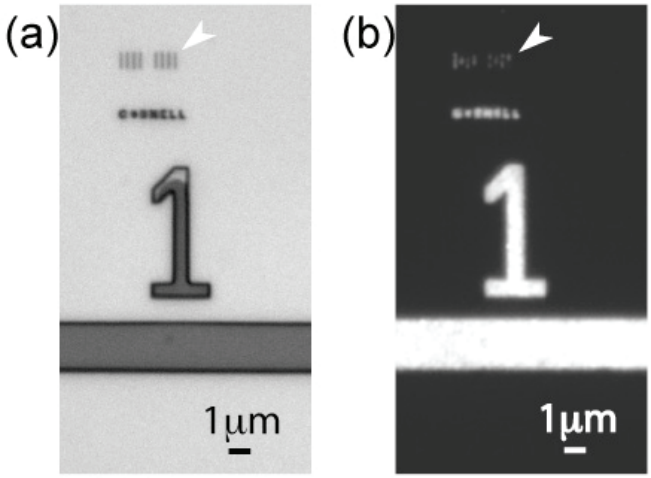

Figure 2.4 Fluorescent immunostaining to confirm the presence and functionality of patterned fibronectin. (a) Differential contrast microscopy image of the original parylene template, with arrays of 180nm lines marked by the arrow. (b) Fluorescence microscopy image showing immunostaining of the fibronectin features successfully patterned onto the surface. The image brightness and contrast have been adjusted, so that the dim fluorescence of the lines demarcated by the arrow could be seen. The arrays of 90nm spots could not be easily visualized by optical microscopy since their size is significantly smaller than the diffraction limit.

2.3.3 Uniform, Multi-Component Antibody Nanoarrays

The PNP approach was developed to take advantage of the high-throughput, multiplexing capabilities of inkjet printing and combine this with the nanopatterning capabilities of parylene peel-off. The right-hand image in Figure 2.5(a) shows a bright field microscopy image of a portion of the fabricated parylene stencil. Each printed spot of antibody ~70–100μm covers a set of nanoscale openings in the parylene stencil, as shown in Figure 2.5(b). As illustrated in Figure 2.5(c), the parylene stencil was then mechanically peeled away to uniformly pattern multi-component antibodies arrays with different nanoscale feature shapes and sizes. Arrays of 600nm lines and 600nm spots of antibodies could be patterned, as shown in Figure 2.5(c), despite inconsistencies in the original inkjet spot morphology and size.

This result demonstrates that the PNP process could be used to clean-up imperfect inkjet printed spots by transforming them into consistently defined features through the application of the parylene stencil. This spot transformation is not limited to nanoscale features, and can also be used to pattern microscale features, provided that the original inkjet spot is larger than the openings in the parylene. The simple alignment approach in the PNP process enables multiple species to be reproducibly patterned onto a surface, circumventing the problem of alignment issues associated with printing multiple components in μCP. This PNP technology can also extend the resolution of regular inkjet printing from micrometers to sub-micrometers, after a single straightforward peeling step to remove the parylene stencil.

Furthermore, PNP can be scaled up to print 1,000s of different components with a high throughput associated with standard microarrayers. The spacing between each set of patterned antibody features in our nanoarrays is currently limited by the 70–100μm diameter of the inkjet printed spot on our hydrophobic parylene surface. Based on this spacing distance, calculations indicate that over 20,000 different

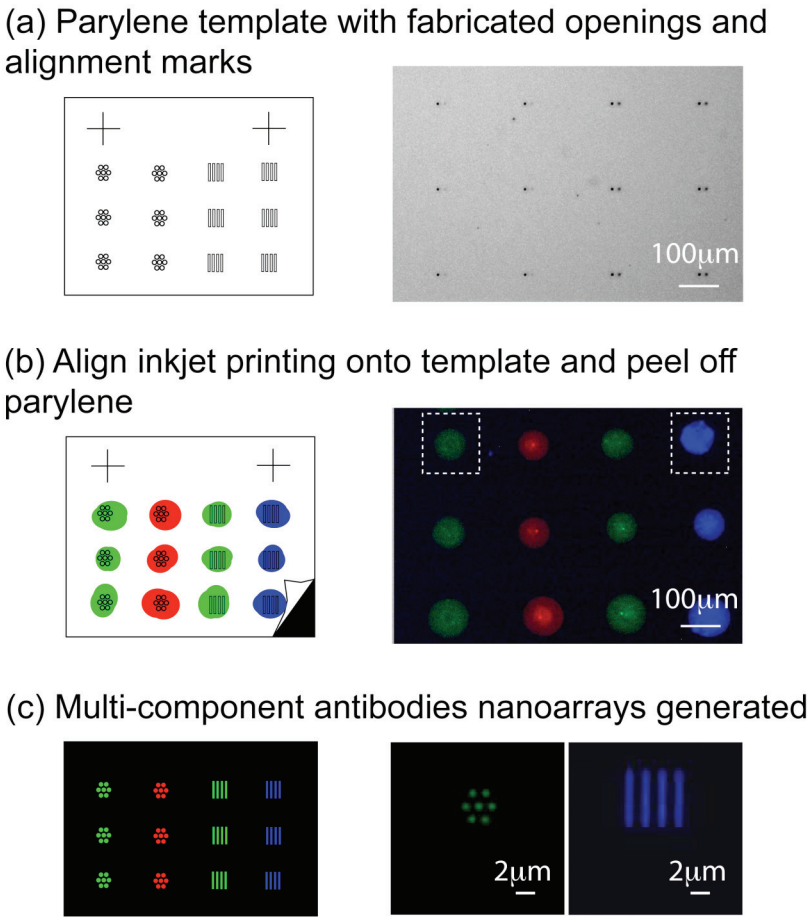

Figure 2.5 The PNP process. Schematic diagram of each step is shown on the left, not drawn to scale. (a) Bright field microscopy image showing a part of the parylene template pre-defined with openings and alignment marks. (b) Pseudo-color merged fluorescence image showing aligned inkjet printing of different antibodies onto parylene. (c) Multi-component antibodies arrays were generated after peel off, corresponding to the boxed region in (b). Array features of different shapes and sizes – 600nm wide lines and spots –were patterned with the PNP process.

antibodies could be printed on a 1 cm x 2 cm chip area at maximum packing density. One of the future aims would be to reduce this spacing to sub-micrometers and achieve an even higher packing density by utilizing multi-layer parylene stencils [41]. This work is the first demonstration where multiple proteins are arrayed on a single surface utilizing parylene peel-off, while previous work involving bath incubation of solutions onto the parylene stencil have been limited to patterning arrays containing at most two different proteins [31]. The antibodies arrays created using our PNP method could potentially be useful for immunoassays, diagnostics, and cytokines screening.

2.3.4 Combinatorial Antibody Nanoarrays

The aligned printing process allows for dramatically extending the utility of these PNP arrays by offering a convenient alternative method to create nanoarrays of mixed proteins. Printing of a second set of spots was immediately superimposed on top of the first set, to create arrays with different combinations of antibodies per feature, as illustrated in the schematic in Figure 2.6(a). The fluorescence images of the inkjet printed spots corresponding to the three fluorophores were collected and merged to yield a pseudo-color image in Figure 2.6(b). Six different combinations of antibodies could be generated from an initial pool of just three different antibodies. After parylene peel-off, arrays of 600nm diameter spots containing various combinations of antibodies were patterned in Figure 2.6(c). These experiments show that the combinations of biomolecules patterned can be potentially increased by increasing the number of different types of antibodies in the initial pool, followed by overlaying more sets of spots per array feature. Although purified proteins and antibodies were used for these experiments, any desired biomaterials ranging from nucleic acids to cells and cell lysates, can be printed in combination or by itself.

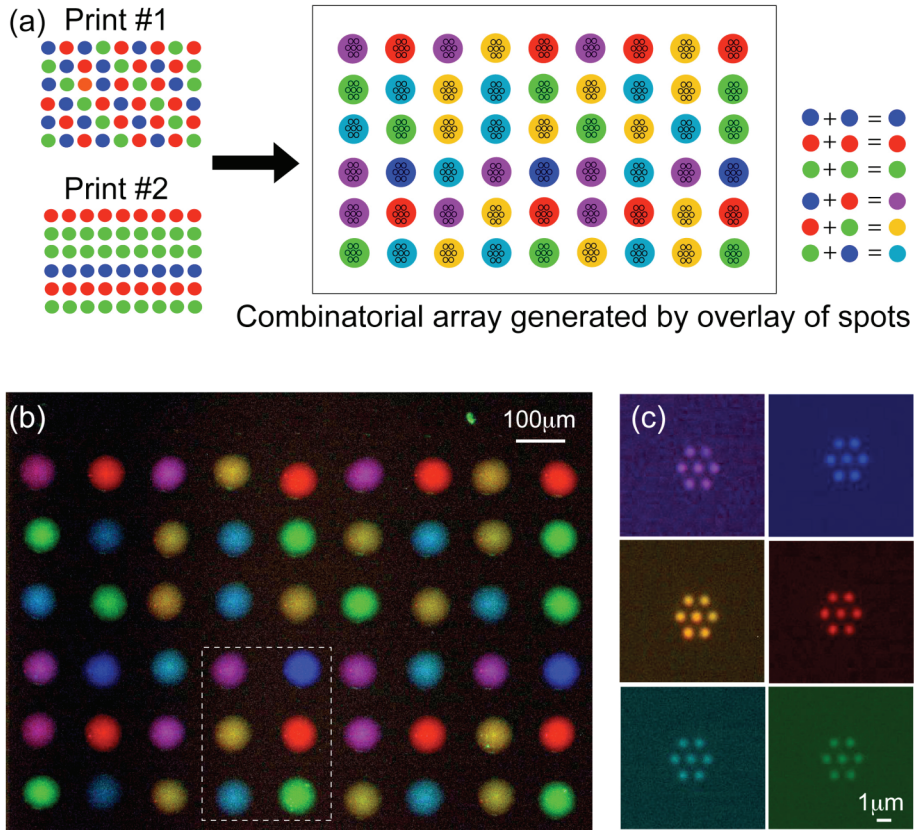

Figure 2.6 The PNP process can generate combinatorial biomolecular nanoarrays. (a) Schematic diagram showing the process of superimposing a second inkjet print-run immediately over the first print to generate six different combinations of antibodies from an initial pool of three separate antibodies. (b) Pseudo-color merged fluorescence image showing the combinatorial array that can be inkjet printed onto the parylene template. (c) Antibodies nanoarrays of six different biomolecular combinations were generated after parylene peel-off, corresponding to the spots demarcated within the boxed region in (b).

Arraying different combinations of biomolecular components has been important in combinatorial screening of pharmaceutical compounds and responses of stem cells to various polymeric surfaces, signaling, growth or transfection cues [16, 17, 42]. The ability of this PNP technology to create combinatorial biomolecular nanoarrays with ease and high throughput will open up future opportunities to explore synergistic and antagonistic combinations of biomolecules in receptor-ligand interactions.

2.3.5 Covalently Immobilized TGF-α and IL-8 Nanoarrays

The PNP technique can be modified to covalently link smaller proteins to the oxidized silicon surface exposed in the parylene openings. While large proteins such as fibronectin (450kDa) and immunoglobulin antibodies (150kDa) can irreversibly adsorb to a surface, smaller proteins may desorb again from surfaces after adsorption [43], necessitating covalent linkage. The schematic in Figure 2.7(a) shows our method for this surface chemistry, which is modified from literature [44]. Figure 2.7(b) shows an inkjet droplet containing IL-8 covering an array of nanoscale line features demarcated by the black arrow. The fluorescent images in Figures 2.7(c) and 2.7(d) correspond to TGF-α and IL-8 patterned chips collected at the appropriate emission wavelengths (centered at 680nm and 530nm respectively). These results demonstrate that the PNP technique can be utilized for nanopatterning arrays of covalently bound proteins, as confirmed by fluorescence immunostaining using antibodies that specifically recognize IL-8 and TGF-α.

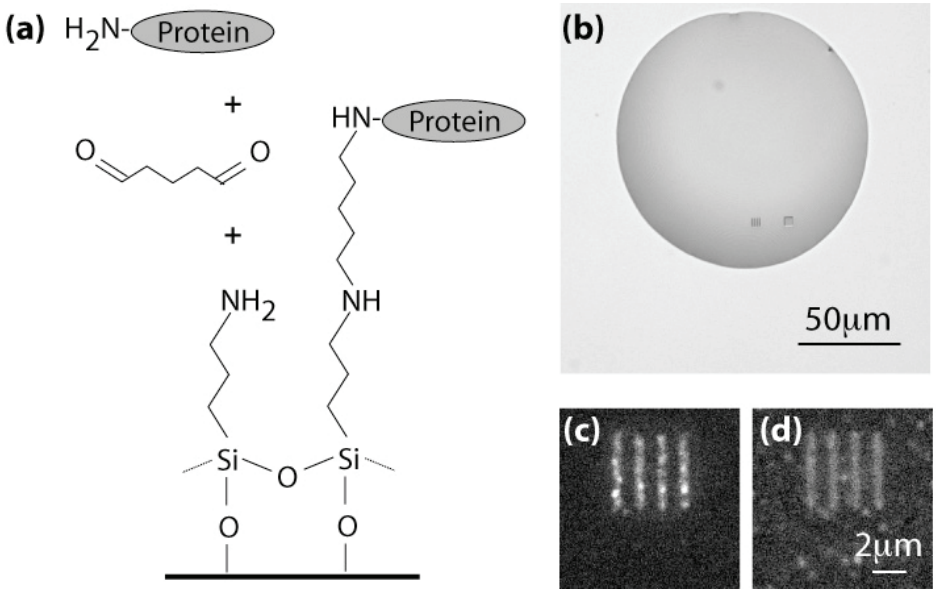

Figure 2.7 (a) Schematic showing the surface modification of our parylene chips utilizing APTES and glutaraldehyde for covalently immobilizing proteins. (b) Brightfield image of an inkjet droplet of IL-8 incubated on the parylene openings that have been treated with glutaraldehyde and aminosilane. (c) Fluorescent image collected (emission wavelength for Alexa Fluor 647) following immunostaining, showing TGF-α covalently bound to the surface as a nanoarray of 600nm line features. (d) Fluorescent image similar to (c) but collected for IL-8 (emission wavelength for Alexa Fluor 488).

2.4 CONCLUSIONS

In conclusion, the PNP technology has been developed that is capable of producing nanoscale resolution, multi-component biomolecular arrays. These nanoarrays can be rapidly produced in a large area format with high throughput using standard inkjet printers or microarrayers utilized in the PNP process. Uniform nanoscale array features can be patterned despite imperfections in the inkjet spot morphologies. The aligned printing process can be further extended to create combinatorial nanoarrays, as well as nanoarrays of covalently linked proteins. In the future, it is anticipated that these multi-component biomolecular nanoarrays will be useful for super high-resolution studies of subcellular biological processes and interactions [45, 46], integrating biochemical functionalities with nanoscale sensors, and engineering cellular and tissue micro- and nanoenvironments.

REFERENCES

1. Khademhosseini, A., *Micro and nanoengineering of the cell microenvironment*. Artech House: Boston, MA, 2008.
2. Blattler, T.; Huwiler, C.; Ochsner, M.; Stadler, B.; Solak, H.; Voros, J.; Grandin, H. M., Nanopatterns with biological functions. *Journal of Nanoscience and Nanotechnology* 2006, 6, 2237-2264.
3. Lee, K. B.; Park, S. J.; Mirkin, C. A.; Smith, J. C.; Mrksich, M., Protein nanoarrays generated by dip-pen nanolithography. *Science* 2002, 295, 1702-1705.
4. Takayama, S.; Ostuni, E.; LeDuc, P.; Naruse, K.; Ingber, D. E.; Whitesides, G. M., Laminar flows - subcellular positioning of small molecules. *Nature* 2001, 411, 1016-1016.
5. Senaratne, W.; Sengupta, P.; Jakubek, V.; Holowka, D.; Ober, C. K.; Baird, B., Functionalized surface arrays for spatial targeting of immune cell signaling. *Journal of the American Chemical Society* 2006, 128, 5594-5595.
6. Torres, A. J.; Wu, M.; Holowka, D.; Baird, B., Nanobiotechnology and cell biology: Micro- and nanofabricated surfaces to investigate receptor-mediated signaling. *Annual Review of Biophysics* 2008, 37, 265-288.
7. Goffin, J. M.; Pittet, P.; Csucs, G.; Lussi, J. W.; Meister, J. J.; Hinz, B., Focal adhesion size controls tension-dependent recruitment of alpha-smooth muscle actin to stress fibers. *Journal of Cell Biology* 2006, 172, 259-268.
8. Chen, C. S.; Mrksich, M.; Huang, S.; Whitesides, G. M.; Ingber, D. E., Geometric control of cell life and death. *Science* 1997, 276, 1425-1428.
9. Arnold, M.; Cavalcanti-Adam, E. A.; Glass, R.; Blummel, J.; Eck, W.; Kantlehner, M.; Kessler, H.; Spatz, J. P., Activation of integrin function by nanopatterned adhesive interfaces. *Chemphyschem* 2004, 5, 383-388.

10. Cui, Y.; Wei, Q. Q.; Park, H. K.; Lieber, C. M., Nanowire nanosensors for highly sensitive and selective detection of biological and chemical species. *Science* 2001, 293, 1289-1292.

11. Domansky, K.; Li, J.; Janata, J., Selective doping of chemically sensitive layers on a multisensing chip. *Journal of the Electrochemical Society* 1997, 144, L75-L78.

12. Waggoner, P. S.; Craighead, H. G., Micro- and nanomechanical sensors for environmental, chemical, and biological detection. *Lab on a Chip* 2007, 7, 1238-1255.

13. St John, P. M.; Davis, R.; Cady, N.; Czajka, J.; Batt, C. A.; Craighead, H. G., Diffraction-based cell detection using a microcontact printed antibody grating. *Analytical Chemistry* 1998, 70, 1108-1111.

14. MacBeath, G.; Schreiber, S. L., Printing proteins as microarrays for high-throughput function determination. *Science* 2000, 289, 1760-1763.

15. Flaim, C. J.; Chien, S.; Bhatia, S. N., An extracellular matrix microarray for probing cellular differentiation. *Nature Methods* 2005, 2, 119-125.

16. Yoshikawa, T.; Uchimura, E.; Kishi, M.; Funeriu, D. P.; Miyake, M.; Miyake, J., Transfection microarray of human mesenchymal stem cells and on-chip sirna gene knockdown. *Journal of Controlled Release* 2004, 96, 227-232.

17. Anderson, D. G.; Levenberg, S.; Langer, R., Nanoliter-scale synthesis of arrayed biomaterials and application to human embryonic stem cells. *Nature Biotechnology* 2004, 22, 863-866.

18. Bailey, S. N.; Ali, S. M.; Carpenter, A. E.; Higgins, C. O.; Sabatini, D. M., Microarrays of lentiviruses for gene function screens in immortalized and primary cells. *Nature Methods* 2006, 3, 117-122.

19. Zhu, H.; Snyder, M., Protein chip technology. *Current Opinion in Chemical Biology* 2003, 7, 55-63.

20. Huo, F. W.; Zheng, Z. J.; Zheng, G. F.; Giam, L. R.; Zhang, H.; Mirkin, C. A., Polymer pen lithography. *Science* 2008, 321, 1658-1660.

21. Mei, Y.; Cannizzaro, C.; Park, H. S.; Xu, Q. B.; Bogatyrev, S. R.; Yi, K.; Goldman, N.; Langer, R.; Anderson, D. G., Cell-compatible, multicomponent protein arrays with subcellular feature resolution. *Small* 2008, 4, 1600-1604.

22. Huo, F. W.; Zheng, G. F.; Liao, X.; Giam, L. R.; Chai, J. A.; Chen, X. D.; Shim, W. Y.; Mirkin, C. A., Beam pen lithography. *Nature Nanotechnology* 2010, 5, 637-640.

23. Coyer, S. R.; Garcia, A. J.; Delamarche, E., Facile preparation of complex protein architectures with sub-100-nm resolution on surfaces. *Angewandte Chemie International Edition* 2007, 46, 6837-6840.

24. Tien, J.; Nelson, C. M.; Chen, C. S., Fabrication of aligned microstructures with a single elastomeric stamp. *Proceedings of the National Academy of Sciences of the United States of America* 2002, 99, 1758-1762.

25. Roth, E. A.; Xu, T.; Das, M.; Gregory, C.; Hickman, J. J.; Boland, T., Inkjet printing for high-throughput cell patterning. *Biomaterials* 2004, 25, 3707-3715.

26. Lee, K. B.; Lim, J. H.; Mirkin, C. A., Protein nanostructures formed via direct-write dip-pen nanolithography. *Journal of the American Chemical Society* 2003, 125, 5588-5589.

27. Braunschweig, A. B.; Huo, F. W.; Mirkin, C. A., Molecular printing. *Nature Chemistry* 2009, 1, 353-358.

28. Zheng, Z. J.; Daniel, W. L.; Giam, L. R.; Huo, F. W.; Senesi, A. J.; Zheng, G. F.; Mirkin, C. A., Multiplexed protein arrays enabled by polymer pen

lithography: Addressing the inking challenge. *Angewandte Chemie International Edition* 2009, 48, 7626-7629.

29. Wang, Y. H.; Giam, L. R.; Park, M.; Lenhert, S.; Fuchs, H.; Mirkin, C. A., A self-correcting inking strategy for cantilever arrays addressed by an inkjet printer and used for dip-pen nanolithography. *Small* 2008, 4, 1666-1670.
30. Tan, C. P., Seo, B. R., Brooks, D. J., Chandler, E. M., Craighead, H. G., Fischbach, C., Parylene peel-off arrays to probe the role of cell-cell interactions in tumour angiogenesis. *Integrative Biology* 2009, 1, 587-594.
31. Ilic, B., Craighead, H.G., Topographical patterning of chemically sensitive biological materials using a polymer-based dry lift off. *Biomedical Microdevices* 2000, 2, 317-322.
32. Moran-Mirabal, J. M.; Tan, C. P.; Orth, R. N.; Williams, E. O.; Craighead, H. G.; Lin, D. M., Controlling microarray spot morphology with polymer liftoff arrays. *Analytical Chemistry* 2007, 79, 1109-1114.
33. Moran-Mirabal, J. M.; Edel, J. B.; Meyer, G. D.; Throckmorton, D.; Singh, A. K.; Craighead, H. G., Micrometer-sized supported lipid bilayer arrays for bacterial toxin binding studies through total internal reflection fluorescence microscopy. *Biophysical Journal* 2005, 89, 296-305.
34. Orth, R. N.; Wu, M.; Holowka, D. A.; Craighead, H. G.; Baird, B. A., Mast cell activation on patterned lipid bilayers of subcellular dimensions. *Langmuir* 2003, 19, 1599-1605.
35. Jinno, S.; Moeller, H. C.; Chen, C. L.; Rajalingam, B.; Chung, B. G.; Dokmeci, M. R.; Khademhosseini, A., Macrefabricated multilayer parylene-c stencils for the generation of patterned dynamic co-cultures. *Journal of Biomedical Materials Research, Part A* 2008, 86A, 278-288.

36. Wright, D.; Rajalingam, B.; Selvarasah, S.; Dokmeci, M. R.; Khademhosseini, A., Generation of static and dynamic patterned co-cultures using microfabricated parylene-c stencils. *Lab on a Chip* 2007, 7, 1272-1279.

37. Lam, R.; Chen, M.; Pierstorff, E.; Huang, H.; Osawa, E. J.; Ho, D., Nanodiamond-embedded microfilm devices for localized chemotherapeutic elution. *ACS Nano* 2008, 2, 2095-2102.

38. Chou, S. Y.; Krauss, P. R.; Renstrom, P. J., Imprint lithography with 25-nanometer resolution. *Science* 1996, 272, 85-87.

39. Bergkvist, M.; Carlsson, J.; Oscarsson, S., Surface-dependent conformations of human plasma fibronectin adsorbed to silica, mica, and hydrophobic surfaces, studied with use of atomic force microscopy. *Journal of Biomedical Materials Research Part A* 2003, 64A, 349-356.

40. Thery, M.; Racine, V.; Piel, M.; Pepin, A.; Dimitrov, A.; Chen, Y.; Sibarita, J. B.; Bornens, M., Anisotropy of cell adhesive microenvironment governs cell internal organization and orientation of polarity. *Proceedings of the National Academy of Sciences of the United States of America* 2006, 103, 19771-19776.

41. Kuribayashi, K., Hiratsuka, Y., Yamamura, T., Takeuchi, S., Sequential parylene lift-off process for selective patterning of biological materials. *IEEE MEMS 2007*, 501-504.

42. Angres, B., Cell microarrays. *Expert Review of Molecular Diagnostics* 2005, 5, 769-779.

43. Sigal, G. B.; Mrksich, M.; Whitesides, G. M., Effect of surface wettability on the adsorption of proteins and detergents. *Journal of the American Chemical Society* 1998, 120, 3464-3473.

44. Tlili, A.; Jarboui, M. A.; Abdelghani, A.; Fathallah, D. M.; Maaref, M. A., A novel silicon nitride biosensor for specific antibody-antigen interaction.

Materials Science & Engineering C-Biomimetic and Supramolecular Systems 2005, 25, 490-495.

45. Fernandez-Suarez, M.; Ting, A. Y., Fluorescent probes for super-resolution imaging in living cells. *Nature Reviews Molecular Cell Biology* 2008, 9, 929-943.

46. Huang, B.; Jones, S. A.; Brandenburg, B.; Zhuang, X. W., Whole-cell 3d storm reveals interactions between cellular structures with nanometer-scale resolution. *Nature Methods* 2008, 5, 1047-1052.

CHAPTER 3

PARYLENE PEEL-OFF ARRAYS TO PROBE THE ROLE OF CELL-CELL INTERACTIONS IN TUMOR ANGIOGENESIS[3]

3.1 INTRODUCTION

Cell-microenvironment interactions regulate cell behavior in general and tumorigenesis in particular. However, the underlying biological mechanisms remain poorly understood. Cells cooperate with their environment by interacting with neighboring cells (*e.g.* via adherens junctions), with their surrounding ECM and by communicating through secreted soluble factors. Typically, these interactions are well-coordinated, but perturbation of the underlying cellular and molecular interplay may affect intracellular signaling pathways, immunological reactions and tissue homeostasis, all of which play a pivotal role in tumor initiation, growth and metastasis. [1]

Alterations in cell-microenvironment interactions influence tumor angiogenesis, a hallmark of cancer. [2] The formation of new blood vessels from pre-existing ones is critical to nutrient and oxygen supply, and also confers a route for tumor cells to metastasize. Vascular endothelial growth factor (VEGF), interleukin-8 (IL-8) and basic fibroblast growth factor (bFGF) are three of the most widely investigated pro-angiogenic factors [3-5] and the expression of these proteins is controlled by microenvironmental conditions. For example, cell-cell interactions [6, 7] and changes in ECM composition [8, 9] alter angiogenic factor secretion by regulating the downstream signaling of the corresponding receptors. Additionally, hypoxia

[3] This chapter is a modified and revised form of the publication: Tan, C.P., Seo, B.R., Brooks, D.J., Chandler, E.M., Craighead, H.G., Fischbach, C., Parylene Peel-Off Arrays to Probe the Role of Cell-Cell Interactions in Tumor Angiogenesis, *Integrative Biology* 2009, 1, 587-594.

mediates the angiogenic switch in agglomerates of tumor cells larger than 200μm in diameter [10]. However, it is still unclear whether the angiogenic potential of a single tumor cell differs from a tumor cell cluster in the absence of oxygen limitations.

μCP using PDMS stamps is frequently used to pattern proteins and cells and to study the role of cell-cell interactions on cell behavior [11, 12]. The elastomeric PDMS suffers from sagging and swelling in solution, which makes it inefficient for patterning uniform features over a large area [13]. However, large and uniform arrays of patterned cells are needed to measure detectable amounts of secreted pro-angiogenic factors in the culture media. Furthermore, μCP frequently involves a drying step that may compromise the bioactivity of the proteins to be printed [14]. PDMS is a low energy polymer and segregates to the surface of the stamp. This can lead to the transfer of PDMS to the substrate, potentially affecting the purity of the biomaterial patterned [15]. Other methods to micropattern arrays of single cells (*e.g.* hydrodynamic microfluidic chips [16], dielectrophoretic trapping [17], optical trapping [18], magnetic positioning [19, 20], SU-8 micropallet arrays [21]) are not routinely applicable due to their complex experimental setup, may involve additional steps of labeling and transfecting cells with nanoparticles, or may not be capable of presenting ECM proteins to cells necessary for cell surface integrin engagement.

Parylene stencils can be used to pattern a variety of biological materials (*e.g.* nucleic acids, lipids and cells) in both dry and aqueous environments and overcome the limitations associated with μCP [22-27]. Because parylene is chemically inert, pinhole free and resists swelling in aqueous medium, it represents an appropriate material to pattern uniform and reproducible features of biomaterials over a large tissue culture surface area, allowing for the profiling of protein secretion in cell culture. Additionally, parylene is biocompatible, and does not elicit an immune response from cells nor alter the biology in cell culture studies. Finally, parylene can

be mechanically peeled off glass surfaces without leaving any residue. This process can be done under aqueous conditions, preserving both the native conformation and purity of the patterned biomaterial.

The goal in this study was to utilize the advantages of parylene peel-off for the novel study of the angiogenic potential of tumor cells in response to cell-cell interactions. To this end, a PeelArray chip was designed that can be readily utilized to pattern and culture large arrays of single cells or cell clusters in a reproducible and controlled manner. The PeelArray chip consists of a glass coverslip with a parylene stencil that can be easily peeled off to uniformly pattern large arrays of fibronectin features against a non-cell adhesive background. Based on the fibronectin feature sizes, either individual or clustered tumor cells were cultured. By comparing the secretion of angiogenic factors in the absence or presence of cell-cell interactions, the synergistic behavior of tumor cells towards angiogenesis was investigated. This novel integration of parylene peel-off patterning approach with the study of tumor angiogenesis may help to define the quantitative relationships by which cell-cell interactions contribute to the tumor angiogenic switch.

3.2 EXPERIMENTAL METHODS

3.2.1 Chip Microfabrication

The microfabrication process for the PeelArray chip is outlined in Figure 3.1(a). Parylene-C (Uniglobe Kisco) was deposited via chemical vapor deposition (Specialty Chemical Systems Labcoter 2) onto a polyethylene glycol (PEG) treated 22mm x 22mm glass coverslip. The PEG coverslips were either purchased from Microsurfaces Inc., coated using the MVD-100 tool (Applied Microstructures), or manually silanized with a 15% PEG-silane (500Da, Gelest) in anhydrous toluene for 14h. The parylene film was measured to be 800nm thick using a profilometer and was

patterned using photolithography. A photoresist layer (Shipley 1827) was spun on top of the parylene, and square patterns were exposed on the photoresist using 405nm ultraviolet light (HTG System III-HR). The photoresist was then developed, serving as an etch mask during oxygen plasma etching of the parylene (PlasmaTherm PT72). Residual photoresist was removed by rinsing the chip with acetone and isopropanol. Each chip was patterned with either 20µm x 20µm or 40µm x 40µm features, suitable for culturing an array of single cells or cell clusters respectively.

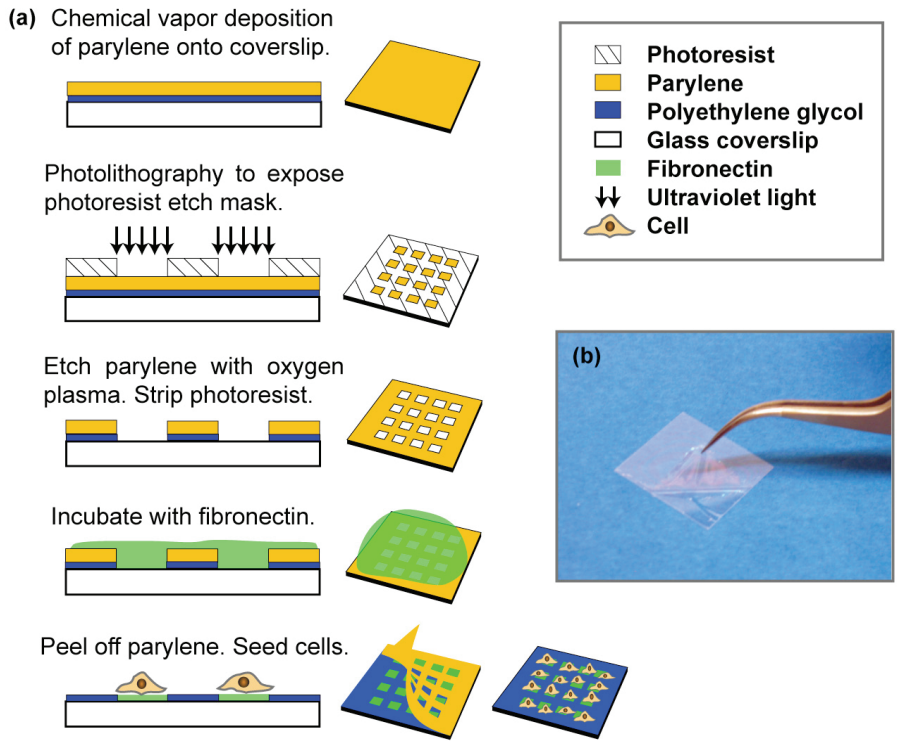

Figure 3.1 (a) Schematic diagrams showing the microfabrication process of the PeelArray chip. (b) Mechanical peeling of the parylene template after fibronectin incubation (shown here in dry condition for the ease of photography, but the actual peeling was performed in aqueous environment).

3.2.2 Patterning Fibronectin Features

The chips were sterilized with 70% ethanol. Next, each chip was incubated with 0.2mg/mL of human fibronectin (Sigma-Aldrich) dissolved in PBS for 1 h at room temperature and then rinsed twice with deionized water to remove unbound fibronectin. Subsequently, the parylene stencil was mechanically peeled off the chip with sterile tweezers (Figure 3.1(b)) to define an array of 20μm x 20μm or 40μm x 40μm fibronectin features. Throughout the whole experiment, the fibronectin was maintained in an aqueous environment. The PEG coating remained on the area surrounding the fibronectin features to prevent nonspecific cell adhesion. To visualize the patterned fibronectin features, immunostaining was performed using rabbit anti-fibronectin antibody (Sigma-Aldrich) and Alexa Fluor 488 conjugated secondary antibody (Invitrogen), following the manufacturer's instructions.

3.2.3 Cell Seeding, Adhesion and Proliferation

Human oral squamous cell carcinoma (OSCC3; a kind gift from Peter Polverini, University of Michigan) and human prostate carcinoma (DU145) cells (American Type Culture Collection) were routinely cultured in Dulbecco's modified Eagle's minimum essential medium (DMEM, Gibco) and Eagle's minimum essential medium (EMEM, Gibco) respectively, supplemented with 10% fetal bovine serum (FBS) and 1% penicillin-streptomycin. Harvested cells were run through a 40μm mesh cell strainer to help break up cell clusters. 10^5 cells in media with 5% FBS were seeded onto each chip. The chips were gently shaken to help distribute the cells evenly, and then left undisturbed for 2 h to establish cell adhesion. Finally, the chips were rinsed to remove non-adherent cells and then cultured in fresh media for a maximum of up to 48 h.

During the course of the experiment, the cells were monitored using phase contrast microscopy (Carl Zeiss AX.10 Observer Z1 inverted microscope). The proliferation index of the cells cultured on each chip was calculated as the ratio:

$$\frac{\text{number of cells per feature at "x" hours post-adhesion}}{\text{number of cells per feature at 4 hours post-adhesion}}$$

where “x” represents the time point of 24 or 48 h post-adhesion.

For these calculations, the number of cells was determined by taking at least 10 representative images of each chip and counting the number of cells on each image. This analysis was repeated for 3 chips per time point and the cell numbers were averaged.

3.2.4 Fluorescent Staining of Cells

At 24 h of sustained culture following cell adhesion, the cells were fixed with 10% formaldehyde in PBS. The nuclei and cytoskeleton of OSCC3 cells were stained with 4',6-diamidino-2-phenylindole (DAPI, Invitrogen) and Alexa Fluor 594 conjugated phalloidin (Invitrogen) respectively, following the manufacturer’s protocols. E-cadherin immunostaining of DU145 cells was performed with an anti E-cadherin antibody (BD Biosciences) and Alexa Fluor 488 conjugated secondary antibody (Invitrogen); counterstaining was conducted with DAPI. The fluorescently stained chips were mounted onto microscope slides with a drop of Prolong Gold antifade reagent (Invitrogen) and imaged using an Zeiss inverted epifluorescence microscope.

3.2.5 Image Analyses of Fluorescently Stained Chips

The surface area of cell spreading on fibronectin was quantified using AxioVision software (Carl Zeiss Microimaging). The total number of cells on each chip and the average cell number per occupied feature were determined by semi-automated counting of the nuclei in the DAPI fluorescence channel. At least 10 images were collected from random positions on each chip for the image analyses.

3.2.6 Cytokine Antibody Arrays and Enzyme-Linked Immunoassays for Screening of Angiogenic Factors

After 24 h of sustained culture following cell adhesion on the PeelArrays, the culture medium was collected from each chip. Human cytokine antibody arrays 3.0 (Panomics) were used to broadly screen for angiogenic factors that were differentially secreted by cells cultured on chips with 20μm x 20μm features and 40μm x 40μm features. Additionally the medium was analyzed using commercially available ELISA kits (Quantikine, R&D System) to more accurately measure the concentrations of VEGF, IL-8 and bFGF. Thereafter, the total amount of each angiogenic factor secreted by tumor cells cultured on the different chips was calculated. All reported values of angiogenic factors secretions have been normalized to the total number of cells per chip quantified as described above.

3.2.7 Inhibition of E-cadherin Signaling

DU145 cells expressing E-cadherin were cultured on conventional glass coverslips. To block E-cadherin signaling, cells were pre-incubated with 10μg/mL of anti E-cadherin antibody (Chemicon International) prior to seeding. Subsequently, the culture medium was supplemented with the same concentration of anti E-cadherin antibody throughout the complete culture period. Control experiments without the

inhibitory antibodies were also performed. Following adhesion, the cells were cultured for 24 h and then stained for nuclei and E-cadherin as described above. The cell medium for each experimental condition was also collected and analyzed using ELISA for angiogenic factor secretions of VEGF and IL-8.

3.2.8 Statistical Analyses

For each experiment, three independent PeelArray chips (n = 3) were used for each feature size, (*i.e.*, three chips for 20μm x 20μm features, and three chips for 40μm x 40μm features). The two-tailed Student's t-test was used for statistical analyses, and $p < 0.01$ was considered statistically significant, except for the experiment evaluating the temporal maintenance of patterns where $p < 0.02$ was considered statistically significant. The data shown in the graphs represent the mean values, while the associated error bars represent $\pm$ standard deviations.

3.3 RESULTS AND DISCUSSIONS

3.3.1 Patterning Fibronectin Arrays

A parylene-C stencil was utilized on the PeelArray chip to define fibronectin features suitable for culturing arrays of single cells or cell clusters. With standard photolithography, micrometer-sized openings of any geometry can be easily fabricated on parylene for a variety of large-area substrates with accuracy and precision. 20μm x 20μm was chosen as the feature dimension for patterning single cells, commensurate with the average surface area of a single cell adhered onto the surface of a conventional culture dish ($440 \pm 130 \mu m^2$). It was reasoned that increasing the feature width by two-fold, as in the case of 40μm x 40μm features, would be appropriate for patterning a cluster of four cells on each feature island. Each feature was separated from the adjacent feature by a distance of 70μm (~3.5 times the width of an adhered

cell) to ensure that cells could only physically interact within the feature, but not between feature islands. To ensure similar cell numbers for the 20μm x 20μm and 40μm x 40μm arrays, the total area of patterned features was kept constant for both conditions.

The features fabricated with the parylene stencils were 20.2μm x 20.2μm or 40.0μm x 40.0μm (Figure 3.2(a) and 3.2(b), left panels), as determined with differential interference contrast microscopy images. Using these parylene stencils, arrays of 20.2μm x 20.2μm or 39.6μm x 39.6μm fibronectin features were patterned, as analyzed from the fluorescent immunostained images taken at random positions on the chips (Figure 3.2(a) and 3.2(b), right panels). The parylene stencil on the PeelArray chip was easily peeled off without any residue, maintaining the integrity of the patterned fibronectin features and leaving a non-adhesive background on the chip (Figure 3.2(a) and 3.2(b), right hand panels).

The fractions of

$$\frac{\text{fibronectin feature width}}{\text{parylene feature width}}$$

were 1.00 and 0.99 for the chips with 20μm x 20μm features and 40μm x 40μm features, respectively, while the fractions of

$$\frac{\text{fibronectin feature area}}{\text{parylene feature area}}$$

were 1.00 and 0.98 (Figure 3.2(c)). Collectively, these results indicate that large arrays of fibronectin features can be patterned uniformly across the chip area and faithfully reproduce the feature sizes of the parylene stencil. Importantly, this approach does not compromise the bioactivity of the patterned protein, since the protein is maintained in an aqueous environment throughout the whole patterning process and experiment.

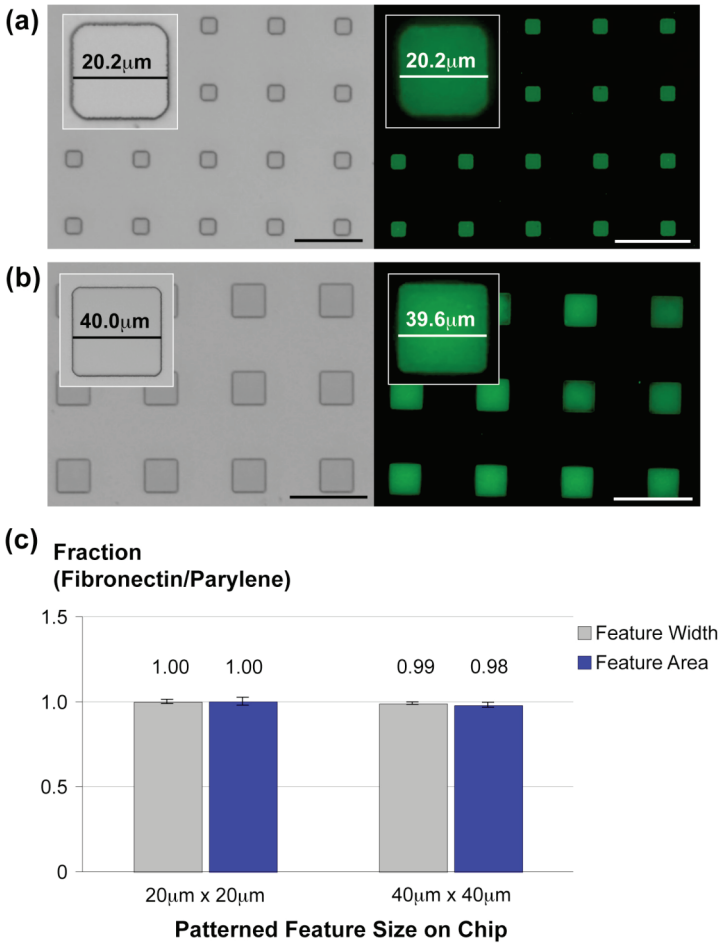

Figure 3.2 Morphology and sizes of the etched 20µm x 20µm ((a), left) and 40µm x 40µm ((b), left) parylene features on the PeelArray chip as evaluated by differential interference contrast microscopy. Morphology and sizes of the corresponding fibronectin patterns after peeling off the parylene template and visualization by immunofluorescent staining of fibronectin (20µm x 20µm [(a), right] and 40µm x 40µm [(b), right] features). (c) Accuracy of fibronectin micropatterning by PeelArray technology.. Inserts show zoomed-in features. Scale bars represent 100µm, unless noted otherwise.

3.3.2 Establishment of OSCC3 Single Cells and Cell Clusters Arrays

OSCC3 cells are representative of an aggressive form of oral epithelial cancer mediated by microenvironmentally controlled angiogenic potential [28, 29]. Using the PeelArray chips, large uniform arrays of OSCC3 cells were established and cultured in the presence or absence of cell-cell interactions for 24 h post-adhesion (Figure 3.3(a)). Fluorescent staining of the cell nuclei, patterned fibronectin and the cell cytoskeleton enabled the visualization and quantification of the number of cells adhered onto the PeelArray chips and the surface area of a cell spreading.

To enable studies in which cell behavior can be tested as a function of variations in direct cell-cell contact rather than differences in paracrine signaling, similar cell numbers were cultured on both 20μm x 20μm and 40μm x 40μm arrays by retaining the total adhesive area in both conditions. More specifically, the total cell number per chip was 33,000 $\pm$ 8,000 cells for the 20μm x 20μm arrays, and 40,000 $\pm$ 6,000 cells for the 40μm x 40μm arrays; no statistically significant differences were detected between the two conditions.

Each 20μm x 20μm feature was occupied by an average of 1.3 cells, while each 40μm x 40μm was occupied by an average of 3.1 cells (Figure 3.3(b)). The disparity between the actual and expected average cell number on the 20μm x 20μm array chip is due to double binding of cells, which occurred for less than 27% of all occupied features. The lower than expected cell number (actual 3.1 *vs*. expected 4 cells per feature) for the 40μm x 40μm array chip raised the question as to whether this difference may be due to increased cell spreading of individual cells on the larger fibronectin features. Since adhesion-dependent changes in cell morphology alter cell behavior [30], the average cell surface area was quantified and a cell shape factor (maximum length/minimum width) for the cells spreading on the fibronectin features was determined. The results indicate no statistically significant difference in the cell

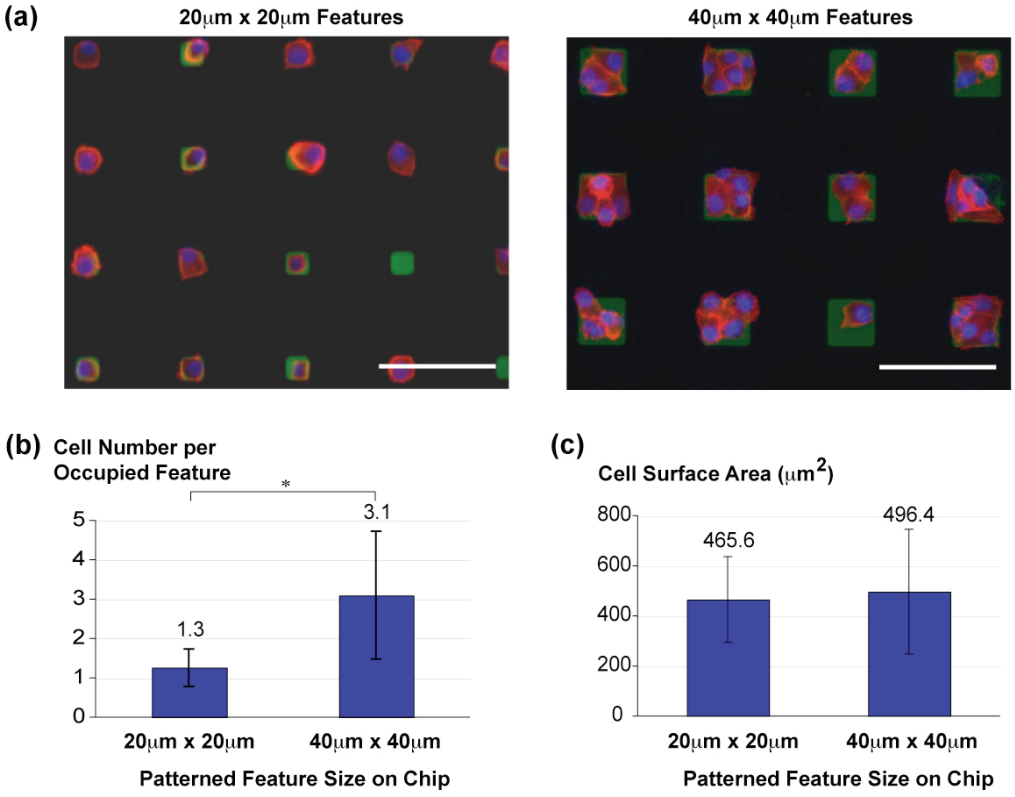

Figure 3.3 Arrays of single cells and cell clusters as developed by culturing OSCC3 cells on PeelArray chips with 20µm x 20µm ((a), left) and 40µm x 40µm ((a), right) features, respectively. Visualization was performed by fluorescent staining of the tumor cells (nuclei [DAPI, blue], cytoskeleton [phalloidin, red]) and patterned fibronectin (anti-human fibronectin, green). (b) Average number of OSCC3 cells per fibronectin feature on the different chips as quantified by image analysis (* $p < 0.01$). (c) The surface area of individual OSCC3 cells adhering onto fibronectin features of single cells arrays was quantitatively similar to the surface area of an individual cell in the clusters adhering onto fibronectin features of the cell cluster arrays (C). Scale bars represent 100µm.

surface area between the different conditions (Figure 3.3(c)). Accordingly, the cell shape factor was similar for cells adhering onto the fibronectin features for single cells arrays (1.47±0.41) and cell cluster arrays (1.43±0.16). These results suggest that the lower than expected cell number on the 40μm x 40μm features was not due to altered cell spreading.

The two major design goals for the 20μm x 20μm array chip were: i) to maintain individual tumor cells devoid of direct physical cell-cell contact, and ii) to create patterns with a high enough number of cells to ensure detectable levels of secreted pro-angiogenic factors by ELISA.

To develop a large array of single cells, different feature widths (10, 15, 20, and 25μm features) were systematically tested. It was found that the 20μm x 20μm feature, as proportional to the size of an adhered OSCC3 cell in conventional 2D culture (440±130μm^2), supported the long-term culture of single cells in the experimental setup. 25μm x 25μm features promoted the adhesion of double cells, while the cells did not adhere onto the 10μm x 10μm features. On the 15μm x 15μm features, cells initially adhered but detached within 24 h, likely due to an inability of the cells to appropriately adhere and spread. These results are shown in Figure 3.4.

Various types of PEG coatings were investigated for their ability to minimize nonspecific cell adhesion in the regions surrounding the fibronectin patterns (Figure 3.5). The commercial PEG coating (Figure 3.5(b)) was the best in reducing cell adhesion, followed by the manual PEG-silane coating (Figure 3.5(a)). On the contrary, the MVD deposited PEG promoted cell adhesion (Figure 3.5(c)).

3.3.3 Temporal Maintenance of Cell Patterns

To determine an appropriate time frame for analysis of angiogenic factor secretion, the establishment and maintenance of defined single cells or cell clusters

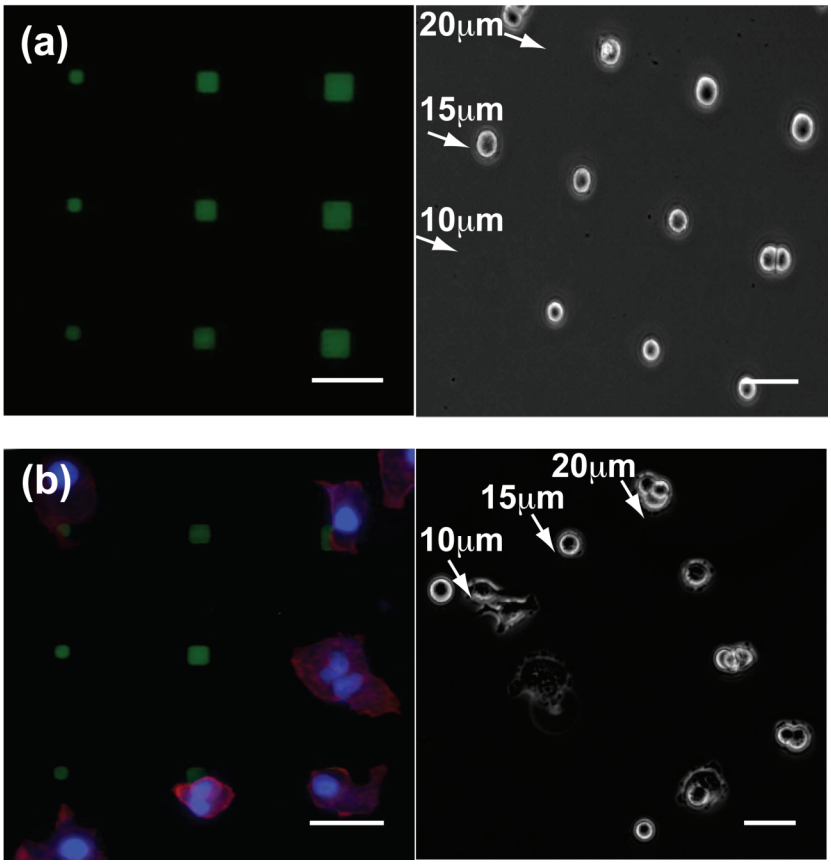

Figure 3.4 Cell adhesion dependence on fibronectin feature size. (a) Left panel: Fluorescent image showing array of 10μm x 10μm, 15μm x 15μm, and 20μm x 20μm square fibronectin (green) features. Right panel: Phase contrast microscopy image showing OSCC3 cells adhered to the fibronectin features 4h after seeding. (b) Left panel: Fluorescent image showing cells that remained on the fibronectin (green) features after 48 h after seeding. Cells were nuclear-stained with DAPI (blue) and phalloidin (red). Cells were adhered mostly on the 20μm x 20μm fibronectin features. Right panel: Phase contrast microscopy image showing cells mostly adhered to the 20μm x 20μm fibronectin features at 48 h.

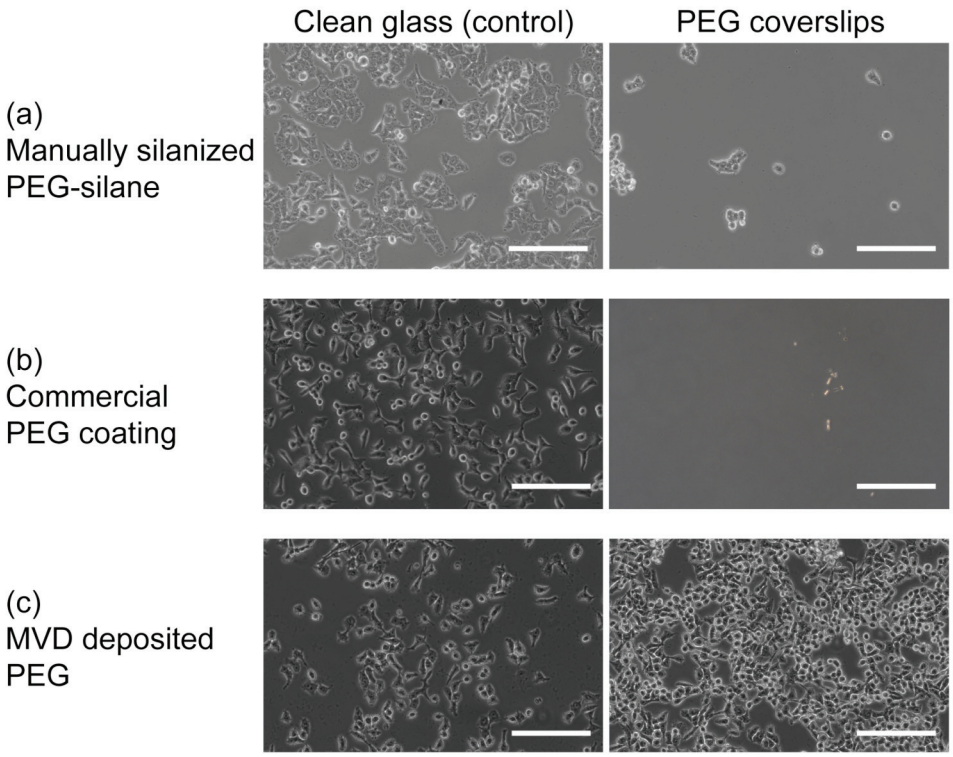

Figure 3.5 PEG coatings tested for reducing nonspecific cell adhesion. The left hand panels show the control glass coverslips without any coatings for each experiment. The right hand panels show (a) manually silanized PEG-silane (Gelest), (b) commercial PEG coated coverslips from Microsurfaces, and (c) MVD deposited PEG. The commercial PEG coverslips reduced cell adhesion the most, while the MVD deposited PEG actually promoted cell adhesion.

were investigated as a function of time (Figure 3.6(a)). Arrays of single cells or cell clusters were established on the fibronectin patterns at 4 h post-adhesion. At 24 h post-adhesion, the spatial patterns of the cells were still robustly maintained for both feature sizes. At 48 h post-adhesion, the cells had undergone proliferation, and more than one cell occupied the individual features on the 20μm x 20μm array chips.

Cell-cell interactions are involved in cell proliferation [31, 32]. To assess whether single tumor cells exhibit different proliferative capacities as compared to tumor cell clusters, the proliferation index of OSCC3 cells was quantified. At 24 h post-adhesion, no significant differences were detected between the different fibronectin feature sizes. At 48 h post-adhesion, the proliferation index of the cells on the 20μm x 20μm features was 1.3, whereas cells cultured on the 40μm x 40μm features exhibited a significantly enhanced proliferation index of 1.8 (Figure 3.6(b)). As a comparison, OSCC3 cells cultured in petri-dishes coated with fibronectin exhibited a proliferation index of 2.0 over 5 days. These results indicate that cell-cell interactions promote the proliferative capacity of OSCC3 cells. Additionally, a culture period of 24 h may be appropriate to both maintain defined cultures of individual cells or clusters of cells while allowing for the onset and establishment of cellular pathways that are involved in expression of angiogenic factors in response to varying cell-cell interactions. Phosphatidylinositol 3-kinase (PI3K) is a likely mediator of increased proliferation on the cell cluster arrays and PI3K inhibitors may be used to block proliferation on the chips in an effort to maintain similar cell numbers over time [32]. However, this approach would compromise the ability to test angiogenic factor secretions in response to cell-cell interactions as PI3K inhibition down-regulates IL-8 secretion [33].

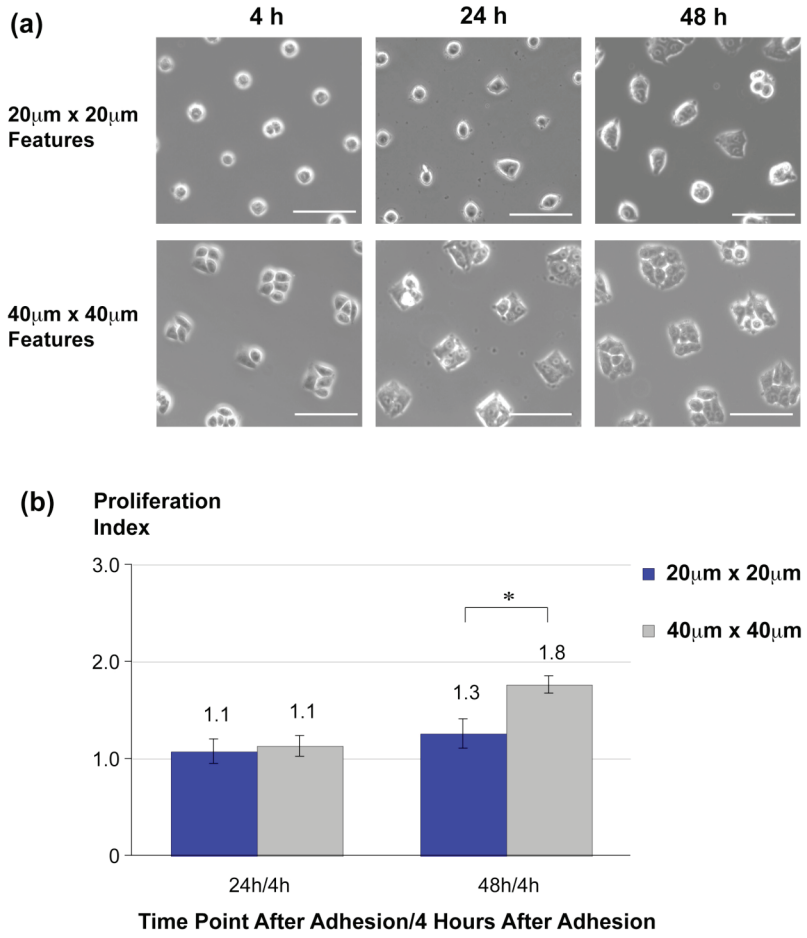

Figure 3.6 (a) Patterns of single cells on 20μm x 20μm features and cell clusters on 40μm x 40μm features over time. At 24 hours post-adhesion, the fidelity of both the single cells and cell cluster pattern is robustly maintained, while the spatial definition of the pattern morphology decreases at 48 hours post-adhesion. (b) OSCC3 proliferation represented as a function of cell-cell interactions. The proliferation index of these cells was significantly enhanced on the 40μm x 40μm features as compared to the 20μm x 20μm features at 48 hours post-adhesion (* $p < 0.02$). No statistically significant difference was observed at 24 hours. Scale bars represent 100μm.

3.3.4 Patterned Arrays of DU145 Expressing E-Cadherin

E-cadherins are involved in adherens junctions formation and impact the signaling of cells in response to cell-cell interactions. OSCC3 cells are representative of a highly invasive tumor cell line that lack expression of E-cadherin [9]. To demonstrate the broad utility of the PeelArray chip in patterning different cell types, and to assess the presence of E-cadherin at cell junctions developed between cells on 40μm x 40μm arrays, but not the 20μm x 20μm arrays, arrays of E-cadherin positive DU145 human prostate carcinoma cells [34].

DU145 cells cultured on the chips over 24 h post-adhesion confirmed that the cell patterns could be temporally maintained, similar to the OSCC3 cells (Figure 3.7(a)). As expected, the average cell number per occupied feature was significantly higher ($p < 0.01$) on the 40μm x 40μm features in comparison with the 20μm x 20μm features (Figure 3.7(b)). In the case of single cells arrays, E-cadherin was diffusively distributed throughout the cells (Figure 3.7(c), left panel). However, for the cell cluster arrays, it was observed that E-cadherin was localized at the boundaries where the cells were physically in contact with each other, likely due to the formation of adherens junctions (Figure 3.7(c), right panel). Consequently, the PeelArray chips are suitable for patterning a variety of cell types over sustained culture periods and studying the effect of cell-cell interactions, and possibly E- cadherin, on their proliferative and angiogenic behavior.

3.3.5 Regulation of Angiogenic Factor Secretion by Cell-Cell Interactions

To determine the effect of cell-cell interactions on the angiogenic potential of cancer cells, VEGF, bFGF and IL-8 secretion by OSCC3 and DU145 cells on the PeelArray chips with different feature sizes were quantified. In the presence of cell-cell interactions, VEGF secretion was increased for both OSCC3 and DU145 cell

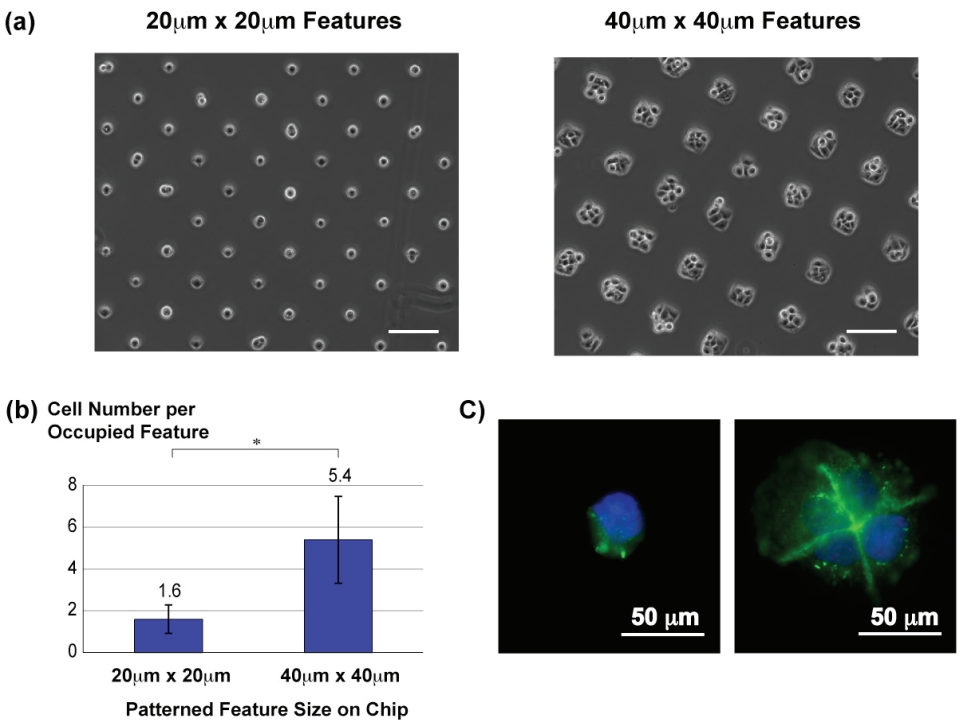

Figure 3.7 (a) Micropatterning of E-cadherin expressing DU145 prostate cancer cells on single cells arrays (20μm x 20μm features) and cell cluster arrays (40μm x 40μm features) as visualized by phase contrast microscopy. (b) The PeelArray chips allowed controlling the number of cell-cell interactions by patterning different sizes of fibronectin features. (c) On cell cluster arrays E-cadherin localized to sites of cell-cell interactions, while on single cells arrays E-cadherin was diffusively distributed throughout the cells as indicated by immunofluorescent staining of E-cadherin (green) and counterstaining with DAPI (blue). Scale bars represent 100μm, unless noted otherwise.

lines: VEGF secretion was up-regulated in cell clusters by 4.2-fold as compared to single cells (29.7 *vs.* 7.0 pg/10,000 cells, $p < 0.01$) for OSCC3 cells and by 1.9-fold (93.4 *vs.* 49.3 pg/10,000 cells, $p < 0.01$) for DU145 cells (Figure 3.8(a)). In contrast, increased cell-cell interactions resulted in an opposite trend of IL-8 secretion between OSCC3 and DU145 cells. More specifically, IL-8 secretion was up-regulated in cell clusters by 2.3-fold as compared to single cells (20.9 *vs.* 9.1 pg/10,000 cells, $p < 0.01$) for DU145 cells, but down-regulated by 2.3-fold (25.9 *vs.* 11.4 pg/10,000 cells, $p < 0.01$) for OSCC3 cells (Figure 3.8(b)). The levels of bFGF secretions were negligibly low under the tested conditions. To more broadly evaluate the angiogenic factors secretion profile in these studies, the collected cell culture medium was additionally analyzed via cytokine antibody arrays. Results from the antibody arrays indicate that interleukin-4 (IL-4) may also be differentially regulated in the presence and absence of cell-cell interactions.

Both VEGF and IL-8 expression regulate tumor angiogenesis as a function of microenvironmental conditions [3-5]. Tumor proliferation beyond a critical mass induces hypoxia, which in turn activates the angiogenic switch [10, 35]. The results from this work here indicate that cell-cell interactions may promote angiogenesis even before the onset of hypoxia through up-regulation of VEGF. Furthermore, cell-cell interactions may play a similar role in stimulating IL-8 mediated angiogenesis as suggested by these results with DU145 cells (Figure 3.8(b)). Accordingly, previously reported data indicate that loss of E-cadherin-mediated cell-cell adhesion down-regulates IL-8 [6]. Nevertheless, increased cell-cell interactions led to decreased IL-8 secretion in E-cadherin negative OSCC3 cells in this work. Epithelial-mesenchymal transition (EMT), a process involved in tumor invasion and metastasis, is characterized by a decrease in epithelial cell-cell adhesion due to loss of E-cadherin [29]. As IL-8 expression is positively correlated with enhanced metastatic

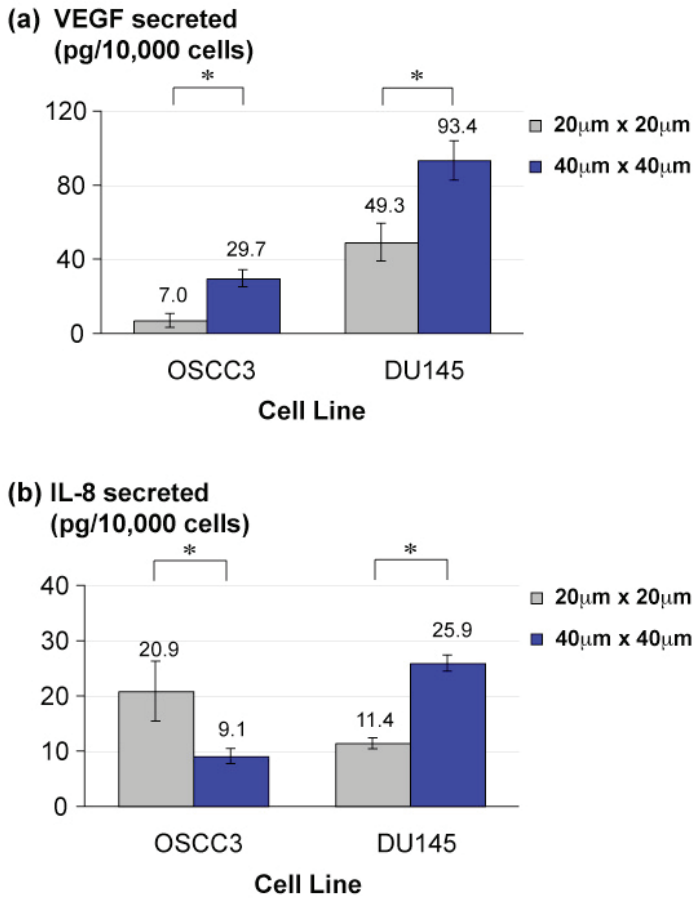

Figure 3.8 (a) VEGF secretion is upregulated in cell clusters as compared to single cells (* $p < 0.01$) for both OSCC3 and DU145 cells, indicating a synergistic role of cell-cell interactions in the up-regulation of VEGF in tumors. (b) IL-8 secretion was down-regulated in cell clusters as compared to single cells for OSCC3 cells, while the converse (*$p < 0.01$) was observed for DU145 cells, suggesting that the regulation of IL-8 secretion in response to varying cell-cell interactions may be cell type dependent (* $p < 0.01$).

potential and tumor cell migration [36, 37], the results in Figure 3.8(b) may suggest that decreased interactions between cells that have undergone EMT and hence loss of E-cadherin, could promote metastasis by up-regulating IL-8.

While these results indicate that increased cell-cell interactions regulate angiogenic factor secretions via modulating E-cadherin signaling, it has to be noted that other microenvironmental changes coincide with higher cell densities. For example, local changes in metabolite levels, pH, oxygen tension, and ECM concentration may affect the angiogenic potential of tumor cells on the subcellular level [5, 38]. By integrating microfluidic channels for subcellular positioning of small molecules [39], the herein described array technology has the potential to enable analysis of local changes of soluble factors in the future.

3.3.6 E-Cadherin and Its Role in Regulating Angiogenic Factor Secretion by Cell-Cell Interactions

To confirm the biological significance of the findings in this study and define a possible role of E-cadherin in VEGF and IL-8 secretions, E-cadherin signaling was inhibited in conventional two-dimensional (2D) culture of DU145 cells. Specifically, E-cadherin was blocked by supplementing the cell culture medium with a neutralizing anti E-cadherin antibody. Fluorescent immunostaining at 24 h after administration of the inhibitor confirmed that E-cadherin was prevented from localizing to sites of cell-cell interactions and hence, the associated signaling (Figure 3.9(a)). Subsequent analysis of VEGF and IL-8 secretions in the presence and absence of E-cadherin inhibitor further revealed that E-cadherin plays a primary role in the upregulation of VEGF and IL-8 secretions by DU145 cells as a function of enhanced cell-cell interactions (Figure 3.9(b)). This data supports the conclusions drawn from the earlier experimental results in Figure 3.8.

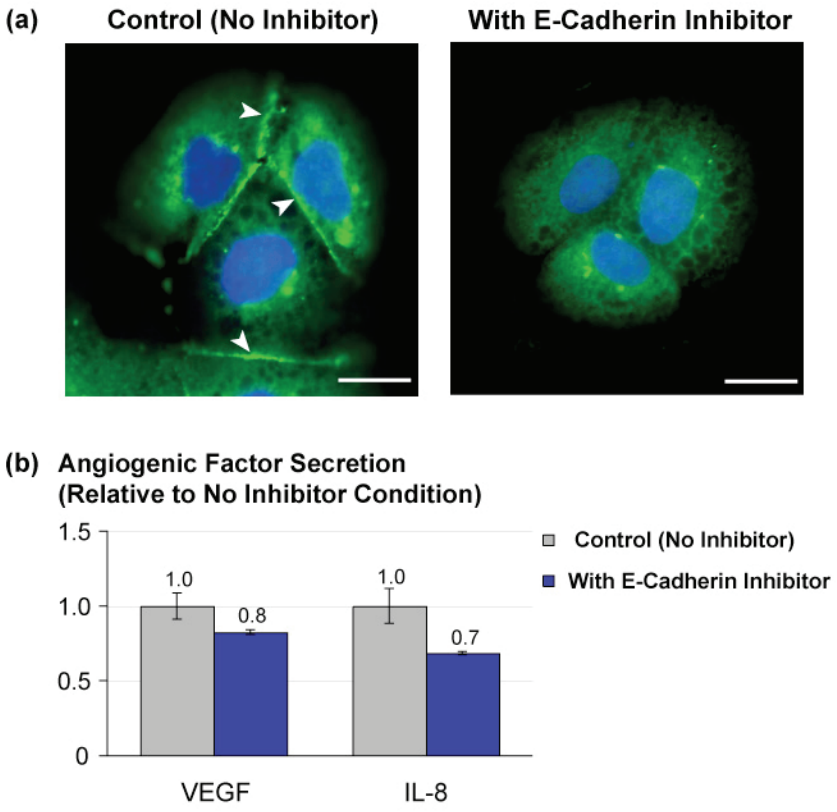

Figure 3.9 (a) Fluorescent immunostaining of E-cadherin (green) and counterstaining with DAPI (blue) in conventional monolayer culture confirmed that administration of E-cadherin blocking antibody prevented the localization of E-cadherin to sites of cell-cell interactions (arrows). (b) Antibody-mediated inhibition of E-cadherin signaling led to a downregulation in VEGF and IL-8 secretions relative to the control conditions. Scale bars represent 20μm.

In summary, this body of work indicates that cell-cell interaction play a synergistic role in regulating the expression of VEGF and IL-8, and that they may work in concert not solely in angiogenesis, but perhaps also in other processes involved in cancer progression (*e.g.* EMT). The PeelArray technology can further quantify the underlying molecular mechanisms, and define the role of E-cadherin in cell-cell contact mediated regulation of angiogenic factor secretion.

3.4 CONCLUSIONS

A PeelArray chip was fabricated that is capable of reproducibly patterning and culturing a large uniform array of cells in the absence or presence of direct cell-cell contact. The results from this study indicate that clusters of tumor cells exhibit enhanced proliferative and angiogenic potential as compared to individual tumor cells, and that these effects may play an important role in the regulation of tumor progression and angiogenesis, even before the onset of tumor hypoxia.

The PeelArray chips are simple to use and broadly applicable, although they are particularly useful for quantitative studies in which a uniform representation of patterned biomaterial on the whole chip is crucial. Such applications may include studies of cellular secretions in co-cultures of multiple cells [26], studies of microenvironmental effects on stem cells [40], single cells behavior [41, 42], mapping global gene expression networks and drug screening [43-45].

REFERENCES

1. Bissell, M. J.; Radisky, D., Putting tumours in context. *Nature Reviews Cancer* 2001, 1, 46-54.
2. Hanahan, D.; Weinberg, R. A., The hallmarks of cancer. *Cell* 2000, 100, 57-70.
3. De, S.; Razorenova, O.; McCabe, N. P.; O'Toole, T.; Qin, J.; Byzova, T. V., VEGF-integrin interplay controls tumor growth and vascularization. *Proceedings of the National Academy of Sciences of the United States of America* 2005, 102, 7589-7594.
4. Lowrie, A. G.; Salter, D. M.; Ross, J. A., Latent effects of fibronectin, alpha 5 beta 1 integrin, alpha v beta 5 integrin and the cytoskeleton regulate pancreatic carcinoma cell IL-8 secretion. *British Journal of Cancer* 2004, 91, 1327-1334.
5. Fischbach, C.; Kong, H. J.; Hsiong, S. X.; Evangelista, M. B.; Yuen, W.; Mooney, D. J., Cancer cell angiogenic capability is regulated by 3D culture and integrin engagement. *Proceedings of the National Academy of Sciences of the United States of America* 2009, 106, 399-404.
6. Grzesiak, J. J.; Smith, K. C.; Chalberg, C.; Burton, D. W.; Deftos, L.; Bouvet, M., Type I collagen and divalent cation shifts disrupt cell-cell adhesion, increase migration, and decrease PTHrP, IL-6, and IL-8 expression in pancreatic cancer cells. *International Journal of Gastrointestinal Cancer* 2005, 36, 131-146.
7. Ahmad, S. A.; Jung, Y. D.; Liu, W. B.; Reinmuth, N.; Parikh, A.; Stoeltzing, O.; Fan, F.; Ellis, L. M., The role of the microenvironment and intercellular cross-talk in tumor angiogenesis. *Seminars in Cancer Biology* 2002, 12, 105-112.

8. Kim, S.; Bell, K.; Mousa, S. A.; Varner, J. A., Regulation of angiogenesis in vivo by ligation of integrin alpha 5 beta 1 with the central cell-binding domain of fibronectin. *American Journal of Pathology* 2000, 156, 1345-1362.

9. Fischbach, C.; Chen, R.; Matsumoto, T.; Schmelzle, T.; Brugge, J. S.; Polverini, P. J.; Mooney, D. J., Engineering tumors with 3D scaffolds. *Nature Methods* 2007, 4, 855-860.

10. Kerbel, R.; Folkman, J., Clinical translation of angiogenesis inhibitors. *Nature Reviews Cancer* 2002, 2, 727-739.

11. Singhvi, R.; Kumar, A.; Lopez, G. P.; Stephanopoulos, G. N.; Wang, D. I. C.; Whitesides, G. M.; Ingber, D. E., Engineering cell-shape and function. *Science* 1994, 264, 696-698.

12. Chen, C. S.; Mrksich, M.; Huang, S.; Whitesides, G. M.; Ingber, D. E., Micropatterned surfaces for control of cell shape, position, and function. *Biotechnology Progress* 1998, 14, 356-363.

13. Cui, Z., Soft lithography. In *Nanofabrication: Principles, capabilities and limits*, Springer Science: New York, NY, 2008; pp 197-202.

14. Kavic, S. M.; Basson, M. D., Environmental factors of temperature, humidity, serum accumulation, and cell seeding increase colon cancer cell adhesion in vitro, with partial characterization of the serum component responsible for pressure-stimulated adhesion. *Journal of Surgical Research* 2001, 98, 89-96.

15. Glasmastar, K.; Gold, J.; Andersson, A. S.; Sutherland, D. S.; Kasemo, B., Silicone transfer during microcontact printing. *Langmuir* 2003, 19, 5475-5483.

16. Di Carlo, D.; Wu, L. Y.; Lee, L. P., Dynamic single cell culture array. *Lab on a Chip* 2006, 6, 1445-1449.

17. Mittal, N.; Rosenthal, A.; Voldman, J., NDEP microwells for single-cell patterning in physiological media. *Lab on a Chip* 2007, 7, 1146-1153.

18. MacDonald, M. P.; Spalding, G. C.; Dholakia, K., Microfluidic sorting in an optical lattice. *Nature* 2003, 426, 421-424.

19. Tanase, M.; Felton, E. J.; Gray, D. S.; Hultgren, A.; Chen, C. S.; Reich, D. H., Assembly of multicellular constructs and microarrays of cells using magnetic nanowires. *Lab on a Chip* 2005, 5, 598-605.

20. Ino, K.; Okochi, M.; Konishi, N.; Nakatochi, M.; Imai, R.; Shikida, M.; Ito, A.; Honda, H., Cell culture arrays using magnetic force-based cell patterning for dynamic single cell analysis. *Lab on a Chip* 2008, 8, 134-142.

21. Wang, Y. L.; Young, G.; Bachman, M.; Sims, C. E.; Li, G. P.; Allbritton, N. L., Collection and expansion of single cells and colonies released from a micropallet array. *Analytical Chemistry* 2007, 79, 2359-2366.

22. Ilic, B., Craighead, H.G., Topographical patterning of chemically sensitive biological materials using a polymer-based dry lift off. *Biomedical Microdevices* 2000, 2, 317-322.

23. Moran-Mirabal, J. M.; Edel, J. B.; Meyer, G. D.; Throckmorton, D.; Singh, A. K.; Craighead, H. G., Micrometer-sized supported lipid bilayer arrays for bacterial toxin binding studies through total internal reflection fluorescence microscopy. *Biophysical Journal* 2005, 89, 296-305.

24. Moran-Mirabal, J. M.; Tan, C. P.; Orth, R. N.; Williams, E. O.; Craighead, H. G.; Lin, D. M., Controlling microarray spot morphology with polymer liftoff arrays. *Analytical Chemistry* 2007, 79, 1109-1114.

25. Orth, R. N.; Wu, M.; Holowka, D. A.; Craighead, H. G.; Baird, B. A., Mast cell activation on patterned lipid bilayers of subcellular dimensions. *Langmuir* 2003, 19, 1599-1605.

26. Wright, D.; Rajalingam, B.; Selvarasah, S.; Dokmeci, M. R.; Khademhosseini, A., Generation of static and dynamic patterned co-cultures using microfabricated parylene-C stencils. *Lab on a Chip* 2007, 7, 1272-1279.

27. Jinno, S.; Moeller, H. C.; Chen, C. L.; Rajalingam, B.; Chung, B. G.; Dokmeci, M. R.; Khademhosseini, A., Microfabricated multilayer parylene-C stencils for the generation of patterned dynamic co-cultures. *Journal of Biomedical Materials Research Part A* 2008, 86A, 278-288.

28. Lingen, M. W., Angiogenesis in the development of head and neck cancer and its inhibition by chemopreventive agents. *Critical Reviews in Oral Biology & Medicine* 1999, 10, 153-164.

29. Choi, S.; Myers, J. N., Molecular pathogenesis of oral squamous cell carcinoma: Implications for therapy. *Journal of Dental Research* 2008, 87, 14-32.

30. Chen, C. S.; Alonso, J. L.; Ostuni, E.; Whitesides, G. M.; Ingber, D. E., Cell shape provides global control of focal adhesion assembly. *Biochemical and Biophysical Research Communications* 2003, 307, 355-361.

31. Gray, D. S.; Liu, W. F.; Shen, C. J.; Bhadriraju, K.; Nelson, C. M.; Chen, C. S., Engineering amount of cell-cell contact demonstrates biphasic proliferative regulation through RhoA and the actin cytoskeleton. *Experimental Cell Research* 2008, 314, 2846-2854.

32. Nelson, C. M.; Chen, C. S., Cell-cell signaling by direct contact increases cell proliferation via a pi3k-dependent signal. *FEBS Letters* 2002, 514, 238-242.

33. Moscova, M.; Marsh, D. J.; Baxter, R. C., Protein chip discovery of secreted proteins regulated by the phosphatidylinositol 3-kinase pathway in ovarian cancer cell lines. *Cancer Research* 2006, 66, 1376-1383.

34. Chunthapong, J.; Seftor, E. A.; Khalkhali-Ellis, Z.; Seftor, R. E. B.; Amir, S.; Lubaroff, D. M.; Heidger, P. M.; Hendrix, M. J. C., Dual roles of E-cadherin in prostate cancer invasion. *Journal of Cellular Biochemistry* 2004, 91, 649-661.

35. Shweiki, D.; Itin, A.; Soffer, D.; Keshet, E., Vascular endothelial growth-factor induced by hypoxia may mediate hypoxia-initiated angiogenesis. *Nature* 1992, 359, 843-845.

36. De Larco, J. E.; Wuertz, B. R. K.; Rosner, K. A.; Erickson, S. A.; Gamache, D. E.; Manivel, J. C.; Furcht, L. T., A potential role for interleukin-8 in the metastatic phenotype of breast carcinoma cells. *American Journal of Pathology* 2001, 158, 639-+.

37. Xie, K. P.; Wei, D. Y.; Huang, S. Y., Transcriptional anti-angiogenesis therapy of human pancreatic cancer. *Cytokine & Growth Factor Reviews* 2006, 17, 147-156.

38. Fang, J. S.; Gillies, R. D.; Gatenby, R. A., Adaptation to hypoxia and acidosis in carcinogenesis and tumor progression. *Seminars in Cancer Biology* 2008, 18, 330-337.

39. Takayama, S.; Ostuni, E.; LeDuc, P.; Naruse, K.; Ingber, D. E.; Whitesides, G. M., Laminar flows - subcellular positioning of small molecules. *Nature* 2001, 411, 1016-1016.

40. LaBarge, M. A.; Nelson, C. M.; Villadsen, R.; Fridriksdottir, A.; Ruth, J. R.; Stampfer, M. R.; Petersen, O. W.; Bissell, M. J., Human mammary progenitor cell fate decisions are products of interactions with combinatorial microenvironments. *Integrative Biology* 2009, 1, 70-79.

41. Chang, H. H.; Hemberg, M.; Barahona, M.; Ingber, D. E.; Huang, S., Transcriptome-wide noise controls lineage choice in mammalian progenitor cells. *Nature* 2008, 453, 544-U510.

42. Rosenfeld, N.; Young, J. W.; Alon, U.; Swain, P. S.; Elowitz, M. B., Gene regulation at the single-cell level. *Science* 2005, 307, 1962-1965.

43. Regelin, A. E.; Fernholz, E.; Krug, H. F.; Massing, U., High throughput screening method for identification of new lipofection reagents. *Journal of Biomolecular Screening* 2001, 6, 245-254.

44. Ziauddin, J.; Sabatini, D. M., Microarrays of cells expressing defined cDNAs. *Nature* 2001, 411, 107-110.

45. Liotta, L. A.; Espina, V.; Mehta, A. I.; Calvert, V.; Rosenblatt, K.; Geho, D.; Munson, P. J.; Young, L.; Wulfkuhle, J.; Petricoin, E. F., Protein microarrays: Meeting analytical challenges for clinical applications. *Cancer Cell* 2003, 3, 317-325.

CHAPTER 4

CONTROLLING MICROARRAY SPOT MORPHOLOGY WITH PARYLENE PEEL-OFF ARRAYS[4]

4.1 INTRODUCTION

While microarrays have become ubiquitous in biological research, microarray data are widely known to be noisy and imprecise [1]. As the data obtained from deoxyribonucleic acid (DNA) microarray-based experiments consist of measurements of thousands of individual genes, confidence in array data is critically dependent upon the printed spot morphology. However, the dynamics that underlie the drying of complex solutions (e.g., DNA contained within the printing solution) are not completely understood. As a result, variation in spot quality occurs both within and between arrays, affecting the reliability of data obtained from any given array and the ability to reproduce these measurements between arrays [2]. To compensate for the lack of spot uniformity, image analysis programs average pixel intensities across a given spot [3]. Also, a number of printing solutions have been introduced to control the drying rate of individual spots [4, 5]. Because these strategies have had only limited success, the development of novel technologies to produce more uniform spots would have a significant impact on the quality and precision of data from microarray experiments [6, 7].

There is limited understanding of the forces that drive drying patterns on microarrays. Prior studies examining the drying of simple, dilute aqueous solutions

[4] This chapter is a modified and revised form of the publication: Moran-Mirabal, J.M, Tan, C.P., Orth, R.N., Williams, E.O., Craighead, H.G., Lin, D.M., Controlling Microarray Spot Morphology with Polymer Liftoff Arrays, *Analytical Chemistry* 2007, 79, 1109-1114. Tan designed experiments, performed microfabrication and silanization, analyzed data, and wrote the article.

have shown that a droplet placed on a hydrophilic surface results in a pinned contact line at the periphery of the area where the solution and surface meet [8]. As evaporation proceeds, the height of the droplet is reduced, but the contact area remains constant. This establishes a capillary flow at the surface that is driven toward the periphery to maintain the original radius of the spot. Dissolved solids are carried by this capillary flow to the periphery, producing the characteristic "coffee ring" pattern upon drying. Although microarray printing buffers are often more complex than the simple solution described in the coffee ring studies [8], it is hypothesized that this capillary flow could explain the morphologically similar "donut" pattern of hybridization seen in many microarray experiments. As most microarrays are printed on hydrophilic, amine-functionalized surfaces, it is theorized that evaporation of the spotted DNA droplets would drive dissolved nucleic acids to the periphery due to the pinned contact line. Upon hybridization, this would result in increased signal at the periphery of the spot and decreased signal in the center. Data from such "donut"-shaped spots would rely on pixel averaging to compensate for the lack of uniformity of the original printed material.

To ameliorate the uneven DNA deposition problem and improve microarray reproducibility and reliability, a hybrid substrate using photolithographically patterned surfaces was developed in this work. This substrate combines a hydrophobic polymeric (parylene-C) surface with patterned openings that expose an amine-functionalized hydrophilic surface beneath the parylene. DNA spotted on the mixed surface would be subject to distinct capillary flow patterns during drying. In the simplest case, the portion of the droplet in contact with the hydrophobic surface would experience depinned contact line drying, and an inward capillary flow [9]. Through evaporation, the spot would shrink until it covered only the hydrophilic

microfabricated openings, resulting in increased uniformity of deposition due to the high DNA concentration within the openings.

This work reports the fabrication and use of these parylene peel-off microarray substrates to address problems associated with microarray-based experiments. This work shows that the hybrid hydrophobic/hydrophilic nature of the parylene arrays improves DNA deposition, spot uniformity, replication, and reproducibility between microarray experiments as compared with conventional substrates. From experimental observations here, an inward convective flow occurs on these hybrid substrates whereas the opposite behavior is observed on simple, hydrophilic surfaces. These parylene peel-off arrays represent a novel approach toward addressing the common coffee ring issue observed in drying of dilute analytes and could be used to improve deposition of other types of arrays.

4.2 EXPERIMENTAL METHODS

4.2.1 Microarray Substrate Fabrication

Parylene peel-off microarray substrates were fabricated on 1 x 3 inches, 1mm-thick Pyrex glass slides (Esco Products) as previously reported [10, 11]. Substrates were cleaned using piranha solution (1:3 v/v sulfuric acid/30% hydrogen peroxide), followed by a short oxygen plasma clean. Polyethylene glycol (1% in water, 200Da, Sigma-Aldrich) was spun on the substrates to reduce nonspecific binding. A 300nm thin conformal coating of parylene-C was vapor deposited in a PDS-2010 Labcoter 2 Parylene deposition system (Specialty Coating Systems). Shipley 1827 positive photoresist was spun on the substrates to a thickness of 2.7μm and baked at 90 °C. Photolithography was performed using an HTG System III-HR Contact Aligner. The exposed photoresist was developed in MIF300 developer for 60 s, followed by a deionized water rinse, and then dried under nitrogen. Exposed regions of the parylene

film were etched in a reactive oxygen ion plasma chamber, and residual photoresist was removed by washing successively with acetone and isopropanol. Substrates were functionalized for DNA adsorption with 3-aminopropyltrimethoxysilane (APTMS) in a MVD-100 tool (Applied MicroStructures). Control slides were functionalized with APTMS in parallel.

4.2.2 DNA Spot Printing and Hybridization

DNA was spotted using a custom-built microarrayer and 946 quill pins (Telechem International). Ambient humidity was maintained between 55 and 60%. A positive control DNA, which has been shown to be an effective measure of hybridization sensitivity, was printed on all arrays [12]. To print the DNA, a buffer containing 1X SSC/0.005% sarkosyl (subsequently referred to as printing buffer) was used. Slides were postprocessed using 1-methyl-2-pyrollidinone [13]. During the washing phase of the postprocessing, the parylene was peeled away and discarded. Slides were briefly washed successively in three washes of 0.1X SSC, water, and 200 proof ethanol and spun dry. Labeled target was generated using the indirect labeling method [14] and Trizol-purified total ribonucleic acid (RNA) from mouse liver. Slides were hybridized in a HS400 hybridization machine (Tecan), although conventional hybridization coverslips can also be used. Slides were preblocked in 3X SSC/0.1% SDS/1% BSA and hybridized at 45°C in 3X SSC/0.1%SDS/50% formamide/20 mM Tris 8.0/0.1 mg/mL BSA/0.1 μg/mL salmon sperm DNA for 18 h. Unbound fluorescent target was removed by an initial wash in 6X SSC/0.005% Triton X-100 followed by three washes in 0.1X SSC/0.005% Triton X-100, and the slides dried under a stream of argon gas. Slides were scanned using an Axon 4000B scanner (Molecular Devices).

4.2.3 Fluorescent Particle Tracking and Confocal Microscopy

Hybridized slides were imaged with a LSM510 Meta laser scanning microscope (Zeiss), with 532nm laser excitation line, and a Plan-Neofluar 20X/0.5 NA objective. The drying profile of spotted droplets was observed with a camera set to record side views of the droplet. Videos were captured with a Panasonic DVD recorder, and frames were extracted using VirtualDub MPEG software. Droplets of different buffers containing fluorescent latex spheres (10^9 spheres/mL; Molecular Probes) were examined for flow patterns using an Olympus IX71 inverted microscope and a Plapon 10X/0.4 NA objective (NY/NJ Scientific). Videos were recorded as the spheres moved in the drying solution using a Cascade 512 cooled CCD camera (Roper Scientific/Biovision).

4.2.4 Microarray Spot Analysis

Fluorescence microscopy images were analyzed using a custom MATLAB (The Mathworks) program based on Otsu's thresholding algorithm [15]. Once a threshold gray scale level was calculated, the raw image was separated into signal and background areas. A two-pixel exclusion region between signal and background was generated to eliminate pixels that average signal and background values due to the image resolution. The program then calculated the mean, median, and standard deviation of pixel intensities for signal and background regions for every printed spot analyzed and generated representative images for each processing step.

For comparative measurement of uniformity and reproducibility, the percentage standard deviation (PSD) of the signal values was obtained for the analyzed spots. Comparison of the PSD values was used to assess the uniformity of spot morphology via confocal fluorescence microscopy and microarray scanner

images. The PSD was also used to compare reproducibility of spot morphology within and across arrays. The PSD was calculated as follows:

$$\text{PSD} = \frac{\text{Signal intensity standard deviation}}{\text{Mean signal fluorescence intensity}} \times 100$$

4.3 RESULTS AND DISCUSSIONS

4.3.1 Parylene-Based Hybrid Substrate for Conventional Microarray Technology

There are multiple microarray platforms currently in use. The most flexible and frequently employed design uses quill pins to spot a variety of biological materials, including proteins, oligonucleotides, cDNAs, genomic DNA, and others [16]. Because the benefits of the proposed approach can be extended to these applications, the parylene peel-off hybrid substrates were designed for general use with conventional microarray equipment. Glass was used as the base for the parylene peel-off arrays because glass is easily functionalized with silane chemistry and 1 x 3 inches slides can be mounted on most microarraying equipment. For the hydrophobic aspect of the parylene peel-off arrays, parylene was chosen since it is a polymer shown to be photolithographically patterned, is nonreactive, and is compatible with a variety of biological molecules [10, 11]. The fabrication of the parylene peel-off arrays is described in the Experimental Section and depicted in Figure 4.1. Contact angle measurements from a prior experiment confirmed that the parylene surface was not amine-functionalized during silanization (Figure 1.3). DNA was then spotted on parylene peel-off arrays and on control APTMS-coated slides. After printing, the parylene was mechanically “peeled off” from the parylene peel-off arrays, leaving behind the patterned, surface-bound DNA. Then, both sets of arrays were hybridized and processed in parallel using standard protocols [17].

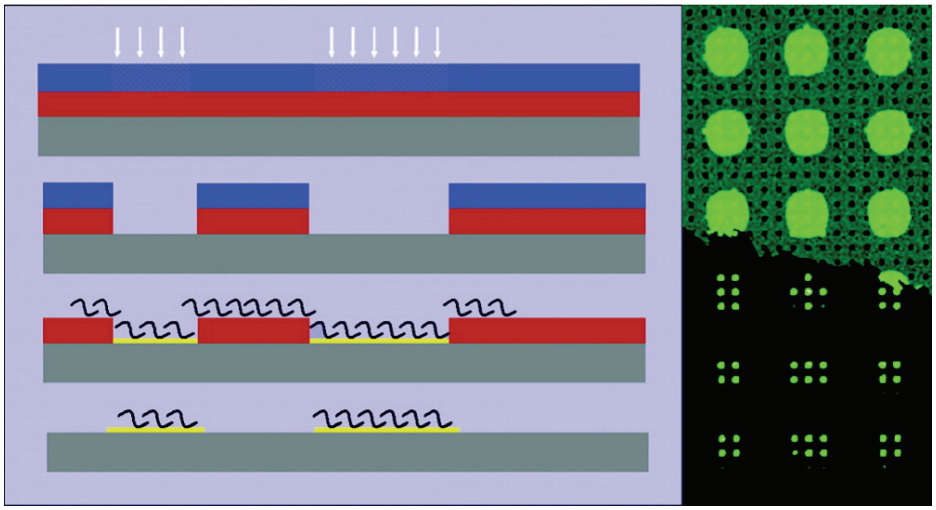

Figure 4.1 Left: fabrication of parylene peel-off arrays. A glass substrate (gray) is coated with parylene (red). Photoresist (blue) is spun on and UV-exposed (white arrows). Exposed resist (cross-hatched area) is removed, and the exposed parylene is etched through. APTMS (yellow) is applied to the exposed glass surface, and DNA is spotted on the surface (black curves). Parylene is then peeled away, leaving behind only the patterned material (bottom). Right: 10μm opening parylene peel-off array. Here, parylene has been partially removed (bottom) after spot printing and drying. Note each printed spot covers multiple openings in the parylene. Each opening covered by a printed spot is considered a subspot for analysis purposes.

4.3.2 Improved Uniformity of Deposition on Parylene Peel-Off Arrays

An advantage of using the parylene peel-off arrays is that the patterning mask can be designed to produce openings of various sizes in the parylene. For the application as a DNA microarray substrate, the openings had to be small enough so that drying was largely governed by the hydrophobic surface while the capillary flow within the hydrophilic openings was minimized. However, the diameter required to achieve this effect could not be predicted a priori. Spot diameters of DNA printed on standard glass slides typically range from 80 to 150μm; parylene peel-off arrays with 10−40μm diameter openings were generated.

An unlabeled, positive control DNA [12]was then printed on these substrates and hybridized with Cy3-labeled target made from total mouse liver RNA. Confocal microscopy was used to assess the uniformity of individual spots. It was observed that for openings with diameters $\geq$ 20μm, DNA dried in a ring-like pattern similar to that of DNA printed on control substrates (Figures 4.2(a), (e)). For 20μm openings, the relative thickness of the ring increased, and more of the opening was filled with the deposited DNA (Figures 4.2(b), (f)). For 10μm openings, the coffee ring pattern was significantly reduced, producing more uniform DNA distribution within the opening (Figures 4.2(c), (g)). While even smaller openings would further improve deposition, most commercial microarray scanners have a maximum resolution of 5 μm/pixel. Thus, insufficient pixel information would be obtained with smaller diameters. Because one of the goals is to make the parylene peel-off arrays compatible with current microarray technology, the opening diameter was maintained at 10μm for the experiments described below.

To quantitatively assess the improvement in uniformity of deposition, the variation of the fluorescence intensity across each printed spot was calculated. Discrimination between signal and background pixel populations was performed with

a MATLAB program based on Otsu's thresholding algorithm [15] as described in the Experimental Section. After the signal and background pixels were identified, the mean and standard deviation from each population was calculated. The PSD was used as a comparative measure of the uniformity of deposition because the standard deviation is a measure of the spread in fluorescence intensity values across each spot. The fraction of the mean signal intensity represented by the standard deviation was calculated to ensure that the observed variations did not stem from differences in the amount of adsorbed material. Figure 4.2(d) shows that the PSD calculated from confocal data for spots printed on control slides is larger than that of spots generated by parylene peel-off arrays with 10-μm openings. The visual and quantitative data obtained from the experiments show that DNA printed and hybridized on parylene peel-off arrays is distributed more uniformly than on control slides.

4.3.3 Uniformity of Intra-Microarray Replicate Spots

A benefit of using 10-μm-wide openings within the parylene stencil is that multiple signals (subspots) are obtained per printed spot. Each one of these highly uniform replicate subspots provides precise data, which represents an obvious advantage over conventional arrays where a single spot is often printed per gene due to spatial constraints. However, because of the relatively low resolution of commercial scanners, each subspot on the parylene peel-off array only generates a small fraction of the pixel information of the average, 100-μm spot. Using a commercial scanner would represent a stringent test of the utility of these subspots, as even small variations in the parylene peel-off array data would have a significant effect on the standard deviation. It would also determine whether existing scanners could be used to analyze data from the parylene peel-off arrays.

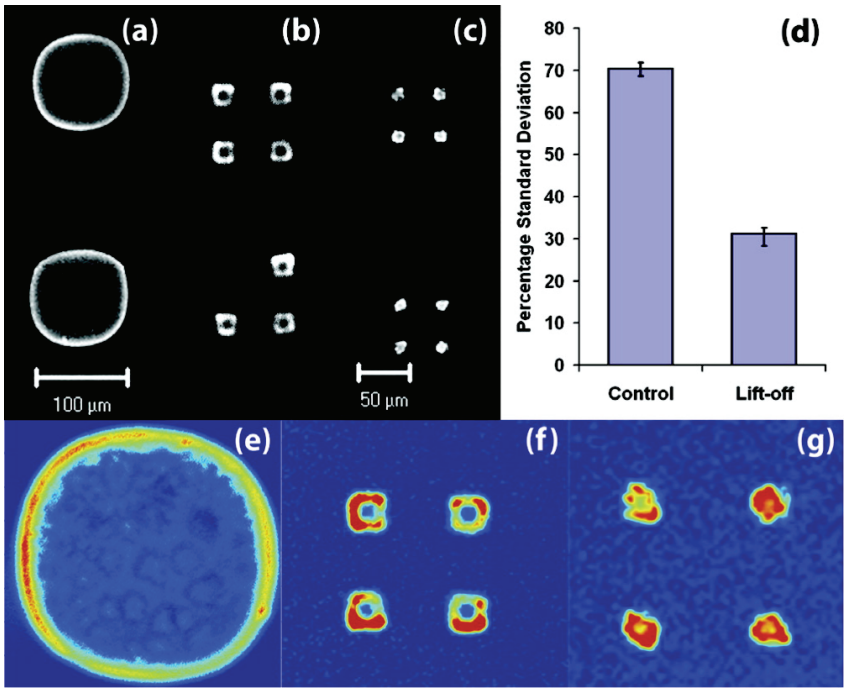

Figure 4.2 Confocal imaging showing the improvement of spot uniformity after hybridization obtained with parylene peel-off arrays. (a–c) Raw images from control and parylene peel-off arrays. (a) Spot printed on amine-functionalized surface shows uneven coffee ring pattern. (b, c) Parylene peel-off arrays with 20- and 10-µm openings. The relative thickness of the coffee ring inside the opening increases as the diameter decreases, yielding the most uniform deposition at 10 µm. Scale is the same for both micropatterned arrays. (d) Comparison of the percentage standard deviation of the mean fluorescence intensity for control vs 10-µm opening parylene arrays. (e–g) Pseudocolor of intensity of arrays in (a–c) for uniformity comparison.

After hybridization and scanning on an Axon scanner (set to 5 μm/pixel resolution), each of the 9−12 subspots generated per printed spot were taken as within-array replicates. The mean and standard deviation of the fluorescence intensity of these replicates was calculated with the algorithm described above. In the simplest case, the PSD can be compared for the population of 9−12 subspots generated per printed spot on the parylene peel-off array against the single printed spot present on the control slide.

However, to gain more insight into the general behavior of these subspots in providing replicate information, the control DNA was spotted four times on each substrate. Each of the four sets of subspots could then be compared against the corresponding spots printed on the standard slide. This experiment was repeated three times and a total of 12 spots and 12 subspot sets were analyzed. The PSD obtained from the sets of subspots generated by each printed spot on parylene peel-off arrays was compared with the PSD for the identical spots on control slides (Figure 4.3).

Variation was greatly reduced for all subspot sets as compared to the spots printed on control slides. Thus, despite the use of a commercial scanner and the concomitant decrease in pixel information associated with the subspot measurements, the data obtained from the subspots was still significantly more precise than that obtained from spots printed on control slides. This is true whether a single spot is printed on each array or if the same DNA is printed multiple times on each array. In the first instance, the subspot data for any given spot (e.g., “spot 1”) is more uniform than that obtained from a spot printed on a control slide. In the latter case, the subspot data across spots (e.g., “spots 1−4”) is less variable than that obtained from a control slide.

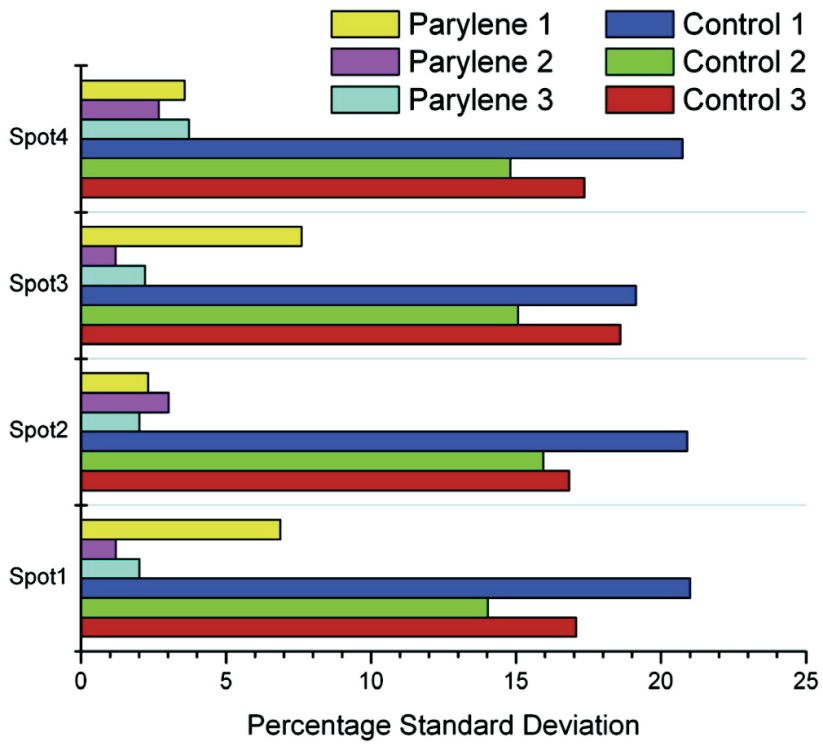

Figure 4.3 Percentage standard deviation from subspot sets generated by individually printed spots. The PSD is lower than that from conventional array spotted data. The PSDs of pixel intensities across each spot are shown for four replicate spots printed on parylene peel-off versus control substrates (3 slide replicates).

4.3.4 Improved Reproducibility from Replicate Microarrays over Standard Arrays

Given the inherent noise in microarray data, technical replicates are often performed using the same RNA source hybridized to two arrays so that the observed measurements can be averaged across experiments. If each gene is printed once on an array, obtaining two measurements for each gene using the same RNA stock can help reduce the effects of variation in printing quality or hybridization conditions. Although the multiple subspots produced on any given parylene peel-off array can improve the precision of the acquired data from that particular slide as described in the previous section, the next test was whether these arrays could improve data acquisition across experiments and arrays at various levels of signal intensity.

Positive control DNA was printed at successive, 2-fold serial dilutions (100 to 0.78 ng/μL) with four replicate spots per dilution. This has been shown to be a means of normalizing data between arrays and enable comparisons of hybridization efficiency between experiments [12]. Comparisons both within and between arrays were performed by comparing measurements from the various spots. All arrays (conventional and parylene peel-off) were processed in parallel and hybridized with an aliquot from a common stock of labeled target. The conditions were designed to be as identical as possible to produce highly similar technical replicates.

After hybridization and scanning, the subspot intensity data across all arrays and dilutions in three independent experiments (12 slides) were determined. Subspot information was averaged for each dilution printed in each slide. Comparison of reproducibility across arrays was determined by averaging pixel intensity across all like arrays and calculating the standard deviation. Significantly lower standard deviation was seen in technical replicates of parylene peel-off arrays than in control arrays (Figure 4.4), arguing for better interarray reproducibility. Thus, despite

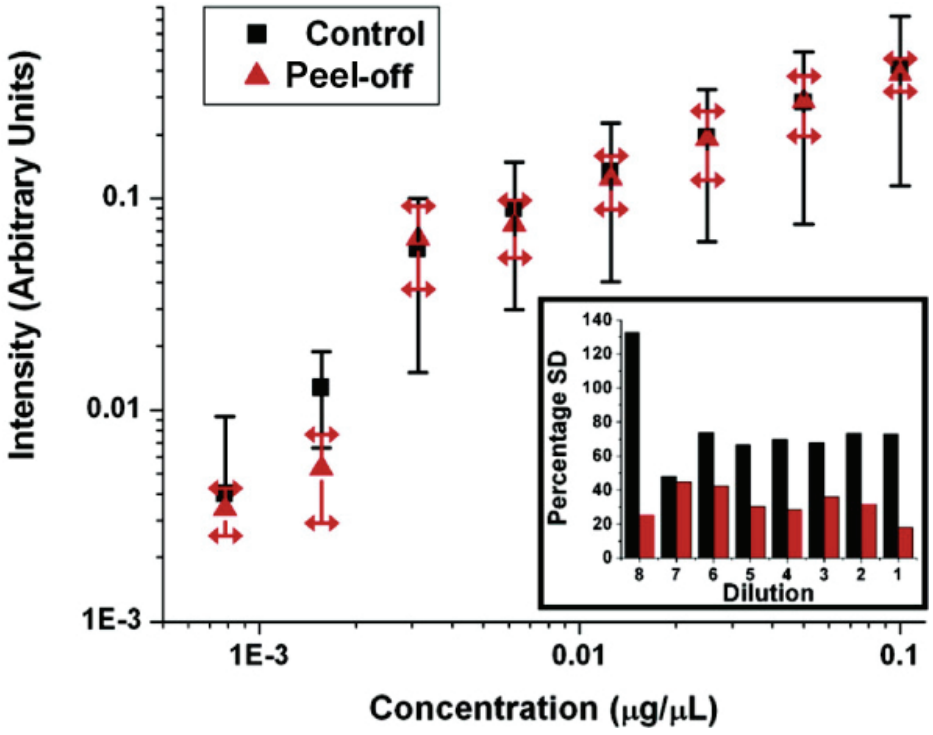

Figure 4.4 Standard deviation associated with measurements of pixel intensities across arrays for successive dilutions. Inset: standard deviation for individual dilutions represented as a percentage of the mean intensity.

performing 12 technical replicates in a manner designed to generate data with highly reduced standard deviations on conventional slides, parylene peel-off arrays still produced more uniform data. While 12 replicates are unlikely to ever be performed in routine experiments, the use of parylene peel-off arrays will improve the quality of data obtained even with just two replicates.

4.3.5 Fluorescent Particle Tracking of Flow Patterns in Drying Spots

To determine whether the increased uniformity of deposition and reproducibility reflect alterations in flow patterns of spotted droplets on the arrays, droplets of printing buffer containing fluorescent latex spheres were spotted on patterned and control surfaces. This approach has been used previously to follow capillary flow in drying droplets of simple solutions [9, 18]. By tracking the fluorescent sphere movement, it was observed the flow in droplets deposited on control substrates was directed toward the periphery of the droplet as shown in Figure 4.5(a). However, flow in droplets deposited on parylene peel-off substrates was directed toward the center of the droplet in Figure 4.5(b). These findings suggest that the capillary flow on parylene peel-off substrates promotes concentration of the material at the center of the droplet while the flow on control surfaces promotes concentration at the periphery. This behavior helps to explain the observation of the reduction of the coffee ring pattern and the enhanced uniformity in the parylene peel-off substrates.

Despite the inward flow, it was observed that the drying profile of a droplet of printing buffer on the patterned slides differed from that of a solution of PBS. As predicted by the model proposed by Deegan and colleagues [8], drying of the aqueous droplet (*i.e.*, PBS) was not constrained by a pinned contact line as seen in Figure 4.5(d). Nevertheless, the droplet containing printing buffer showed a pinned contact line in Figure 4.5(c). Thus, the observed flow behavior cannot be uniquely associated

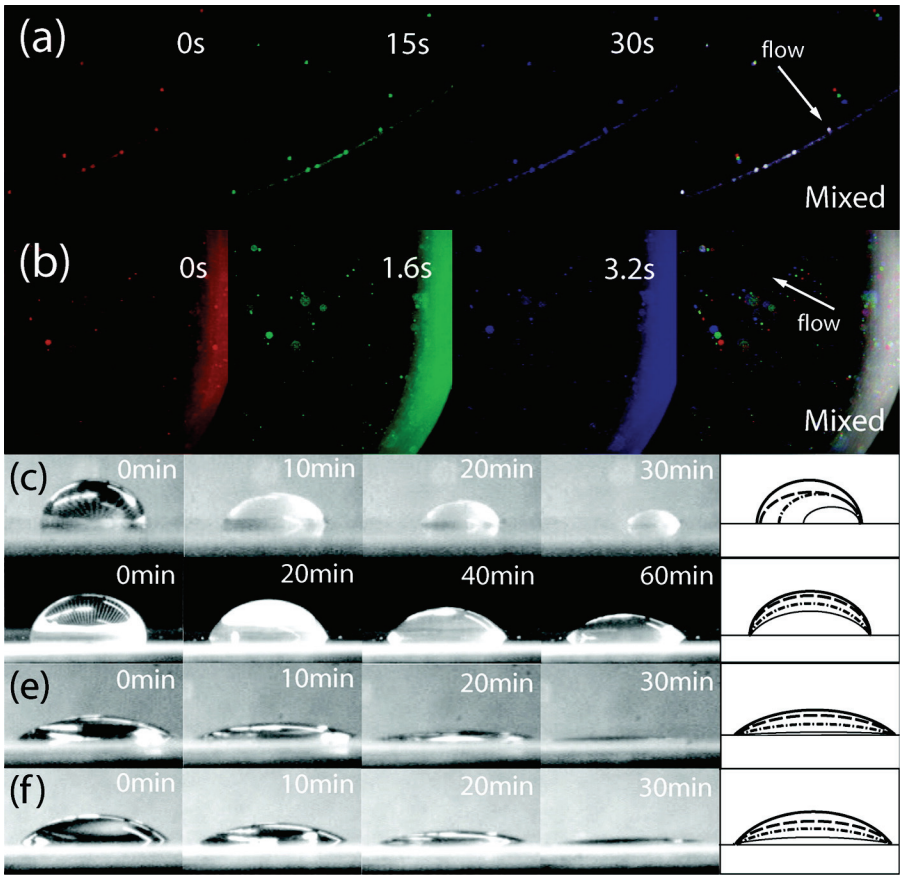

Figure 4.5 Drying behavior of the printing buffer. Drying is different on parylene peel-off substrates than on control slides. Panels a, b: capillary flow behavior near the substrate surface for amine-functionalized control slides (a) and for parylene peel-off substrates (b). Fluorescent beads were used as markers for the flow behavior. Different color images are snapshots in time extracted from recorded videos. Panels (c−f): drying droplet profile for an aqueous solution (PBS) and printing buffer on parylene peel-off and control substrates. Individual images show snapshots of the recorded video as the droplet dried. Final image on each panel shows the droplet profile for each of the previous shots. Treatments: (c) aqueous solution on parylene, (d) printing buffer on parylene, (e) aqueous solution on control slide, and (f) printing buffer on control slide.

with the presence of a pinned contact line as in the proposed model. On the other hand, the drying profiles of both PBS and printing buffer on control surfaces were the same as showin in Figures 4.5(e-f). The observed differences in the drying profiles can be attributed to the presence of a small percentage of detergent in the printing buffer that effectively disrupts the polar interactions of the solution with the parylene substrate. It has previously been shown that the coffee ring pattern can be suppressed by the Marangoni effect, which generates additional vortices in the drying solution [19]. The interactions of a complex fluid (i.e., printing buffer) with a mixed hydrophilic/hydrophobic surface may require further modeling to help explain the observed effects. This is beyond the scope of the present paper, which aims to demonstrate the use of parylene peel-off arrays to improve spot morphology in DNA microarrays.

4.4 CONCLUSIONS

In this work, it has been shown that the parylene peel-off substrates can be easily adapted to conventional microarray technology. The increase in uniformity, replication, and reproducibility demonstrates the advantages of parylene peel-off over conventional arrays. It is anticipated that these results can be applied to other biomolecule arrays [20] (e.g., protein, antibody, RNA) and platforms and should be particularly valuable in creation of matrix-assisted laser desorption/ionization targets. The results in this study suggest that the benefits of parylene peel-off arrays stem directly from the constrained deposition of DNA into targeted openings by the tailored surface properties. The use of these substrates could be extended to experiments that require controlled drying of biological materials, with potential applications such as concentration of dilute analytes [21] or particle self-assembly [22].

REFERENCES

1. Churchill, G. A., Fundamentals of experimental design for cDNA microarrays. *Nature Genetics* 2002, 32, 490-495.
2. Auburn, R. P.; Kreil, D. P.; Meadows, L. A.; Fischer, B.; Matilla, S. S.; Russell, S., Robotic spotting of cDNA and oligonucleotide microarrays. *Trends in Biotechnology* 2005, 23, 374-379.
3. Heyer, L. J.; Moskowitz, D. Z.; Abele, J. A.; Karnik, P.; Choi, D.; Campbell, A. M.; Oldham, E. E.; Akin, B. K., Magic tool: Integrated microarray data analysis. *Bioinformatics* 2005, 21, 2114-2115.
4. Rickman, D. S.; Herbert, C. J.; Aggerbeck, L. P., Optimizing spotting solutions for increased reproducibility of cDNA microarrays. *Nucleic Acids Research* 2003, 31.
5. Diehl, F.; Beckmann, B.; Kellner, N.; Hauser, N. C.; Diehl, S.; Hoheisel, J. D., Manufacturing DNA microarrays from unpurified PCR products. *Nucleic Acids Research* 2002, 30.
6. Dufva, M., Fabrication of high quality microarrays. *Biomolecular Engineering* 2005, 22, 173-184.
7. Tran, P. H.; Peiffer, D. A.; Shin, Y.; Meek, L. M.; Brody, J. P.; Cho, K. W. Y., Microarray optimizations: Increasing spot accuracy and automated identification of true microarray signals. *Nucleic Acids Research* 2002, 30.
8. Deegan, R. D.; Bakajin, O.; Dupont, T. F.; Huber, G.; Nagel, S. R.; Witten, T. A., Capillary flow as the cause of ring stains from dried liquid drops. *Nature* 1997, 389, 827-829.
9. Petsi, A. J.; Burganos, V. N., Evaporation-induced flow in an inviscid liquid line at any contact angle. *Physical Review E* 2006, 73.

10. Moran-Mirabal, J. M.; Edel, J. B.; Meyer, G. D.; Throckmorton, D.; Singh, A. K.; Craighead, H. G., Micrometer-sized supported lipid bilayer arrays for bacterial toxin binding studies through total internal reflection fluorescence microscopy. *Biophysical Journal* 2005, 89, 296-305.

11. Ilic, B., Craighead, H.G., Topographical patterning of chemically sensitive biological materials using a polymer-based dry lift off. *Biomedical Microdevices* 2000, 2, 317-322.

12. Yang, Y. H.; Dudoit, S.; Luu, P.; Lin, D. M.; Peng, V.; Ngai, J.; Speed, T. P., Normalization for cDNA microarray data: A robust composite method addressing single and multiple slide systematic variation. *Nucleic Acids Research* 2002, 30.

13. *DNA microarrays: A molecular cloning manual*, Bowtell, D.; Sambrook, J., Eds. Cold Spring Harbor Laboratory Press: Cold Spring Harbor, NY, 2003.

14. Hughes, T. R.; Mao, M.; Jones, A. R.; Burchard, J.; Marton, M. J.; Shannon, K. W.; Lefkowitz, S. M.; Ziman, M.; Schelter, J. M.; Meyer, M. R.; Kobayashi, S.; Davis, C.; Dai, H. Y.; He, Y. D. D.; Stephaniants, S. B.; Cavet, G.; Walker, W. L.; West, A.; Coffey, E.; Shoemaker, D. D.; Stoughton, R.; Blanchard, A. P.; Friend, S. H.; Linsley, P. S., Expression profiling using microarrays fabricated by an ink-jet oligonucleotide synthesizer. *Nature Biotechnology* 2001, 19, 342-347.

15. Otsu, N., Threshold selection method from gray-level histograms. *IEEE Transactions on Systems Man and Cybernetics* 1979, 9, 62-66.

16. Koczan, D.; Thiesen, H. J., Survey of microarray technologies suitable to elucidate transcriptional networks as exemplified by studying krab zinc finger gene families. *Proteomics* 2006, 6, 4704-4715.

17. Lin, D. M.; Yang, Y. H.; Scolnick, J. A.; Brunet, L. J.; Marsh, H.; Peng, V.; Okazaki, Y.; Hayashizaki, Y.; Speed, T. P.; Ngai, J., Spatial patterns of gene expression in the olfactory bulb. *Proceedings of the National Academy of Sciences of the United States of America* 2004, 101, 12718-12723.

18. Deegan, R. D.; Bakajin, O.; Dupont, T. F.; Huber, G.; Nagel, S. R.; Witten, T. A., Contact line deposits in an evaporating drop. *Physical Review E* 2000, 62, 756-765.

19. Hu, H.; Larson, R. G., Marangoni effect reverses coffee-ring depositions. *Journal of Physical Chemistry B* 2006, 110, 7090-7094.

20. Olle, E. W.; Messamore, J.; Deogracias, M. P.; McClintock, S. D.; Anderson, T. D.; Johnson, K. J., Comparison of antibody array substrates and the use of glycerol to normalize spot morphology. *Experimental and Molecular Pathology* 2005, 79, 206-209.

21. Yanagimachi, I.; Nashida, N.; Iwasa, K.; Suzuki, H., Enhancement of the sensitivity of electrochemical stripping analysis by evaporative concentration using a super-hydrophobic surface. *Science and Technology of Advanced Materials* 2005, 6, 671-677.

22. Lee, M.; Cho, Y. W.; Park, J. H.; Chung, H. S.; Jeong, S. Y.; Choi, K. W.; Moon, D. H.; Kim, S. Y.; Kim, I. S.; Kwon, I. C., Size control of self-assembled nanoparticles by an emulsion/solvent evaporation method. *Colloid and Polymer Science* 2006, 284, 506-512.

CHAPTER 5

PARYLENE-BASED PAPER MICROFLUIDICS[5]

5.1 INTRODUCTION

Paper-based microfluidics – devices that transport fluids along patterned conduits in paper – retain the advantages of traditional microfluidics (*e.g.* low sample volume consumption, portable assays), and additionally bring new benefits (*e.g.* passive fluid wicking without the need for external pumps, high surface-area-to-volume ratios for biosensor applications) [1, 2]. Paper-based microfluidics have been utilized in several applications, such as biosensors, electrochemical and immunoassays [3-7]. To support enhanced capabilities for next-generation paper microfluidics (*e.g.* mechanically flexible devices, programmable devices, advanced microfluidic functions), there is a continued interest in new methods for patterning fluid conducting channels in paper, and to discover new materials that are compatible with paper towards this aim. Currently, there are two main strategies to pattern fluid transporting channels in paper: i) directly cutting channels out from paper, typically of millimeter dimensions [8, 9], and ii) defining hydrophilic microchannels in paper treated with hydrophobic polymers [10-16]. Of the patterning strategies, photolithography has the best patterning resolution at ~190μm, however photolithography patterned paper is brittle. While inkjet printing solvents onto hydrophobic sized paper can produce flexible paper microfluidic devices, the patterning resolution is relatively large ~1mm compared to other techniques.

Programmable devices are emerging as an important innovation for next-generation paper microfluidics [17-20]. For instance in biosensor applications, it is

[5] This chapter is a modified and revised form of the article: Tan, C.P., Szeto, K., Pilarz, C.J., Craighead, H.G., Parylene-Based Paper Microfluidics, 2010, submitted for review.

useful to control fluid flow speeds in paper-based microfluidics for programming sequential arrival of reagents in an immunoassay. Millimeter-sized channels directly cut out from paper with different lengths and widths have been utilized to program the sequential arrival of reagents for two-dimensional (2D) immunoassays [9, 21]. While increasing channel length and width can reduce flow speed, there exist two tradeoffs: i) increased sample volumes are required to fill the channels and to counter the loss of capillary pumping over long distance, and ii) the device footprint is increased [19]. Recently, on-chip timers have been created in three-dimensional (3D) paper microfluidic devices by printing drops of wax sandwiched between layers of photoresist-patterned paper to control vertical flow speeds [19, 20].

Parylene is a unique family of polymer coatings deposited via CVD. Parylene-C is flexible, biocompatible, conformal and hydrophobic (water contact angle $\geq 87^{o}$). Parylene CVD is a scalable high-throughput coating process traditionally used in semiconductor, electronics and biomedical industries [22]. Additionally, parylene has been used to preserve paper and books that withstand total immersion in water for years without damage to the paper or print [23]. During paper preservation, the parylene vapor forms a thin conformal coating around each cellulose fibril that confers the properties of parylene to the paper. At parylene thickness <10μm, the physical structure of the cellulose fibril is unaltered and parylene does not fill the gaps between the fibrils [23, 24]. This process of creating hydrophobic paper is different from other paper sizing treatments that may involve adding fillers into the gaps, and thus retains the high surface area (porous) nature of paper.

In this work, parylene-coated paper was investigated as a new substrate for next-generation paper-based microfluidics with enhanced capabilities such as tunable flow speeds programmed into the channels, combinatorial mixing, concentration gradient generators and protein detection. The physico-mechanical properties of

parylene are incorporated with the porous paper matrix to create mechanically flexible and waterproof devices. This work first reports on the fabrication of a parylene-paper composite patterned with hydrophilic channels. Two new approaches are described and characterized: i) using adhesive tape to mask the channel regions during parylene CVD, and ii) oxygen plasma etching the parylene-coated paper using adhesive tape stencils to expose the channel regions. Using the second method, the parylene-paper surface can be modified by oxygen plasma treatment to program fluidic channels with varying levels of hydrophilicity. This new patterning approach was utilized to create a single 2D paper microfluidic device containing regions of different lateral flow speeds, without the need to use multiple paper layers (3D devices) [19, 20] or increasing the reagent volume in the case of direct paper cut-outs [9, 21]. By selectively exposing different regions to varying levels of oxygen plasma treatment using peelable adhesive tabs, the fluidic channels can be programmed to deliver fluid flows sequentially. Furthermore, several enhanced functions in parylene-based paper microfluidics were demonstrated: combinatorial mixing of two color dyes in a Y-shaped paper microfluidic channel, and generating and detecting a BSA protein concentration gradient using bifurcated paper microfluidic channels.

5.2 EXPERIMENTAL METHODS

5.2.1 Patterning Microchannels in Paper Using Parylene and Tape

Method 1: Microchannel designs were drawn in a computer-assisted design software (ROBOCraft) and cut out from sheets of transparent adhesive tape (Con-Tact® clear adhesive laminate) using a tabletop craft cutter (QuicKutz). The adhesive tape cut-outs were positioned face down on a carrier mat (QuicKutz Silhouette CR09308K) to remove the backing. Filter paper (Whatman #1 or #50) was placed on top of the cut-outs, which were transferred onto the paper by a rolling pin to ensure

uniform attachment of the tape to the paper. Multiple devices were simultaneously created on a sheet of filter paper, and the maximum packing density of the devices depends on each device footprint. The paper-tape constructs were removed from the carrier mat and coated with parylene-C (Uniglobe Kisco) via CVD (Specialty Coating Systems Labcoter 2). The channel cut-outs (adhesive tape) served as a masking material during parylene CVD, while the parylene vapor conformally coated the cellulose fibrils in the unmasked regions. Finally, the cut-outs were peeled off to reveal hydrophilic channels in hydrophobic paper as shown in Figure 5.1(a). The specific Con-Tact® adhesive tape used in the experiments leaves no residue and does not damage the underlying paper, as confirmed by high-resolution scanning electron microscopy (SEM) images in Figure 5.4(e-f).

Method 2: The inverse of the channel design was cut out from adhesive tape to create stencils, which were transferred onto sheets of filter paper pre-coated with parylene. The backside of the paper was taped to protect from oxygen plasma treatment. Upon oxygen plasma treatment with a Harrick Plasma expanded plasma cleaner, regions on the paper with exposed parylene were etched to create hydrophilic channels, depicted in the schematic in Figure 5.1(b). If desired, the stencil can be left on the paper without affecting the performance of the microfluidic device, or can be peeled off without damaging the underlying hydrophobic parylene coating.

5.2.2 Contact Angle Measurements of Parylene Coated Filter Paper

Strips of Whatman #1 and #50 filter paper were coated with parylene, either 0.15g, 0.3g, 0.5g or 1.0g. A 1μL drop of deionized water was dispensed onto each strip using an automated syringe pump. Static water contact angles (WCA) were measured on the parylene-coated paper with a goniometer (VCA Optima XE, AST Products) immediately when the drop of water first touched the paper. Replicate strips

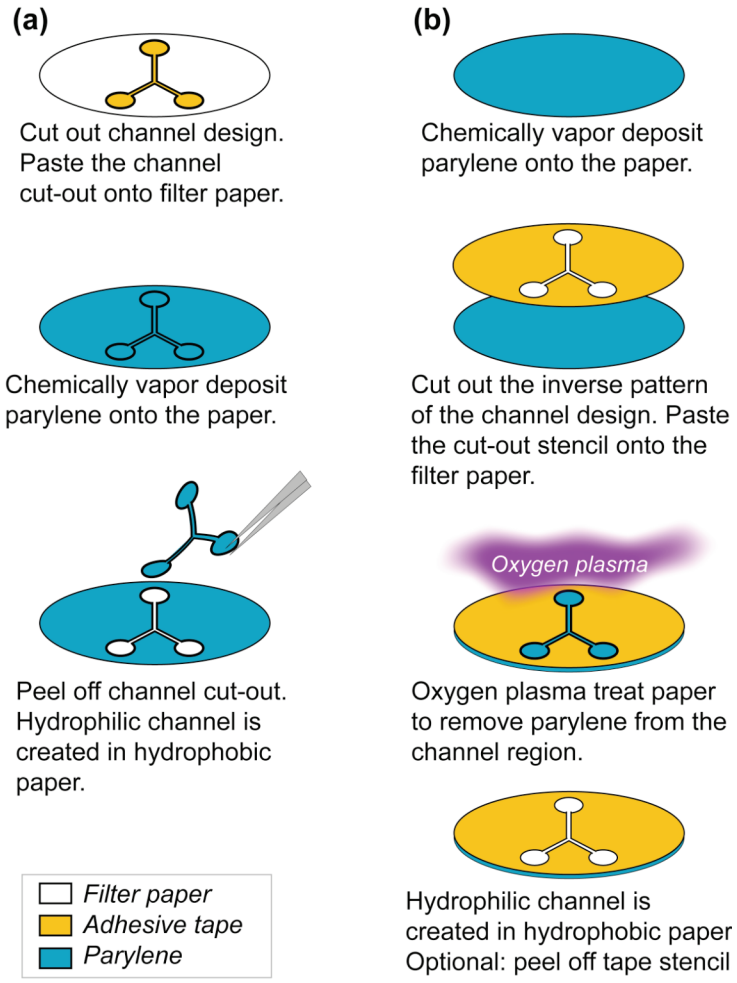

Figure 5.1 Fabrication of paper microfluidics using parylene using: (a) Method 1 and (b) Method 2.

(n=3) were measured for each parylene mass data point and paper type. Water droplets were also positioned on three different regions on each strip to obtain an average WCA. Each data point plotted in Figure 5.3 represents an average WCA and its standard deviation from the independent measurements. While dynamic contact angles (advancing and receding) may be used for surface analysis, the static method is preferred in this instance since any loose filter paper fibrils would impede the motion of the receding contact line. Uncoated filter paper, as well as oxygen plasma treated parylene-coated paper, wicked water immediately and hence their WCAs were not measured.

5.2.3 Test for Resolution of Patterning Methods

Microchannels or the inverse design (200μm to 1mm widths) with 100μm increments, were cut out from the laminate adhesive sheet. Microchannels were created using Methods 1 or 2 on two types of filter paper (Whatman #1 or #50) coated with different amounts of parylene (0.5g or 1.0g). The microchannels were connected to a large inlet reservoir, where blue food dye was loaded to visualize the hydrophilic channels. Images of replicate microchannels (n=3) were captured using a high-resolution microscope camera. The criterion for a successfully patterned microchannel is one that completely transported fluid across the complete length of the channel. The widths of the patterned smallest microchannel were measured at three different regions on each replicate channel, to calculate an average width and the standard deviation for each type of paper, amount of parylene deposited, and patterning method.

5.2.4 Characterization of Flow Speeds as a Function of Oxygen Plasma Treatment Time

Hydrophobic parylene-coated filter paper is waterproof, but can be made to

conduct fluid in a microchannel rendered hydrophilic by oxygen plasma treatment using Method 2. This change in the hydrophilicity of the parylene-paper surface is due to the introduction of oxygen-containing polar species into the chemical structure of parylene, similar to the etching process of parylene films by oxygen plasma [25, 26]. To understand the behavior and characterize the flow speed in parylene-paper composites as a function of oxygen plasma treatment, we focused on the Whatman #50 paper pre-coated with 0.5g of parylene. Sheets of this parylene-coated paper were cut into 50mm x 5mm strips. Pencil markings were made on the strips to demarcate the distance traveled (5mm, 10mm *etc*.) at 5mm intervals. The strips were then subjected to oxygen plasma treatment for 0s, 15s, 30s, 60s, 120s or 300s. The time traveled by the dye front towards each distance mark was measured using a split lap stopwatch. Replicate strips (n=3) were measured for each oxygen plasma treatment time and distance traveled to obtain an average flow speed and standard deviation. All flow assays described henceforth were performed at room temperature (25^{o}C) and 50% humidity.

5.2.5 Patterning Regions with Different Flow Speeds on a Single Paper Microfluidic Device

To pattern regions with different lateral flow speeds on a single paper microfluidic device, adhesive tape stencils with peelable tabs were cut and transferred onto the parylene-coated filter paper. The tabs covered various regions of a paper microfluidic device and could be peeled off to expose the underlying parylene-coated paper to oxygen plasma treatment using Method 2. By sequentially peeling off these tabs as shown in Figure 5.6(a), channels containing regions with varying hydrophilicity – and hence different lateral flow speeds – could be patterned and programmed onto a single device. 4μL of blue or yellow dye was loaded at the end

reservoirs to help visualize the flow speeds in each microchannel section, as the dyes flowed toward the central mixing chamber. The diameter of the central mixing chamber was enlarged relative to the channel width to contain the blue and yellow dyes for mixing. The dyes diffused and mixed inside the central chamber to give a green coloration that was easily visualized.

5.2.6 Combinatorial Mixing, Concentration Gradient Generator and Protein Detection

Bifurcated channels were patterned to create a combinatorial mixer and a microfluidic gradient generator. Parylene-coated Whatman #50 paper with an adhesive tape stencil was subjected to 120s oxygen plasma treatment. Blue and yellow food dyes were loaded into the reservoir inlets to help visualize the color gradient generated. A separate device was prepared for protein detection by spotting 0.3μL tetrabromophenol blue (TBPB, Sigma) in 70% v/v ethanol/water solution with a capillary micropipette onto each outlet reservoir and allowed to dry [10]. BSA (Sigma) was dissolved in sodium acetate buffer (pH 5.5) to a 75μM BSA solution. A 5μL volume of the BSA solution was loaded into the left inlet reservoir, while 5μL of sodium acetate buffer was loaded into the right inlet simultaneously. A concentration gradient of BSA was formed at the reservoir outlets, which was detected colorimetrically by turning the orange-yellow TBPB blue: the intensity of blue color correlates to the amount of BSA protein detected. The BSA concentrations at each outlet of the gradient generator were calculated as previously described [27]. The image of the BSA concentration gradient was converted to grayscale using ImageJ (National Institutes of Health) and inverted so that the brightest outlet (leftmost) corresponds to the highest BSA concentration detected. Intensity histograms were generated for the 812 pixels circular area of each outlet, and the average intensity per

pixel (A.U./pixel) and associated standard deviation were recorded. These average intensity values were corrected by subtracting the background average intensity per pixel (average intensity of the outlet with no BSA), and then plotted as a function of BSA concentration.

5.2.7 Scanning electron microscopy (SEM)

Pieces of the Whatman filter papers: i) uncoated, ii) parylene-coated, iii) adhesive tape peeled off, and iv) parylene-coated and oxygen plasma treated, were mounted with carbon paste onto the sample holders. A thin 5nm layer of gold-palladium was sputter deposited onto the paper samples to reduce charging and enhance imaging contrast. The filter paper samples were imaged at 0.7kV with a 20μm aperture size using a Zeiss LEO 1550 field emission SEM.

5.3 RESULTS AND DISCUSSIONS

5.3.1 Water Contact Angles of Parylene-Coated Filter Paper

Parylene CVD is a conformal coating since the monomeric vapor can penetrate deeply into a substrate and afterwards polymerize to form a parylene film. As an example, sugar cubes that have undergone parylene CVD can be boiled off to leave behind an exact replica of the sugar cube's original porous structure made entirely of parylene [23]. After parylene coating, the Whatman filter papers remained flexible but became hydrophobic and waterproof. Droplets of water, which would otherwise wick immediately into the paper, beaded up and remained on the surface of the parylene-coated filter paper.

To characterize wetting behavior on the two types of filter paper coated with different amounts of parylene, static WCAs were measured. As shown in Figure 5.2, overall parylene-coated Whatman #1 filter paper exhibited higher WCAs than that of

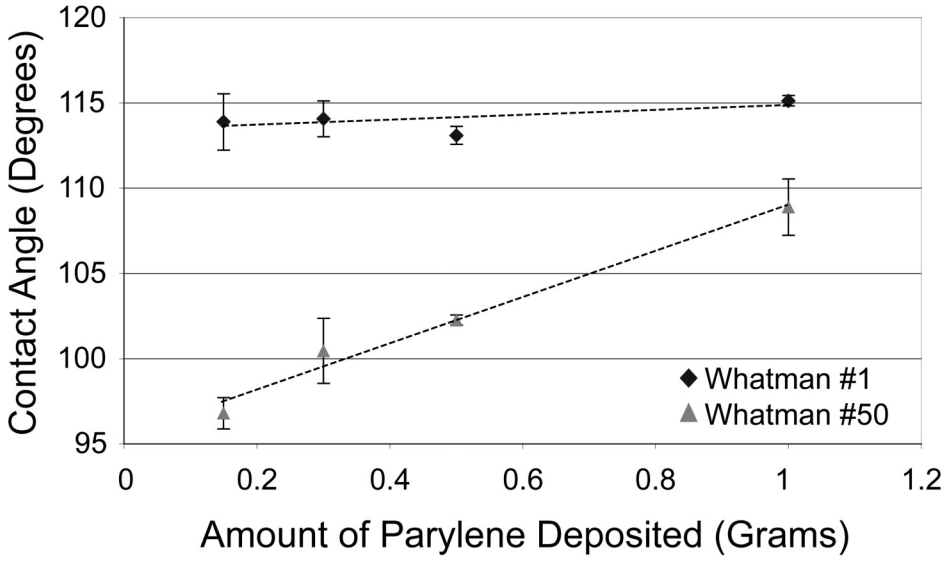

Figure 5.2 WCA on parylene-coated filter papers across a range of parylene mass deposited. Lines are linear fits of the data points. Measurements were performed on replicate samples (n=3) for each data point.

parylene-coated Whatman #50. The WCAs of the coated Whatman #1 filter paper were consistently high (>112^{o}) across the range of parylene deposited, while the WCAs of the coated Whatman #50 paper increased linearly with the mass of parylene deposited. These differences in WCAs of Whatman #1 and #50 can be explained by the paper pore size and type of finish.

The manufacturer reports that the particle retention sizes (approximate pore sizes) for Whatman #1 and #50 filter papers are 11μm and 2.7μm respectively. Additionally the Whatman #1 surface is unfinished with visible loose fibrils, while the Whatman #50 surface is glazed. SEM images of the uncoated filter papers confirmed that the gaps between fibrils are larger that in Whatman #1 (Figure 5.3(a)) compared to Whatman #50 (Figure 5.4(a)). Figures 5.3(b) and 5.4(b) show the surface detail of the cellulose fibrils of Whatman #1 and #50 at high magnification. The approximate pore dimensions we observed for both types of paper were much larger than that reported by the manufacturer, however this can be attributed to difference in the methods used to determine the pore size. The larger pore size of Whatman #1 allowed the parylene vapor to easily penetrate and coat the cellulose fibrils quickly, resulting in relatively constant WCAs throughout. The smaller pore size of Whatman #50 reduced parylene vapor penetration into the paper, and thus the WCAs increased as more parylene is deposited. The reason for Whatman #1 having an overall higher WCA compared to Whatman #50 (for the same parylene mass) is not only a function of pore size, but may also depends on the type of surface finish. Assuming the Wenzel model of wetting, our hypothesis is that the parylene-coated loose fibrils on the surface of Whatman #1 paper increased apparent surface roughness resulting in an increase in WCA (and hydrophobicity) [28]. Conversely, Whatman #50's proprietary glazed surface with less loose fibrils would have a reduced apparent surface roughness compared to Whatman #1.

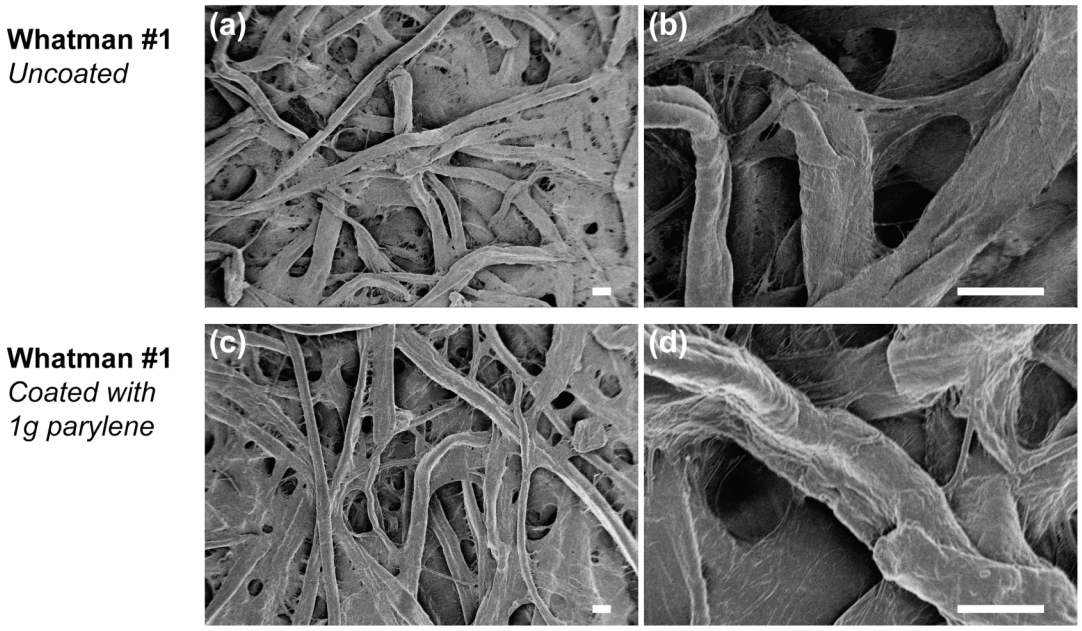

Figure 5.3 Representative SEM images of Whatman #1 filter paper that is: (a-b) uncoated, as purchased from the manufacturer, and (c-d) coated with 1g of parylene. Images (b) and (d) show the details of the surface of uncoated and coated cellulose fibrils at high magnification. Note that parylene does not coat or fill the gaps between the cellulose fibrils as seen from images (a) and (c), but rather conformally coat each fibril. The fibrils do not appear to be modified as a consequence of the parylene deposition, as shown in images (b) and (d). Scale bars represent 20μm.

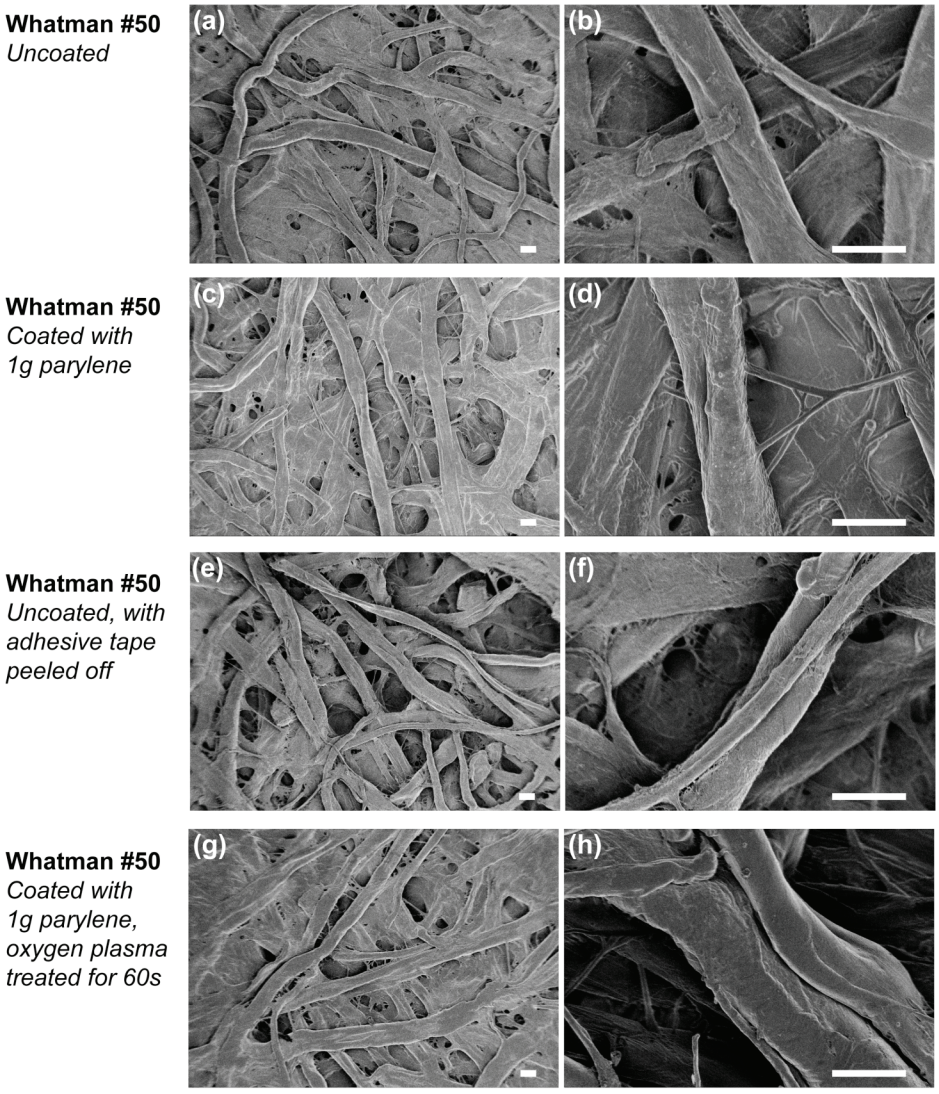

Figure 5.4 Representative SEM images of Whatman #50 filter paper that is: (a-b) uncoated, as purchased from the manufacturer, (c-d) coated with 1g of parylene, (e-f) uncoated filter paper with adhesive tape peeled off, and (g-h) coated with 1g of parylene and oxygen plasma treated for 60s. Images (b), (d), (f), and (h) show the surface details of cellulose fibrils at high magnification. The adhesive tape did not leave residue or damage the fibrils in (e-f) as compared to the original filter paper (a-b). Oxygen plasma treatment did not alter the physical structure of paper or the surface roughness of the fibrils in (g-h) as compared to parylene-coated filter paper (c-d). Scale bars represent 20μm.

Comparisons of SEM images of uncoated Whatman #1 filter paper as purchased from manufacturer (Figure 5.3(a)) and parylene-coated Whatman #1 filter paper (Figure 5.3(c)) confirm previous report in literature that thin parylene conformally coats the cellulose fibrils and does not fill or coat the gaps between the fibrils [23]. There are no apparent differences in the overall paper structure between the SEM images of uncoated and coated filter paper, even at high magnification in Figure 5.3(b) and (d). Furthermore, the high magnification images do not show any apparent physical modification of the fibrils after parylene coating consistent with a previous study [24]. These observations are also true for Whatman #50 – Figure 5.4(a-b) show the filter paper as purchased from the manufacturer, while Figure 5.4(c-d) show the filter paper after coating with 1g of parylene.

5.3.2 Smallest Channel Widths Patterned Using Parylene Vapor-Based Methods

SEM images in Figure 5.4(e-f) showed that the adhesive tape did not leave any residue on the paper surface nor damaged the paper fibrils. The average smallest hydrophilic channel that can be patterned with Method 1 was 275$\pm$15μm (using Whatman #1), which varies about $\pm$5% depending on the type of paper and amount of parylene deposited as shown in Figure 5.5. Replica PDMS structures and shadow masks have been previously used to mask regions on substrates during parylene CVD and pattern feature widths down to 25μm [29, 30].

The resolution of Method 1 is mainly limited by the smallest channel width that can be cut by the craft cutter (~200μm) and thereafter completely transferred onto the filter paper. Hydrophilic channels patterned via Method 1 took a long time (>10mins) to fill when dry, presumably due to some parylene vapor penetrating underneath the tape mask during CVD. Moistening the channels first with water

enabled immediate filling. The smallest hydrophilic channel width that could be patterned using Method 2 was 365±16μm (Whatman #50) as shown in Figure 5.5. Overall for Method 2, Whatman #50 paper with 1g of parylene had the best patterning resolution of 365±16μm. The patterning resolution of the two methods is influenced by the paper pore size. For example, Whatman #1 with larger pores allowed better penetration of parylene to define a smaller channel width in Method 1, while Whatman #50 with smaller pores reduced oxygen plasma penetration under the adhesive tape mask. Based on the paper type and porosity, either Method 1 or 2 can be employed for the optimal patterning and the resolution of the patterned microchannels. These results show that the parylene-based patterning approach is versatile enough to allow for fluidic channels to be created in paper, in a manner that is independent of the substrate type and porosity.

The smallest patterning resolutions of Method 1 and 2 (275±15μm and 365±16μm) are improvements over most of the current methods such as wax printing (561±45μm) [12, 13], inkjet printing of solvents to dissolve hydrophobic polymers (420±50μm) [14, 15], direct plotting with PDMS (1mm) [16]. While the patterning resolution of photolithography patterned paper is the best (186±13μm) [2], parylene-paper composites offer the advantage of being mechanically flexible and foldable unlike brittle photolithography patterned paper. Increase in the mechanical strength of ligneous and nonligneous paper were also reported after parylene coating [31]. Photolithography can also leave behind undesirable polymeric scum in the hydrophilic channels since they are exposed to solvents and liquid hydrophobic polymers [2]. Although this can be alleviated by removing the scum with oxygen plasma treatment, directly incorporating oxygen plasma in the parylene-based patterning approach would reduce the number of processing steps. Compared to photolithography, the parylene-based method has the advantages of being solvent-free with fewer processing steps.

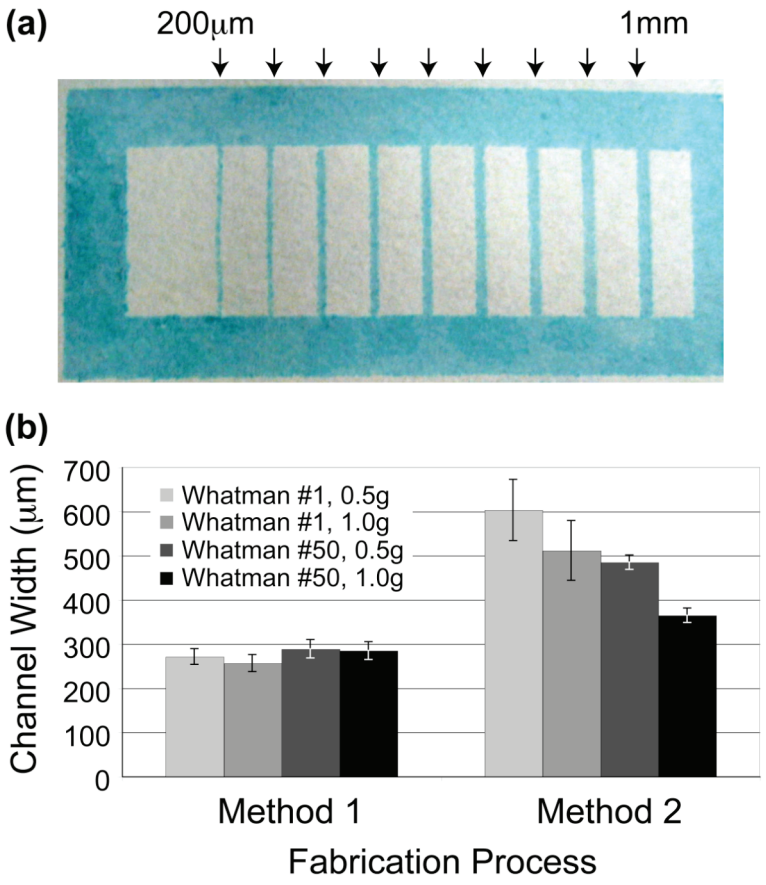

Figure 5.5 Patterning resolution of Methods 1 and 2. (a) A representative image showing a series of patterned hydrophilic channels widths in 100μm intervals, ranging from 200μm to 1mm. In this instance, Whatman #1 paper with 0.5g of parylene was patterned with Method 1. The arrows point to the locations of microchannels of different widths. The criterion for a successfully patterned channel is one that transports fluid across the entire length of the channel. (b) Graph showing the average widths (n=3) of the smallest hydrophilic channel and the associated standard deviations that could be patterned on the different types of paper coated with various amounts of parylene for each fabrication method.

5.3.3 Controlling Lateral Flow Speed by Modifying Channel Hydrophilicity with Oxygen Plasma Treatment

Next, the influence of oxygen plasma treatment time on the flow speeds of liquids in Whatman #50 paper strips coated with 0.5g parylene was investigated. As shown in Figure 5.6, the flow speeds increased with longer oxygen plasma times due to the channels becoming more hydrophilic. It is postulated that this change in the hydrophilicity of the parylene-paper surface is due oxygen-containing polar species introduced into the chemical structure of parylene, similar to the etching process of parylene films by oxygen plasma [25, 26].

SEM images of Whatman #50 filter paper coated with parylene and oxygen plasma treated in Figure 5.4(g-h) did not show any apparent changes in surface roughness or porosity compared to the original filter paper. The unaltered physical structure of the cellulose fibrils and paper porosity are attractive for applications (*e.g.* sensors, batteries) that would benefit from retention of the high surface area of the porous paper after surface modification [32, 33].

It was observed that the flow speeds decreased with farther distances traveled by the fluid on the paper, agreeing with what has been previously reported and attributed to increased counteracting viscous forces or fiber swelling [15, 34]. From the graph in Figure 5.6, 120s oxygen plasma resulted in the highest flow speed for all distances traveled. Oxygen plasma times (>120s) did not improve the flow speed, and started lateral wicking of fluids from the channel. The distance traveled by the fluid front on the etched parylene-coated paper strips scaled linearly with time$^{1/2}$ for the various oxygen plasma treatments is shown Figure 5.7, consistent with the Washburn relation governing capillary flows in porous media [35]:

$$t^{1/2} \propto \left(\frac{4\eta}{D\,\gamma \cos\theta} \right)^{1/2} \ell$$

where t is the time taken for the fluid front to travel the distance ℓ, for a fluid with viscosity η, surface tension γ inside a porous medium with average pore diameter D and θ is the apparent fluid contact angle that depends on surface hydrophilicity.

The slopes of the Washburn plots in Figure 5.7 decrease with longer oxygen plasma treatment times, due to changes in the surface energy of the parylene-coated paper fibrils as the surface rendered made more hydrophilic. Hydrophobic sized paper have also demonstrated different fluid flow speeds after being subjected to oxygen plasma treatment [18]. Table 5.1 displays the slope values of the Washburn plots with various oxygen plasma treatment times. The plots better approximates linear Washburn flows as oxygen plasma treatment time is increased. This can be explained by the reduced surface tension forces resisting fluid flow by the hydrophobic parylene. A consequence of these results is that by simply altering the oxygen plasma treatment time, one could tune the fluid flow speed in these parylene-coated paper microfluidic devices, which would be useful for timing the sequential arrival of fluids in paper immunoassays [21]. To achieve this, the parylene and adhesive tape patterning approach in this work allows for patterning regions of tunable flow speeds in a single 2D parylene-based microfluidic device as shown in Figure 5.8.

5.3.4 Patterning Regions with Different Lateral Flow Speeds on a Parylene Paper Microfluidic Device

Channels with regions having different flow speeds were patterned on a single device. Peelable tabs were fabricated in the adhesive tape stencil for selectively exposing various regions of the channel to different oxygen plasma treatment times.

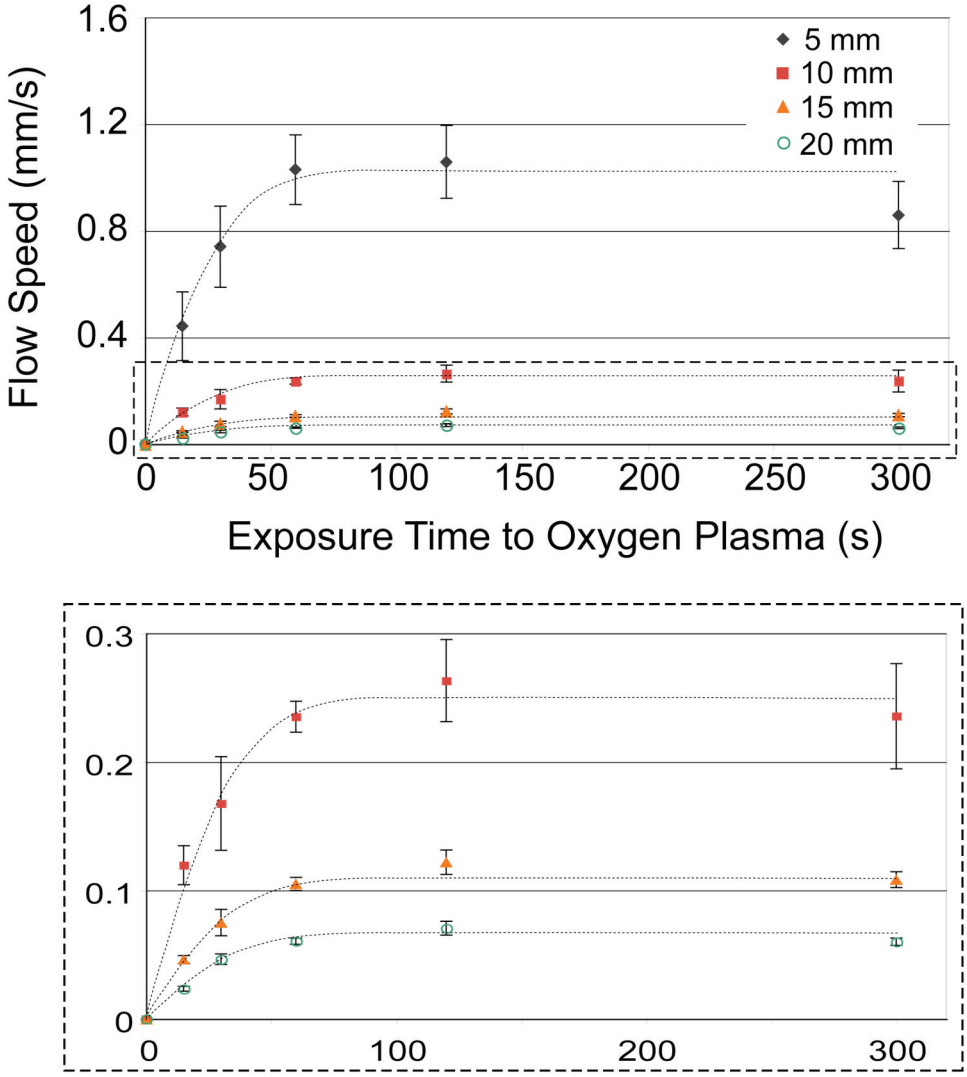

Figure 5.6 Flow speeds of dye as a function of oxygen plasma treatment time (0, 15, 30, 60, 120, and 300s) for Whatman #50 paper strips coated with 0.5g parylene. n=3 strips were tested for each oxygen plasma treatment time. The flow speeds decreased the farther the distance traveled by the dye front, due to counteracting viscous forces or fiber swelling. Bottom graph: zoomed in view of the boxed region in the top graph. Curves are added to guide the eye.

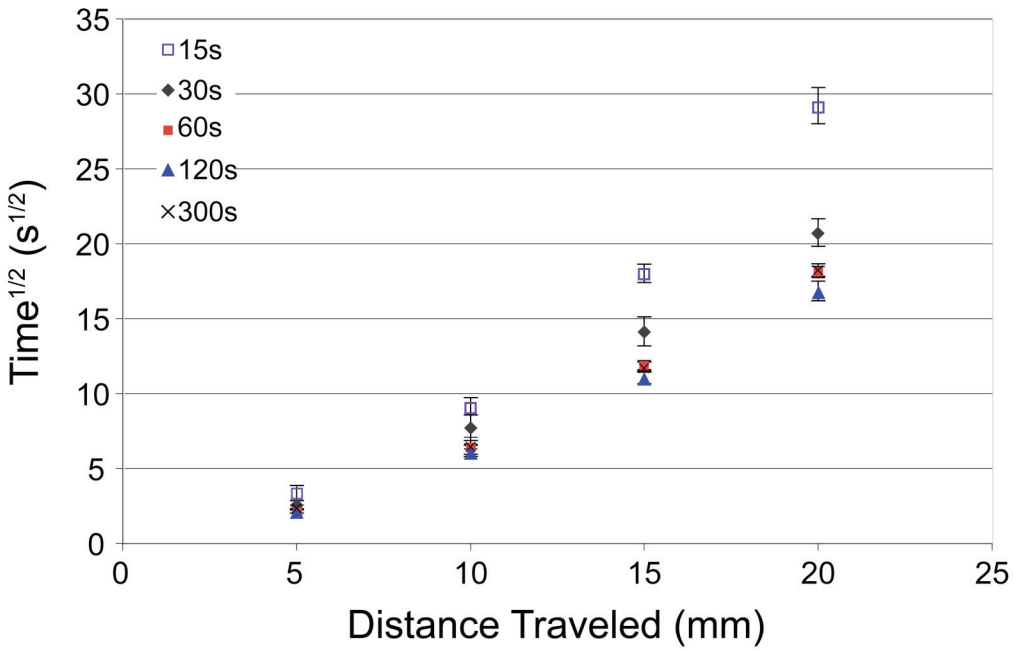

Figure 5.7 Washburn plots for parylene-coated paper strips with various oxygen plasma treatment times.

Table 5.1 Slopes of Washburn relation with different oxygen plasma treatment times.

Oxygen Plasma Treatment (s)	Slope of Washburn plot	R^2 for linear regression
15	1.28	0.90
30	0.96	0.94
60	0.83	0.93
120	0.77	0.94
300	0.82	0.93

An example of using these adhesive tabs to pattern straight channels with two inlet reservoirs leading into a central mixing chamber is shown in Figure 5.8(a). Channels with other geometries can also be patterned. Region 1 of the channel was exposed to a total of 120s oxygen plasma, while region 2 was exposed to only 60s of oxygen plasma. 4μL of blue or yellow dye was pipetted into the inlet reservoirs and time-lapsed images of the dyes in Figure 5.8(b) revealed that the fluid flow in region 2 (yellow dye) was slower than in region 1 (blue dye) because of decreased channel hydrophilicity. Finally, the central chamber showed diffusive mixing of the two dyes to form a green coloration, despite the differences in arrival times of the dyes. One way to minimize the lateral spreading is to use clamped metal stencils [18] or PDMS replicas [29, 30]. However these materials are unable to pattern the freestanding structures (*e.g.* the microfluidic gradient generator in Figure 5.9(b-c)).

Next-generation programmable paper microfluidics have demonstrated enhanced capabilities such as valves [17, 18] on-chip timers [19, 20], and ability to sequentially control the arrival of flows [20, 21]. The ability to tune flow speeds is attractive for paper microfluidic assays that require the certain reagents to react before others. The results in Figure 5.8 demonstrate that 2D parylene-based paper microfluidics devices can be engineered with tunable lateral flow speeds without the need for multiple paper layers (3D devices) [19, 20], and does not compromise on the device portability or need to increase sample volume compared to direct paper cut-outs [9, 21].

5.3.5 Enhanced Capabilities of Parylene-Based Paper Microfluidics

Three enhanced capabilities of parylene-based paper microfluidics were demonstrated: i) Y-shaped microchannel combinatorial mixer, ii) bifurcated channel concentration gradient generator, and iii) microfluidic biosensor for protein detection.

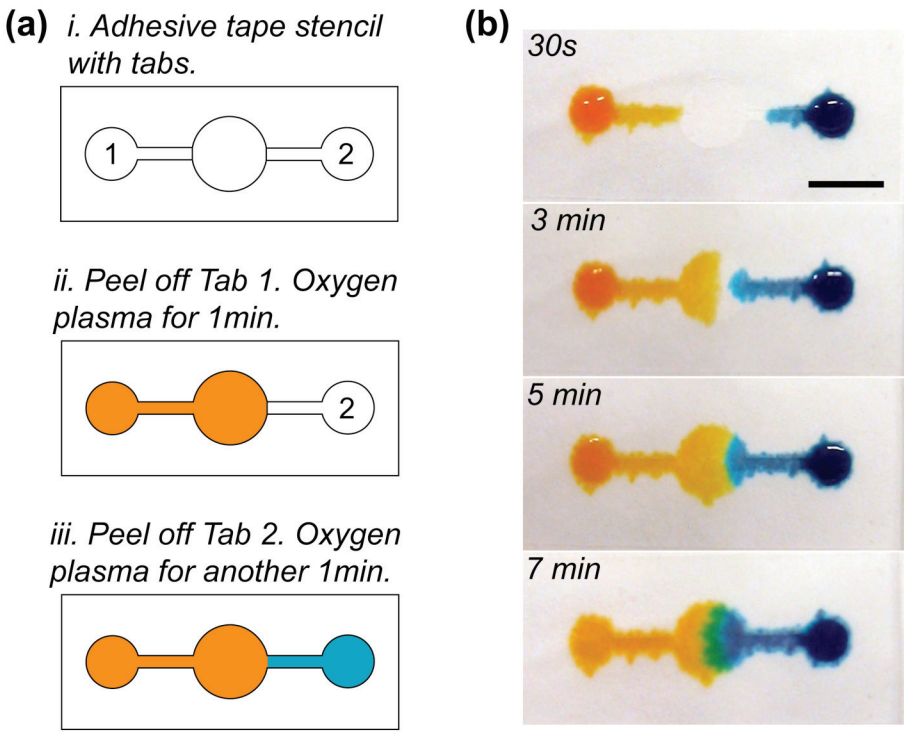

Figure 5.8 2D parylene-based paper microfluidic device with regions of tunable lateral flow speeds without having to increase channel dimensions and hence sample volume. (a) Schematic showing peelable tabs that controlled the amount of oxygen plasma treatment in the channels. (b) Time lapsed images showing a single patterned paper microfluidic device with faster flow (yellow dye) left channel than the flow (blue dye) in the right channel. The dyes were contained in the central mixing chamber and eventually merged to give a green coloration. Scale bar represents 5mm.

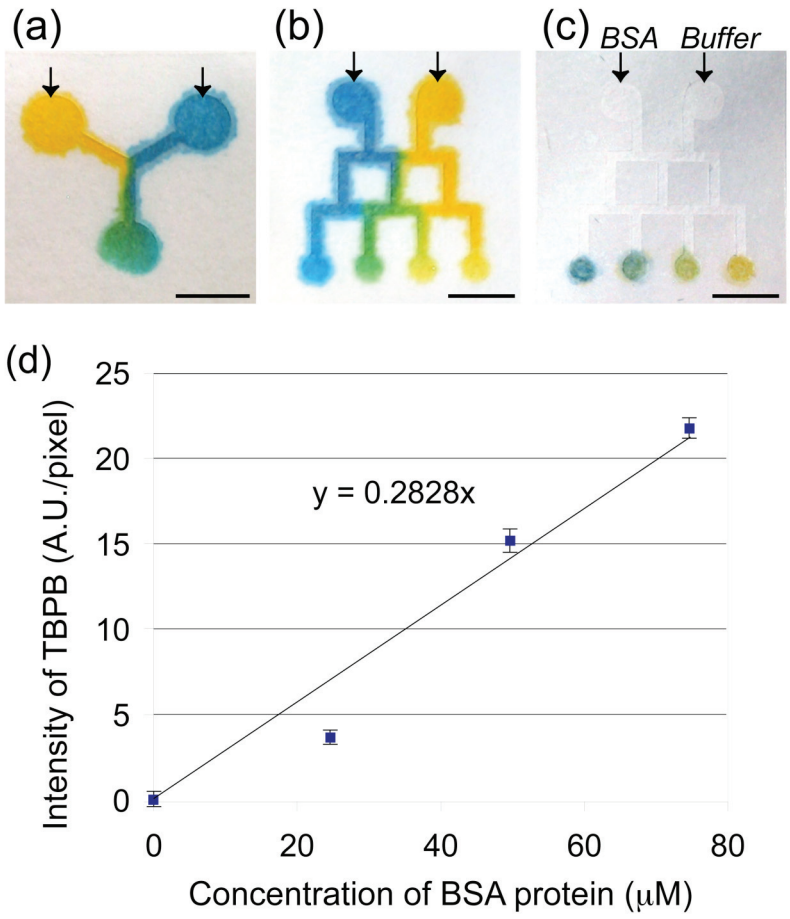

Figure 5.9 Enhanced capabilities of parylene-based paper microfluidics. (a) Y-shaped fluidic channel can also be patterned; shown here is the mixing of two laminar flows of blue and yellow dyes. (b) Combinatorial mixing of blue and yellow dyes by the gradient generator. (c) Protein detection using the gradient generator: BSA and buffer were loaded into the two inlets to create a BSA protein gradient, which was colorimetrically detected by the TBPB spots at the outlets. Arrows point to the inlet reservoirs. (d) Graph showing the intensity of TBPB as a function of BSA concentration, analyzed from the image in (c). Scale bar represents 5mm.

Y-shaped microchannel geometry was patterned on parylene-coated filter paper and yellow and blue dyes were added to the two inlet reservoirs to demonstrate combinatorial mixing as shown in Figure 5.9(a). Upon meeting, the dyes retained their laminar trajectories briefly before diffusing to form a green flow upstream. This is consistent with previous literature whereby laminar flow have been shown in porous paper medium [9, 34].

As shown in Figure 5.9(b), the bifurcating channel concentration gradient generator produced a color gradient resulting from the combinatorial mixing of blue and yellow dyes. The same bifurcating channel geometry was used to create a BSA protein concentration gradient in Figure 5.9(c). A monotonically increasing darker blue intensity of TBPB (buffered under acidic condition) was detected, corresponding to an increasing concentration of BSA from right to left, as shown in Figure 5.9(d). It is important to buffer the acidic pH of the BSA solution, since TBPB is also a pH indicator and turns pH$\geq$7 solutions blue. This is the first demonstration of a paper-based microfluidic concentration gradient generator.

5.4 CONCLUSIONS

This work reports on a novel parylene-based paper composite that is mechanically flexible, waterproof and yet retains the porosity of paper. Two fabrication methods utilizing adhesive tape were used to pattern hydrophilic channels in the parylene-coated paper that passively wicked fluids without any external pumps. The smallest channel widths that can be patterned with Methods 1 and 2 are 275$\pm$15μm and 365$\pm$16μm, which are improvements over most of the current patterning techniques (with the exception of photolithography). However parylene-based microfluidic devices offer the advantage of being mechanically flexible and foldable unlike photolithography-patterned paper that is brittle. Enhanced capabilities

for next-generation paper-based microfluidics were demonstrated using the parylene-based paper microfluidic devices: combinatorial mixing, concentration gradient generation, protein detection, and tunable flow speeds that were programmed into the channels via hydrophilicity. This is the first demonstration of concentration gradient generator using paper-based microfluidics. By using peelable tabs that varied the level of oxygen plasma treatment, sequential arrival of fluids can be programmed into 2D parylene-based paper microfluidic device without having to use multiple paper layers (3D devices) or increasing sample volumes. This work is the first study of its kind showing the feasibility of using parylene as a material in patterning paper microfluidics. In the future, parylene films with reactive amine groups [36, 37] may be used to add surface functionalities and covalently link proteins to create bioactive paper for sensors [4]. It is envisioned this solventless parylene CVD patterning method may be extended to patterning other porous substrates such as membranes [38], and further expand the capabilities of next-generation paper microfluidics.

REFERENCES

1. Yager, P.; Domingo, G. J.; Gerdes, J., Point-of-care diagnostics for global health. *Annual Review of Biomedical Engineering* 2008, 10, 107-144.
2. Martinez, A. W.; Phillips, S. T.; Whitesides, G. M.; Carrilho, E., Diagnostics for the developing world: Microfluidic paper-based analytical devices. *Analytical Chemistry* 2010, 82, 3-10.
3. Li, X.; Tian, J. F.; Shen, W., Progress in patterned paper sizing for fabrication of paper-based microfluidic sensors. *Cellulose* 2010, 17, 649-659.
4. Pelton, R., Bioactive paper provides a low-cost platform for diagnostics. *Trends in Analytical Chemistry* 2009, 28, 925-942.
5. Nie, Z. H.; Nijhuis, C. A.; Gong, J. L.; Chen, X.; Kumachev, A.; Martinez, A. W.; Narovlyansky, M.; Whitesides, G. M., Electrochemical sensing in paper-based microfluidic devices. *Lab on a Chip* 2010, 10, 477-483.
6. Stevens, D. Y.; Petri, C. R.; Osborn, J. L.; Spicar-Mihalic, P.; McKenzie, K. G.; Yager, P., Enabling a microfluidic immunoassay for the developing world by integration of on-card dry reagent storage. *Lab on a Chip* 2008, 8, 2038-2045.
7. Li, X.; Tian, J. F.; Shen, W., Quantitative biomarker assay with microfluidic paper-based analytical devices. *Analytical and Bioanalytical Chemistry* 2010, 396, 495-501.
8. Fenton, E. M.; Mascarenas, M. R.; Lopez, G. P.; Sibbett, S. S., Multiplex lateral-flow test strips fabricated by two-dimensional shaping. *ACS Applied Materials & Interfaces* 2009, 1, 124-129.
9. Fu, E.; Lutz, B.; Kauffman, P.; Yager, P., Controlled reagent transport in disposable 2D paper networks. *Lab on a Chip* 2010, 10, 918-920.

10. Martinez, A. W.; Phillips, S. T.; Butte, M. J.; Whitesides, G. M., Patterned paper as a platform for inexpensive, low-volume, portable bioassays. *Angewandte Chemie International Edition* 2007, 46, 1318-1320.

11. Martinez, A. W.; Phillips, S. T.; Wiley, B. J.; Gupta, M.; Whitesides, G. M., Flash: A rapid method for prototyping paper-based microfluidic devices. *Lab on a Chip* 2008, 8, 2146-2150.

12. Lu, Y.; Shi, W. W.; Jiang, L.; Qin, J. H.; Lin, B. C., Rapid prototyping of paper-based microfluidics with wax for low-cost, portable bioassay. *Electrophoresis* 2009, 30, 1497-1500.

13. Carrilho, E.; Martinez, A. W.; Whitesides, G. M., Understanding wax printing: A simple micropatterning process for paper-based microfluidics. *Analytical Chemistry* 2009, 81, 7091-7095.

14. Abe, K.; Suzuki, K.; Citterio, D., Inkjet-printed microfluidic multianalyte chemical sensing paper. *Analytical Chemistry* 2008, 80, 6928-6934.

15. Li, X.; Tian, J. F.; Garnier, G.; Shen, W., Fabrication of paper-based microfluidic sensors by printing. *Colloids and Surfaces B: Biointerfaces* 2010, 76, 564-570.

16. Bruzewicz, D. A.; Reches, M.; Whitesides, G. M., Low-cost printing of poly(dimethylsiloxane) barriers to define microchannels in paper. *Analytical Chemistry* 2008, 80, 3387-3392.

17. Martinez, A. W.; Phillips, S. T.; Nie, Z. H.; Cheng, C. M.; Carrilho, E.; Wiley, B. J.; Whitesides, G. M., Programmable diagnostic devices made from paper and tape. *Lab on a Chip* 2010, 10, 2499-2504.

18. Li, X.; Tian, J. F.; Nguyen, T.; Shen, W., Paper-based microfluidic devices by plasma treatment. *Analytical Chemistry* 2008, 80, 9131-9134.

19. Noh, N.; Phillips, S. T., Metering the capillary-driven flow of fluids in paper-based microfluidic devices. *Analytical Chemistry* 2010, 82, 4181-4187.

20. Noh, N.; Phillips, S. T., Fluidic timers for time-dependent, point-of-care assays on paper. *Analytical Chemistry* 2010, 82.

21. Fu, E.; Kauffman, P.; Lutz, B.; Yager, P., Chemical signal amplification in two-dimensional paper networks. *Sensors and Actuators B: Chemical* 2010, 149, 325-328.

22. Tan, C. P.; Craighead, H. G., Surface engineering and patterning using parylene for biological applications. *Materials* 2010, 3, 1803-1832.

23. Humphrey, B. J., Paper strengthening with gas-phase parylene. Polymers: Practical considerations. *Restaurator* 1990, 11, 48-68.

24. Carrapella, E. E.; Powell, E. M.; Rutiser, C. A.; Barger, M. S., Changes in paper morphology caused by resizing treatments. *Restaurator* 1990, 11, 219-235.

25. Chang, T. Y.; Yadav, V. G.; De Leo, S.; Mohedas, A.; Rajalingam, B.; Chen, C. L.; Selvarasah, S.; Dokmeci, M. R.; Khademhosseini, A., Cell and protein compatibility of parylene-C surfaces. *Langmuir* 2007, 23, 11718-11725.

26. Hwang, K. S.; Park, J. H.; Lee, J. H.; Yoon, D. S.; Kim, T. S.; Han, I.; Noh, J. H., Effect of atmospheric-plasma treatments for enhancing adhesion of Au on parylene-c-coated protein chips. *Journal of the Korean Physical Society* 2004, 44, 1168-1172.

27. Dertinger, S. K. W.; Chiu, D. T.; Jeon, N. L.; Whitesides, G. M., Generation of gradients having complex shapes using microfluidic networks. *Analytical Chemistry* 2001, 73, 1240-1246.

28. Marmur, A., Wetting on hydrophobic rough surfaces: To be heterogeneous or not to be? *Langmuir* 2003, 19, 8343-8348.

29. Chen, H. Y.; Elkasabi, Y.; Lahann, J., Surface modification of confined microgeometries via vapor-deposited polymer coatings. *Journal of the American Chemical Society* 2006, 128, 374-380.

30. Chen, H. Y.; Lahann, J., Vapor-assisted micropatterning in replica structures: A solventless approach towards topologically and chemically designable surfaces. *Advanced Materials (Weinheim, Germany)* 2007, 19, 3801-3808.

31. Carter, H. A., The chemistry of paper preservation part 3. The strengthening of paper. *Journal of Chemical Education* 1996, 73, 1160-1162.

32. Hu, L. B.; Choi, J. W.; Yang, Y.; Jeong, S.; La Mantia, F.; Cui, L. F.; Cui, Y., Highly conductive paper for energy-storage devices. *Proceedings of the National Academy of Sciences of the United States of America* 2009, 106, 21490-21494.

33. Nystrom, G.; Mihranyan, A.; Razaq, A.; Lindstrom, T.; Nyholm, L.; Stromme, M., A nanocellulose polypyrrole composite based on microfibrillated cellulose from wood. *Journal of Physical Chemistry B* 2010, 114, 4178-4182.

34. Fu, E.; Ramsey, S. A.; Kauffman, P.; Lutz, B.; Yager, P., Transport in two-dimensional paper networks. *Microfluidics and Nanofluidics* 2010, doi: 10.1007/s10404-10010-10643-y.

35. Washburn, E. W., The dynamics of capillary flow. *Physics Review* 1921, 17, 273-283.

36. Lahann, J.; Balcells, M.; Lu, H.; Rodon, T.; Jensen, K. F.; Langer, R., Reactive polymer coatings: A first step toward surface engineering of microfluidic devices. *Analytical Chemistry* 2003, 75, 2117-2122.

37. Miwa, J.; Suzuki, Y.; Kasagi, N., Adhesion-based cell sorter with antibody-coated amino-functionalized-parylene surface. *Journal of Microelectromechanical Systems* 2008, 17, 611-622.

38. Lu, Y.; Shi, W. W.; Qin, J. H.; Lin, B. C., Fabrication and characterization of paper-based microfluidics prepared in nitrocellulose membrane by wax printing. *Analytical Chemistry* 2010, 82, 329-335.

CHAPTER 6

MULTIPLEXED APTAMERS SELECTION AND RECOVERY WITH PARYLENE PEEL-STRIPS[6]

6.1 INTRODUCTION

Multiplexed affinity-based screening is widespread in biology, whereby potential biomolecular candidates in a sample pool are screened against capturing biomolecules immobilized on an array surface. For example, DNA microarrays enable the massively parallel screening of sample RNA that may hybridize to any of thousands of gene sequences arrayed on a surface. It is often useful to recover the bound biomolecule species afterwards for complete identification (*e.g.* DNA sequencing) and to generate more copies (*e.g.* PCR amplification), particularly if the original sample pool is a priori unknown. One such instance is the identification of previously uncharacterized corona viruses such as SARS, whereby viral nucleic acids hybridized to a DNA microarray were individually scraped off using tungsten needles for PCR [1]. Although this approach is simple, its disadvantages include contamination, loss and destruction of samples.

Current technologies fail to combine both multiplexed affinity-based screening and sample recovery. Whatman's FTA® Elute have been used to recover total DNA without specificity from whole blood or buccal cheek cells [2-5]. HPLC systems allow for affinity-based screening and sample recovery, but multiple columns and the systems can be prohibitively expensive. Microfluidic systems have had some early success at addressing these problems. For example, nucleic acid aptamers that showed

[6] This chapter is a modified and revised form of the article being prepared for submission to a journal: Tan, C.P., Ceniccola, K.E., Szeto, K., Pilarz, C.J., Lin, D.M., Craighead, H.G., Multiplexed Aptamers Selection and Recovery Using Functional Parylene Peel-Strips.

binding to protein have been selected from a sample library pool and recovered using heating electrodes [6] or micromagnetic beads [7]. The challenge remains to reliably isolate and individually recover biomolecule species of interest after multiplexed screening.

Aptamers are short length nucleic acids that bind to proteins, and are emerging as potential therapeutic molecules that could target proteins involved in disease. Systematic evolution of ligands by exponential enrichment (SELEX) is a process utilized to select aptamers with high affinity binding to proteins. SELEX requires both affinity-based screening and subsequent recovery of aptamers that binds to proteins for PCR amplification. With each cycle of SELEX, the stringency of binding in the screening process is increased, and at the end of several SELEX rounds, aptamers with high binding affinity are systematically evolved. SELEX is time consuming and microfluidics have been shown to shorten the process [7-9]. However these microfluidic systems involve selection against one protein at a time; it would be desirable to develop a microfluidic system capable of multiplexed selection and screening simultaneously.

Parylene is a family of CVD deposited polymers used in engineering surfaces for biological applications [10], such as micropatterning [11, 12] or direct coating to create bioactive surfaces. Parylene films are biocompatible, conformal with high surface coverage uniformity, and able to withstand a variety of solvents without degradation or swelling. Chemically reactive parylene-A films containing substituted amine groups can be coated onto nearly any surface to confer new functional group for covalent linkage of biomolecules or drugs [13-16]. This is an advantage over traditional surface chemistries, such as silanization or thiol self-assembly on gold that require specialized surfaces to work.

This work reports on the fabrication and use of the novel parylene-based "peelable" strips (Peel-Strips) array surface that combines both affinity-based screening and recovery of aptamers from a sample pool. Parylene-A layer was used to confer amine groups to the Peel-Strips for the covalent immobilization of a different protein on each strip. The Peel-Strips array patterned with proteins were then incorporated into a microfluidic format and exposed to a sample mixture containing aptamers for affinity-based screening. Microfluidics enable low reagent volume consumption through the miniaturization. Afterwards, each individual Peel-Strip could be simply peeled off to recover the aptamers that bound to the specific protein. As an initial proof of principle, aptamers known to bind to proteins implicated in disease (thrombin, VEGF, PDGF-BB) were tested for affinity binding and recovery. Aptamers recovery was quantified via fluorospectrometry and rolling circle amplification. Aptamer concentrations down to 1.6nM could be recovered and detected, depending on the aptamer affinity for the protein of interest. The work was then extended towards SELEX of a random ssDNA library pool, in an attempt to screen and recover aptamers against proteins (VEGF, PDGF-BB, TNF-α). Two cycles of SELEX was performed and results from fluorescent activated cell sorting (FACS) the recovered aptamer pool at the end of Round 2 did not show significant binding to the protein targets displayed on yeast cells. This is a preliminary study into SELEX and the experimental conditions and parameters need to be optimized to ensure success.

The advantages of Peel-Strips are: i) the ability to combine multiplexed affinity-based screening and individual sample recovery, ii) highly simplified sample recovery by peeling off each Peel-Strip without specialized equipment, and iii) preservation of sample integrity. In the future, Peel-Strips may be expanded to 96-wells format with many broad applications for recovering a diversity of affinity-captured biomolecules and cells in a compact and easy-to-use system.

6.2 EXPERIMENTAL METHODS

6.2.1 Fabrication of Peel-Strips

2.5mm of parylene-C (diX-C, Uniglobe Kisco) was conformally coated onto 22mm x 22mm thermally oxidized silicon chips via CVD using a Specialty Coating Systems Labcoter 2. This layer of parylene-C served as mechanical support to enable easy peeling and handling. 250nm of parylene-A (diX-A, Uniglobe Kisco) was deposited on top of the parylene-C layer using the same CVD process, to confer surface amine groups suitable for protein immobilization. The boundaries of the Peel-Strips were created by mechanically scoring with a razor blade to create 3mm wide rectangular strips. For future work in miniaturizing the Peel-Strips further, Peel-Strips with micrometer lengths and widths can be easily defined with photolithography and oxygen plasma etching as previously described for microfabrication of parylene stencils [11].

6.2.2 Covalent Immobilization of Proteins onto Peel-Strips

The top surface of the Peel-Strips (parylene-A layer) was treated with 500μL of 2.5% glutaraldehyde, a homobifunctional linker that would covalently cross-link amine groups on the Peel-Strip surface and the proteins [15]. The schematic in Figure 6.1 outlines the surface chemistry, while Figure 6.2 shows the process flow. To attach a biotinylated protein to the surface, the process was modified to first immobilize streptavidin with the surface amine groups, followed by incubation with the protein of interest (Figure 6.2). The proteins used in this study are listed in Table 6.1. All the incubation reactions were performed on the chips inside a humidified dish to reduce evaporation and prevent the solution droplets from drying out.

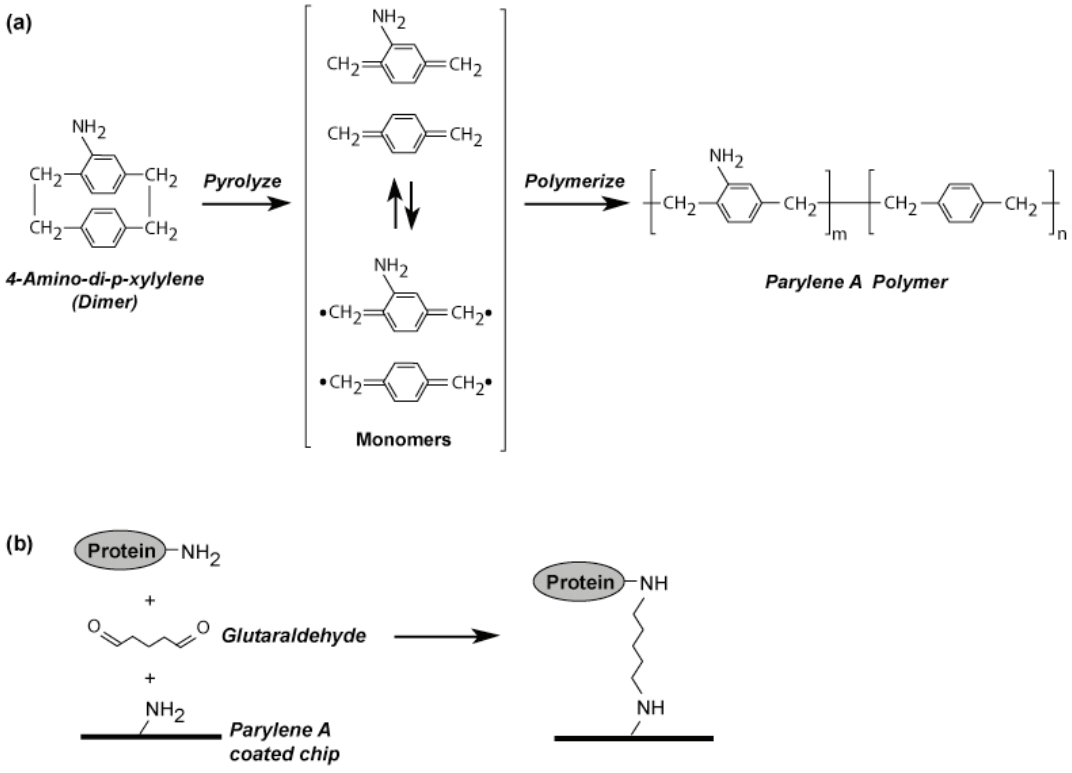

Figure 6.1 Schematic showing: (a) Parylene-A chemical structure and the CVD deposition process, and (b) covalent linkage of proteins to the parylene Peel-Strip surface.

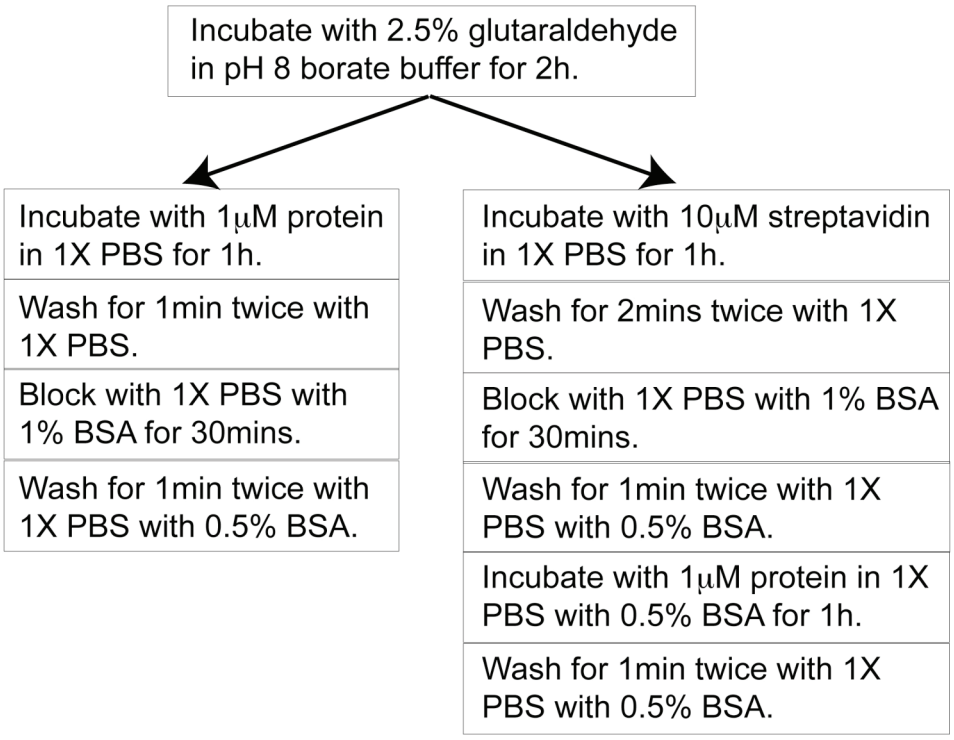

Figure 6.2 Process flow of protein immobilization onto Peel-Strips surface.

6.2.3 Fluorescent Immunostaining to Detect Protein Covalently Immobilized on Parylene-A

Proteins were immobilized on test chips coated with 250nm of parylene-A as described. Fluorescent was performed immunostaining using a primary antibody against the protein and a corresponding fluorophore conjugated secondary antibody, to confirm the presence of the protein on the surface. Chips immobilized with BSA served as negative controls for the fluorescent immunostaining. The primary antibodies were purchased from the same sources as the protein antigens in Table 6.1. AlexaFluor labeled secondary antibodies were obtained from Invitrogen. The primary antibodies were incubated on the chips at 50μg/mL diluted in 1X PBS with 0.5% BSA for 1h, and then washed twice for 2mins with 1X PBS with 0.5% BSA. Afterwards, the secondary antibodies were diluted 1:100 in 1X PBS with 0.5% BSA for 1h, and also washed similarly as before. Chips were imaged using fluorescence microscopy (Olympus AX70) using filter cubes designed for the specific fluorophores.

Table 6.1 Proteins used in this study.

Protein	MW (kDa)	Source
Human TNF-α	17.5	R&D Systems
Human $VEGF_{165}$	20	R&D Systems
Human PDGF-BB	24.3	Abcam
Human PSA	30	Biodesign International
Human α-Thrombin	37	Haematologic Technologies
Human biotinylated α-Thrombin	37	Haematologic Technologies

6.2.4 Fluorescence Assay to Test for Bioactivity of Covalently Immobilized Thrombin

Since α-thrombin is a serine protease, it was convenient to also test the bioactivity of the covalently immobilized enzyme. SN-59, a fluorogenic substrate for thrombin, was purchased from Haematologic Technologies and used to probe the bioactivity of thrombin. 10μM of BSA and thrombin were immobilized on parylene-A coated chips and three 2μL drops of 100μM SN-59 were incubated on the chips. The BSA chip served as a negative control for this assay. The fluorescence of the drop on the chip surface was imaged using fluorescence microscopy after 60 mins. As a comparison, the reaction of thrombin with SN-59 in free solution was also tested. SN-59 and thrombin were mixed in a 50μL volume inside a microcentrifuge tube at 100μM and 1μM final concentrations. The control tube contained a SN-59 and BSA mixture. Three 2μL drops of each mixture were removed at 0, 20, 30, 45, and 60mins, and imaged using fluorescence microscopy on a glass coverslip. The fluorescence of the three drops on each chip was averaged for each time point.

6.2.5 Fluorescence Microscopy Image Analysis

At least three images were collected at random positions on each chip for the analyses, both from the center of the chip where the protein was incubated and the peripheral region of the chip where no protein was incubated (background). Fluorescence intensity per pixel was recorded for each image using the histogram function in ImageJ software (National Institutes of Health). For background correction on each chip, the average fluorescence signal from background was subtracted from the average fluorescence signal from the center region.

6.2.6 Incorporation of Peel-Strips with Microfluidics Assembly

Table 6.2 lists the flow conditions used for the microfluidic experiments. 10μL of each protein was spotted and immobilized on each Peel-Strip as described. A 1mm thick silicone gasket (Grace Biolabs) defined with a 4mm wide x 20mm long fluidic channel was placed on the parylene Peel-Strips and sealed at the top with a 1mm thick glass coverslip containing two fluidic ports as shown in Figures 6.3(a), (b), (e). The NanoPort (Idex) at the outlet reservoir enabled mating with tubing connected to a peristaltic pump (Idex) that controlled the flow rate by withdrawing fluid. Two binder clips were used to clamp and seal the whole microfluidic assembly. Binding buffer (20mM Tris-HCl, 140mM NaCl, 5mM KCl, 1mM $MgCl_2$, 1mM $CaCl_2$) was utilized for all the microfluidic aptamer experiments. The coverslip and gasket can be reversibly separated from the chip to facilitate peeling of the Peel-Strips. Table 6.3 summarizes the samples flowed in various microfluidic experiments.

Table 6.2 Microfluidic chip flow conditions.

Step	Reagent	Flow Rate (μL/min)	Time (min)	Total Volume (μL)
Filling fluidic channel	Binding buffer	20	1	20
Introduce aptamers	Sample (see Table 6.4)	20	5	100
Wash	Binding buffer with 0.5% BSA	40	2.5	100

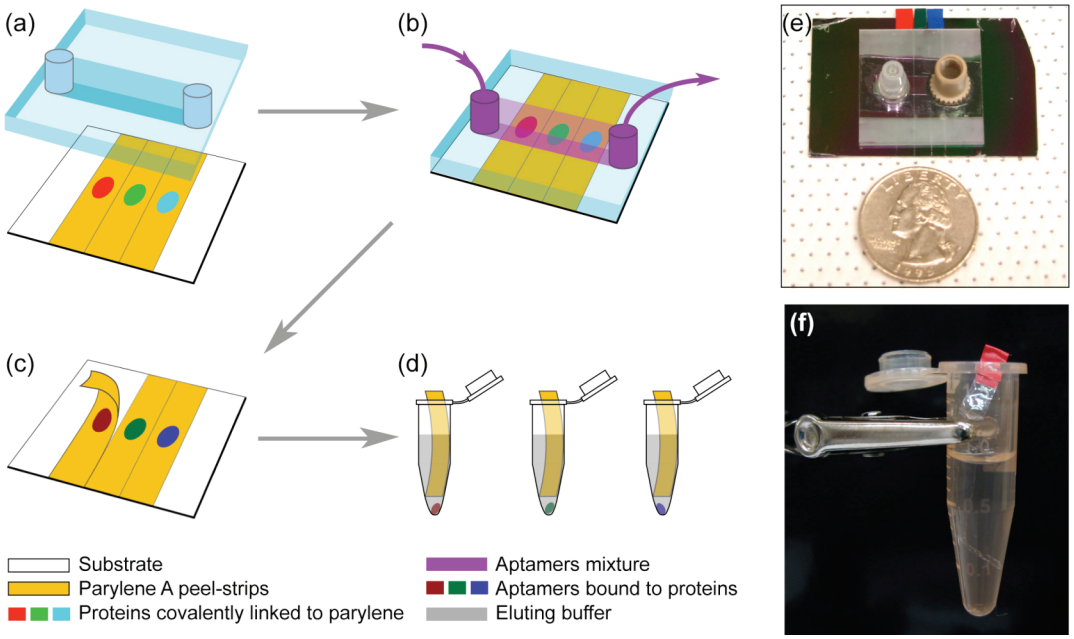

Figure 6.3 (a-d) Schematic showing integration of Peel-Strips with microfluidics, and the process for separating and recovering aptamers. (e) Photograph of actual device – the assembled Peel-Strips with microfluidics. (f) Recovery of bound aptamers as the strip is placed into an eluting buffer inside a microcentrifuge tube. Buffer is shown here for illustrative purpose, and does not represent the actual volume used.

Table 6.3 Samples introduced in various microfluidic experiments.

Experiment	Sample
Binding of known fluorescent aptamers	Fluorescent aptamers mixed in binding buffer to a final 5μM concentration each.
Binding of RCA aptamer-primers	Thrombin and PDGF-BB aptamer-primers mixed in binding buffers to final concentrations of 5μM, 1μM, 200nM, 40nM, 8nM, 1.6nM each.
SELEX Negative selection round	5μM DNA library in binding buffer.
SELEX Round 1	Flow-through solution collected from outlet in negative selection round.
SELEX Round 2	Bound aptamers eluted from peel-strips; PCR amplified by 12 cycles.

6.2.7 Individual Recovery of Bound Fluorescent Aptamers by Peel-Strips

All DNA sequences were purchased and purified by Integrated DNA Technologies. Known aptamer sequences for thrombin [17], PDGF-BB [18], and VEGF [19] were modified to contain the fluorophore AlexaFluor 488, 594, and 647 respectively (Table 6.4). Each Peel-Strip containing the bound aptamers was mechanically peeled off using sterile tweezers (Figure 6.3(c)) and placed inside a microcentrifuge tube. Milty Zerostat3 was used to neutralize static charges on the strips. 20mM sodium hydroxide (Figure 6.3(d-f)) was added to elute off the aptamers. After 1min, the sodium hydroxide solution was retrieved by a pipette into a clean tube and neutralized with a 1M hydrochloric acid. Each strip was washed again with 10μL deionized water, which was then collected and pooled with the previous eluent. Relative amounts of fluorescent aptamers eluted from each strip were detected using a Nanodrop ND3300 fluorospectrometer.

Table 6.4 Sequences of DNA used

Name	Sequence (5'->3')	Bases
AlexaFluor 488 thrombin aptamer	*AlexaFluor488*-TTTTTTTTTTTT GGTTGGTGTGGTTGG	27
AlexaFluor 594 PDGF-BB aptamer	*AlexaFluor594*-TTTTTTTTTTTT TACTCAGGGCACTGCAAGCAATTGTGGTCCCAATGGGCTGAGTAT	57
AlexaFluor 647 VEGF aptamer	*AlexaFluor647*-TTTTTTTTTTTT CCCGTCTTCCAGACAAGAGTGCAGGGG	39
Thrombin template	*phos*-AGGACACGCATTTTACTAGATAGCTAGCTTTCGATCGTTCTGAGCAGACAACG	53
Thrombin aptamer-primer	GGTTGGTGTGGTTGG TTTTTTTTT AATGCGTGTCCTCGTTGTCTGCTC	48
PDGF-BB template	*phos*-TAGCACGGACATATATGATGGTACCGCAGTATGAGTATCTCCTATCACTACTAAGTGGAAGAAATGTAACTGTTTCCTTC	80
PDGF-BB aptamer-primer	TACTCAGGGCACTGCAAGCAATTGTGGTCCCAATGGGCTGAGTAT TTTTTT TGTCCGTGCTAGAAGGAAACAGTTAC	77
DNA Library	GGGAGAATTCAACTGCCATCTAGGC -N_{60}- GTACTACAAGCTTCTGGACTCGGT	109
Libfwd	GGGAGAATTCAACTGCCATCTAGGC	25
Librev1	ACCGAGTCCAGAAGCTTGTAGTAC	24
Librev2	*phos*-ACCGAGTCCAGAAGCTTGTAGTAC	24

6.2.8 Rolling Circle Amplification of Recovered Aptamers

Rolling circle amplification (RCA) was exploited as a more sensitive detection method to analyze the recovered aptamers, since some of the aptamers used (*e.g.* thrombin-aptamer with 15 bases) were too short to be used as a template for PCR. The known aptamers for thrombin and PDGF-BB tested in Section 6.2.7 were each modified to contain a unique primer region (aptamer-primer, sequences shown in Table 6.4). In the presence of the aptamer-primer with sequence complementary to the circular template, the highly processive isothermal ϕ29 polymerase linearly amplifies and also displaces the growing ssDNA strand continuously to create a large MW RCA product (Figure 6.4).

Phosphorylated ssDNA template with the complementary sequence to the each aptamer-primer (Table 6.4) was ligated using CircLigase I enzyme from Epicentre Biotechnologies (Table 6.5) to create the circular templates. Unligated ssDNA templates were removed via ExoI/III digestion. To verify successful ligation, 2μL of the ligase reaction were loaded and electrophoresed in a 10% TBE urea denaturing polyamcrylamide gel (Novex, 180V, 40mins), together with the negative controls of unligated ssDNA template and unligated ssDNA template with ExoI/III treatment.

RCA was performed under the conditions in Table 6.6. After polymerase inactivation, 5μL of each RCA reaction were loaded into a 1% agarose gel and electrophoresed to visualize the large MW RCA products. Table 6.7 shows the design of experiment for microfluidic selection and recovery of the aptamer-primers by Peel-Strips functionalized with thrombin, PDGF-BB, and VEGF. Aptamer-primers eluted from each strip were probed with thrombin and PDGF-BB circular templates to confirm the correct capture of the aptamer-primer by the proteins and nonspecific binding if any. Mixtures of aptamer-primers with 5-fold concentration dilutions were used in the microfluidic experiments to determine the limit of detection of RCA.

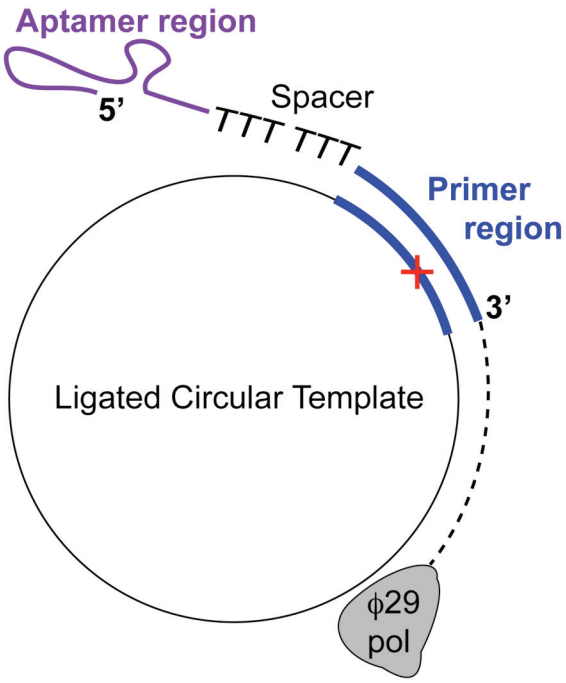

Figure 6.4 Schematic of RCA detection scheme. Each aptamer was designed to carry a primer region that was complementary to a specific ligated circular template. Note that the sequences of the PDGF-BB and thrombin ligated circular templates are different and unique as shown in Table 6.4. Upon successful hybridization of the primer region to the correct template, the ϕ29 polymerase then continuously amplify and displace the growing ssDNA strand from the circle template. Hence, a large MW ssDNA product is created if and only if the aptamer bearing the correct primer region is present.

Table 6.5 Reaction for ligating phosphorylated ssDNA

Components	**Stock**	**Final Concentration**	**Volume (μL)**
Phosphorylated ssDNA template	10μM	0.5μM	2
10X CircLigase reaction buffer	10X	1X	4
ATP	1mM	50μM	2
Manganese chloride	50mM	2.5mM	2
CircLigase I*	100U/μL	5U/μL	4
Water			26
		Total volume	40

*Heat mixture at 95^{o}C for 5mins and snap cool on ice before adding CircLigase I.
Incubate at 60^{o}C for 2h.
Inactivate ligase at 80^{o}C for 10mins and snap cool on ice.
Add 1μL each of ExoI (stock 20U/μL) and ExoIII (stock 200U/μL).
Incubate at 37^{o}C for 1h.
Inactivate exonucleases at 80^{o}C for 15mins.

Table 6.6 RCA reaction conditions.

Components	Stock	Final Concentration	Volume (μL)
Circular template	Ligase reaction	N/A	2
Aptamer-primer	Eluent from Peel-Strip	N/A	4
10X RepliPHI buffer	10X	1X	1
dNTP	25mM each	2.5mM	1
DTT	100mM	5mM	0.5
ϕ29 polymerase	100U/uL	5U/uL	0.5
Water			1
		Total volume	10
Incubate at 30°C for 3h. Inactivate polymerase at 65°C for 10mins.			

Table 6.7 RCA design of experiment for testing Peel-Strips eluent.

Eluent from Peel-Strip of:	**PDGF-BB**	**PDGF-BB**	**Thrombin**	**Thrombin**	**VEGF**	**VEGF**
Perform RCA with circular Template:	PDGF-BB ligated circle	Thrombin ligated circle	PDGF-BB ligated circle	Thrombin ligated circle	PDGF-BB ligated circle	Thrombin ligated circle

6.2.9 Systematic Evolution of Ligands by Exponential Enrichment of Aptamers from an Initial Random ssDNA Library

Next, microfluidic Systematic Evolution of Ligands by Exponential Enrichment (SELEX) was attempted to isolate aptamer candidates for three proteins (TNF-a, PDGF-BB, and VEGF), from an initial random pool of ssDNA library. The original DNA library used contained a 60 random bases variable region, flanked on each end by a constant primer region (24–25bases) as shown in Table 6.4. Figure 6.5 illustrates the process flow of SELEX.

In this initial test, two rounds of SELEX were performed using the microfluidic Peel-Strips after one round of negative selection. Negative selection is important to reduce nonspecific binding of aptamers to the device or specific aptamers that bind to BSA.

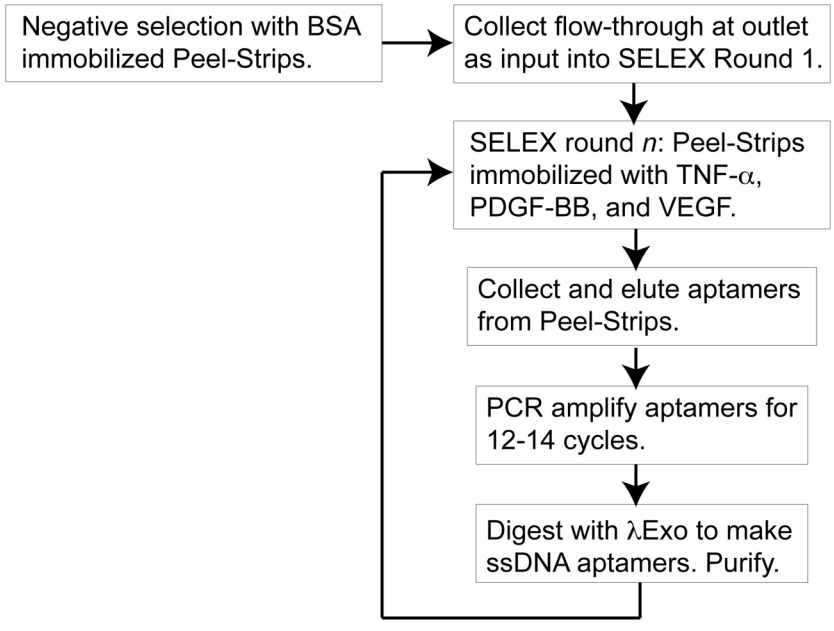

Figure 6.5 Flow chart showing microfluidic SELEX process.

The ssDNA pool that flowed through the BSA functionalized Peel-Strips microfluidic device was collected at the output, and then introduced into a new device functionalized with the three proteins. ssDNA captured on each Peel-Strip with different protein was eluted as described before, and then amplified using KOD Hot Start polymerase (Novagen) under the conditions in Table 6.8. The reverse primer for PCR amplifcation was intentionally modified to carry a 5'phosphate as listed in Table 6.4. λExo preferentially digests 5'phosphorylated DNA, and was used after PCR to remove the 5'phosphate reverse DNA strand to create ssDNA aptamers (forward DNA strand). Specifically, 20μL of λExo (Epicentre Biotechnologies, 10U/μL) and 13μL of 10X λExo reaction buffer was added to the PCR reaction volume, and then incubated at 37^{o}C for 30mins. Subsequently, λExo was inactivated at 75^{o}C for 10mins.

Table 6.8 PCR amplification reaction

Components	**Stock**	**Final Concentration**	**Volume (μL)**
Primers (forward & reverse)	10uM each	200nM	4
Aptamer eluted from Peel-Strips	N/A	N/A	18
Magnesium sulfate	25mM	1.5mM	6
10X KOD buffer	10X	1X	10
dNTP mix	2mM	200uM	10
KOD Hot Start polymerase	1U/uL	0.01U/uL	1
Water			51
		Total volume	100
Pre PCR Cycle	95^{o}C for 5mins, 55^{o}C for 1min, 72^{o}C for 5mins		
12x PCR Cycles	95^{o}C for 30s, 55^{o}C for 1min, 72^{o}C for 1min		
Polishing Step	72^{o}C for 10mins		

6.2.10 Fluorescence Activated Cell Sorting to Test Binding Efficacy of Aptamer Pools

Yeast surface display system was used to express proteins (either TNF-α, PDGF-BB, or VEGF) on the yeast cell wall (a kind gift from Dr. Moonsoo Jin) [20, 21]. Yeast cells were induced for specific protein expression in selective galactose medium. Negative controls were yeast cells that have not been induced. Good display of expressed protein on the yeast cell wall was shown by the binding of antibodies against Flag or c-myc tags that are cloned onto and carried on the protein C-terminus.

The original ssDNA library and the Round 2 ssDNA pool were fluorescently labeled by hybridizing the biotinylated reverse primer (Table 6.4) to the ssDNA in a 1:1 ratio, followed by incubating the biotinylated ssDNA with streptavidin-PE in a 4:1 ratio. The PE fluorescently labeled ssDNA aptamer pools were then incubated at 100nM concentration with harvested yeast cells (either induced and negative control) in a V-bottom 96-wells plate at 30^{o}C for 20mins with shaking. After incubation, the cells were washed in 100μL binding buffer with 0.5% BSA, and resuspended in 100μL binding buffer for FACS analysis (Coulter). To test for expression of proteins on yeast surface, induced and control yeast cells were incubated with anti-c-myc and anti-Flag primary antibodies, followed by fluorescent secondary antibodies and then washed and resuspended for FACS. Results were analyzed using the WinMDI 2.9 freeware from the Scripps Institute.

6.2.11 Statistical Analyses

Student's t-test was used to determine statistical significance ($p<0.01$). At least n=3 replicate chips were used for each experiment. Furthermore, three images at random positions were taken on each chip. These measurements were then averaged. The bar graphs show the average values and the error bars show standard deviations.

6.3 RESULTS AND DISCUSSIONS

6.3.1 Presence of Covalently Immobilized Proteins on Peel-Strips

Figure 6.6 shows the fluorescent immunostaining results of various proteins immobilized on the Peel-Strips. Compared to the control (BSA) surface, the chips that have been incubated with proteins show a statistically significant increase in fluorescence due to the antibodies detecting the proteins present on the surface ($p<0.01$). These results indicate that proteins of a range of molecular weights can be immobilized on the parylene-A surface. These findings are consistent with another report that showed antibody binding to proteins covalently linked to parylene-A coated polystyrene microplates [15].

However, the fluorescent immunostaining results can only be qualitative due to differences in the background fluorescence values at various excitation and emissions wavelengths. This is due to the background autofluorescence of parylene-A, which is shown in Figure 6.7 collected at the emission wavelengths corresponding to different AlexaFluor fluorophores. The chips were excited at the optimum peak excitation wavelengths of the fluorophores. Parylene-A showed the highest autofluorescence at the 616nm emission wavelength and the least autofluorescence at the 670nm. Parylenes also have extraordinarily large autofluorescence at UV wavelengths and are rapidly bleached upon excitation (data not shown). To minimize interference from background autofluorescence, it is recommended to conduct fluorescence studies that involve parylene as the substrate at the red emission wavelengths. For this qualitative study simply to detect the presence or absence of proteins from the parylene-A surface, the autofluorescence of parylene did not pose a problem since the signals from the antibodies were much higher than the background autofluorescence.

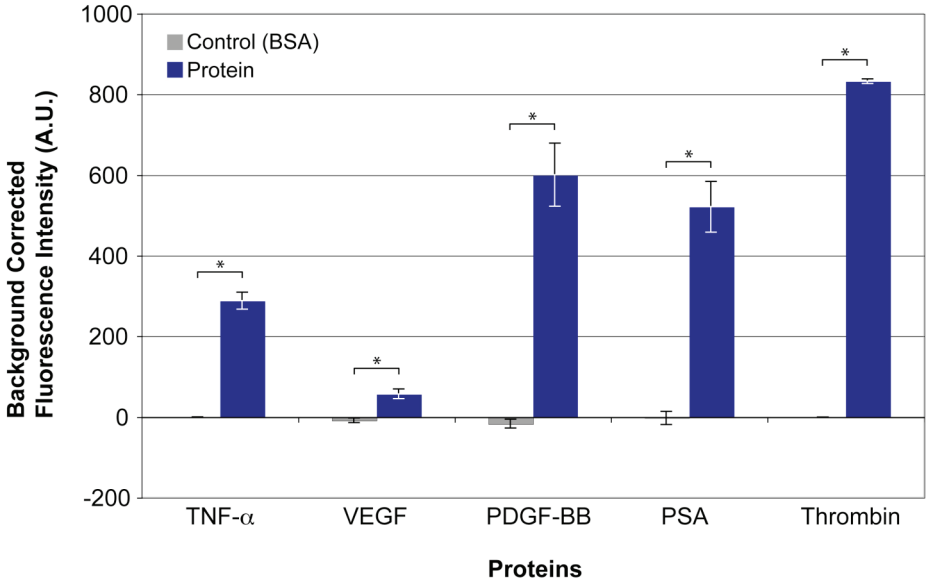

Figure 6.6 Fluorescent immunostaining of covalently immobilized proteins on parylene-A coated chips. Chips functionalized with BSA served as a control for each protein-antibody pair tested. All proteins tested are present on the parylene-A surface (*$p<0.01$).

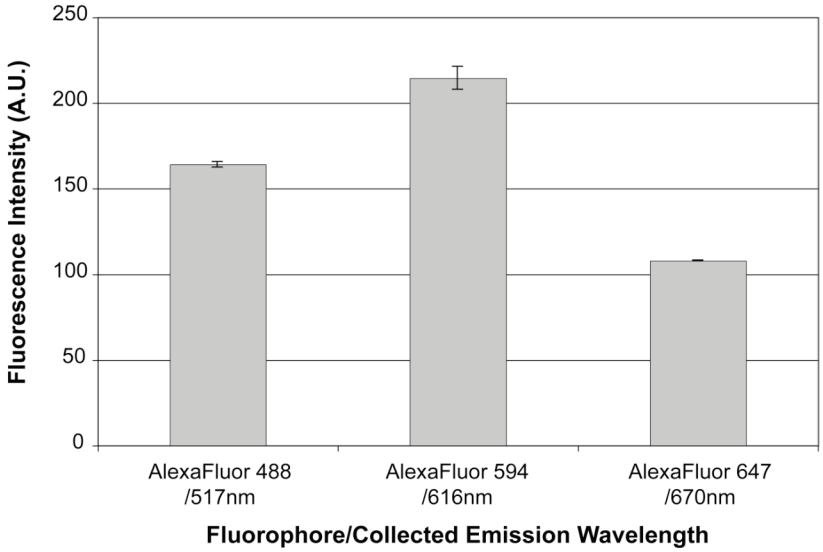

Figure 6.7 Autofluorescence of parylene-A corresponding to the emission wavelengths for different fluorophores.

6.3.2 Bioactivity of Immobilized Thrombin on Parylene-A

Thrombin is a serine protease that can recognize and cleave a range of peptide sequences, amongst which is the valine-proline-arginine sequence. SN-59 is a 6-amino-1-napthalenesulfonamide based fluorogenic substrate for thrombin that contains the valine-proline-arginine sequence. Once cleaved from this peptide moiety, SN-59 exhibits a 1,000-fold increase in fluorescence intensity.

Figure 6.8(a) shows the curve of fluorescence increase with time as more SN-59 was cleaved by thrombin in free solution. Figure 6.8(b) shows a 300-fold increase in fluorescence of the chip immobilized with 10μM thrombin compared to the control chip immobilized with BSA, comparable to the fluorescence of 1μM thrombin incubated with the same SN-59 concentration in free solution.

While this one assay is not an exhaustive conclusion that thrombin bioactivity is wholly maintained, the results do indicate that immobilized thrombin retains some bioactivity, in this case for recognizing and cleaving the valine-proline-arginine peptide sequence. This result here is important to show that thrombin retains some bioactivity. Most studies thus far only test for the presence of immobilized proteins via antibody binding, but not the functional bioactivity of an immobilized protein on parylene-A surface [15, 22], except in one study by Lahann *et al.* whereby r-hirudin protein was immobilized in metallic implant devices to resist blood clotting *in vivo* [13].

6.3.3 Binding of Fluorescent Aptamers to Proteins Immobilized on Peel-Strips in Microfluidics

Fluorescently labeled known aptamers for thrombin, PDGF-BB, and VEGF (Table 6.4) were first individually tested for binding to proteins immobilized on parylene-A coated chips, following similar process steps as the fluorescent

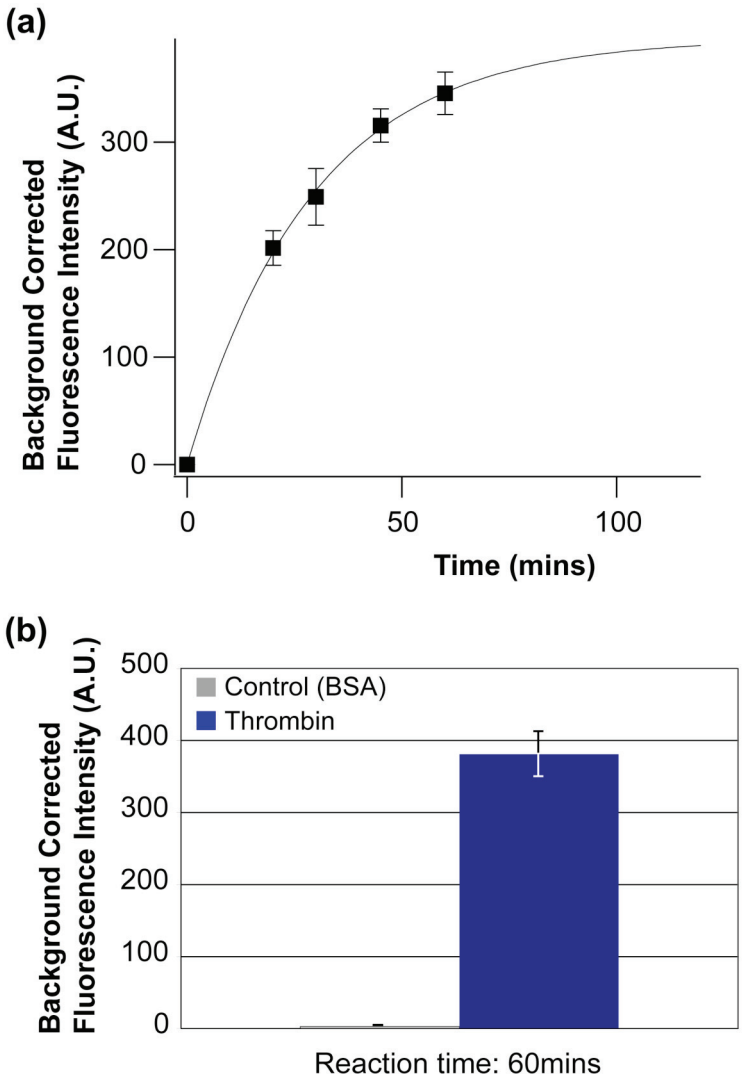

Figure 6.8 Fluorescence assay of thrombin cleaving the fluorogenic substrate SN-59 in (a) free solution at 10μM thrombin concentration, and (b) immobilized thrombin incubated at 1μM concentration.

immunostaining studies but only using aptamers instead of antibodies. Figure 6.9 shows the successful binding of the fluorescent aptamers to their corresponding proteins ($p<0.01$). Control chips with BSA showed little to no fluorescent signal (no binding). Even though immobilized thrombin was present on the chips as verified by fluorescent immunostaining in 6.3.1 and its bioactivity was retained in 6.3.2, however the 15-mer AlexaFluor 488 thrombin-aptamer did not bind to thrombin (data not shown). The thrombin-aptamer could only bind to biotinylated thrombin that was indirectly immobilized via streptavidin method described in Figure 6.2. The thrombin in Figure 6.9 was biotinylated and immobilized via streptavidin, and its corresponding control chip was functionalized with biotin-BSA.

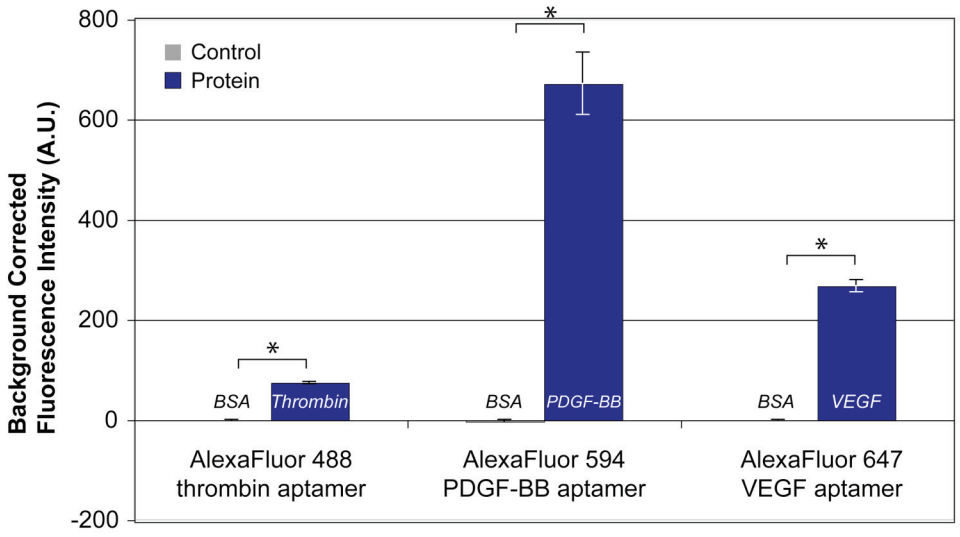

Figure 6.9 Fluorescence intensity showing aptamers binding to the correct proteins tested (thrombin, PDGF-BB, and VEGF, *$p<0.01$). Aptamers showed little to no binding to the BSA control chips. The thrombin protein (biotin-thrombin) was immobilized on the Peel-Strip via indirect streptavidin linkage, and the corresponding control chip was functionalized with biotin-BSA.

The fluorescent aptamers were then mixed in a 100μL volume to 5μM final concentrations (Table 6.4) and flowed through the microfluidic Peel-Strips device. Three Peel-Strips are present in each microfluidic device and each strip was spotted and immobilized with a different protein. After washing, the glass coverslip and silicone gasket were removed from the chip. Each individual Peel-Strip was imaged using fluorescence microscopy before peeling off (Figure 6.10) to check for successful binding of the aptamer to the correct protein and also to test for non-specific binding. The results in Figure 6.10 showed specific and high affinity binding of the aptamers for their corresponding proteins. The AlexaFluor 647 VEGF-aptamer showed some non-specific binding for PDGF-BB protein on the Peel-Strip. Thrombin aptamer preferentially bound to the thrombin Peel-Strip to give a ~1.8 fold increase in fluorescence signal over the other strips, while PDGF-BB and VEGF aptamers gave a ~2.9 fold and ~2.5-fold increase respectively. Presumably, these differences in fold-increase of fluorescence are due to the different affinity of aptamers binding to the proteins, but could also be convolved with parylene-A autofluorescence. Hence, the captured fluorescent aptamers on each strip was eluted with sodium hydroxide and measured using fluorospectrometry to mitigate the issue of parylene autofluorescence.

Fluorescence measurements of the eluted aptamers from each Peel-Strip by the fluorospectrometer confirmed that the aptamers bound specifically and with high affinity to their correct proteins, as shown in Figure 6.11. However differences in the amount of nonspecific binding (albeit low) to the irrelevant proteins could be observed. While the aptamers still showed high signal binding to the correct proteins, the increase in fluorescence intensity over the irrelevant proteins are different from Figure 6.10. The results in Figure 6.11 should be more accurate in reflecting the affinity binding of aptamers to the proteins, since the problem of parylene autofluorescence is eliminated.

However, even though a relatively high concentration of fluorescent aptamers was used (5μM each), unfortunately the fluorescence R.F.U. measured was already at the limit of detection of the fluorospectrometer. A more sensitive method for detecting the eluted aptamers is needed, such as RCA that is utilized in section 6.3.4.

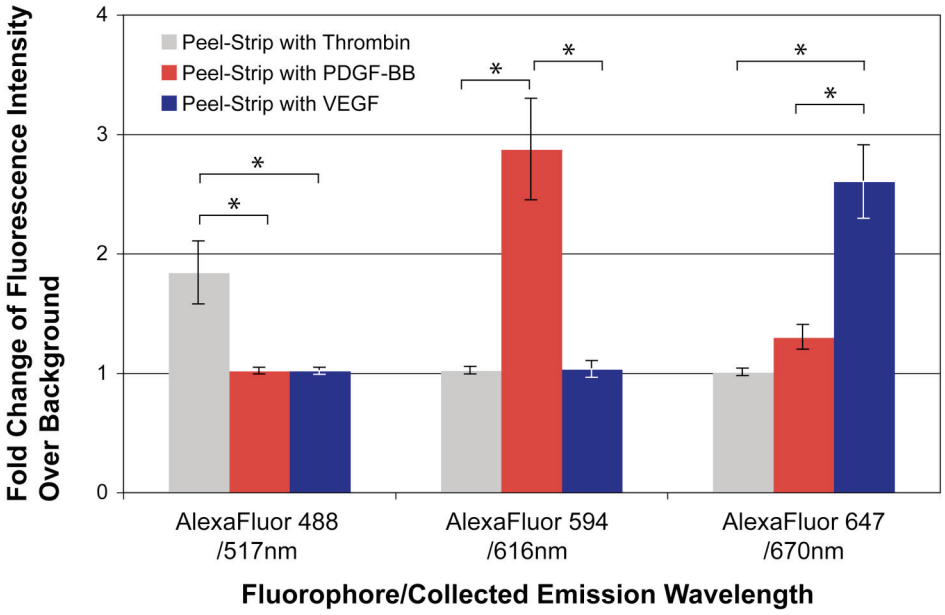

Figure 6.10 Fluorescence microscopy of Peel-Strips showing aptamers binding to the correct proteins (*$p<0.01$). Fluorescence intensities are normalized over the background as fold-changes to account for differences in parylene-A autofluorescence over the various emission wavelengths.

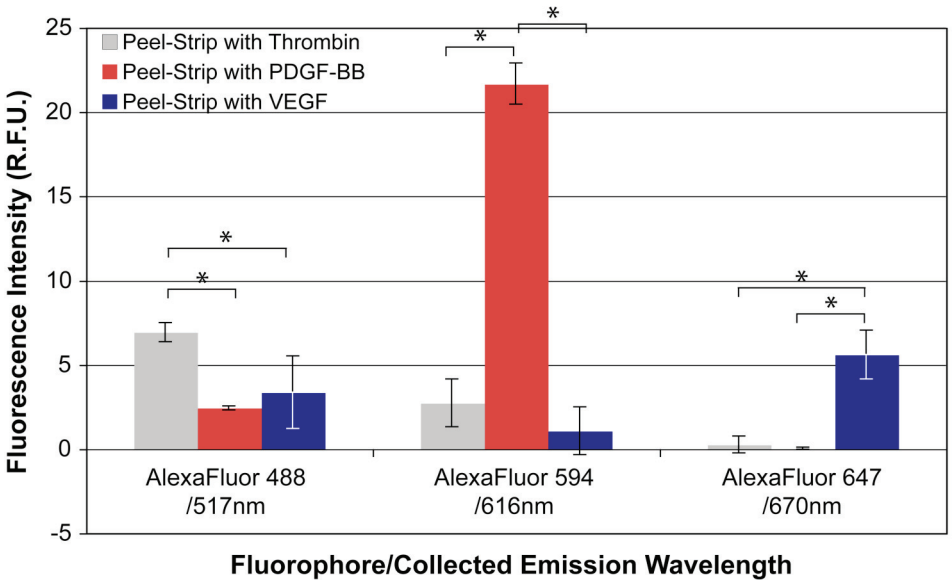

Figure 6.11 Fluorospectrometer measurements of aptamers eluted from different Peel-Strips confirmed again that the aptamers bound specifically and with high affinity to the correct proteins compared to other nonspecific proteins (*$p<0.01$).

6.3.4 RCA of Aptamers Recovered by Microfluidic Peel-Strips

RCA was exploited as a potentially more sensitive detection method to analyze the recovered aptamers, since the limit of detection of fluorometry was reached in section 6.3.3 and PCR-based methods are inapplicable due to the short aptamer length (the 15 bases long thrombin-aptamer is smaller than a PCR primer).

The denaturing polyacrylamide gel in Figure 6.12 shows that ligated circles were successfully ligated from 5'phosphorylated ssDNA templates (PDGF-BB template and thrombin template, Table 6.4). The electrophoretic mobility of circular ssDNA is slower than that of linear ssDNA, which can be seen from the upwards shift in the bands in lanes 2 and 5 (ligated circles) compared to the bands in lanes 3 and 6 (linear ssDNA). Another confirmation is the presence of the bands in lanes 2 and 5

after ExoI/III digestion, since circular DNA is not digested. On the contrary, ssDNA were digested and the DNA bands were absent in lanes 4 and 6.

RCA was performed with the circle templates and aptamer-primers. As shown in the 1% agarose gel, RCA products larger than 10kbp were formed and remained in the loading wells of lanes 2 and 4, corresponding to PDGF-BB circle template/PDGF-BB aptamer-primer and thrombin circle template/thrombin aptamer-primer. Smears of incomplete RCA products of various molecular weights were also formed in these lanes. RCA did not occur when the circle templates were mixed with a non-complementary irrelevant aptamer-primer (lanes 3 and 5), showing specificity of the RCA reaction depending on whether the correct aptamer-primer is present.

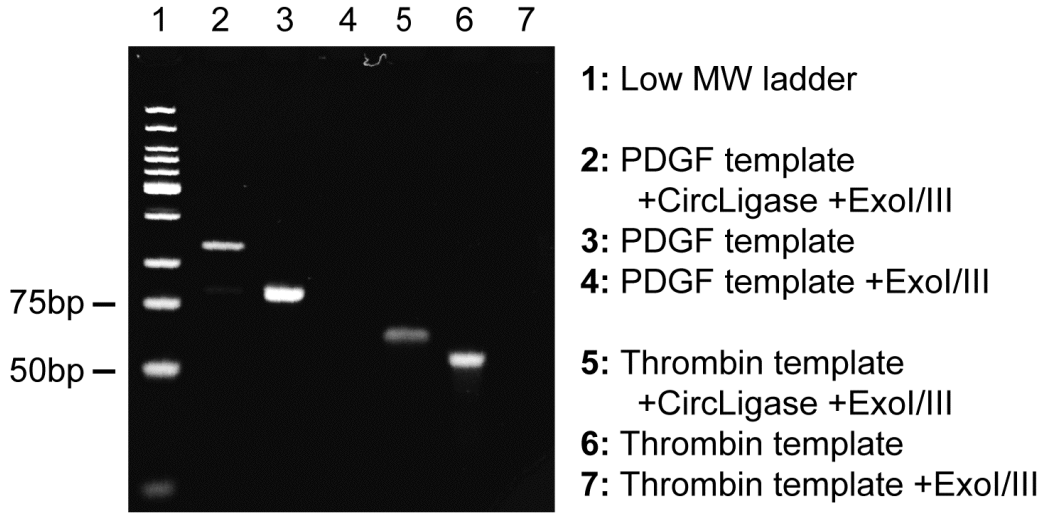

Figure 6.12 10% TBE urea denaturing polyacrylamide gel of ligated circle products. Circularized ssDNA (lanes 2, 5) migrates slower than linear ssDNA (lanes 3, 6). Additionally, circularized ssDNA is not digested by ExoI and III (lanes 2, 5), while linear ssDNA is digested by ExoI and III (absence of bands in lanes 4, 7). The PDGF-BB template (80bases) has a different sequence from the thrombin template (53bases).

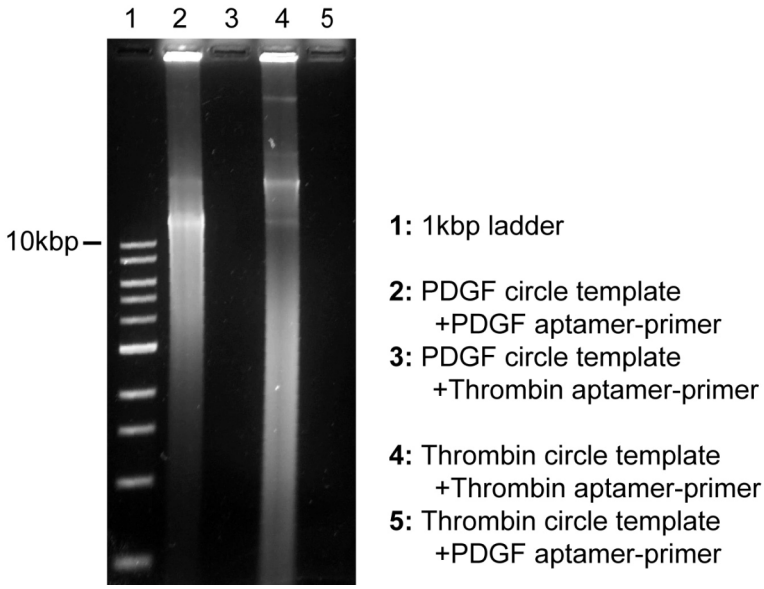

Figure 6.13 1% agarose gel. RCA products were formed (DNA product larger than 10kbp that remained inside the loading wells, and smears of various MW DNA products) when PDGF circle templates were incubated with the PDGF aptamer-primer (lane 2), and when thrombin circle templates were incubated with the thrombin aptamer-primer (lane 4). No RCA products were formed when the circles were incubated with the irrelevant aptamer-primers (lanes 3 and 5).

The eluted aptamer-primers from each Peel-Strip were split into two tubes for RCA reactions with PDGF-BB circle template and thrombin circle template. This was performed for each Peel-Strip chip flowed with a different starting concentration of aptamer-primers as described in Table 6.3 and Table 6.7. Figure 6.13 shows the 1% agarose gels of the RCA reaction products using eluents from the Peel-Strips. At high concentrations of the aptamer-primer mixtures (5μM and 1μM) flowed into the microfluidic device, nonspecific binding of the aptamer-primers to the Peel-Strips was abundant and could be seen by the RCA products formed for all lanes 2-7. In the

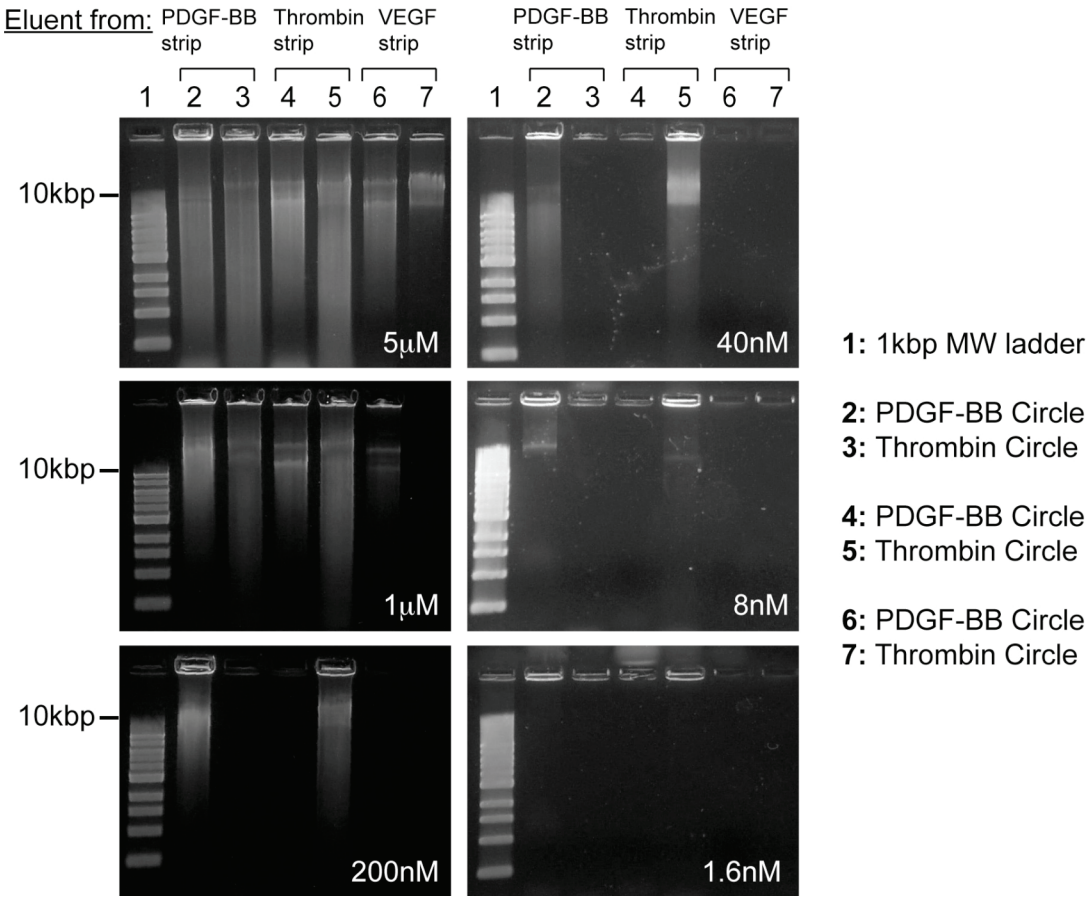

Figure 6.14 1% agarose gel. RCA products of PDGF-BB and thrombin aptamer-primers recovered from Peel-Strips immobilized with proteins.

future, more rigorous washing could potentially reduce this nonspecific binding, either by increasing the flow rate or lengthening the washing times. For mixture flowed with a reduced aptamer-primer concentration (200nM and below), the nonspecific binding of the aptamer-primer to the irrelevant proteins is greatly reduced as seen in Figure 6.14. Only lanes 2 and 5 showed RCA products formed as expected, since they are the only RCA reactions containing circle templates with the correct aptamer-primers. As the mixture concentration of aptamer-primers flowed into the microfluidic device decreased, the smears in the lane gradually diminished as less incomplete RCA products were formed. The detection limit of the RCA reaction (stopping at 3h) is about 1.6nM of starting aptamer-primers mixture flowed into the microfluidic device. The gel for 1.6nM aptamer-primers still showed the large RCA products inside the loading wells of lanes 2 and 5 in Figure 6.14.

6.3.5 SELEX of Aptamers From an Initial Random ssDNA Library

The reaction conditions of λExo to digest dsDNA with a 5'phosphorylated reverse strand were tested. Two pilot PCR reactions were performed on the ssDNA library using regular primers (Libfwd and Librev1) and with regular forward/5'phosphorylated reverse primer (Libfwd and Librev2). Each PCR reaction were split into two tubes (with or without λExo added). The digested reactions were purified via a Qiaquick PCR purification kit, and electrophoresed on a 10% TBE urea denaturing polyacrylamide gel. As shown in Figure 6.15, two separate bands are present in each lane (lanes 2 and 3), which are the two denatured DNA strands formed from regular PCR. Lane 6 shows a single strong band that represent the ssDNA from the unamplified initial library. Lane 4 has one band since the 5'phosphorylated reverse strand was digested by λExo, while lane 5 shows two bands since there is no enzyme added.

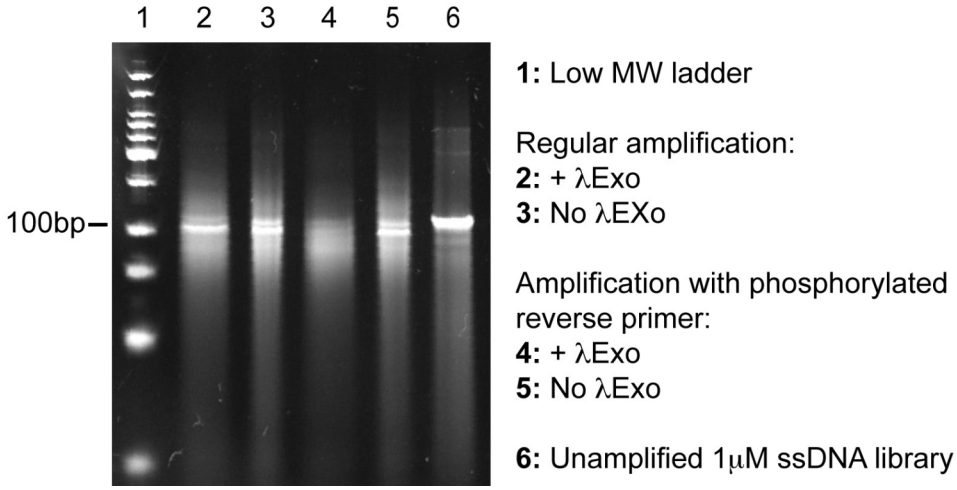

Figure 6.15 10% TBE urea denaturing polyacrylamide gel showing PCR products with and without λExo digestion. Two bands were seen in each lane (for lanes 2, 3, 5), since reverse strands were not digested. Lane 6 shows one band since library is ssDNA. Lane 4 shows one band after digestion of the 5'phosphorylated reverse strand.

From the negative selection round, Lanes 5 and 6 in Figure 6.16 show the ssDNA collected from a Peel-Strip functionalized with BSA and the flow-through ssDNA pool (<5μM) collected from the outlet reservoir. As expected, most of the ssDNA flowed through the microfluidic device, while a small fraction bound to the BSA on the Peel-Strip. Lanes 2, 3, and 4 are PCR amplified and λExo digested products from the aptamers eluted from the Peel-Strips after SELEX Round 2. These three lanes show a strong band of amplified product near 100bp, which corresponds to the expected size of the PCR products. There is an unexplained faint band at ~200bp for the eluent from the PDGF-BB Peel-Strip, which could be a contaminant from the environment. The PCR amplified and λExo digested reactions were purified via Qiaquick PCR purification kit and their concentrations were measured using the Nanodrop spectrophotometer to determine the dilution factor for FACS analysis.

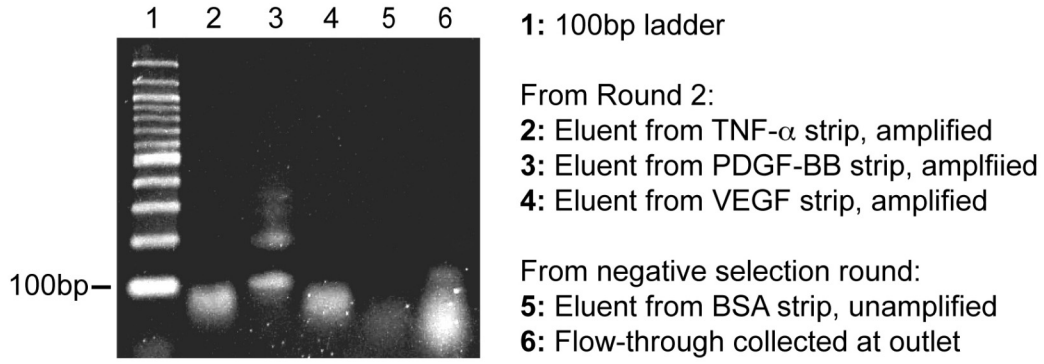

Figure 6.16 3% agarose gel showing PCR amplification products from SELEX Round 2, as well as the collected ssDNA from the negative selection round.

Yeast cells showed good display of PDGF-BB and VEGF on the cell wall, as verified by fluorescent immunostaining of c-myc tags co-expressed on the C-terminus of the expressed proteins. For both PDGF-BB and VEGF expressing cells, the FACS histograms show an increase in the number of induced yeast cells with a higher fluorescence intensity (histogram curve shifts to the right) compared to the control noninduced yeast cells (curve with shaded gray area) in Figure 6.17. Unfortunately, induced yeast cells did not seem to express TNF-α, since the histogram curve directly overlays the control non-induced yeast cells. For yeast cells expressing VEGF, the original ssDNA library did not show binding to the VEGF (histogram curve shifts to the left compared to non-induced control yeast histogram), while the SELEX Round 2 aptamer pool showed perhaps slight binding to VEGF (histogram curve showed negligible shift to the right compared to non-induced control yeast histogram). For yeast cells expressing PDGF-BB, the original ssDNA library showed binding to the PDGF-BB (histogram curve shifts to the right compared to non-induced control yeast), while the SELEX Round 2 aptamer pool showed some binding to PDGF-BB

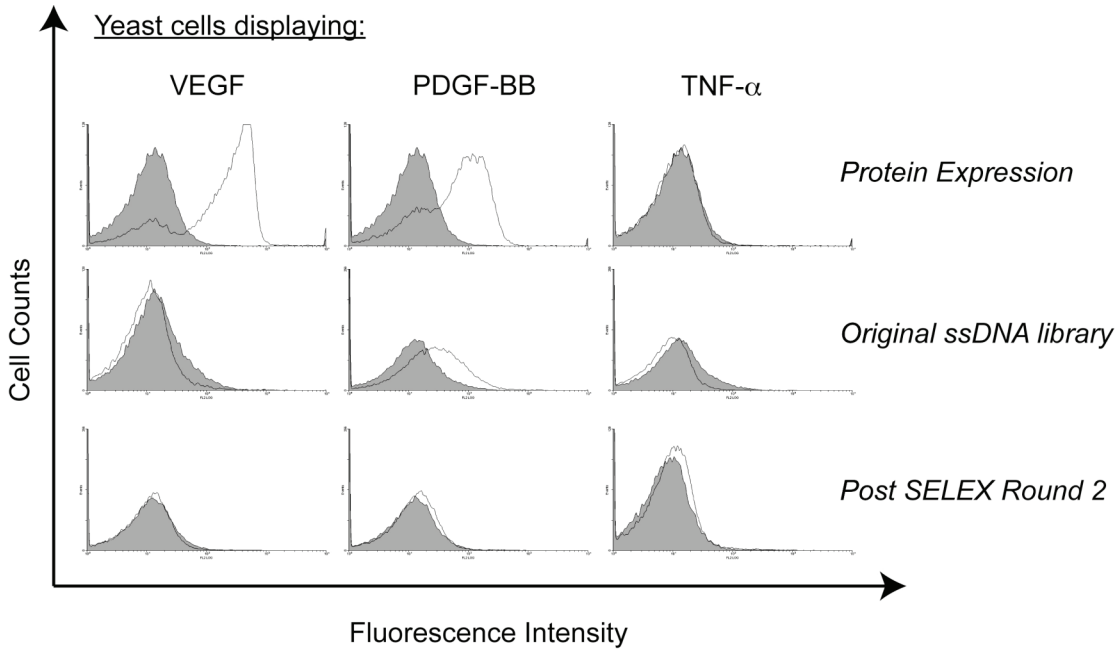

Figure 6.17 FACS analysis of fluorescent immunostaining and fluorescent aptamer binding to proteins expressed on yeast surface. Yeast cells showed good display of VEGF, PDGF-BB, but not TNF-α on the surface from the antibodies immunostaining. The original ssDNA library showed negligible binding to VEGF, but surprisingly favored binding to PDGF-BB. Post SELEX round 2 aptamer pools showed very small binding to VEGF and PDGF-BB over the control non-induced yeast cells (histograms with gray areas). TNF-α data was not considered since the yeast failed to express/display the protein.

(histogram curve showed negligible shift to the right compared to non-induced control yeast histogram), but less than the original library. TNF-α was not considered since the induced yeast cells did not express the protein.

It was surprising that the original ssDNA library showed more binding to PDGF-BB compared to SELEX Round 2 aptamer pool. However, the isoelectric point of PDGF-BB is at pH 9.8 [23] and so the protein is cationic (positively charged) in the SELEX binding buffer pH 8.0<<9.8. Nonspecific electrostatic interactions may be occurring between the original DNA library and the PDGF-BB. The isoelectric point of VEGF is at pH 7.9 [24], and so the protein is neutral at pH 8.0 (binding buffer) unlike PDGF-BB. Yeast cells expressing TNF-α should also be optimized for protein expression. More cycles of PCR should be performed after each SELEX round to ensure that abundant aptamer pools are generated, as the 12-14 cycles of PCR performed here were only enough for one experiment with FACS. For future work, more rounds of SELEX could be performed for better evolution of aptamer pools. In literature, microfluidic-based SELEX have been shown to achieve aptamer pools for high affinity binding with proteins after only three rounds [8] or even one round of SELEX [7]. It is worth noting that one of these studies involve selecting aptamers for PDGF-BB [8] and the original synthesized library may already be biased [25] in favor of binding to PDGF-BB (as seen from Figure 6.17).

6.4 CONCLUSIONS

A simple chip consisting of parylene-A coated Peel-Strips was developed for covalent immobilization of biomolecules (in this study, proteins) to the amine groups on the Peel-Strip surface. Proteins were determined to be functionalized on the surface via fluorescent immunostaining. Furthermore, the bioactivity of one of the proteins (thrombin) was retained after immobilization. The Peel-Strips were then individually

spotted and immobilized with a different protein on each strip and incorporated into a microfluidic format for affinity-based screening of aptamers in a mixture binding to the proteins. Afterwards, the Peel-Strips could be mechanically peeled off to recover and elute the bound aptamers for post-screening processing such as DNA amplification. This study is the first demonstration of using parylene-A based Peel-Strips for aptamers separation and recovery. The recovered aptamers were detected by fluorospectrometry and also RCA to verify specific binding to the correct proteins and successful recovery. The limit of detection via the RCA detection scheme is 1.6nM starting concentration of aptamers flowed into the microfluidic device. Two rounds of SELEX were attempted to enrich and isolate aptamers from a random ssDNA library against three proteins (TNF-, PDGF-BB, and VEGF), but the SELEX process needs to be further optimized. The microfluidic parylene Peel-Strips platform is not limited to screening and recovering aptamers-proteins, but could be generalized to other biomolecular interactions such as protein-protein, protein-cells interactions, nucleic acids hybridization *etc.* Scaling up may be feasible in the future to high-density smaller strips (*e.g.* 96-wells format), which can be potentially processed and automated using robotics. This can be extended to other fields such as the screening and selection of rare stem cells, induced pluripotent stem cells *etc.* Future use of Peel-Strips could also include drug screening for therapeutic aptamers for proteins involved in diseases using SELEX.

REFERENCES

1. Wang, D.; Urisman, A.; Liu, Y. T.; Springer, M.; Ksiazek, T. G.; Erdman, D. D.; Mardis, E. R.; Hickenbotham, M.; Magrini, V.; Eldred, J.; Latreille, J. P.; Wilson, R. K.; Ganem, D.; DeRisi, J. L., Viral discovery and sequence recovery using DNA microarrays. *Plos Biology* 2003, 1, 257-260.
2. Harty, L. C.; Garcia-Closas, M.; Rothman, N.; Reid, Y. A.; Tucker, M. A.; Hartge, P., Collection of buccal cell DNA using treated cards. *Cancer Epidemiology Biomarkers & Prevention* 2000, 9, 501-506.
3. Higgins, J. A.; Jenkins, M. C.; Shelton, D. R.; Fayer, R.; Karns, J. S., Rapid extraction of DNA from escherichia coli and cryptosporidium parvum for use in pcr. *Applied and Environmental Microbiology* 2001, 67, 5321-5324.
4. Sigurdson, A. J.; Ha, M.; Cosentino, M.; Franklin, T.; Haque, K. A.; Qi, Y.; Glaser, C.; Reid, Y.; Vaught, J. B.; Bergen, A. W., Long-term storage and recovery of buccal cell DNA from treated cards. *Cancer Epidemiology Biomarkers & Prevention* 2006, 15, 385-388.
5. Zhong, K. J. Y.; Salas, C. J.; Shafer, R.; Gubanov, A.; Gasser, R. A.; Magill, A. J.; Forney, J. R.; Kain, K. C., Comparison of isocode stix and fta gene guard collection matrices as whole-blood storage and processing devices for diagnosis of malaria by pcr. *Journal of Clinical Microbiology* 2001, 39, 1195-1196.
6. Park, S. M.; Ahn, J. Y.; Jo, M.; Lee, D. K.; Lis, J. T.; Craighead, H. G.; Kim, S., Selection and elution of aptamers using nanoporous sol-gel arrays with integrated microheaters. *Lab on a Chip* 2009, 9, 1206-1212.
7. Lou, X. H.; Qian, J. R.; Xiao, Y.; Viel, L.; Gerdon, A. E.; Lagally, E. T.; Atzberger, P.; Tarasow, T. M.; Heeger, A. J.; Soh, H. T., Micromagnetic

selection of aptamers in microfluidic channels. *Proceedings of the National Academy of Sciences of the United States of America* 2009, 106, 2989-2994.

8. Cho, M.; Xiao, Y.; Nie, J.; Stewart, R.; Csordas, A. T.; Oh, S. S.; Thomson, J. A.; Soh, H. T., Quantitative selection of DNA aptamers through microfluidic selection and high-throughput sequencing. *Proceedings of the National Academy of Sciences of the United States of America* 2010, 107, 15373-15378.
9. Qian, J. R.; Lou, X. H.; Zhang, Y. T.; Xiao, Y.; Soh, H. T., Generation of highly specific aptamers via micromagnetic selection. *Analytical Chemistry* 2009, 81, 5490-5495.
10. Tan, C. P.; Craighead, H. G., Surface engineering and patterning using parylene for biological applications. *Materials* 2010, 3, 1803-1832.
11. Tan, C. P.; Seo, B. R.; Brooks, D. J.; Chandler, E. M.; Craighead, H. G.; Fischbach, C., Parylene peel-off arrays to probe the role of cell-cell interactions in tumour angiogenesis. *Integrative Biology* 2009, 1, 587-594.
12. Tan, C. P.; Cipriany, B. R.; Lin, D. M.; Craighead, H. G., Nanoscale resolution, multicomponent biomolecular arrays generated by aligned printing with parylene peel-off. *Nano Letters* 2010, 10, 719-725.
13. Lahann, J.; Pluster, W.; Klee, D.; Gattner, H. G.; Hocker, H., Immobilization of the thrombin inhibitor r-hirudin conserving its biological activity. *Journal of Materials Science: Materials in Medicine* 2001, 12, 807-810.
14. Nandivada, H.; Chen, H.-Y.; Elkasabi, Y.; Lahann, J., Reactive polymer coatings for biological applications. In *Polymers for biomedical applications*, American Chemical Society: Washington, DC, 2008; pp 283-298.
15. Jeon, B. J.; Kim, M. H.; Pyun, J. C., Parylene-a coated microplate for covalent immobilization of proteins and peptides. *Journal of Immunological Methods* 2010, 353, 44-48.

16. Jeon, B. J.; Kim, M. H.; Pyun, J. C., Application of a functionalized parylene film as a linker layer of spr biosensor. *Sensors and Actuators B: Chemical* 2010, doi:10.1016/j.snb.2010.1001.1035.

17. Bock, L. C.; Griffin, L. C.; Latham, J. A.; Vermaas, E. H.; Toole, J. J., Selection of single-stranded-DNA molecules that bind and inhibit human thrombin. *Nature* 1992, 355, 564-566.

18. Zhou, L.; Ou, L. J.; Chu, X.; Shen, G. L.; Yu, R. Q., Aptamer-based rolling circle amplification: A platform for electrochemical detection of protein. *Analytical Chemistry* 2007, 79, 7492-7500.

19. Potty, A. S. R.; Kourentzi, K.; Fang, H.; Jackson, G. W.; Zhang, X.; Legge, G. B.; Willson, R. C., Biophysical characterization of DNA aptamer interactions with vascular endothelial growth factor. *Biopolymers* 2009, 91, 145-156.

20. Jin, M.; Song, G.; Carman, C. V.; Kim, Y. S.; Astrof, N. S.; Shimaoka, M.; Wittrup, D. K.; Springer, T. A., Directed evolution to probe protein allostery and integrin i domains of 200,000-fold higher affinity. *Proceedings of the National Academy of Sciences of the United States of America* 2006, 103, 5758-5763.

21. Hu, X. B.; Kang, S.; Lefort, C.; Kim, M.; Jin, M. M., Combinatorial libraries against libraries for selecting neoepitope activation-specific antibodies. *Proceedings of the National Academy of Sciences of the United States of America* 2010, 107, 6252-6257.

22. Miwa, J.; Suzuki, Y.; Kasagi, N., Adhesion-based cell sorter with antibody-coated amino-functionalized-parylene surface. *Journal of Microelectromechanical Systems* 2008, 17, 611-622.

23. Park, Y. J.; Lee, Y. M.; Lee, J. Y.; Seol, Y. J.; Chung, C. P.; Lee, S. J., Controlled release of platelet-derived growth factor-BB from chondroitin

sulfate-chitosan sponge for guided bone regeneration. *Journal of Controlled Release* 2000, 67, 385-394.

24. Lauten, E. H.; VerBerkmoes, J.; Choi, J.; Jin, R.; Edwards, D. A.; Loscalzo, J.; Zhang, Y. Y., Nanoglycan complex formulation extends VEGF retention time in the lung. *Biomacromolecules* 2010, 11, 1863-1872.

25. Hall, B.; Micheletti, J. M.; Satya, P.; Ogle, K.; Pollard, J.; Ellington, A. D., Design, synthesis, and amplification of DNA pools for in vitro selection. *Current Protocols in Molecular Biology* 2009, doi: 10.1002/0471142727.mb0471142402s0471142788.

CHAPTER 7

ADDITIONAL EXPLORATIONS OF PARYLENE[7]

7.1 SUMMARY

This chapter highlights several unpublished explorations using parylene for biological applications, namely: i) using parylene as a substrate for cell culture, ii) investigating the viability of protein after parylene has been deposited on top, iii) extending parylene peel-off to pattern alginate hydrogels, iv) multi-layer paryleen peel-off stencils, and v) parylene-based hydrophobic separation barriers to control distance between two populations of cells. Each section starts with a motivation for the small body of work, followed by a short description of the experimental methods and finally the results and their implications. Some of these studies were pursued simply out of curiosity; while most of them were motivated by several biological questions encountered during the course of the author's Ph.D studies. It is hoped that these additional explorations would someday encourage or inspire new work on using parylene-based surface patterning methods for understanding biology.

7.2 AMINATED PARYLENE CONTACT ANGLES AND CELL CULTURE

7.2.1 Motivation

The ability to spatially control and direct cell growth can be useful in studying disease progression (*e.g.* role of cell-cell interaction in tumor angiogenesis in Chapter 3), creating *in vitro* models of cellular processes, and tissue engineering. Cells are known to adhere to poly-lysine or aminosilane treated surfaces [1, 2]. A possible reason is that the cells, typically carrying a negative charge, are attracted to the positively charged surfaces abundant with amine groups. Cells have also been reported

[7] The results and observations presented in this chapter are unpublished.

to prefer hydrophilic surfaces over hydrophobic alkylsilane surfaces [3]. Parylene-C films under different treatments (*e.g.* oxygen plasma) have been investigated for their ability to promote cell adhesion [4]. Here, aminated parylene films were explored for their ability to support cell adhesion and growth. The hypothesis was that cells might preferentially bind to the aminated parylene regions over glass. The WCAs on aminated parylene under different surface treatment conditions were also characterized. Bladder carcinoma cells (HTB-4) were then cultured on the photolithographically patterned aminated parylene surfaces on glass coverslips.

7.2.2 Experimental Methods

Glass coverslips (Fisher Scientific) were solvent-cleaned and oxygen plasma treated for 2 mins. 0.25g of parylene-A or parylene-AM were coated onto the coverslips. Parylene-A and parylene-AM film thicknesses were measured using a profilometer and determined as 210$\pm$30nm and 100$\pm$30nm respectively. Shipley 1827 photoresist was spun on top of the parylene and a concentric pattern of aminated parylene and glass surface was fabricated using a similar photolithography process as previously mentioned in Chapter 3. These patterned parylene-A coverslips were cleaned with 70% ethanol before using in cell culture. HTB-4 cells were cultured in T75 flasks to 80% confluence in McCoy's 5A modified medium supplemented with 10% FBS. The cells were then detached with 0.25% trypsin-EDTA, then diluted 1:5 in cell culture medium/10% FBS and incubated onto the patterned parylene coverslips. Cells were cultured for 48, 96 h and imaged with phase contrast microscopy.

Additionally, to characterize the hydrophilicity of various parylene surfaces, WCAs were measured using the VCA Optima XE goniometer on: i) freshly deposited parylene surfaces, ii) parylene surfaces that were directly oxygen plasma etched for

30s, and iii) photoresist coated parylene surfaces that were immediately stripped off with acetone and isopropanol.

7.2.3 Results and Discussion

Parylene-A and parylene-AM surfaces were hydrophobic; the WCAs measured were 76.0° and 86.7° in Figure 7.1. The parylene films became hydrophilic upon direct etching with oxygen plasma. The parylene-A film was more hydrophilic (WCA 20.5°) compared to the parylene-AM film (WCA 29.0°) with the same plasma treatment time in Figure 7.1. Surprisingly, coating the parylene films with photoresist and immediately stripping it off resulted in a significant decrease in WCA for both parylene-A and parylene-AM to 52.7° and 53.2° respectively.

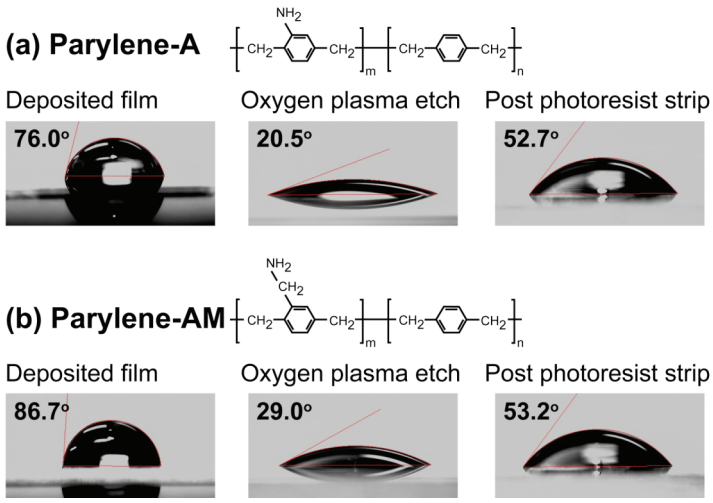

Figure 7.1 Chemical structures and WCAs of: (a) parylene-A and (b) parylene-AM surfaces.

As a comparison, the WCA is typically more than 90^{o} for freshly deposited parylene-C, and decreases to 87^{o} post photoresist stripping. For applications whereby the final hydrophobicity of the parylene films may be important, parylene-A and parylene-AM surfaces are not suitable for photolithography patterning, since the photoresist and its subsequent removal modifies the parylene films rendering them hydrophilic. In such instances, parylene-C should be considered as an alternative.

Figure 7.2(a) shows patterned coverslips with concentric alternating patterns of parylene-A and glass surfaces. Parylene-AM films were not tested for cell culture. HTB-4 cells randomly attached and proliferated on the coverslip, showing no preference for parylene-A or glass in Figure 7.2(b). One possible explanation for this observation is the nonspecific binding of serum proteins in the cell culture medium to both the parylene-A and glass surfaces that promoted cell adhesion. As discussed in Chapter 3, PEG coatings were required to prevent protein adhesion on surfaces; otherwise the epithelial cells would adhere.

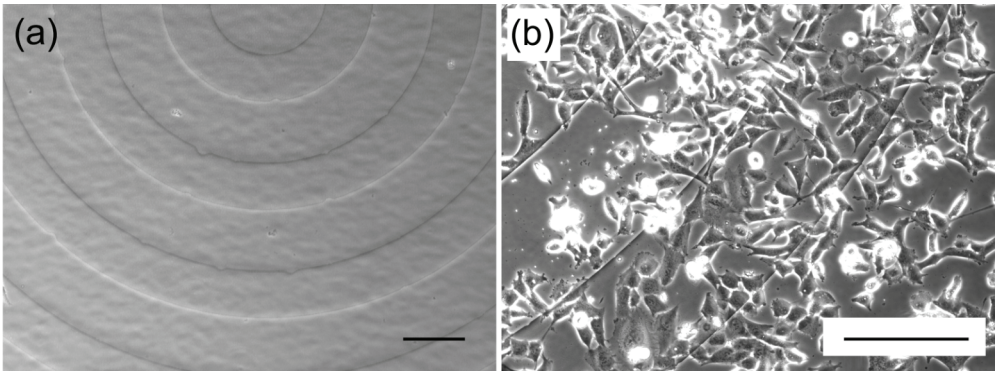

Figure 7.2 (a) Concentric ring pattern of alternating parylene-A and glass surfaces. (b) HTB-4 cells cultured on the patterned surfaces, showing no preference for parylene-A or glass.

The conclusion from this study was that epithelial cells (HTB-4) did not preferentially adhere and grow on parylene-A films compared to glass surfaces. To specifically control and direct epithelial HTB-4 cell adhesion and growth, further surface modifications need to be made to the parylene-A and glass surfaces – for instance, coupling PEG-silane or alkylsilane onto glass to prevent cell adhesion, and also covalently coupling ECM proteins that promotes cell adhesion to the amine groups of parylene-A. Strips of parylene-C on glass have been utilized to guide and pattern neuronal growth [5] since neurons do not typically grow on glass. Behavior of cells on various patterned parylene substrates appears to vary for different cell types.

7.3 PARYLENE DEPOSITION ON PROTEIN

7.3.1 Motivation

An interesting spatial pattern for study consists of large arrays of cells, whereby each cell lies in a central region surrounded by patterned regions of different proteins that may as guidance cues for cell growth or chemotaxis. This unit of the array is depicted in Figure 7.3(c). However, if all the different patterned proteins are presented to cells during cell seeding, the cells may already adhere on top of these proteins even before the study of the effects of the proteins can commence. One suggestion to circumvent this problem could be to utilize multiple parylene layers for patterning. The first layer of parylene stencil would be utilized to spatially pattern the different proteins. Afterwards a second layer of parylene would be coated over the proteins to 'hide' them as shown in Figure 7.3(a). Openings can then be microfabricated in this second parylene layer to create a region for incubating

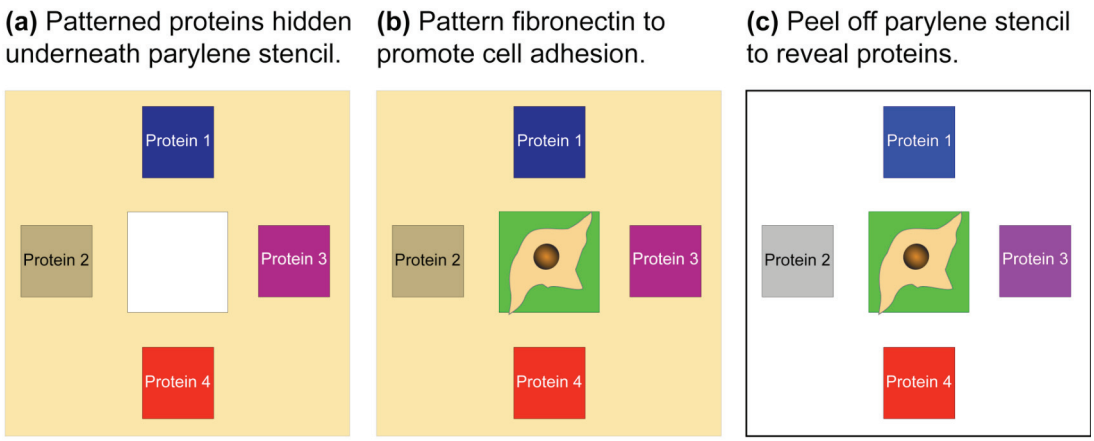

Figure 7.3 Schematic of a patterned cell surrounded by proteins cues. (a) Four different types of proteins (blue, magenta, grey, and red) can be first patterned and then a parylene film (beige) can be deposited on top to 'hide' the protein patterns. An opening can be microfabricated to expose the glass surface in the center of the protein patterns for cell adhesion. (b) A molecule that promotes cell adhesion (*e.g.* fibronectin) can be incubated and a cell would adhere to the central opening. (c) The parylene film can then be peeled off to reveal the four protein patterns. This spatial pattern is potentially useful for studying the effects of various proteins for mediating cellular behavior (*e.g.* growth, chemotaxis *etc.*). The distances between the proteins and the central cell can be readily varied using photolithography.

a molecule that promotes cell adhesion. After the cells have adhered as shown in Figure 7.3(b), the parylene stencil can then be peeled off to reveal the originally patterned proteins as depicted in Figure 7.3(c).

It is not immediately obvious whether the proteins would remain on the surface or retain their bioactivity after the second layer of parylene is deposited. Fibronectin, a model ECM protein that is involved in promoting cell adhesion, was utilized as a test protein to determine if this process would be viable. Figure 7.4 is a schematic showing the process of first creating the fibronectin patterns, followed by depositing a second parylene layer on top of the patterned surface and then peeling it off. After the second parylene layer was peeled off, two experiments were conducted. The first experiment involved fluorescence immunostaining the coverslip after the second layer of parylene was peeled off (Figure 7.4, 5(a)) to verify the presence of fibronectin remaining on the glass surface. The second experiment in Figure 7.4, 5(b), involved culturing cells on top of the fibronectin patterns to determine if the fibronectin retained its ability to promote cell adhesion (bioactivity).

7.3.2 Experimental Methods

The first parylene stencil layer with 40μm x 40μm square openings was microfabricated on PEG-coated glass coverslips as described in Chapter 3, Section 3.2.1. Fibronectin was incubated on the parylene stencil in the same fashion as in Chapter 3, Section 3.2.2. After parylene peel-off, a second parylene layer was deposited on top of the glass coverslip with the fibronectin patterns. This second parylene layer was peeled-off and the coverslips were either immunostained as previously described in Chapter 3, Section 3.2.2, or seeded with OSCC3 cells as described in Chapter 3, Section 3.2.3. After 24h of culture, the cells were fixed and stained with DAPI, while the fibronectin was immunostained.

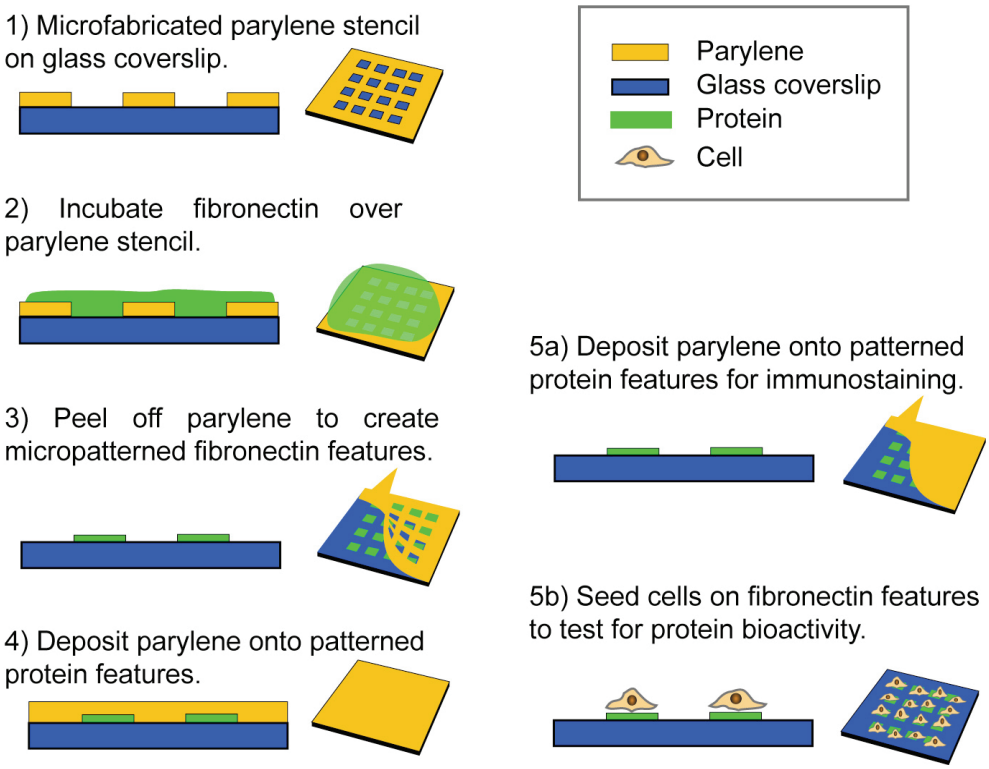

Figure 7.4 Schematic of parylene deposited on protein (1-4). Experiments to test for fibronectin presence (5a) and bioactivity (5b) after second layer parylene deposition and peel-off.

7.3.3 Results and Discussion

Ordered arrays of cells were successfully patterned on the fibronectin features 4h after seeding, as seen from the phase contrast microscopy image in Figure 7.5(a). The patterned cells continued to grow and adhere to the patterns 24h after seeding, shown in Figure 7.5(b). Fluorescence staining confirmed the presence of the fibronectin patterns and cell nuclei in Figure 7.5(c). The average fluorescence intensity (A.U.) of the fibronectin features in Figure 7.5(c) was ~70% that of immunostained fibronectin features without a second parylene layer deposited. This apparent loss in fibronectin could be due to the protein adhering to the second parylene layer as it was peeled off, or due to protein denaturation during the parylene deposition vacuum process. In the future, a higher initial concentration of fibronectin could be incubated to improve the amount of fibronectin adhered.

In conclusion, the results in Figure 7.5 cumulatively suggest that the fibronectin patterns remained on the glass coverslip and retained their bioactivity even after parylene deposition on top of the patterns and subsequent parylene peel-off. These promising results indicate that the proposed spatial patterning of a cell surrounded by multiple proteins in Figure 7.3(c) may be realized in the future for many diverse cell studies (*e.g.* axonal guidance, cell migration, and chemotaxis of bacteria *etc.*).

7.4 PATTERNED ARRAYS OF CALCIUM ALGINATE HYDROGELS

7.4.1 Motivation

The cellular microenvironment is highly complex and can exert an influence on cellular behavior through mechanical cues and/or biochemical signaling. For example, a cell can sense and respond to matrix stiffness (mechanical cue) or to paracrine signaling molecules secreted by neighboring cells (biochemical cues) [6]. In

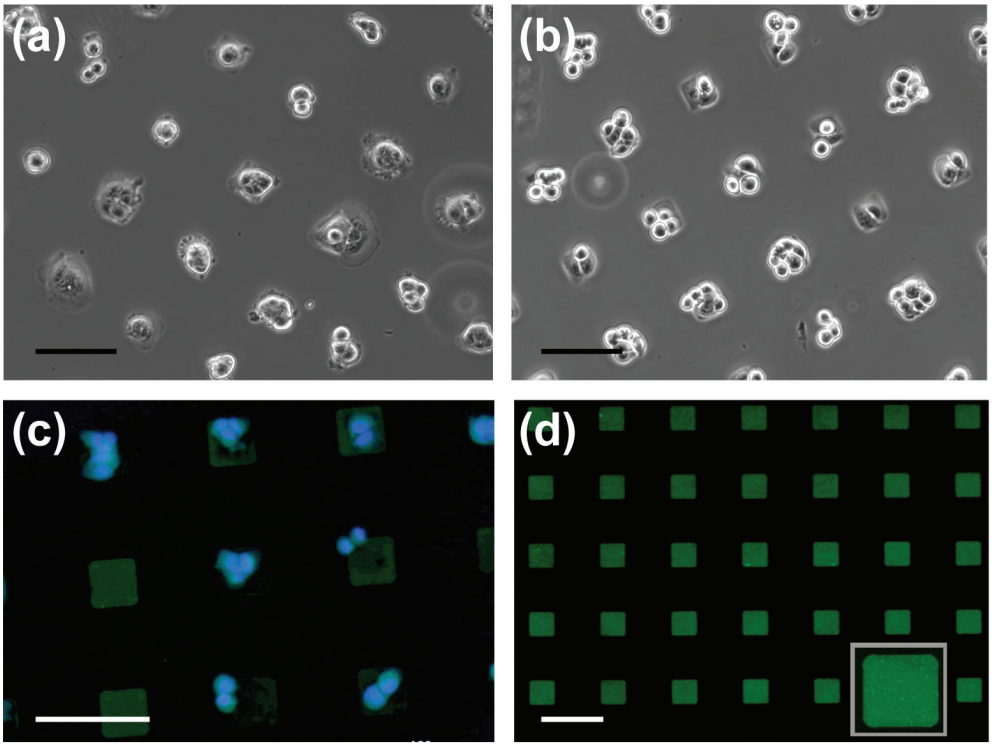

Figure 7.5 Fibronectin patterns remained on the glass surface and retained bioactivity after parylene deposition and peel-off. Phase contrast microscopy image showing cells growing on the fibronectin patterns (a) 4h post-seeding, and (b) 24h post-seeding. (c) Fluorescence microscopy image showing immunostained fibronectin features (green) and DAPI counter-stained cell nuclei (blue). Cells attached and grew on the fibronectin features. (d) Arrays of fluorescence immunostained fibronectin features (green) on the glass coverslip; this coverslip was not used for cell culture. Scale bars represent 100μm.

diseases such as breast cancer, one of the first symptoms is an increase in the elastic modulus of tumor tissue (detection of a hard lump) compared to normal soft breast tissue [7, 8]. Mechanical cues from changes in the ECM stiffness have been shown to transform normal cells to malignant cells through integrins engagement [8].

Alginate hydrogels is a class of biomaterial that is useful for applications such as tissue engineering and 3D tumor models [9, 10]. Cells can be encapsulated in hydrogels to create 3D models that better mimic *in vivo* microenvironments. Cellular behavior in a 3D environment can be markedly different from that in 2D. For example, pro-angiogenic factors are differentially secreted by tumor cells in 3D culture compared to 2D culture [11]; furthermore, unlike in 2D cultures, cells in 3D cultures do not form focal adhesions aggregates [12]. These distinctions are significant enough to warrant studies using 3D culture models. While alginate hydrogels do not naturally support cell adhesion, alginate chains can be covalently modified with a short peptide chain (arginine-glycine-aspartic acid [RGD]) that can be recognized by integrins for cell adhesion [9, 10]. Various groups have attempted to micropattern hydrogels using soft embossing, photopolymerization, and dielectrophoresis [13-16]. In addition to providing an aqueous 3D cell culture model, alginate hydrogels crosslinked by calcium ions with different mechanical stiffness have been created [17]. Thus alginate hydrogels also provide an opportunity to study the effects of mechanical stiffness on cellular behavior.

In this study, the feasibility of using parylene peel-off stencils to micropattern alginate hydrogels with different mechanical stiffness was investigated. One of the final goals is to characterize the behavior of tumor cells cultured on these patterned alginate hydrogels. By controlling the surface area of the hydrogels, the effects of cell-cell interactions can be synergistically studied with stiffness effects. Alternatively, cells can also be encapsulated inside the patterned hydrogels for 3D culture studies.

7.4.2 Experimental Methods

Purified sodium alginate was dissolved to a 3% or 1.5% w/v solution in 50mM HEPES buffer and agitated overnight. The alginate solution was spun coated to a uniform thickness onto 1μm thick parylene stencils on glass coverslips. The alginate chains carrying negatively charged hydroxyl groups were then crosslinked with divalent calcium ions (0.1M calcium chloride in 50mM HEPES) to form an 'egg-box' hydrogel structure as shown in Figure 7.6(a). The parylene can then be peeled off to pattern arrays of alginate hydrogels. This patterning process is outlined in Figure 7.6(b).

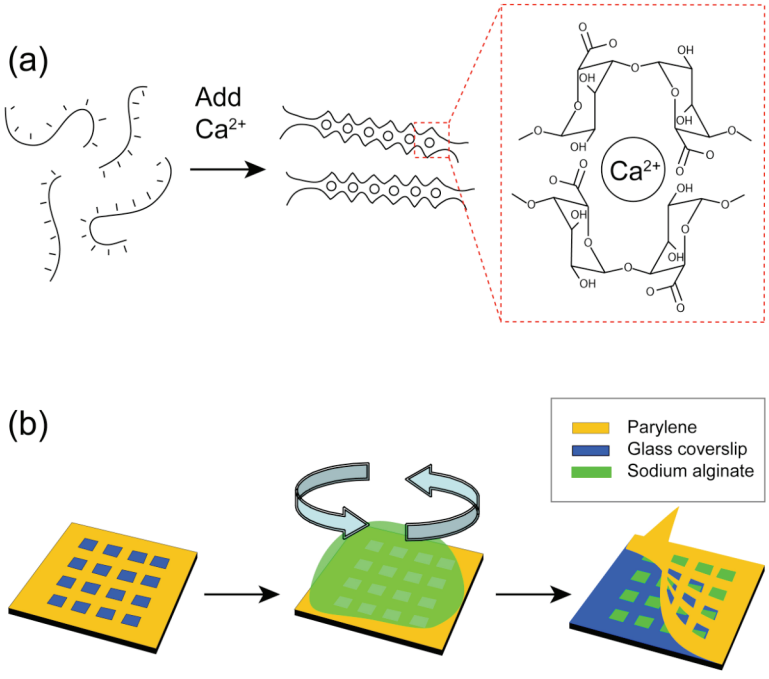

Figure 7.6 (a) Crosslinking of alginate with calcium ions to form hydrogels. (b) Process of patterning alginate hydrogels using parylene peel-off.

7.4.3 Results and Discussion

Arrays of crosslinked 1.5% alginate hydrogel were patterned as seen in Figure 7.7. The smallest hydrogel feature attempted was 10μm wide. Large arrays of 1.5% alginate hydrogels can be patterned, except for the 3% alginate that was too viscous to be uniformly spin coated for the range of spin speeds.

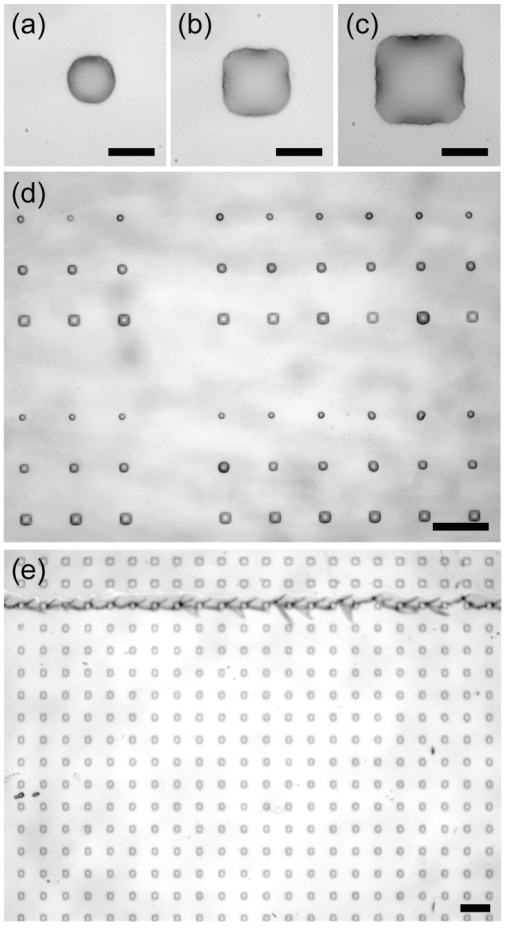

Figure 7.7 Optical images of the crosslinked 1.5% alginate hydrogel arrays. Hydrogel features patterned with widths of (a) 10μm, (b) 15μm, and (c) 20μm. (d) Whole array of hydrogels with different feature widths. (e) Top: Parylene stencil with hydrogel. Bottom: Arrays of hydrogels with 40μm feature width after parylene peel-off. (a-c) Scale bars represent 10μm. 1(d-e) Scale bars represent 100μm.

Figure 7.8(a) shows the thickness of calcium crosslinked 1.5% alginate hydrogel that can be obtained at different spin speeds. A similar graph could not be obtained for 3% alginate as the solution was too viscous to be spin coated uniformly; the result was a small patch of alginate with uneven thickness in the center of the coverslip. The aggregate moduli of the hydrogels at different alginate concentrations in Figure 7.8(b) were measured by Emily Chandler (Fischbach group). The average aggregate modulus of crosslinked 3% alginate hydrogel was 12kPa, significantly different compared to the 5kPa aggregate modulus of the 1.5% alginate hydrogel ($p<0.05$). Cross-sections of 1.5% alginate hydrogel features were uniform in thickness (860±50nm) when spun coated at 5000rpm. The 3% alginate hydrogel features (2.0±0.2μm) were less uniform and ~2.3 times thicker at the same spin speed.

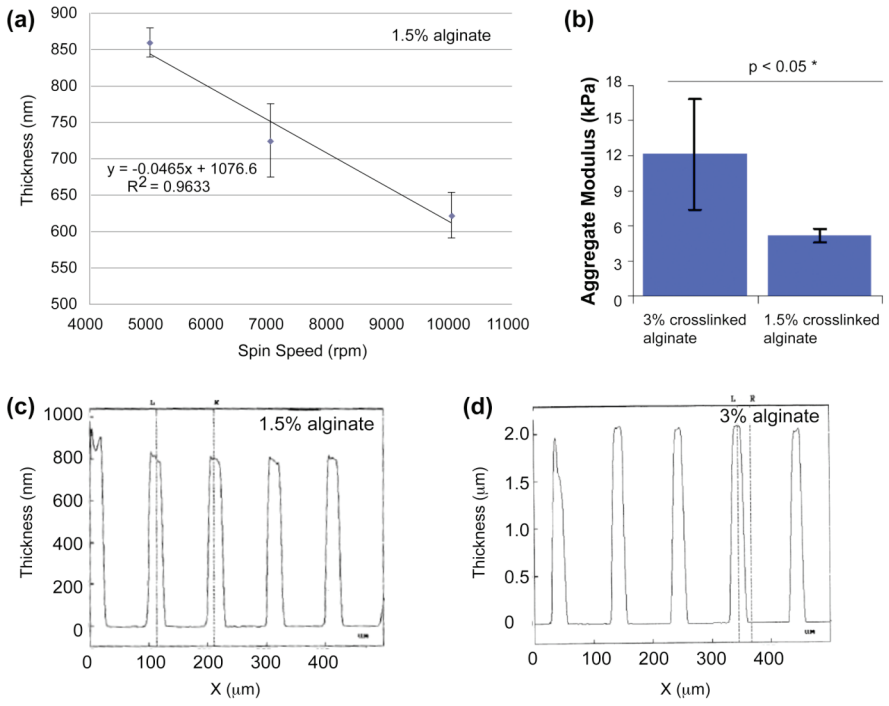

Figure 7.8 (a) 1.5% alginate hydrogel thickness as a function of spin speed. (b) Aggregate moduli of alginate hydrogels. Cross-sectional thickness of (c) 1.5% and (d) 3% alginate hydrogel measured by profilometry. Note difference in y-axes units (c- d).

Crosslinking the alginate first before peeling off the parylene stencil is critical for forming well-defined hydrogel features. Conversely, peeling the stencil first followed by crosslinking failed to define hydrogel features. In the latter case, Figure 7.9(a) shows only residue left at the boundary of the square but no hydrogel formed. Profilometry was performed and no appreciable thickness of hydrogel was measured. This failure to form hydrogels was observed for both 1.5% and 3% alginate.

In conclusion, arrays of calcium crosslinked 1.5% alginate hydrogels can be patterned over a large area. The thickness and uniformity of these hydrogels can be reliably controlled. However it was difficult to spin coat the 3% alginate solution due to its high viscosity. One possible way to overcome this problem is to manually spread the alginate solution on the parylene stencil coverslip by harnessing surface tension effects. However, even if the 3% alginate could be applied on top of the parylene stencil and crosslinked, very thick (>>1μm) hydrogels would be obtained that would tear upon parylene peel-off as shown in in Figure 7.9(b). Parylene peel-off is suitable for patterning 1.5% alginate hydrogels, but not 3% alginate hydrogels at this time.

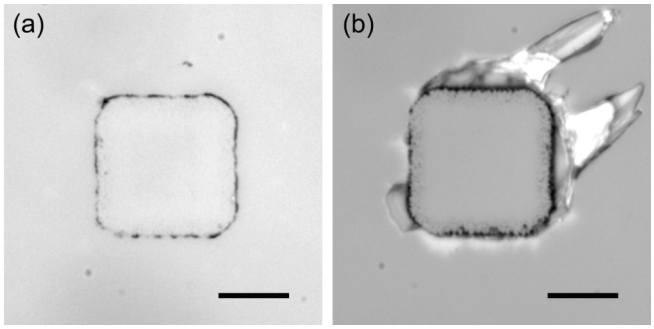

Figure 7.9 (a) Peeling off the parylene stencil first before crosslinking results in no hydrogel formed. A faint boundary of the hydrogel remains. (b) Peeling off the parylene stencil for > 1μm thick crosslinked 3% alginate hydrogel causes the hydrogel to directionally tear in the direction of peeling. Scale bars represent 10μm.

7.5 MULTI-LAYER PARYLENE PEEL-OFF STENCILS

7.5.1 Motivation

The concept of multi-layer parylene stencils was first demonstrated in 2007 by Kuribayashi and colleagues [18]. An advantage of using multi-layer parylene stencils is that smaller distances can be achieved between patterns of different biomolecules compared to inkjet printing. Reducing the interval between two patterned features will increase the packing density of features on a microarray, to enable the screening of more biomolecular candidates per unit area. Additionally, array-based biosensors can be further miniaturized. The ability to pattern two different biomolecules in close proximity will present new opportunities to engineer cellular microenvironments that more closely resemble those *in vivo*, which can be useful for studying interactions between two different cell types.

As discussed in Chapter 2, the distance between two patterned features containing different biomolecules is limited by the size of the inkjet printed spots. To avoid merging of two spots, the interval between them must be at least the diameter of a spot. The use of multi-layer parylene stencil can alleviate this problem through the sequential patterning of biomolecules, outlined in Figure 7.10. In this case, the distance between two features is determined by the resolution of the lithography used to fabricate the parylene stencils. Two assumptions made in the multi-layer parylene patterning process are: i) the surface first exposed is saturated with the first type of biomolecule (red, Figure 7.10) such that this surface does not absorb or react with the second type of biomolecule (blue, Figure 7.10), and ii) the first biomolecule is irreversibly attached to the first surface (*e.g.* covalent linkage or irreversible adsorption) and does not contaminate the subsequent pattern. Blocking or quenching agents can be used to saturate the first exposed surface after patterning the first biomolecule, to reduce nonspecific adsorption or reaction of the second biomolecule.

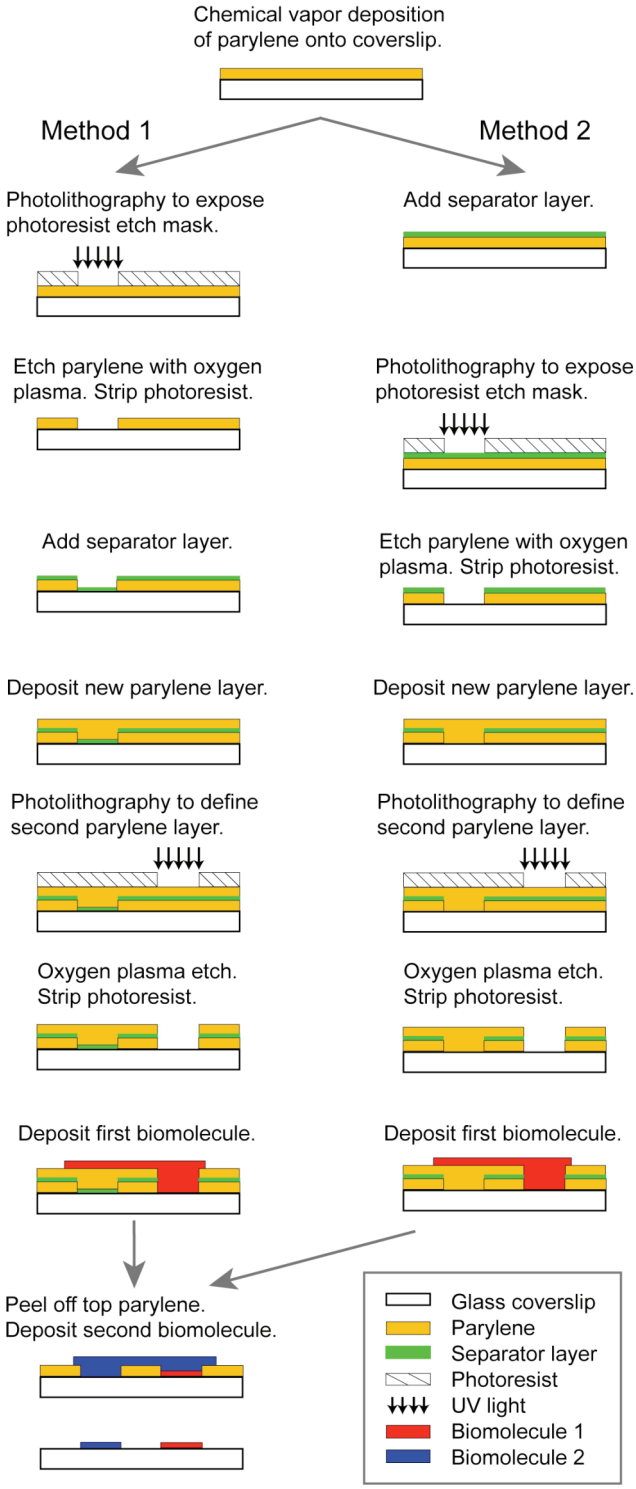

Figure 7.10 Schematic showing multi-layer parylene stencils fabrication and patterning.

An important aspect of multi-layer parylene stencils is the separator layer between each parylene layer. Two sequentially coated parylene layers are stuck to each other and cannot be individually peeled off without a separator. Suitable candidates for the separator include BSA, surfactants, and thin metal films. Two methods of creating multi-layer parylene stencils are shown in Figure 7.10. Method 1 involves adding the separator layer (green) after the first parylene stencil is photolithographically created, while the separator layer is added to the first parylene film before photolithography in Method 2. In Method 1, the separator material is also deposited on top of the surface exposed in the parylene stencil layer. In the later patterning steps, this separator will hinder the second biomolecule (blue) from attaching or reacting with the surface, unless this separator material is soluble in aqueous solutions and can be easily rinsed away without affecting the first biomolecule (red) already patterned. Method 2 circumvents the problem of the separator deposited onto the surface, however the separator layer must be photolithography compatible and not easily removed when the photoresist etch mask is stripped off. The investigation in this section is to determine the suitability of different materials as the separator layer for Methods 1 and 2, towards optimizing the fabrication of multi-layer parylene stencils.

7.5.2 Experimental Methods

The first experiment involved selecting suitable materials and concentrations for the separator layer. Parylene was coated onto glass coverslips. Various separators were incubated on these parylene coverslips and left to dry. The materials tested for the separator layer include PBS, Tween-20, PEG (MW 200Da, Sigma Aldrich), BSA at different concentrations and 15nm thermally evaporated Al film. A second parylene film was then coated on top of the separator layer on each coverslip. The parylene film

stack was fully scored along the edges of the coverslip using a razor blade or a pair of sharp tweezers. Peeling of the top-most (second) parylene film was initiated using adhesive tape. If the separator works, the top parylene film would detach from the underlying (first) parylene film. Otherwise the two parylene films would remain stuck to each other and both films would be peeled off completely from the glass coverslip.

The second experiment involves incorporating the successful separators (from the first experiment) in the microfabrication process to create the multi-layer parylene stencils. The GCA AS200 Autostep 5X i-line stepper was chosen as the tool to expose photoresist due to the ease and accuracy of locating the alignment marks etched in the parylene stencils. Each parylene stencil layer was microfabricated using photolithography as shown in Figure 7.10.

7.5.3 Results and Discussion

Table 7.1 shows the results of the different materials tested as the separator layer in the first experiment. PBS, Tween-20, PEG, BSA and Al were successful in separating the two parylene films. PBS and BSA only worked at higher concentrations ($\geq$1% w/v), while Tween-20 and PEG still worked at lower concentrations ($\geq$0.025% w/v). It was important to keep the concentration of Tween-20 to a minimum if lipids and cells are to be patterned, since Tween-20 is a detergent and disrupts lipid bilayers and cell membranes. Even though these materials showed preliminary success, there are many problems in incorporating them into the photolithography process for the next step.

PBS is a biology-compatible buffer and water-soluble, which is potentially suitable for Method 1. However upon drying, PBS leaves a thick film of dried salt crystals that prevents the alignment marks from being seen while attempting to expose the photoresist for defining the second parylene stencil. Both Tween-20 and PEG dry

non-uniformly across the parylene surface and leave either residue or interference fringes due to uneven film thickness, as shown in Figure 7.11, which disrupt the visualization of the alignment marks during photolithography (Method 1). Spin coating was explored as an alternative to letting the Tween-20 and PEG dry; however the spin-coated Tween-20 and PEG failed to separate the two parylene films. BSA dissolved in deionized water is optically transparent when dry, however it is not suitable for Method 1, as BSA will irreversibly adsorb to the glass surface and prevent patterning of the second biomolecule. Hence BSA was tested as a candidate for Method 2. Unfortunately, the process (step 3 in Method 2) – "post-oxygen plasma etch" removal of the remaining photoresist etch mask using acetone and isopropanol – also removed the BSA separator layer. Tween-20 and PEG were also removed during photolithography processing, and were thus unsuitable for Method 2.

The thin Al layer was the best separator layer for Method 2. Al did not work for Method 1, since it is not optically transparent for visualizing the alignment marks. During photoresist development using the AZ-MIF300 developer, the exposed Al was also wet-etched isotropically. This is due to the base in the developer dissolving the Al. After that, the underlying exposed parylene film could be oxygen plasma etched. Al was not removed by acetone and isopropanol during the "post-etch" stripping of the photoresist etch mask. A caveat to this approach is that Al cannot be used again in later processing steps, either as an etch mask for fabricating nanoscale openings as described in Chapter 2 or as a separator layer, since it would obscure the alignment marks.

In summary, several materials were explored as separator layer between the parylene stencil layers. Of the materials explored, none were suitable for Method 1 since they were not optically transparent or would block the patterning of the second biomolecule. Al was the best material for Method 2, although it cannot be used again

in later processing steps due to its optical opacity. The other materials tested for Method 2 were removed during the lithography processing steps and failed to work as separator layers. For multi-layer parylene stencils that are more than two layers, other alternative materials as separator layers should be explored.

Table 7.1 Materials tested as separator layers in the first experiment. Y indicates success, N indicates failure, N/A means not applicable.

Concentration (w/v)	PBS	Tween-20	PEG	BSA	Al
2%	Y	Y	Y	Y	N/A
1%	Y	Y	Y	Y	N/A
0.10%	N	Y	Y	N	N/A
0.025%	N	Y	Y	N	N/A
N/A	N/A	N/A	N/A	N/A	Y

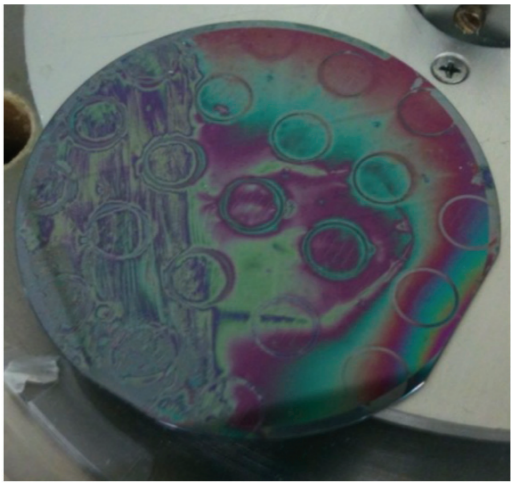

Figure 7.11 Residue (left side on wafer) and interference patterns (right side of wafer) due to uneven thickness of Tween-20 on the parylene coated wafer.

7.6 HYDROPHOBIC PARYLENE SEPARATION BARRIERS

7.6.1 Motivation

As discussed in Section 7.3.1, the cellular microenvironment plays a role in regulating cell fate and function. Micromachined silicon combs have been utilized to spatiotemporally vary cell-cell interactions in real-time [19]. Briefly, the two micromachined parts containing interlocking comb fingers can be reconfigured using a mechanical mechanism to either bring cells into contact or to separate the cells at a pre-defined gap. A different cell type was seeded and cultured on each micromachined part before mechanically altering the distance between the two cell populations.

As an alternative of the micromechanical silicon combs by Hui and Bhatia, the purpose of this study is to explore whether hydrophobic parylene can serve as an effective separation barrier on a glass coverslip to allow for the culture of two cell types. The schematic in Figure 7.12 illustrates the concept. A central strip of parylene defines the spacing between the left and the right side of the coverslip (w), as well as the distance between each 'finger' of the pattern (d_1 and d_2), hence controlling the dimensions where cell-cell interactions occur. Solutions containing cells had to be incubated for cell adhesion before the central parylene strip was peeled off.

7.6.2 Experimental Methods

The first test was whether two different solutions can be adequately separated by a hydrophobic parylene barrier. To investigate this, a 2μm thick parylene film was first coated on the coverslip and photolithographically patterned to form three peelable strips (orange 1, 2, and 3) in Figure 7.12(a). The gaps between each strip after lithography were 10μm wide. Strip 1 (left) was peeled off and a PBS buffer solution (2–10μL) containing a green fluorescent protein (green, Alexa Fluor 488 conjugated antibody 50μg/mL) was incubated on the left side of the coverslip in Figure 7.12(b).

Next, strip 2 (right) was peeled off and a PBS buffer solution (2–10μL) containing a red fluorescent protein (red, Alexa Fluor 647 conjugated antibody 50μg/mL) was incubated on the right side of the coverslip in Figure 7.12(c). Finally the central parylene strip was peeled off in Figure 7.12(d). The protein solutions were left to dry and fluorescence microscopy using appropriate filter cubes was used to image the coverslip. The red and green fluorescence images were merged using ImageJ to form a pseudocolor image. Alternatively, strips 1 and 2 were simultaneously peeled off and the coverslip was oxygen plasma treated for 10s using a barrel oxygen plasma reactor (Harrick Plasma) to improve wetting of the solutions into the comb 'finger' regions.

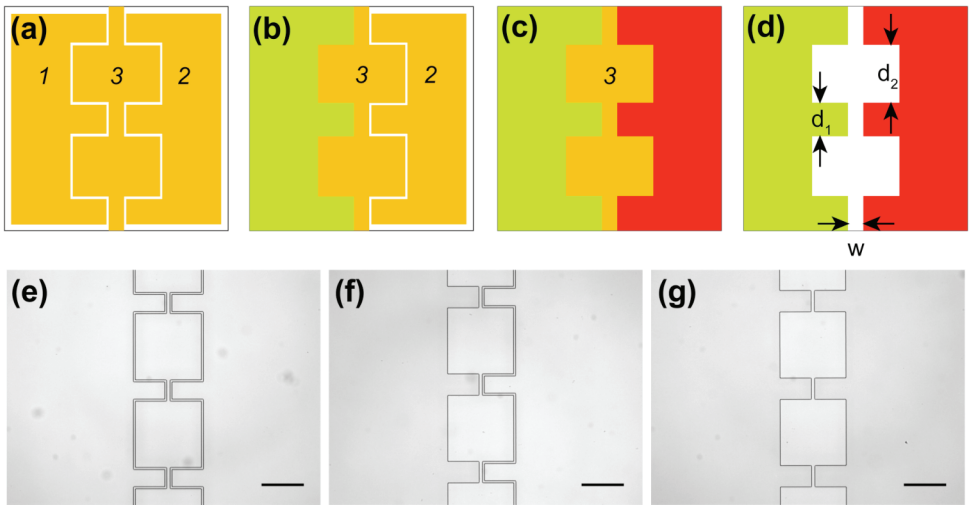

Figure 7.12 Schematic of hydrophobic parylene barriers for controlling cell-cell interactions. (a) 2μm thick parylene (orange) was photolithography patterned into three strips. (b) Strip 1 was peeled off and a solution of Alexa Fluor 488 conjugated antibody (green) was incubated on the left side. (c) Strip 2 was peeled off and a solution Alexa Fluor 647 conjugated antibody (red) was incubated on the right side. (d) The central parylene strip was peeled off. (e-g) Optical image showing the sequential peeling of the three strips (1, 2, 3). Scale bars represent 200μm.

7.6.3 Results and Discussion

Figure 7.12(e-g) shows that the parylene strips (d_1=100μm, d_2=320μm, w=40μm) could be individually peeled off without tearing. The length d_2>>w was chosen to reduce paracrine signaling between adjacent cells of the same type. As an initial test, d_2 was fixed at 320μm since experiments and mathematical modeling show that at distance >300μm away from a point source, the concentrations of VEGF and IL-8 (signaling molecules) decrease to less than 50% of the original concentration at source [11].

A problem was that the aqueous solution did not wet the 'finger' regions of the comb, as shown by the arrow in Figure 7.13(a). Increasing the volume of solution added did not improve wetting and resulted in the solution rolling over the central parylene strip barrier onto the other side. Coverslips with strips 1 and 2 peeled off were thus oxygen plasma treated for 10s to render the glass surface hydrophilic.

While the oxygen plasma improved solution wetting into the 'finger' region demarcated by the arrow in Figure 7.13(b), the central parylene barrier also became more hydrophilic. The decrease in surface tension of the solution at the parylene boundary reduced the volume of solution that could be confined on each side to 2μL, and the solutions dried quickly before the coverslip could be imaged as seen in Figure 7.13(b). Figure 7.13(c –d) show the fluorescence images of the dried antibodies corresponding to the Alexa Fluor 488 and 647 emission wavelengths respectively. Figure 7.13 (e) is a pseudocolor image of the merged fluorescence images, demonstrating that the two antibody solutions can be separated by the parylene barrier and sufficiently wet the 'fingers' of the microcomb structure.

Although this process was adequate in patterning two types of antibodies in close proximity, the limitation in extending this to cell culture was that the small solution volumes evaporated too quickly in the timeframe required for cell seeding

(1h). Thicker (>10μm) parylene barriers could be constructed in the future to increase the volume confined, however the time required to etch through the parylene to create the strips could be prohibitively long (~60 minutes as parylene etch rate in oxygen plasma is 150nm/min).

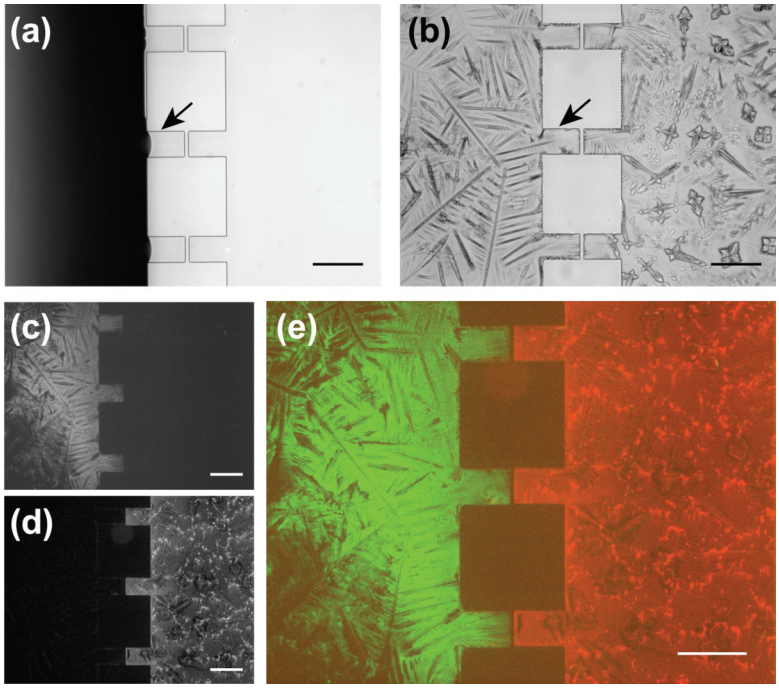

Figure 7.13 Separating two aqueous solutions of fluorescently labeled antibodies by a central hydrophobic parylene microcomb barrier. (a) Solution did not wet the 'finger' region of the microcomb structure as demarcated by the arrow. (b) Solutions wet the 'finger' regions demarcated by the arrow after a brief 10s oxygen plasma treatment. However the central parylene strip became hydrophilic after the oxygen plasma treatment and less solution volume could be confined on each side. The antibody solutions dried quickly and left salt crystals. Fluorescence images taken at Alexa Fluor 488 and 647 emission wavelengths. (e) Pseudocolor fluorescence image of (c) and (d) merged. Scale bars represent 200μm.

7.7 CONCLUSIONS

Even though this chapter is an incomplete body of work motivated by biological questions encountered during the author's Ph.D. studies, some of the preliminary results demonstrate early success and also pose several challenges that need to be overcome. In particular, the microfabrication process of multi-layer parylene stencils (including choice of separator layers and their compatibility with biology and photolithography) is worth pursuing, so as to extend the application of parylene peel-off stencils to more sophisticated biological nano- and micropatterns. The ability to accurately recreate cellular microenvironments, together with subcellular nanopatterns of ligands, will enable understanding of cells and biological systems at a global (microscale) and local (nanoscale) level. Parylene-based surface patterned arrays are a versatile toolbox that can in the future, be integrated with current technologies such as high-throughput inkjet printing [20], bulk or single molecule localization microscopy [21-23] and in the future, super-resolution microscopy techniques (electron microscopy [24], super-resolution fluorescence microscopy).

.

REFERENCES

1. Corey, J. M.; Wheeler, B. C.; Brewer, G. J., Micrometer resolution silane-based patterning of hippocampal neurons: Critical variables in photoresist and laser ablation processes for substrate fabrication. *IEEE Transactions on Biomedical Engineering* **1996,** 43, 944-955.
2. Kleinfeld, D.; Kahler, K. H.; Hockberger, P. E., Controlled outgrowth of dissociated neurons on patterned substrates. *Journal of Neuroscience* **1988,** 8, 4098-4120.
3. Oliver, A. E.; Ngassam, V.; Dang, P.; Sanii, B.; Wu, H. W.; Yee, C. K.; Yeh, Y.; Parikh, A. N., Cell attachment behavior on solid and fluid substrates exhibiting spatial patterns of physical properties. *Langmuir* **2009,** 25, 6992-6996.
4. Chang, T. Y.; Yadav, V. G.; De Leo, S.; Mohedas, A.; Rajalingam, B.; Chen, C. L.; Selvarasah, S.; Dokmeci, M. R.; Khademhosseini, A., Cell and protein compatibility of parylene-c surfaces. *Langmuir* **2007,** 23, 11718-11725.
5. Unsworth, C. P.; Graham, E. S.; Delivopoulos, E.; Dragunow, M.; Murray, A. F., First human hNT neurons patterned on parylene-C/silicon dioxide substrates: Combining an accessible cell line and robust patterning technology for the study of the pathological adult human brain. *Journal of Neuroscience Methods* **2010**, doi:10.1016/j.jneumeth.2010.1009.1022.
6. Liotta, L. A.; Kohn, E. C., The microenvironment of the tumour-host interface. *Nature* **2001,** 411, 375-379.
7. Samani, A.; Zubovits, J.; Plewes, D., Elastic moduli of normal and pathological human breast tissues: An inversion-technique-based investigation of 169 samples. *Physics in Medicine and Biology* **2007,** 52, 1565-1576.

8. Paszek, M. J.; Zahir, N.; Johnson, K. R.; Lakins, J. N.; Rozenberg, G. I.; Gefen, A.; Reinhart-King, C. A.; Margulies, S. S.; Dembo, M.; Boettiger, D.; Hammer, D. A.; Weaver, V. M., Tensional homeostasis and the malignant phenotype. *Cancer Cell* **2005,** 8, 241-254.

9. Augst, A. D.; Kong, H. J.; Mooney, D. J., Alginate hydrogels as biomaterials. *Macromolecular Bioscience* **2006,** 6, 623-633.

10. Fischbach, C.; Chen, R.; Matsumoto, T.; Schmelzle, T.; Brugge, J. S.; Polverini, P. J.; Mooney, D. J., Engineering tumors with 3D scaffolds. *Nature Methods* **2007,** 4, 855-860.

11. Fischbach, C.; Kong, H. J.; Hsiong, S. X.; Evangelista, M. B.; Yuen, W.; Mooney, D. J., Cancer cell angiogenic capability is regulated by 3D culture and integrin engagement. *Proceedings of the National Academy of Sciences of the United States of America* **2009,** 106, 399-404.

12. Fraley, S. I.; Feng, Y. F.; Krishnamurthy, R.; Kim, D. H.; Celedon, A.; Longmore, G. D.; Wirtz, D., A distinctive role for focal adhesion proteins in three-dimensional cell motility. *Nature Cell Biology* **2010,** 12, 598-U169.

13. Albrecht, D. R.; Tsang, V. L.; Sah, R. L.; Bhatia, S. N., Photo- and electropatterning of hydrogel-encapsulated living cell arrays. *Lab on a Chip* **2005,** 5, 111-118.

14. Albrecht, D. R.; Underhill, G. H.; Wassermann, T. B.; Sah, R. L.; Bhatia, S. N., Probing the role of multicellular organization in three-dimensional microenvironments. *Nature Methods* **2006,** 3, 369-375.

15. Ding, Z. W.; Salim, A.; Ziaie, B., Squeeze-film hydrogel deposition and dry micropatterning. *Analytical Chemistry* **2010,** 82, 3377-3382.

16. Liu, V. A.; Bhatia, S. N., Three-dimensional photopatterning of hydrogels containing living cells. *Biomedical Microdevices* **2002,** 4, 257-266.

17. Kuo, C. K.; Ma, P. X., Maintaining dimensions and mechanical properties of ionically crosslinked alginate hydrogel scaffolds in vitro. *Journal of Biomedical Materials Research Part A* **2008,** 84A, 899-907.

18. Kuribayashi, K., Hiratsuka, Y., Yamamura, T., Takeuchi, S., Sequential parylene lift-off process for selective patterning of biological materials. *IEEE MEMS 2007*, 501-504.

19. Hui, E. E.; Bhatia, S. N., Micromechanical control of cell-cell interactions. *Proceedings of the National Academy of Sciences of the United States of America* **2007,** 104, 5722-5726.

20. Tan, C. P.; Cipriany, B. R.; Lin, D. M.; Craighead, H. G., Nanoscale resolution, multicomponent biomolecular arrays generated by aligned printing with parylene peel-off. *Nano Letters* **2010,** 10, 719-725.

21. Hiyama, S.; Gojo, R.; Shima, T.; Takeuchi, S.; Sutoh, K., Biomolecular-motor-based nano- or microscale particle translocations on DNA microarrays. *Nano Letters* **2009,** 9, 2407-2413.

22. Yoshida, Y.; Yokokawa, R.; Suzuki, H.; Atsuta, K.; Fujita, H.; Takeuchi, S., Biomolecular linear motors confined to move upon micro-patterns on glass. *Journal of Micromechanics and Microengineering* **2006,** 16, 1550-1554.

23. Moran-Mirabal, J. M.; Santhanam, N.; Corgie, S. C.; Craighead, H. G.; Walker, L. P., Immobilization of cellulose fibrils on solid substrates for cellulase-binding studies through quantitative fluorescence microscopy. *Biotechnology and Bioengineering* **2008,** 101, 1129-1141.

24. Teramoto, K., Rapid characterization of bacteria using Clairscope and SpiralTOF. *JEOL News* **2010,** 45, 38-41.

CHAPTER 8

CONCLUDING REMARKS AND FUTURE OUTLOOK

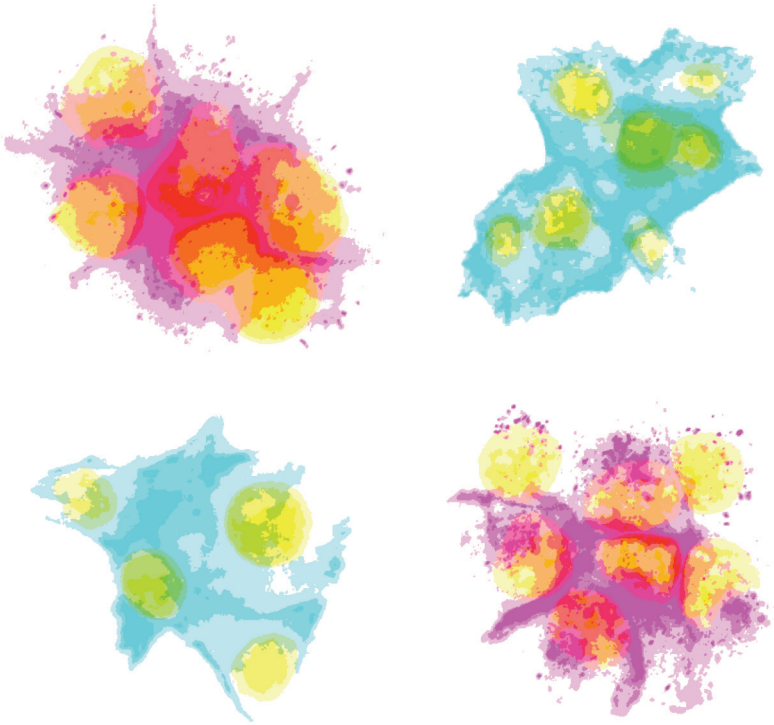

Patterned Cell Arrays © 2011 Christine Tan.

8.1 CONCLUDING REMARKS

Spatially patterned biomolecules and cells on surfaces are important in mimicking and engineering biologically relevant microenvironments. In a cellular microenvironment, cells interact with their neighboring cells at the microscale level, while the specific receptors on the cell membrane interact with ligands on the extracellular matrix at nanoscale dimensions. The ability to manipulate and position biomolecules with both nano- and micrometer scale precision is critical for applications such as chemical functionalization of biosensors, tissue engineering, and fundamental studies in biophysical and molecular chemistry. However there are also several challenges associated with biochemical surface patterning, that the work in this dissertation has attempted to address. Ideally, the patterning method must be biocompatible and preserve the bioactivity of the molecules. Additional desirable features include the ability to achieve patterning nanoscale resolution, high throughput patterning on large area surfaces, the ease of utility, and in some cases the ability to recover molecules that have been bound to the patterned surface.

This work presents parylene, a unique family of CVD polymers, for several applications in surface patterning. Parylene is easily deposited in a CVD process that requires minimum user intervention – just add the appropriate mass of dimer powder – and utilizes an efficient green chemistry that converts 100% of the dimer into a polymer film. In addition, parylene is highly conformal, biocompatible, amenable to photolithography processing, can be made reactive or chemically inert depending on the substituted functional groups, and does not swell in aqueous environments, all of which are crucial features to facilitate biological patterning on surfaces. The two key themes featured in this dissertation are: i) the use of parylene-C films with nano/microfabricated openings as a stencil tool for surface patterning, and ii) the

application of parylene (parylene-C and parylene-A) coatings to directly modify and pattern surfaces.

Related to the first theme, a new nanofabrication method for creating parylene peel-off stencils has been developed in Chapter 2 of this work. An Al etch mask was utilized instead of a photoresist etch mask, creating parylene stencils that enabled the patterning of nanoscale protein arrays down to 90nm resolution. Furthermore, parylene peel-off stencils were combined with inkjet printing to rapidly generate high throughput arrays of multi-component proteins on a single surface. Overlaying sets of printed spots can also generate combinatorial patterned arrays of biomolecules. Combinatorial screening is especially important in biology since most proteins do not bind only to one target, but to a plethora of target proteins. Additionally, interacting with different combinations of target proteins can elicit diverse biological responses and cellular behaviors. Such a complexity of molecular interactions in biology can only be systematically unraveled through the use of combinatorial and highly multiplexed assays.

Chapter 3 highlights the versatility of parylene peel-off and how this simple patterning approach can bring rich new insights into the underlying mechanisms of tumor angiogenesis. Specifically, parylene peel-off was utilized to spatiotemporally control cell-cell interactions in micropatterned tumor cells with high reproducibility over a large area surface. The parylene peel-off patterned tumor cell arrays were probed for cellular secretions of pro-angiogenic factors (IL-8 and VEGF). Secretion of these two factors correlated with the level of physical cell-cell interactions, of which E-cadherin was found to be a critical mediator. The biological significance of this study was that tumor angiogenesis could be regulated and triggered by cell-cell interactions, perhaps even before the onset of hypoxia that is traditionally believed to be the angiogenic trigger in advanced stages of tumor progression.

In Chapter 4, a new substrate incorporating parylene peel-off with aminosilane glass slides chemistry was fabricated and utilized for DNA microarray studies. The new parylene peel-off microarray slide is a hybrid surface with hydrophobic polymer regions surrounding a hydrophilic aminosilane opening, showing the adaptability of incorporating various surface chemistries with parylene peel-off. Flow patterns of a drying printed DNA spot were shown to be directed inwards towards the center of the spot on a parylene peel-off slide compared to outward flow patterns on a traditional hydrophilic aminosilane slide, thus reducing the coffee-ring effect of dried DNA spots. Using the parylene peel-off slides resulted in more reproducible DNA microarray experiments compared to an aminosilane only slide.

These three studies demonstrate that parylene peel-off is a versatile technology for patterning surfaces, which can be adapted for many biological applications. Furthermore, parylene peel-off is simple to use, compatible and easily integrated with existing technologies like inkjet printing, cell culture techniques (microscopy and plastic dishes), DNA microarray scanners and slide processors.

Parylene is also amenable for directly patterning surfaces, in line with the second theme. Chapter 5 illustrates using a direct coating of parylene-C onto filter paper to create a new parylene-paper composite with tunable surface properties. The highly conformal nature of parylene caused the paper to become hydrophobic without changing its porous nature and high surface area. Hydrophilic channels with the smallest width of 275μm were patterned in parylene-coated paper for paper-based microfluidics. 2D parylene-based paper microfluidics with regions of different lateral flow speeds were fabricated by tuning surface hydrophicility and used to program the sequential arrival of fluids. This simple device obviates the need for multiple paper layers (3D devices) or significantly increasing sample volume by changing channel dimensions. Biological applications of parylene-based paper microfluidics were also

demonstrated for combinatorial mixing, generating protein concentration gradients and detecting proteins. The vapor-based and solventless methods of patterning paper microfluidics reported in this dissertation may be extended for patterning other porous media (e.g. membranes) and expand the repertoire of programmable next-generation paper-based assays.

Previous work in literature have shown that reactive forms of parylene, such as parylene containing amine functional groups (parylene-A), can be directly utilized as a surface for covalently immobilizing proteins and other biochemical molecules. This is a convenient method to modify virtually any surface, compared to other surface modification techniques that require specific sbstrates, such as silanization on hydroxyl-rich surfaces (glass) and self-assembly of thiol monolayers on gold. Related to the second theme in this dissertation, parylene-A was not only utilized as a surface for immobilizing proteins, but also extended as a tool for recovering the molecules that show affinity binding for the immobilized species in Chapter 6. One of the challenges in microarray technology is the inability to recover bound species after the initial round of affinity-based screening. It is often useful to identify or create more copies of the bound species by performing post-screening processing (*e.g.* DNA sequencing or amplification). Parylene-A peel-strips were created and incorporated into a microfluidic format for multiplexed SELEX analysis in Chapter 6. Each parylene peel-strip contained a different target protein directly immobilized on the parylene surface. The strip was mechanically peeled away after affinity binding with aptamers to recover the bound aptamers. This new peel-strip microfluidic system is a powerful approach for individually addressable sample screening and recovery, which can also be easily extended to a plate-format containing 96 or more wells.

8.2 FUTURE OUTLOOK

Overall the body of work in this dissertation has shown that parylene is a versatile polymer that enables the creation of a diversity of surface patterned arrays, for various biological applications. There are clearly many interesting directions for future work utilizing parylene, some of which have been explored to different degrees in Chapter 7. Parylene peel-off is a simple and adaptable patterning technique that would undoubtedly continue to find many more biological applications. These examples include neuron patterning, axonal guidance studies, tumor microenvironment studies, and combining nanoscale patterning with ultra high resolution electron and fluorescence microscopy techniques to elucidate biological processes down to single-molecule resolution. Without repeating the possibilities for future work that have already been proposed under the auspices of the other chapters, other additional challenges include lithography-free fabrication of parylene peel-off stencils, and 3D parylene structures for biomimetic membranes and blood vessels.

A barrier towards widespread adoption of parylene peel-off patterning is that the stencils have to be fabricated in the cleanroom. While the tool for parylene deposition has become smaller and relatively self-contained, there is still a need for a reactive ion etcher to directionally etch openings in parylene. Laser ablation has been used to micromachine structures in glass and silicon [1, 2], and can be explored as an alternative to photolithography and oxygen plasma etching. A printing method that can uniformly deposit metal or metal salts on a surface can be exploited to generate masked areas during parylene deposition and later lifted off to create openings in the parylene. The choice of material is crucial here since parylene shows little to no deposition on certain metals and their salts [3-5], whereas the parylene coating would form a conformal film on top of other materials.

Parylene is both biocompatible and hemocompatible, and has been utilized to coat implantable coronary stents. Recently, polymer-based artificial blood-brain barriers have been created to evaluate drug transport [6]. This work is relevant for pharmaceutical industries as *in vitro* models can help predict the uptake of potential drugs through blood-brain barrier before costly animal model testing and clinical trials. Biomimetic membranes have also been created across arrays of parylene openings for simulating ion channel currents [7]. The work in this dissertation have shown that cells can be cultured on parylene and furthermore, parylene is amenable to lithography-based patterning (*e.g.* electron beam lithography) to create nanoscale openings with controlled accuracy and precision. Such precisely machined openings can systematically mimic the naturally occurring openings and fenestrations in membranes and blood vessels, potentially even allowing cells growing on top of the parylene film to form cellular extensions through the fenestrations. Additionally, parylene films can be mechanically rolled up [8] or pinched off using an underlying high aspect ratio mold structure [9] to form microchannels and microtubes. In the future, this may be combined with surface protein patterning and cell seeding to create artificial blood vasculature. There is a potential for parylene to be utilized for tissue engineering applications. Parylene-based surface patterning techniques are emerging as versatile toolboxes for patterning nano- and microarrays towards many biological applications.

REFERENCES

1. Gattass, R. R.; Mazur, E., Femtosecond laser micromachining in transparent materials. *Nature Photonics* **2008,** 2, 219-225.
2. Schaffer, C. B.; Brodeur, A.; Garcia, J. F.; Mazur, E., Micromachining bulk glass by use of femtosecond laser pulses with nanojoule energy. *Optics Letters* **2001,** 26, 93-95.
3. Chen, H. Y.; Lai, J. H.; Jiang, X. W.; Lahann, J., Substrate-selective chemical vapor deposition of reactive polymer coatings. *Advanced Materials* **2008,** 20, 3474-3480.
4. Vaeth, K. M.; Jackman, R. J.; Black, A. J.; Whitesides, G. M.; Jensen, K. F., Use of microcontact printing for generating selectively grown films of poly(p-phenylene vinylene) and parylenes prepared by chemical vapor deposition. *Langmuir* **2000,** 16, 8495-8500.
5. Vaeth, K. M.; Jensen, K. F., Transition metals for selective chemical vapor deposition of parylene-based polymers. *Chemistry of Materials* **2000,** 12, 1305-1313.
6. Shayan, G.; Choi, Y. S.; Shusta, E. V.; Shuler, M. L.; Lee, K. H., Murine in vitro model of the blood-brain barrier for evaluating drug transport. *European Journal of Pharmaceutical Sciences* **2010**, doi: 10.1016/j.ejps.2010.1011.1005.
7. Le Pioufle, B.; Suzuki, H.; Tabata, K. V.; Noji, H.; Takeuchi, S., Lipid bilayer microarray for parallel recording of transmembrane ion currents. *Analytical Chemistry* **2008,** 80, 328-332.
8. Kuribayashi, K., Hiratsuka, Y., Yamamura, T., Takeuchi, S., Sequential parylene lift-off process for selective patterning of biological materials. *IEEE MEMS 2007*, 501-504.

9. Ilic, B.; Czaplewski, D.; Zalalutdinov, M.; Schmidt, B.; Craighead, H. G., Fabrication of flexible polymer tubes for micro and nanofluidic applications. *Journal of Vacuum Science and Technology B* **2002,** 20, 2459-2465.

APPENDIX 1

MATLAB ALGORITHM FOR COUNTING NUCLEAR STAINED CELLS

This MATLAB m-file automates cell counting using fluorescence images of nuclear-stained cells (.jpg, RGB format) as the input. At the input stage, the user has the ability to crop the fluorescence image to remove the scale bar if necessary. The user should manually change the size of the structuring elements (se and se2) to fit the cell size in the cell types that they are counting. The cells counted by the algorithm can be overlaid on the original fluorescence image for the user to visually check the counting accuracy. Output files are ASCII texts containing the cell numbers corresponding to the input images.

```
% -=-=-=-=-=-=-=-=-=-=-=-=-=-=-=-=-=-=-=-=-=-=-=-=-=-=-=-=-=-=-=-=-=-=-=-=-=-=-=-=-=
%  CELL COUNTING PROGRAM
% CREATED BY CHRISTINE TAN, 19 MARCH 2009
% -=-=-=-=-=-=-=-=-=-=-=-=-=-=-=-=-=-=-=-=-=-=-=-=-=-=-=-=-=-=-=-=-=-=-=-=-=-=-=-=-=
% !-Make sure your .jpg file is in RGB format-!
% -=-=-=-=-=-=-=-=-=-=-=-=-=-=-=-=-=-=-=-=-=-=-=-=-=-=-=-=-=-=-=-=-=-=-=-=-=-=-=-=-=

close all
clear all

% == Prompt user ==
user = input('Enter the file name: ', 's');
flag = input('Crop image? y/n: ', 's');  %allows cropping to remove scale bar
flag2 = 0;
```

```
count = 0;
y = strcmp(flag,'y');
n = strcmp(flag,'n');
if (y|n)==1, flag2=1;
end;
if flag2==0, flag = input('Crop image? y/n: ', 's');
end;
if ((flag2)&&(y))==1, count=1;
end;

% == Read In Colour Image, Convert to Grayscale and Adjust Contrast ==
file = strcat(user,'.JPG');
RGB = im2double(imread(file));  %-Read image and convert to double
GrayIm = rgb2gray(RGB);  %-Convert to grayscale
%figure('NumberTitle','on','Name',file), imshow(GrayIm);
if count==1, GrayIm = imcrop(GrayIm);
end;

% == Perform Thresholding to Get Rid of "Spurious" Cells ==
globallevel = graythresh(GrayIm);
GlobalBW  = im2bw(GrayIm,globallevel);
GlobalSignal = GlobalBW .* GrayIm;
%figure('NumberTitle','on','Name','Thresholded image'), imshow(GlobalSignal);

% == Creating Flat Areas Representing Cells - Image Reconstruction ==
se = strel('disk', 2);  %-Structuring element size; will change with cell size
```

```
Ierode = imerode(GlobalSignal, se);
I1 = imreconstruct(Ierode, GlobalSignal);
I2 = imdilate(I1, se);
I3 = imreconstruct(imcomplement(I2), imcomplement(I1));
I3 = imcomplement(I3);
Im1 = imregionalmax(I3);

% == Smoothing Areas with Closing ==
se2=strel('disk', 2);  %-Again, will change with cell size
Im2 = imclose(Im1, se2);

% == Removing Areas with Too Small Pixel Areas ==
Im3 = bwareaopen(Im2, 4);  %-Set pixel area threshold here
Original = GlobalSignal;
Original(Im3) = 255;
figure, imshow(Original)
title('Cell regions superimposed on original image')  %-Shows cells found overlaid on
original image

% == Counting Cell Number ==
bw = bwlabel(Im3);
CellNumber = max(max(bw));%-double(count.*4);

% == Save File ==
save(strcat('CellNumber_',user),'CellNumber','-ASCII');
```

APPENDIX 2

MATLAB ALGORITHM FOR MICROARRAY SPOT INTENSITY ANALYSIS

The series of algorithms was developed and written for analyzing the intensity per pixel of the DNA microarrays spots in Chapter 4. There are two m-files: one for the Corning and/or regular aminosilane slides, and another for the parylene Peel-Off hybrid slides. For each type of slides, the pixels in each spot are analyzed based on Otsu's thresholding algorithm as discussed in Chapter 4. The m-file then outputs several data files containing the mean intensity per pixel for each DNA spot, standard deviation of these intensities etc. for one particular block of DNA spots (15x20 spots). The process is repeated for the next block of DNA spots until all spots in the whole slide have been analyzed. There is also an m-file to group all the data from each microarray sub-blocks of spots together for the entire microarray slide.

<u>m-file for regular aminosilane slides:</u>

```
% -=-=-=-=-=-=-=-=-=-=-=-=-=-=-=-=-=-=-=-=-=-=
% IMAGE ANALYSIS/PROCESSING PROGRAM
% FOR CORNING ARRAY SPOTS
% OTSU's THRESHOLDING
% CHRISTINE TAN AND JOSE MORAN-MIRABAL, 12 JULY 2008

close all
clear all
```

```
% == Read Original File and Generate Initial Image ==
Bigfile = im2double(imread('/Users/nagelneu/Working/Corning/C1/532/corning1-
brain(cy5) kidney 1(cy3) 630-550_532','tiff'));
BigfileAdj = imadjust(Bigfile);
figure('NumberTitle','on','Name','Bigfile'), imshow(BigfileAdj);
[hb,lb] = ginput(1);
Initial = imcrop(Bigfile,[hb,lb,900,700]); %change for different crop area
InitAdj = imadjust(Initial);
figure('NumberTitle','on','Name','Original Image'), imshow(InitAdj);
[h,l] = ginput(3); %get coordinates for top left & right, and bottom left

% == Calculate Global Background levels ==
globallevel = graythresh(Initial);
GlobalBW  = im2bw(Initial,globallevel);
GlobalSignal = GlobalBW .* Initial;
%GlobalSignalFig = figure, imshow(GlobalSignal);
%saveas(GlobalSignalFig,'GlobalSignal','tif');
DilateMask = strel('square',3);
GlobalExpanded = imdilate(GlobalBW,DilateMask);
GlobalExpandedSignal = GlobalExpanded .* Initial;
GlobalBackground = Initial - GlobalExpandedSignal;
%GlobalBackgroundFig = figure, imshow(GlobalBackground);
%saveas(GlobalBackgroundFig,'GlobalBackground','tif');
GlobalBackgroundMedian = median(nonzeros(GlobalBackground));
save('GlobalBackgroundMedian','GlobalBackgroundMedian','-ASCII');
Global =  Initial .* im2bw(Initial,GlobalBackgroundMedian);
```

```
% == Set Initial Positions to Count Spots ==
name = 'C1-532-1a-';
initpositionx = (h(1) + h(3))/2;
initpositiony = (l(1) + l(2))/2;
intervalx = (h(2) - h(1))/19; %change value for #rows
intervaly = (l(3) - l(1))/14; %change value for #columns

% == Loop to Analyze Individual Spots ==
for R=1:15;
for I=1:20;

% == Generate Box Around Spot ==
    x = initpositionx - (intervalx/2) + intervalx*(I-1);
    y = initpositiony - (intervaly/2) + intervaly*(R-1);
    lastcolumn = int2str(I);
    lastrow = int2str(R);
    nameinitial = horzcat(name,lastrow);
    namesecond = horzcat(nameinitial,'-');
    fullname = horzcat(namesecond,lastcolumn);
    signalname = horzcat(fullname,'-sign');
    hisname = horzcat(fullname,'-hist');
    surfname = horzcat(fullname,'-surf');

% == Crop Area for Single Spot ==
    B1D1(I).Original = imcrop(Initial,[x-2,y-2,intervalx+2,intervaly+2]);
```

```
%B1D1(I).FigOriginal = figure('NumberTitle','on','Name','Single Spot Initial Image'),
imshow(B1D1(I).Original)
   CropArea = (intervalx+2)*(intervaly+2);

% == Thresholding, and Binary Image Generation ==
   %level = max(nonzeros(B1D1(I).Original)) * .10;
   level = graythresh(nonzeros(B1D1(I).Original));
   if level <= 0;
      level = 0.0000001;
   else
   end

   B1D1(I).BW = im2bw(B1D1(I).Original,level);
   %figure('NumberTitle','on','Name','Thresholded Image'), imshow(B1D1(I).BW);
   decision = sum(sum(B1D1(I).BW));
   if decision == 0; %assign bkgd value for no spot
      B1D1(I).BinarySignal = im2double(B1D1(I).BW) ;
      B1D1(I).NumberSigPix = 0;
   else
      % == Count Objects (Fragments) & Generate Square Statistics ==
      [B1D1(I).BWLabel,B1D1(I).NumObjects] = bwlabel(B1D1(I).BW,4);
      B1D1(I).RGB_Label = label2rgb(B1D1(I).BWLabel);
      %figure('NumberTitle','on','Name','RGB Label'), imshow(B1D1(I).RGB_Label);
      B1D1(I).Square_Data = regionprops(B1D1(I).BWLabel,'Area');
      B1D1(I).Areas = [B1D1(I).Square_Data.Area] ;
```

```
        B1D1(I).Squares = find(B1D1(I).Areas > 100 & B1D1(I).Areas < 2000); %set
area range to threshold for signal
        B1D1(I).Sig_Matrix = ismember(B1D1(I).BWLabel,B1D1(I).Squares);
        B1D1(I).BinarySignal = im2double(B1D1(I).Sig_Matrix) ;
        B1D1(I).NumberSigPix = sum(sum(B1D1(I).BinarySignal));
        B1D1(I).PercNumberSigPix = B1D1(I).NumberSigPix / CropArea;
        %figure('NumberTitle','on','Name','Signal_Matrix'),
imshow(B1D1(I).BinarySignal);
    end

% == Generate Signal Image and Compute Signal Values ==
    B1D1(I).Signal = B1D1(I).Original .* B1D1(I).BinarySignal;
    %B1D1(I).FigSignal = figure('NumberTitle','on','Name','Signal'),
imshow(B1D1(I).Signal);
    B1D1(I).MeanSignal = mean(nonzeros(B1D1(I).Signal));

% == Signal Area Expansion by 1 Pixel ==
    B1D1(I).IM2 = imdilate(B1D1(I).BinarySignal,DilateMask);
    %figure('NumberTitle','on','Name','Expansion by 1 pixel'),
    %imshow(B1D1(I).IM2);

% == Generate Background Image ==
    B1D1(I).Background = B1D1(I).Original - (B1D1(I).IM2 .* B1D1(I).Original);
    B1D1(I).PercNumberBGNDPix = 1 - (sum(sum(B1D1(I).IM2))/CropArea);
    B1D1(I).NumberBGNDPix = B1D1(I).PercNumberBGNDPix * CropArea;
```

```
    %figure('NumberTitle','on','Name','Background'), imshow(B1D1(I).Background);
    %safety check - assigning values for NaN error pixels
    if isnan(B1D1(I).MeanSignal) == 1
       B1D1(I).MeanSignal = mean(nonzeros(B1D1(I).Background));
       B1D1(I).Median = median(median(nonzeros(B1D1(I).Background)));
    else
       B1D1(I).Median = median(median(nonzeros(B1D1(I).Signal)));
    end
      B1D1(I).StDevSignal = std(nonzeros(B1D1(I).Signal));
    if isnan(B1D1(I).StDevSignal) == 1
       B1D1(I).StDevSignal = std(nonzeros(B1D1(I).Background));
    end

% == Generate Surface Plot of Signal ==
    % if B1D1(I).MeanSignal == 0;
    % else
    % B1D1(I).Surf = figure('NumberTitle','on','Name','Topography'),
surf(B1D1(I).Signal);
    %    shading interp;
    %    axis([0 intervalx+4 0 intervaly+4 0 1 0 1]);
    %    colormap(jet);
    %    shading interp;
    %    colorbar;
    %    view(-70,100);
    %    saveas(B1D1(I).Surf,surfname,'tif');
    %end
```

```
% == Generate Median and Mean Threshold Signal Images ==
   %B1D1(I).HisFig = figure('NumberTitle','on','Name','Signal Histogram'),
hist(nonzeros(B1D1(I).Signal),20);

   % Setting Upper and Lower Confidence Interval Limits for Mean & Median
   boundary1 = B1D1(I).Median - (2*B1D1(I).StDevSignal);
   if boundary1 <= 0
      boundary1 = 0;
   end
   boundary2 = B1D1(I).Median + (2*B1D1(I).StDevSignal);
   if boundary2 >= 1
      boundary2 = 1;
   end
   B1D1(I).UpperBSigMed = im2bw(B1D1(I).Signal,boundary2);
   B1D1(I).LowerBSigMed = im2bw(B1D1(I).Signal,boundary1);
   B1D1(I).ThreshMed = (B1D1(I).LowerBSigMed - B1D1(I).UpperBSigMed);
   %figure('NumberTitle','on','Name','MedianThresh'), imshow(B1D1(I).Signal .*
B1D1(I).ThreshMed);
   boundary3 = B1D1(I).MeanSignal - (2*B1D1(I).StDevSignal);
   if boundary3 <= 0
      boundary3 = 0;
   end
   boundary4 = B1D1(I).MeanSignal + (2*B1D1(I).StDevSignal);
   if boundary4 >= 1
      boundary4 = 1;
```

```
    end
    B1D1(I).UpperBSigMean = im2bw(B1D1(I).Signal,boundary4);
    B1D1(I).LowerBSigMean = im2bw(B1D1(I).Signal,boundary3);
    B1D1(I).ThreshMean = (B1D1(I).LowerBSigMean - B1D1(I).UpperBSigMean);
    %figure('NumberTitle','on','Name','MeanThresh'), imshow(B1D1(I).Signal .*
B1D1(I).ThreshMean);
    B1D1(I).PercMean =
sum(sum(B1D1(I).ThreshMean))/sum(sum(B1D1(I).BinarySignal)) * 100;
    B1D1(I).PercMedian =
sum(sum(B1D1(I).ThreshMed))/sum(sum(B1D1(I).BinarySignal)) * 100;

% == Generate Exclusion Area of 1 Pixel Around Signal ==
    B1D1(I).Exclusion = B1D1(I).Original - B1D1(I).Signal - B1D1(I).Background;
    %figure('NumberTitle','on','Name','Exclusion'), imshow(B1D1(I).Exclusion);

% == Compute Local Background Values ==
    B1D1(I).MeanBackground = mean(nonzeros(B1D1(I).Background));
    B1D1(I).StDevBackground = std(nonzeros(B1D1(I).Background));
    B1D1(I).MedianBackground = median(median(nonzeros(B1D1(I).Background)));

% == Generate Signal to Noise Ratios ==
    B1D1(I).SNRatio = (B1D1(I).MeanSignal - B1D1(I).MeanBackground) /
B1D1(I).MeanBackground;

% == Save Original and Signal Image ==
    %saveas(B1D1(I).FigSignal,signalname,'tif');
```

```
    %saveas(B1D1(I).FigOriginal,fullname,'tif');
    %saveas(B1D1(I).HisFig, hisname,'tif');
    close all
end

Signal(R,:) = [B1D1.MeanSignal];
Background(R,:) = [B1D1.MeanBackground];
SNR(R,:) = [B1D1.SNRatio];
StdSignal(R,:) = [B1D1.StDevSignal];
StdBackground(R,:) = [B1D1.StDevBackground];
SignalPixel(R,:) = [B1D1.NumberSigPix];
BGNDPixel(R,:) = [B1D1.NumberBGNDPix];
PercSigMean (R,:) = [B1D1.PercMean];
PercSigMedian (R,:) = [B1D1.PercMedian];
Median (R,:) = [B1D1.Median];
MedianBackground (R,:) = [B1D1.MedianBackground];
%close all;
end

save('CropArea','CropArea','-ASCII');
save('Signal','Signal','-ASCII');
save('Background','Background','-ASCII');
save('StDevBackground','StdBackground','-ASCII');
save('StDevSignal','StdSignal','-ASCII');
save('SNR','SNR','-ASCII');
save('SignalPixel','SignalPixel','-ASCII');
```

```
save('BackgroundPixel','BGNDPixel','-ASCII');
save('PercSignalMedian','PercSigMedian','-ASCII');
save('PercSignalMean','PercSigMean','-ASCII');
save('Median','Median','-ASCII');
save('MedianBackground','MedianBackground','-ASCII');
```

<u>m-file for parylene slides:</u>

```
% -=-=-=-=-=-=-=-=-=-=-=-=-=-=-=-=-=-=-=-=-=
% IMAGE ANALYSIS/PROCESSING PROGRAM
% FOR PARYLENE ARRAY SPOTS
% OTSU's THRESHOLDING
% CHRISTINE TAN AND JOSE MORAN-MIRABAL, 9 JULY 2008
% -=-=-=-=-=-=-=-=-=-=-=-=-=-=-=-=-=-=-=-=-=

close all
clear all

% == Read Original File and Generate Initial Image ==
Bigfile = im2double(imread('/Users/nagelneu/Working/Parylene/JHA1/532/jh01-
brain(cy5) kidney 1(cy3) 800-600_532','tiff'));
BigfileAdj = imadjust(Bigfile);
figure('NumberTitle','on','Name','Bigfile'), imshow(BigfileAdj);
[hb,lb] = ginput(1);
Initial = imcrop(Bigfile,[hb,lb,900,700]); %change for different crop area
InitAdj = imadjust(Initial);
```

```
figure('NumberTitle','on','Name','Original Image'), imshow(InitAdj);
[h,l] = ginput(3); %get coordinates for top left & right, and bottom left

% == Initialize Matrix where All Single Square Data Are Stored and Generate
Counter
DataSpots = zeros(20,300);
counter = 0;
counter2 = 0;

% == Calculate Global Background Levels ==
globallevel = graythresh(Initial);
GlobalBW  = im2bw(Initial,globallevel);
GlobalSignal = GlobalBW .* Initial;
%GlobalSignalFig = figure, imshow(GlobalSignal);
%saveas(GlobalSignalFig,'GlobalSignal','tif');
DilateMask = strel('square',3);
GlobalExpanded = imdilate(GlobalBW,DilateMask);
GlobalExpandedSignal = GlobalExpanded .* Initial;
GlobalBackground = Initial - GlobalExpandedSignal;
%GlobalBackgroundFig = figure, imshow(GlobalBackground);
%saveas(GlobalBackgroundFig,'GlobalBackground','tif');
GlobalBackgroundMedian = median(nonzeros(GlobalBackground));
save('GlobalBackgroundMedian','GlobalBackgroundMedian','-ASCII');
Global =  Initial .* im2bw(Initial,GlobalBackgroundMedian);
```

```
% == Set Initial Positions to Count Spots ==
name = 'JHA1-532-1a-';
initpositionx = (h(1) + h(3))/2;
initpositiony = (l(1) + l(2))/2;
intervalx = (h(2) - h(1))/19;
intervaly = (l(3) - l(1))/14;

% == Loop to Analyze Individual Spots ==
for R=1:15;
for I=1:20;
counter = counter + 1;

% == Generate Box Around Spot ==
    x = initpositionx - (intervalx/2) + intervalx*(I-1);
    y = initpositiony - (intervaly/2) + intervaly*(R-1);
    lastcolumn = int2str(I);
    lastrow = int2str(R);
    nameinitial = horzcat(name,lastrow);
    namesecond = horzcat(nameinitial,'-');
    fullname = horzcat(namesecond,lastcolumn);
    signalname = horzcat(fullname,'-sign');
    hisname = horzcat(fullname,'-hist');
    surfname = horzcat(fullname,'-surf.tif');
    objectname = horzcat(fullname,'-objects');
```

```
% == Crop Area for Single Spot ==
   B1D1(I).Original = imcrop(Initial,[x-2,y-2,intervalx+2,intervaly+2]);
   %B1D1(I).Max = max(B1D1(I).Original);
   %B1D1(I).FigOriginal = figure('NumberTitle','on','Name','Single Spot Initial
Image'), imshow(B1D1(I).Original);
   CropArea = (intervalx+2)*(intervaly+2);

% == Thresholding, and Binary Image Generation ==
   %level = max(nonzeros(B1D1(I).Original)) * .10;
   level = graythresh(nonzeros(B1D1(I).Original));
   if level <= 0;
      level = 0.0000001;
   else
   end

   B1D1(I).BW = im2bw(B1D1(I).Original,level);
   %figure('NumberTitle','on','Name','Thresholded Image'), imshow(B1D1(I).BW);
   decision = sum(sum(B1D1(I).BW));
   if decision == 0; %assign bkgd value for no spot
      B1D1(I).BinarySignal = im2double(B1D1(I).BW) ;
      B1D1(I).NumberSigPix = 0;
   else
      % == Count Objects & Generate Square Statistics ==
      [B1D1(I).BWLabel,B1D1(I).NumObjects] = bwlabel(B1D1(I).BW,4);
      B1D1(I).NumObjects;
      B1D1(I).RGB_Label = label2rgb(B1D1(I).BWLabel);
```

```
        %figure('NumberTitle','on','Name','RGB Label'), imshow(B1D1(I).RGB_Label);
        B1D1(I).Square_Data = regionprops(B1D1(I).BWLabel,'Area');
        B1D1(I).Areas = [B1D1(I).Square_Data.Area] ;
        B1D1(I).Squares = find(B1D1(I).Areas > 3 & B1D1(I).Areas < 100);
        B1D1(I).Sig_Matrix = ismember(B1D1(I).BWLabel,B1D1(I).Squares);
        B1D1(I).BinarySignal = im2double(B1D1(I).Sig_Matrix) ;
        B1D1(I).NumberSigPix = sum(sum(B1D1(I).BinarySignal));
        B1D1(I).PercNumberSigPix = B1D1(I).NumberSigPix / CropArea;
        %figure('NumberTitle','on','Name','Signal_Matrix'),
imshow(B1D1(I).BinarySignal);

        % == Store Signal of Individual Sub-Spot ==
        [B1D1(I).BWLabelSignal,B1D1(I).NumObjectsSignal] =
bwlabel(B1D1(I).BinarySignal,4)
        B1D1(I).BWRESC = B1D1(I).BWLabelSignal ./ B1D1(I).NumObjectsSignal;
        interv = 0.99/B1D1(I).NumObjectsSignal;
        Segment = 1.01;
        if B1D1(I).NumObjectsSignal <= 20 & B1D1(I).NumObjectsSignal >= 3;
          for J = 1:B1D1(I).NumObjectsSignal;
              Segment = Segment - interv;
              Objects(J).Binary = im2bw(B1D1(I).BWRESC,Segment);
              %figure, imshow(Objects(J).Binary);

              % == Loop to Ensure Only Consideration of the Jth Subspot
              if J==1;
                 Objects(J).Signal = Objects(J).Binary .* B1D1(I).Original;
```

```
            else
               Temp = Objects(J).Binary - Objects(J-1).Binary;
               Objects(J).Signal = Temp .* B1D1(I).Original;
            end

            %figure, imshow(Objects(J).Signal);
            Objects(J).MeanSignal = mean(nonzeros(Objects(J).Signal));
            SignalObjects(J,:) = Objects(J).MeanSignal;
            DataSpots(J,counter) = Objects(J).MeanSignal;
         end
         save(objectname,'SignalObjects','-ASCII');
         clear SignalObjects;
      else
      end
   end
   StdObjects(:,counter) = std(nonzeros(DataSpots(:,counter)));
   MeanSpotObjects(:,counter) = mean(nonzeros(DataSpots(:,counter)));
   MedianSpotObjects(:,counter) = median(nonzeros(DataSpots(:,counter)));

% == Generate Signal Image and Compute Signal Values ==
   B1D1(I).Signal = B1D1(I).Original .* B1D1(I).BinarySignal;
   %B1D1(I).FigSignal = figure('NumberTitle','on','Name','Signal'),
imshow(B1D1(I).Signal);
   B1D1(I).MeanSignal = mean(nonzeros(B1D1(I).Signal));
```

```
% == Signal Area Expansion by 1 Pixel ==
   B1D1(I).IM2 = imdilate(B1D1(I).BinarySignal,DilateMask);
   %figure('NumberTitle','on','Name','Expansion by 1 pixel'),
   %imshow(B1D1(I).IM2);

% == Generate Background Image ==
   B1D1(I).Background = B1D1(I).Original - (B1D1(I).IM2 .* B1D1(I).Original);
   B1D1(I).PercNumberBGNDPix = 1 - (sum(sum(B1D1(I).IM2))/CropArea);
   B1D1(I).NumberBGNDPix = B1D1(I).PercNumberBGNDPix * CropArea;
   %figure('NumberTitle','on','Name','Background'), imshow(B1D1(I).Background);

   %safety check - assigning values for NaN error pixels
   if isnan(B1D1(I).MeanSignal) == 1;
      B1D1(I).MeanSignal = mean(nonzeros(B1D1(I).Background));
      B1D1(I).Median = median(median(nonzeros(B1D1(I).Background)));
   else
      B1D1(I).Median = median(median(nonzeros(B1D1(I).Signal)));
   end
   B1D1(I).StDevSignal = std(nonzeros(B1D1(I).Signal));
   if isnan(B1D1(I).StDevSignal) == 1
      B1D1(I).StDevSignal = std(nonzeros(B1D1(I).Background));
   end

% == Generate Surface Plot of Signal ==
   if B1D1(I).MeanSignal == 0;
      counter2 = counter2 + 1;
```

```
    else
        % figure('NumberTitle','on','Name','Topography'), surf(B1D1(I).Signal);
        % shading interp;
        % axis([0 intervalx+4 0 intervaly+4]);
        % colormap(jet);
        % shading interp;
        % colorbar;
        % view(-45,70);
        %saveas(B1D1(I).Surf,surfname,'tif');
        %F = getframe(gcf);
        %Image = frame2im(F);
        %imwrite(Image,surfname,'tif')
    end

% == Generate Median and Mean Threshold Signal Images ==
    %B1D1(I).HisFig = figure('NumberTitle','on','Name','Signal Histogram'),
hist(nonzeros(B1D1(I).Signal),20);

    % Setting Upper and Lower Confidence Interval Limits for Mean & Median
    boundary1 = B1D1(I).Median - (2*B1D1(I).StDevSignal);
    if boundary1 <= 0;
        boundary1 = 0;
    end
    boundary2 = B1D1(I).Median + (2*B1D1(I).StDevSignal);
    if boundary2 >= 1;
        boundary2 = 1;
```

```
    end
    B1D1(I).UpperBSigMed = im2bw(B1D1(I).Signal,boundary2);
    B1D1(I).LowerBSigMed = im2bw(B1D1(I).Signal,boundary1);
    B1D1(I).ThreshMed = (B1D1(I).LowerBSigMed - B1D1(I).UpperBSigMed);
    %figure('NumberTitle','on','Name','MedianThresh'), imshow(B1D1(I).Signal .*
B1D1(I).ThreshMed);
    boundary3 = B1D1(I).MeanSignal - (2*B1D1(I).StDevSignal);
    if boundary3 <= 0;
       boundary3 = 0;
    end
    boundary4 = B1D1(I).MeanSignal + (2*B1D1(I).StDevSignal);
    if boundary4 >= 1;
       boundary4 = 1;
    end
    B1D1(I).UpperBSigMean = im2bw(B1D1(I).Signal,boundary4);
    B1D1(I).LowerBSigMean = im2bw(B1D1(I).Signal,boundary3);
    B1D1(I).ThreshMean = (B1D1(I).LowerBSigMean - B1D1(I).UpperBSigMean);
    %figure('NumberTitle','on','Name','MeanThresh'), imshow(B1D1(I).Signal .*
B1D1(I).ThreshMean);
    B1D1(I).PercMean =
sum(sum(B1D1(I).ThreshMean))/sum(sum(B1D1(I).BinarySignal)) * 100;
    B1D1(I).PercMedian =
sum(sum(B1D1(I).ThreshMed))/sum(sum(B1D1(I).BinarySignal)) * 100;

% == Generate Exclusion area of 1 Pixel around signal ==
    B1D1(I).Exclusion = B1D1(I).Original - B1D1(I).Signal - B1D1(I).Background;
```

```
    %figure('NumberTitle','on','Name','Exclusion'), imshow(B1D1(I).Exclusion);

% == Compute Local Background Values ==
    B1D1(I).MeanBackground = mean(nonzeros(B1D1(I).Background));
    B1D1(I).StDevBackground = std(nonzeros(B1D1(I).Background));
    B1D1(I).MedianBackground = median(median(nonzeros(B1D1(I).Background)));
% == Generate Signal to Noise Ratios ==
    B1D1(I).SNRatio = (B1D1(I).MeanSignal - B1D1(I).MeanBackground) /
B1D1(I).MeanBackground;
    % == Save original and signal image ==
    %saveas(B1D1(I).FigSignal,signalname,'tif');
    %saveas(B1D1(I).FigOriginal,fullname,'tif');
    %saveas(B1D1(I).HisFig, hisname,'tif');
    close all
end

Signal(R,:) = [B1D1.MeanSignal];
Background(R,:) = [B1D1.MeanBackground];
SNR(R,:) = [B1D1.SNRatio];
StdSignal(R,:) = [B1D1.StDevSignal];
StdBackground(R,:) = [B1D1.StDevBackground];
SignalPixel(R,:) = [B1D1.NumberSigPix];
BGNDPixel(R,:) = [B1D1.NumberBGNDPix];
PercSigMean (R,:) = [B1D1.PercMean];
PercSigMedian (R,:) = [B1D1.PercMedian];
Median (R,:) = [B1D1.Median];
```

```
MedianBackground (R,:) = [B1D1.MedianBackground];
NumObjectsSignal (R,:) = [B1D1.NumObjectsSignal];
end

DataStops = DataSpots';
StDevObjects = StdObjects';
MeanSpotObject = MeanSpotObjects';
MedianSpotObject = MedianSpotObjects';

save('CropArea','CropArea','-ASCII');
save('StDevObjects','StDevObjects','-ASCII');
save('MeanSpotObjects','MeanSpotObject','-ASCII');
save('MedianSpotObjects','MedianSpotObject','-ASCII');
save('DataSpots','DataStops','-ASCII');
save('Signal','Signal','-ASCII');
save('Background','Background','-ASCII');
save('StDevBackground','StdBackground','-ASCII');
save('StDevSignal','StdSignal','-ASCII');
save('SNR','SNR','-ASCII');
save('SignalPixel','SignalPixel','-ASCII');
save('BackgroundPixel','BGNDPixel','-ASCII');
save('PercSignalMedian','PercSigMedian','-ASCII');
save('PercSignalMean','PercSigMean','-ASCII');
save('Median','Median','-ASCII');
save('MedianBackground','MedianBackground','-ASCII');
save('NumObjectsSignal','NumObjectsSignal','-ASCII');
```